PALEOMAGNETIC, PETROGRAPHIC AND GEOCHEMICAL STUDIES OF THE ROCKS OF PARTS OF CENTRAL AND EASTERN NAGALAND

WATITEMSU

DEPARTMENT OF GEOLOGY
NAGALAND UNIVERSITY
2013

PALEOMAGNETIC, PETROGRAPHIC AND GEOCHEMICAL STUDIES OF THE ROCKS OF PARTS OF CENTRAL AND EASTERN NAGALAND

BY

WATITEMSU

Submitted

In partial fulfillment of the requirement of the Degree of
Doctor of Philosophy in Geology
of Nagaland University

NAGALAND UNIVERSITY

September 2013

DECLARATION

I, Mr. Watitemsu, hereby declare that the subject matter of this thesis is the record of work done by me, that the contents of this thesis did not form basis of the award of any previous degree to me or to the best of my knowledge to anybody else, and that the thesis has not been submitted by me for any research degree in any other University/Institute.

This is being submitted to the Nagaland University for the degree of Doctor of Philosophy in Geology.

Candidate

Head

Supervisor

Co-Supervisor

HEAD
Department of Geology
Nagaland University, Kohima

i

Dr. Vikoleno Rino
Assistant Professor
Department of Geology

Mobile : 09436016695
E-mail : vikoleno_rino@yahoo.co.in

Dated Kohima the 11th September 2013

CERTIFICATE

The thesis presented by Mr. Watitemsu, M.Sc., bearing Registration No. 295/2007 (14.06.2007) embodies the results of investigations carried out by him under my supervision and guidance.

I certify that this work has not been presented for any degree elsewhere and that the candidate has fulfilled all conditions laid down by the University.

(V. RINO)
Supervisor

NAGALAND

Glenn T. Thong
Professor of Geology

☎/Fax : 0370-2240515
Mobile : 09436000479
E-mail : glen2t03@yahoo.com
nagalandslide@yahoo.com

UNIVERSITY

Dated Kohima the 11th September 2013

CERTIFICATE

The thesis presented by Mr. Watitemsu, M.Sc., bearing Registration No. 295/2007 (14.06.2007) embodies the results of investigations carried out by him under my supervision and guidance.

I certify that this work has not been presented for any degree elsewhere and that the candidate has fulfilled all conditions laid down by the University.

(G.T. THONG)
Co-Supervisor

Acknowledgements

(**Watitemsu**)

PREFACE

Nagaland, one of the easternmost states of the Indian Union, is made up of high hills and deep valleys and gorges. It represents a young tectonically active mobile belt with diverse rocks and sediments ranging in age from Upper Jurassic to Holocene. Most of the rocks are structurally deformed and weathered to varying degrees. The deformations are a result of the subduction of the Indian plate beneath that of the Burmese.

Numerous geological, structural, paleontological, petrological and geochemical studies have been undertaken on portions of these rocks to decipher their origin and other related geological aspects. Much of the sedimentaries are also devoid of fossils. Hence, accurate dating of rocks is a problem. Moreover, paleomagnetic and magnetostratigraphic studies of the rocks of Nagaland are yet to begin.

With this in mind the present study has been undertaken to corroborate earlier findings and synthesize all available data to determine the origin of the Upper Disang sediments of part of the Inner Fold Belt and basalt of the Naga Hills Ophiolite belt. This study is also an attempt at dating the rocks through paleomagnetic means and determining sedimentation rates and correlating the same with other adjacent sedimentary horizons.

The study area comprises rocks of diverse character such as shale, chert, serpentinite, plagiogranite, spilite, various metamorphics, etc. but these have not been taken up for study. The Lower Disang comprising shales are highly jointed and weathered to varying extents. As a consequence they are very brittle, so it is not possible to obtain workable cores. The other rocks listed are magnetically weak or are metamorphosed to varying extents so are very poor for paleomagnetic studies.

Paleomagnetic studies of basalts provided very limited data off two samples only. The reason for this may be partial spilitization or slight metamorphism of much of the basalt. Further detailed paleomagnetic studies from all possible basalt horizons may provide better results.

CONTENTS

LIST OF TABLES

LIST OF FIGURES

LIST OF PLATES

PARTICULARS OF CANDIDATE

NAME OF THE CANDIDATE   : Mr. Watitemsu

DEGREE   : PhD

DEPARTMENT   : Geology

TITTLE OF DISSERTATION :

Paleomagnetic, petrographic and geochemical studies of the rocks of parts of central and eastern Nagaland

DATE OF ADMISSION   : 14th June 2007

APPROVAL OF RESEARCH
PROPOSAL   : 14th June 2007

REGISTRATION No. & DATE   : 295/2007 (14.06.2007)

13/9/2013

Head

HEAD
Department of Geology
Nagaland University, Kohima

xx

Chapter 1

INTRODUCTION

Nagaland, the sixteenth state of the Indian Union lies in the extreme northeast with a geographic area of 16,579 km^2. It is bounded by Myanmar in the east, Manipur in the south, Arunachal Pradesh on the northwest, and Assam in the west.

The Naga Hills represents part of the Assam-Arakan Yoma basin where copious accumulations of Cenozoic and Mesozoic sediments have taken place. The sediments of the Assam-Arakan basin are broadly categorized into two distinct facies, the shelf and basin (Mathur and Evans, 1964). Cenozoic sediments of the Naga Hills forms part of a basinal facies represented by the Disang Group (Upper Cretaceous-Upper Eocene), Barail Group (Upper Eocene-Oligocene), Surma Group (Lower Miocene), Tipam Group (Middle to Late Miocene), Namsang Beds (Upper Miocene-Pliocene), Dihing Group (Plio-Pleistocene) and the Naga Hills Ophiolite (NHO) of Upper Cretaceous-Lower Eocene age. The basinal facies marked by strong folding and overthrusting (Ghose and Singh, 1981) are encountered in the Inner Fold Belt (IFB). These sediments, however, lack in reliable criteria for stratigraphic correlations such as age-diagnostic fauna, marker horizons and widespread lateral litho-facies variation. In consequence Mathur and Evans (1964) have given the Cenozoic stratigraphic succession of the region on the basis of lithological variation. Thus this has provided a challenging task to have proper insight of the basinal evolution and necessitates the establishment of high-resolution stratigraphy and its correlation to different sequences within the basin. Ganguly (1993) opines that the regional stratigraphy of these sediments is yet to be established.

Paleomagnetism is a proven robust tool for documenting and more precisely dating rocks for stratigraphic correlation. The earth's magnetic field has been switching over its polarity at irregular intervals, resulting in alternating periods of normal and reverse polarity. This arbitrary reversal pattern of the earth's polarity provides a unique record - the key to paleomagnetism. Charting the long term history of the earth's geomagnetic field by recording fossil magnetism in rocks and sediments, enables dating of sediment formed over geologic time. Magnetic polarity reversal is a global event that provides for correlation and is the basis for chronostratigraphy.

Paleomagnetic stratigraphy or magnetostratigraphy is a recent technique that has been effectively used throughout the world in varied depositional environments for stratigraphic correlation (Harsland *et al.*, 1990; Opdyke and Channel, 1996). Magnetic polarity is independent of lithogenic constraints such as lateral litho-facies variations, permitting good correlation amongst Cenozoic successions (Tauxe and Opdyke, 1982; Tandon *et al.*, 1984; Johnson *et al.*, 1985; Raynold and Johnson, 1985; Appel, *et al.*, 1991; Tandon, 1991; Rao, 1993; Sangode *et al.*, 1996, 1999; Brozovik and Burbank, 2000; Kotlia *et al.*, 2002; Sangode and Kumar, 2003; Sangode and Bloemendal, 2004).

Very limited studies have been carried out on paleomagnetism and magnetostratigraphy in the north-eastern region. This has created a wide gap in our understanding of the geology of this terrain. Hence, the present study is an attempt at a detailed paleomagnetic study to establish magnetic properties of the rocks, pattern of polarity zone and its correlation with global polarity time scale (GPTS) to construct the magnetic polarity stratigraphy of the study area. The study will throw light on the rate of sediment deposition and magnetomineralogy.

However, in recent years some attention has been directed to petrographic and geochemical studies of various types of rocks of the region. The present study is devoted to paleomagnetism, petrography and geochemistry of select rocks of the study area including basalt and Upper Disang shale and sandstone. Other rock types in the region include the Lower Disang shale and various rock types of the ophiolite complex. The Lower Disang have not been considered for the present study as they comprise highly jointed and brittle shales at various stages of weathering that are difficult to sample for paleomagnetic studies. Most of the other rocks of the ophiolite complex are metamorphosed and so are also not suitable for the same as also much of the basalts that are altered to spilite.

1.1   Aims and Objectives of the Study

The study includes petrographic, geochemical and paleomagnetic studies of the basalt of the NHO and sandstone and shale of the Upper Disang rocks. However, for magnetostratigraphic correlation the Laisong sediments have also been sampled and analysed. The aims and objectives of the present study may be summarized in brief as follows:

i)   Petrographic studies of basalt to understand their characteristics.

ii)   Petrographic studies of Upper Disang sandstone for their classification provenance.

iii)   Heavy mineral analyses for determination of provenance of the Upper Disang sediments.

iv)   Geochemical studies to establish petrogenesis and tectonic setting of the basalt.

v)   Geochemical studies of the Upper Disang sandstone and shale to decode their provenance, tectonic setup, sorting and recycling effects, weathering history, paleoclimate and depositional environment.

vi)   Magnetic mineral studies to infer magnetic carriers of characteristic remanent magnetization (ChRM) in the basalt.

vii)   Magnetic mineral studies to infer magnetic carriers of ChRM in the Upper Disang and Laisong sediments.

viii) To establish the rate of deposition of the Upper Disang and Laisong sediments of the study area through paleomagnetic means.

ix)   To construct high-resolution stratigraphy of the study area through paleomagnetic means.

1.2   Location and Accessibility

The study area, including parts of central and eastern Nagaland, falls in Kohima and Phek districts. The basalt areas under study are incorporated in the Survey of India (SoI) toposheet 83 K/13 and lies within 25°33' & 25°41' north latitude and between 94°42' & 94°49' east longitudes. The Upper Disang lies between east longitudes 94°07' & 94°30' and north latitudes 25°30' & 25°41' in SoI toposheet 83 K/2 and K/6.

The area is well connected to the rest of the region by the NH 150 and AH 1. Several metalled and un-metalled roads connect the numerous small towns and villages. The nearest airport and railhead are located at Dimapur. Helipads at Chakhabama, Lacham, Waziho and Ziphu facilitate military and exploratory reconnaissance.

Lithostratigraphic columns of Paleogene sediments for magnetostratigraphic studies have been constructed at Leshimi and Viswema in Phek and Kohima districts

respectively. The Leshimi section lies at 25°31'39"N latitude and 94°13'57.30"E longitude while the Viswema section lies between 25°34'13.11"N and 94°7'22.94"E.

1.3   Physiography

The study area is highly dissected and immature, depicting a second order topography with synclinal ridges and anticlinal valleys. High hills, narrow valleys, steep cliffs, deep gorges devoid of any plateau or tableland are the common physiographic features. The countryside, as a whole, commands a majestic landscape.

1.4   Climate and Rainfall

The study area enjoys sub-temperate to temperate type of climate. Summers are warm and humid while winters are dry and cold. January is the coldest month of the year. In winter the temperature falls normally to 5°C or less and in summer it rises up to 32°C. The area receives abundant rainfall during the monsoon which commences from May and continues till September. Maximum rainfall, which is contributed by the south-west monsoon, is noted during July-August. Cloudbursts and thunderstorms are common phenomena in this part of the country. The average annual rainfall varies within wide limits from 2000 to 2800 mm.

1.5   Drainage

The terrain is highly dissected by a number of perennial and seasonal streams which have excavated 'V' shaped valleys and gorges. The drainage is topographically, lithologically and structurally controlled. There are two main trends, viz., NE-SW and NW-SE. These are mainly dendritic and trellis with occasional parallel or sub-parallel patterns. The drainage density is higher in the Disang shale dominated areas. The major perennial streams are Sedzü, Zungki, Tizü, Lanyi and Layoti.

1.6   Flora

Variations in altitude, physiography, rainfall and soil coupled with the geology have given rise to diverse vegetation in the region. Besides, the intensity of biotic interference, either singly or in combination, creates a striking variety in the ecological situation. Exposed to the heavy rainfall, the area is endowed with rich flora. The terrain

is adorned majestically with both indigenous and exotic flora (angiosperm and non-angiosperm) and includes *Bauhinia variegata*, *Erythrina indica*, *Bombax ceiba*, *Gmelina arborea* (gamari), *Alnus nepalensis* (alder), *Tectona grandis* (teak), *Terminalia myriocarpa* (hollock*)*, *Juglans regia* (walnut), *Spondias pinnata*, *Sapindus rarak* (soap berry tree), *Schima wallichii* (needle tree), *Mangifera indica* (mango), *Quercus sp.* (oak), *Emblica officinalis* (gooseberry), *Rhus semialata* (Naga tenga), *Ficus cunia* (fig), *Ficus auriculata* (fig), *Docynia indica* (wild apple), etc. *Cyphomandra betacea* (tree tomato), *Zanthoxylum sp.* (mechinga), *Rubus ellipticus* (raspberry), *Curculigo capitulate*, *Centella asiatica* (Indian pennywort), *Colacassia sp.*, *Zingiber officinale* (ginger), *Elettaria cardamomum* (cardamom), *Phrynium pubinerve*, *Thysanolaena maxima* (broom), *Musa sp.* (banana), etc. are some of the common shrubs and herbs available in the study area. Climbers include such as *Passiflora edulis* (passion flower), *Sechium edule* (chow chow), *Diascorea sp.* (yam), *Calamus tenius* (cane), etc. A large variety of bamboo is also found (*Bambusa balcooa*, *Bamnusa tulda*, etc). A myriad species of orchids and lichens splendidly clad the natural forest adding brilliance to nature. Pine forests (*Pinus sp.*) abound along the higher hills and ridges in the eastern-most fringe. Jhum cultivation, unrestrained forest fire and indiscriminate felling of trees for timber and firewood are the major factors for large scale deforestation in the region.

1.7   Fauna

Major parts of the study area are uninhabited, being adorned with thick forests that provide an ideal habitat for a numerous and diverse faunal species. The mammals include *Melursus ursinus* (bear), *Muntaiqus muntjak* (barking deer), *Bos frontalis* (mithun), *Canis sp.* (fox), *Talpa* (guinea pig), *Panthera pardus* (leopard), *Herpester sp.* (mongoose), *Hystrix bengalensis* (porcupine), *Callosciuras sp.* (squirrel), *Sus scrofa* (wild boar), *Filis chaus* (wild cat), *Cynoptirius sphinx* (bat), etc. The reptiles are represented by a number of species of poisonous and non-poisonous snakes and lizards. The forests also provide habitat for numerous species of birds like *Bubo nepalensis* (owl), *Dicrurus sp.* (tailed drongo), *Pycnouotus jocosus* (whiskered bulbul), *Passer domesticus* (sparrow), *Gallus gallus* (jungle fowl), *Mengalaima sp.* (barbet), *Psittacula krameri* (parakeet), woodpecker, pigeon and the endangered *Tragopan blythii*, etc. Innumerable species of insects, bees, snails, frogs, fish, etc., abound in the region.

1.8 Previous Literature

Geological studies of the Naga Hills commenced with attempts for locating and evaluating Tertiary coal deposits by Mallet (1876). Oldham (1883) discussed the geology of parts of Kohima and Manipur. Hayden (1910) described some coal fields of Nagaland while Pascoe (1912) conducted a geological traverse from Dimapur to Saramati. Evans (1932) and Mathur and Evans (1964) proposed a lithostratigraphic classification and described the structures and tectonic framework of parts of NE India. Goswami (1960) referred to Nagaland while describing the geology of Assam. Brunnschweiler (1966, 1974) described the regional geology and tectonic history of the Indo-Burman ranges. The geological evolution of the rocks of the Upper Cretaceous-Tertiary basin has been dealt with in detail by Raju (1968) and Bhandari *et al*. (1973). Krishnan (1968) gave a general description of the geology and tectonic framework of Nagaland. The Directorate of Geology & Mining, Nagaland (DGM, 1978) gave importance in unravelling the geology and mineral resources of parts of the state leading to refinement of the stratigraphy of the rocks of Nagaland.

Systematic geological mapping of the NHO belt was undertaken by geologists of the Geological Survey of India (GSI) and DGM (Chattopadhyay and Roy, 1975; Singh and Adiga, 1976; Agrawal, 1977; Srivastava *et al*., 1978; Agrawal and Kacker, 1980; Roy and Kacker, 1980). Geological details of the NHO belt were synthesized in several publications by Sen and Chattopadhyay (1978), Chattopadhyay *et al*. (1983) and Kacker *et al*. (1984). Based on paleontological records the age of the Ophiolite has been placed at Upper Cretaceous-Eocene (Brunnschweiler, 1966; Chattopadhyay *et al*., 1983). Bhattacharjee (1997) dealt with the tectonism of the Indo-Burman area.

Petrography and geochemistry of the Ophiolites, particularly the mafics and ultramafics, was initiated by Ghose (1979), Singh (1979), Ghose and Singh (1980), Agrawal (1985), Agrawal and Ghose (1986) and Chattopadhyay *et al*. (1983). All these workers have distinguished the existence of litho-assemblages of dismembered bodies of the ophiolite. In recent years Rao *et al*. (2003), Subba Rao *et al*. (2004, 2005) and Srikanth *et al*. (2004) contributed to the geology of the NHO. Ezung (2007) undertook detailed geochemical and petrographic studies of the basalt and spilite of the NHO.

Sporadic studies have been carried out in the IFB comprising Upper Cretaceous-Tertiary sediments in the last few decades. Sarmah (1983) gave a detailed account of the Disang and Barail sandstones of Kohima town and its surroundings.

Thong (1993) used geochemistry and petrography of the Palaeogene sandstones around Botsa to decipher their provenance and depositional environment. Baruah (2003) studied the Disang sediments of Chakhabama also to understand their provenance and depositional environment. Vineetha (2004) discussed the geochemistry of the shale of Kohima town to arrive at their origin. Thong and Rao (2006) gave an account of the provenance and depositional environment of the Disang sandstones of Botsa. Srivastava and Pandey (2011) discussed the provenance of the Barail sandstones of Kohima.

1.8.1 Paleomagnetic Studies

Though several workers contributed to the geology of Nagaland, very little interest was given to paleomagnetism. During the late 1980s, the GSI attempted paleomagnetic investigations on the magnetite of the NHO of Phokpur and Kiphire districts. The very first work on magnetostratigraphic attributes of the Tertiary rocks of the northeastern region was along the Hari River section in Meghalaya (Tiwari *et al*., 2006). A 3500 m thick succession of Cenozoic sediments comprising Sylhet limestone, Kopili, Laisong, Jenam, Renji and Lower, Middle and Upper Bhuban formations has been studied. This entire sequence has been inferred to have been deposited in a time span of 30 Ma. Tiwari *et al*. (2007) worked in parts of the Middle Bhuban sequence in Aizawl for magnetostratigraphic attributes where a total of seven normal and reverse magneto zones have been delineated. Recently, magnetostratigraphy of the Neogene sediments of the eastern Himalaya in Arunachal Pradesh has been investigated by Chirouze *et al*. (2012). In parts of the Indian subcontinent paleomagnetic and magnetostratigraphic studies have been extensively carried out by several workers but in the northeastern region such studies are far from expectation although there is scope for such studies.

Chapter 2

GEOLOGY AND TECTONIC FRAMEWORK

2.1 Overview

The Naga Hills represents the western most expanse of the Mesozoic-Cenozoic Indo-Sinian collisional domain extending for about 200 km along the Indo-Myanmar border. Morphotectonically, this north trending Tertiary orogen is a part of a Burmese arc and is bounded by the Cenozoic belt of Burma (Myanmar) in the east and by the Assam Tertiary shelf sediments and Precambrian Mikir Hills' massif in the west and on the northwest by the Brahmaputra trough lineaments. To the north this fold passes into the eastern syntaxial bend and to the south it can be linked through the Chin Hills, Arakan-Yoma and Andaman-Nicobar islands with the Indonesian island arc off the coast of Sumatra (Mitchell and Mckerrow, 1975; Tripathi, 1989). It provides an ideal setting for geodynamic processes involved in the evolution of the north-eastern Indian crustal block during the Mesozoic-Cenozoic.

2.2 Tectono-Stratigraphy

The stratigraphy and tectonic framework of Assam and Nagaland (Fig. 2.1) was established by Mathur and Evans (1964). The stratigraphy of Nagaland (Table 2.1) was subsequently modified by the DGM (1978). The geological layout of Nagaland includes four main tectono-stratigraphic divisions (Ghose *et al*., 1987) from east to west (Fig. 2.2).

    a) Metamorphic Complex

    b) Naga Hills Ophiolite

    c) Inner Fold Belt

    d) Belt of Schuppen

2.2.1 Metamorphic Complex

This complex lying to the east of the NHO belt includes the Naga Metamorphics and the Saramati and Nimi formations.

8

LEGEND

Thrust
Fault
Dauki Fault
River

Alluvium
Dihing and Dupitila
Tipam and Surma Group
Barail Group
Jaintia and Disang Group
Langpar and Mahadek Beds

Ophiolite
Lower Gondwana System
Metamorphic and Igneous Rocks
Water Body

Details in country south-east of overthrust belt are necessarilly largely conjectural

Compiled from survey by the Geologists of the Burma Oil Co. Ltd. and associated companies and by the Geological Survey of India.

100   0   100 Km

Fig. 2.1: Tectono-stratigraphic framework of Nagaland (after Mathur and Evans, 1964)

Table 2.1: Stratigraphy of Nagaland

(Modified after Mathur and Evans, 1964; DGM, 1978; Ghose *et al.*, 2010)

Age	Group	Litho-formations			
		Outer and Intermediate Hills			Eastern High Hills
Recent - Pleistocene		Alluvium and high level terraces			
	Dihing	Boulder beds			
--------Unconformity--------					
Mio-Pliocene	Dupi Tila	Namsang Beds			
--------Unconformity--------					
Miocene	Tipam	Girujan Clay / Tipam Sandstone			
	Surma	Upper Bhuban / Lower Bhuban			
--------Unconformity--------					
Oligocene	Barail	Renji	Tikak Parbat		Jopi / Phokphur Formation
		Jenam	Baragolai		Tuffaceous shale, sandstone, greywacke, grit and conglomerate. Minor limestone and carbonaceous matter
		Laisong	Naogaon		
Upper Cretaceous - Eocene	Disang	Upper			Shale/slate/phyllite with calcareous lenses in basal sections and invertebrate and plant fossils in upper sections with brine springs
		Lower			
---------Base not seen---------				--------Fault/Thrust--------	
Chert Kimmeridgian to mid-Tithonian Middle Jurassic - Cretaceous	**Ophiolite Complex**				Zepuhu Formation Marine sediments (shale, phyllite, greywacke, iron-rich sediments, chert and limestone with radiolaria and coccoliths), volcanics (basalt, spilite, volcaniclastics), metabasics greenschist, glaucophane schist/ glaucophane-bearing metachert, eclogite), layered cumulate sequence (peridotite, pyroxenite, gabbroids, plagiogranite, anorthosite), and peridotite tectonite and serpentinite associated with deposits of podiform chromite and nickeliferous magnetite, minor Cu-Mo sulphides associated with late felsic intrusions and some dolerite dykes
--------Fault/Thrust--------					
Pre-Mesozoic (?)	**Naga Metamorphic Complex**				Nimi Formation Weakly metamorphosed limestone, phyllite, quartzite and quartz-sericite schist Naga Metamorphics Mica schist, granitoid gneiss and feldspathic metagreywacke with tectonic slices of ophiolite in variable dimensions

Fig. 2.2: Tectono-stratigraphic framework of Nagaland (after Ghose *et al*., 1987)

2.2.1a Naga Metamorphics

The Pre-Cenozoic basement 'subnappe' of the eastern Naga Hills represent a belt of crystalline rocks which include quartzite, phyllite/phyllonite, limestone, marble, quartzo-felspathic schist and gneiss, mica schist and sheared granite with minor serpentinite (Brunnschweiler, 1966; Roy and Kacker, 1980). However, slices of sheared granite, volcanics and minor serpentinites have also been recorded (Chattopadhyay and Roy, 1977; Singh *et al*., 1983). The litho-types of the Naga metamorphics are apparently indicative of a neritic environment. The Naga Metamorphics are thrusted over the Upper Cretaceous-Eocene turbidite and ophiolite (Brunnschweiler, 1966). The contact between the Naga Metamorphics and ophiolites is interpreted as a thrust due to the abrupt change in lithology, metamorphic grade and degree of folding and topographical breaks (Vidyatharan *et al*., 1986). Brunnschweiler (1966) considers this Naga Metamorphic complex as Pre-Mesozoic and correlated it with the Precambrian Chaung Magyi series (Rao, 1983).

2.2.1b Saramati Formation

Tectonic slices of metasediments occurring east of the NHO belt was designated Saramati Formation (Acharyya *et al*., 1982). These are extensive lithostratigraphic units of schistose quartzite, quartz-mica schist and carbonaceous phyllite exhibiting banded structures. This formation is well developed in and around Saramati peak. The sedimentary nature of this formation is indicated by the clastic nature of the rocks, bedded sequence marked by arenaceous and argillaceous alternations, current and graded bedding and cut-and-fill structures. The banded nature is observed throughout but in the upper members, banding is less conspicuous. In the absence of any radiometric age data or fossil occurrence, the stratigraphic status of Saramati Formation is rather enigmatic.

2.2.1c Nimi Formation

Named after Nimi Village, the type locality where these meta-sedimentary rocks are exposed, it forms the eastern fringe of Nagaland. This is probably a detached part of the Pre-Tertiary Burmese continental crust. It is accorded a Pre-Mesozoic age (DGM, 1978). They are exposed along the Indo-Myanmar border over a stretch of 18x12 km. The dominant members of this formation consist of non-crystalline limestone, quartzite, phyllite, carbonaceous phyllite, quartz-sericite schist

and schistose granite. The phyllite is light green to deep grey in colour while the associated rocks are dirty white feldspathic quartzite and smoky white quartzite. The alignment of sericite or muscovite imparts a foliation to the latter. Quartzite invariably interbedded with phyllite locally shows a gritty nature with sub-rounded quartz grains. Phyllite and quartzite are associated with limestone which occurs both as major bands and minor lenses with thicknesses varying from 5-100 m. Locally whitish grey to grey crystalline limestone and marble are generally associated with this formation. Brunnschweiler (1966) opines that this formation is lithologically and homotaxially analogous with the Pansat Beds of Myanmar.

2.2.2 Ophiolite Complex

The NNE-SSW trending NHO belt is tectonically sandwiched between the Disang flysch in the west and low grade metamorphic rocks in the east. The linear belt about 90 km in length and 5 to 15 km in breadth comprises a wide variety of litho-members derived from oceanic, volcano-clastic and volcano-plutonic realms (Roy and Kacker, 1980).

The litho-units include serpentinite, peridotite (mainly harzburgite with minor lherzolite), pyroxenite, dunite, gabbro, amphibolite, basalt, spilite, basaltic andesite, trachyte, diorite, plagiogranite, tuffaceous volcanics, chert, limestone, inter-layered chert-volcanics, agglomerate tuff, greywacke, tuffaceous shale/phyllite, glaucophane schist, basic schist, etc. The sharp tectonic contact of this suite of rocks with the epimetamorphosed slate and phyllite along the Moya Thrust in the Naga Hills (Ganju *et al.*, 1986) and the absence of intrusive contacts, contact minerals and contact halos around them (Brunnschweiller, 1966) suggest that these are allochthonous in nature. They are considered an "obducted mass" of the ocean crust. The ultramafic differentiates exhibit both tectonite fabrics and cumulate texture (Roy and Kacker, 1980). The ophiolite sequence exhibits signatures of severe tectonic slicing, fracturing, shearing, mylonitization, silicification and tectonic agglomeration of the litho-units. The overall situation indicates tectonically dismembered Ophiolites. Tectonic emplacement took place towards the end of Early Alpine-Himalayan movements during Late Eocene-Early Oligocene (Roy and Kacker, 1980). Imbricate fish-scale thrust sheets on either side of the NHO belt are conspicuous (Mathur and Evans, 1964; Nandy, 1980). The presence of radiolaria and coccoliths indicate that the NHO probably are Maestrichtian-Eocene in age which is equivalent to the Lower

Disang (Agrawal and Ghose, 1986). The ophiolites are unconformably overlain by ophiolite-derived volcaniclastics and open marine sediments designated as the Phokphur Formation. Metamorphism is marked by complete serpentinization of the rocks.

2.2.2a <u>Salumi Formation</u>

These rocks are exposed in the Luthur-Salumi area of Tuensang district. Oceanic pelagic sediments of this formation form a non-conformable cover over the basaltic crust. The rocks consist of shale, thin interbedded chert and limestone that are distributed in patches. Chert, limestone and phyllite are often intercalated with the volcanics. Chert contains radiolaria and forams such as *Omnatospyris sp.*, *Kassina sp.*, *Spongprunum sp.* and *Textularia sp*. The presence of *Kassina* is the basis for assignment of a Cretaceous age for this formation. The pelagic limestone has yielded a rich microforaminiferal biota consisting of *Globorotalia cf. lehneri*, *Globigerina cf. fringa* and *Globigerina cf. lineaparta* of Paleocene-Lower Eocene age, which indicates that the oceanic realm prevailed up to Lower Eocene.

2.2.2b <u>Jopi Formation</u>

It is tentatively considered to be equivalent to the Barail. This formation unconformably lying over the ophiolite occupies various topographic levels. It consists of thick piles of alternating and repeated sequences of polymictic conglomerate-grit, pebbly and cobbly sandstone, sub-greywacke and shale. Individual cycles vary in thickness in this formation which is over 6000 m. The basal conglomerate unit contains angular to sub-rounded boulders, cobbles and pebbles derived from the underlying ophiolite suite and embedded in reworked tuffaceous/siliceous cements. The succession grades upward into grit, lithic greywacke, siltstone, sandstone and shale. The sandstone gradually becomes arkosic towards the top.

2.2.3 Inner Fold Belt

The IFB, a part of which constitutes the study area, occupies the central portion of the Naga Hills and is confined between two major tectonic zones, the Disang Thrust on the west and NHO on the east. Thick monotonous turbidite sequences of splintery shale, slate and phyllite inter-bedded with sandstone forms the

lithotype of this formation. This sequence is capped with occasional outliers of Barail sandstone. This sequence primarily exposed in the Kohima Synclinorium (Ghose *et al*., 1987) covers a 70 km wide tract between the Disang Thrust and the NHO belt. The Kohima Synclinorium encompassing Disang-Barail sequences along with a Surma core occupies the southern part of the IFB while the Patkai Synclinorium lying to the north comprises only Disang and Barail sequences (Banerjee, 1979). The presence of foraminifera and invertebrate fossils reported in the sediments indicate an Upper Cretaceous-Eocene age (Chattopadhyay *et al*., 1983).

2.2.4 Belt of Schuppen

The Belt of Schuppen (BoS) in the western part of Nagaland forms the most prominent morphotectonic unit of the Naga Hills. This narrow linear belt covers an area of 4500 km^2. It is a zone of imbricate thrust slices which follows the boundary of the Assam valley alluvium extending over a 200 km strike length and width of 20-25 km (Evans, 1932). Mathur and Evans (1964) opine that the Tertiary sediments of this belt encompasses eight or possibly more over-thrusts overriding each other, along which the Naga Hills thrust north-westward relative to the Precambrian crystalline Foreland Spur.

Surface geological investigations and regional mapping carried out by GSI, ONGC and DGM have shown the presence of four to five thrust slices including the Disang, Kongan, Chongliyimsen, Lakhuni and Naga thrusts. However, recent studies on regional structural configuration and seismic patterns of the BoS (Srinivasan, 2007) have revealed the presence of two major thrusts, the Haflong-Naga Thrust and Disang Thrust along with three minor thrusts (ST-1, ST-2, ST-3). These thrusts are of the same general geometry, each repeating the strata and all dipping in the same general direction. This type of imbricate thrust system has been described by Suess (1904) as 'schuppen structure'. The BoS is delineated on the west by a complex set of intersecting faults known as the Naga Thrust and on the east by the Disang Thrust (Rao, 1983). The Naga Thrust separates the sharply folded sediments of the BoS from the little affected, flat to gently dipping beds lying north of this belt. These thrusts have NE trends with homoclinal moderate easterly dips.

Anticlinal folds are generally present in the hanging walls of the thrusts, but those with effective closures are preserved in the outermost thrust sheet where younger formations with more ductile lithologies prevail. Fold axes are parallel with

thrusts and folds characteristically asymmetric towards the foreland. Outcropping formations are older from the internal to the external side of the thrust belt (Rao and Samanta, 1987).

In the southwest at the southern fringe of the Shillong plateau Haflong-Naga Thrust and Disang Thrust merge to form a major E-W fault known as the Dauki-Haflong Thrust. The rocks comprising the BoS are fresh/brackish water molassic sediments deposited in intra-deep troughs over the basinal sediments were derived from the adjacent Precambrian Mikir Hills' craton and newly cratonized Early Tertiary belt (Roy and Kacker, 1980). The lithology of the different geological formations of this belt has been described in detail by various workers like Evans (1932, 1964), Mathur and Evans (1964) and Rao (1983).

2.2.5   Tertiary Sequence in the IFB and BoS

2.2.5a   Disang Group

This group comprises flysch sediments (DGM, 1978). It was first described by Mallet (1876) as a thick monotonous sequence of splintery grey shale interbedded with fine grained sandstone and siltstone. This was later designated 'Disang Series' as the lithologic suite was found to be almost uniform and not divisible into mapable units. The identification of two distinct lithologic units, a basal argillaceous and an upper arenaceous stratum in parts of Nagaland by systematic mapping led to the renaming of this suite as the Disang Group, consisting of two formations, the Upper and Lower Disang formations (Sinha *et al*., 1982). The lower formation comprises dark grey to greenish grey argillaceous shale intercalated with thin bands of grey siltstone and fine grained sandstone while the upper formation comprises arenaceous, dark grey splintery shale intercalated with sandy shale and siltstone. Rao (1983) observes that the upper part of the Disang between the Disang Thrust and the NHO belt are unmetamorphosed sequences of dark grey splintery shale, sandstone and massive siltstone with concretions whereas the lower part is a metamorphosed sequence of rocks. The Disang comprise a 3000 m thick sequence of well-bedded, splintery, dark grey shale intercalated with fine grained, well cemented and thin, flaggy sandstones. The sandstones are just a few centimetres thick at the base but become very prominent near the top with the gradual depletion of shale. Rao (1983) assigns a Maestrichtian age for the Lower Disang. The shale are moderately to highly carbonaceous and exhibit fine laminations and curved or concentric surfaces.

Carbonaceous shale intercalated with massive shale and occasionally fine grained sandstone also occurs in certain areas, especially at the junction of faults. The beds are commonly crumpled and squeezed.

The Upper Disang grades laterally and vertically into the Barail (Ganju *et al*., 1986). Based on planktic foraminifers the Upper Disang is considered Bartonian (Late Middle Eocene) to Priabonian (Late Eocene) in age (Lokho *et al*., 2005).

The Disang are tectonically overlain from the east by the NHO which bear all characteristics of a dismembered oceanic crust (Agrawal and Kacker, 1980; Ghose and Singh, 1981; Roy *et al*., 1982; Chattopadhyay *et al*., 1983; Agrawal and Ghose, 1989).

The Disang are penetrated by numerous thin quartz veins and serpentinized intrusions at places. Towards the east a marked degree of metamorphism is noted with the development of hard, glossy, dark greyish to blue slates. Further east they grade into phyllite, generally talcose and chloritic, and even into schist. Ferruginous concretionary structures and nodules, ripple marks, sole marks and graded bedding are common. Iron pyrites are common as also brine and sulphur springs. The Disang also include black slate, quartzite, limestone and coloured slate along the eastern parts of Nagaland and Manipur (Oldham, 1883; Goswami, 1960). They abut against an igneous body further southeast which may be a projection of the parent rock of the Arakan-Yoma.

2.2.5b Barail Group

The Barail was formerly christened 'Barail Series' by Evans (1932) after the Barail Range in the North Cachar Hills of Assam. Barail outcrops near Jaintiapur run up to the neighbourhood of Kohima. Thereafter the outcrop sweeps to the southeast and south and follows the high ranges west of the Kohima-Imphal road as far as the Manipur border and probably runs further south into the western Manipur plains. This arenaceous suite of rocks, later re-designated the Barail Group (DGM, 1978) consists of flysch sediments. The Barail comprise thick sequences of sandstone intercalated with very thin papery shale. These rocks, ranging in age from Upper Eocene to Oligocene, are scattered in patches in Nagaland. They are exposed in southern Kohima, the eastern parts of Nagaland and all along the western margin of the state. The type area of Barail is limited to the northwest by the Haflong-Disang Thrust

trending roughly NE-SW. They conformably overlie the Disang. They attain a thickness of about 4000 to 6000 m.

The Barail are divided into three formations in the south and southwest of Nagaland (Evans, 1932) including the Laisong, Jenam and Renji formations. The Laisong Formation consists of very hard, grey, thin to thick bedded sandstones with ferruginous concretions. Occasional massive sandstones with intercalations of carbonaceous shale are not uncommon. Thin streaks of coal are also encountered. The thickness of this formation varies from 900 to 2000 m. The Jenam Formation with thicknesses varying from 900 to 2000 m exhibits a gradational contact with the underling and overlying formations. The sandstones are dominantly grey to dark grey and thin to thick bedded with carbonaceous shales. They are commonly interbedded with silts. The Renji Formation is the youngest member of the Barail Group. This formation extends into Assam and Manipur. The sandstones are massive, very thick bedded, hard and ferruginous and with intercalated with minor shale. They form a thick forested range with high peaks such as Japfü (3015 m) on the southwest of Kohima.

The Naogaon Formation is exposed in the north-western parts of Nagaland where it forms high ranges and covers extensive areas. These rocks branch out into narrow strips towards the south, one such branch of which extends into northern Manipur. Sandstones of this formation are hard, grey, thin bedded and fine to medium grained. Some shale and carbonaceous shale are intercalated with the sandstones. Concretionary structures are noted in some areas. The sandstones are thick and massive with occasional thin shale partings towards the southern border of Nagaland. The Naogaon sandstones are indistinguishable from those of the Laisong of Lower Assam. Their thickness varies from 800 to 1000 m. The Baragolai Formation bears a gradational contact with the Naogaon and Tikak Parbat formations. It comprises interbedded sandstone and shale with distinct coal seams. The thickness varies from 2500 to 3000 m. The overlying Tikak Parbat comprises sand-shale alternations with thick coal seams. The thickness of this formation varies between 170 and 700 m.

Of the two parallel divisions of the Barail, the Laisong, Jenam and Renji formations are well developed to the south of the BoS as intermittent isolated outliers, being split up by a system of strike faults while the Naogaon, Baragolai and Tikak Parbat formations lie dominantly along the north of the BoS.

The Barail exhibit a number of sedimentary structures such as ripple marks, load casts, flute marks, current bedding, etc. These rocks, essentially marine to estuarine in origin, are poor in fossils. Coal is restricted to a very few places such as the Borjan Coal Field, Tiru Valley Coal Belt, Jhanji-Desai Valley Coal Belt and the Tuensang Coal Belt.

2.2.5c Surma Group

The Lower Miocene molasse ranging in thickness from 2900 to over 4000 m unconformably overlie the Barail. They comprise alternations of well bedded sandstone, shaly sandstone, mudstone, sandy shale and thin beds of conglomerate. These rocks are exposed in the BoS in the form of a number of long narrow strips running along almost the entire length of Nagaland on the western margin. They gradually thin out toward the north. The Surma are subdivided into the Bhuban and Boka Bil formations, the former characterised by some conglomerate and fragmented shells. The Boka Bil passes vertically and laterally into the overlying Tipam Group.

2.2.5d Tipam Group

The Tipam conformably overlie the Surma without any perceptible break (Mallet, 1876). The Tipam succession was first described in the Tipam River section in Upper Assam. This molasse facies ranges in thickness from 3000 to 4000 m. It is made up of massive sandstone with subordinate clay and shale. The Tipam are subdivided into Tipam Sandstone and Girujan Clay formations (Evans, 1932).

The Tipam Sandstone Formation comprises coarse, friable, massive and false-bedded. These sandstones contain calcareous cementing material and occasionally very thin bands of impure limestone. Local patches of ferruginous matter and streaks of lignite are common. The friable nature of these sandstones is due to poor compaction and cementation. The sandstones are commonly green in colour due to the presence of glauconite but are found to be weathering to different shades of brown. Mottled clay too is occasionally noted with beds of grit and conglomerate. The Tipam Sandstone is exposed along the western fringe of Nagaland in the BoS as long narrow strips due to strike faulting. They have been assigned a Mio-Pliocene age.

The Girujan Clay Formation overlying the Tipam Sandstone essentially comprises variegated and mottled clays with some impersistent inter-beds of argillaceous sandstones. This formation with a thickness of about 1800 m is exposed

in the western parts of Nagaland in the BoS. The formation also contains bluish-grey mottled clay with minor sandstone. The Girujan Clay has yielded some plant fossils that have been identified as *terminalia sp*. (Rao, 1983).

2.2.5e Namsang Beds

These beds belong to the Dupi Tila Group. They consist of sandstone, pebbles of lignite, conglomerate, grit, mottled clay and lenticular seams of lignite that are poorly consolidated. The beds are unconformably overlain by a succession of well-rounded boulder and pebble beds with interspersed lenses of soft sand and clay. The beds reflect a fresh phase of uplift of the Naga-Patkai hinterland.

2.2.5f Dihing Group

They contain conglomerate, grit, sandstone and clay that overlie the Dupi Tila/ Namsang beds. Mathur and Evans (1964) opine that these rocks indicate a transgressive phase as the pebble beds rest over Girujan Clays in the south of Digboi. Locally, the base of the Dihing pebble beds is underlain by unconsolidated sands with relatively few pebbles known as Dekiajuli Beds. Lignite bands are also commonly noted in the Dihing. These rocks have been assigned a Plio-Pleistocene age. These rocks have undergone late phases of folding and faulting (Aier *et al*., 2011) due to which they are often steeply dipping. The boulders and pebbles are undoubtedly products of the Barail. They attain a thickness of about 800 m and are confined to a few patches in the BoS.

2.2.5g Alluvium and High-level Terraces

Alluvium and high-level terraces cover extensive portions of Nagaland. The high-level terraces are dominantly boulder beds with coarse sand, gravel and unassorted clay at various levels above the present rivers. Older alluvium occupies the north-eastern tract of the Naga-Patkai ranges while newer alluvium covers the western border of Nagaland.

2.3 Structure and Geodynamics

NE-SW trending anticlines with several structural highs and lows form the major structural setup of the region. Tectonically the study area is very intricate (Fig. 2.3). Besides the BoS, Goswami (1960), Mathur and Evans (1964) and DGM (1978)
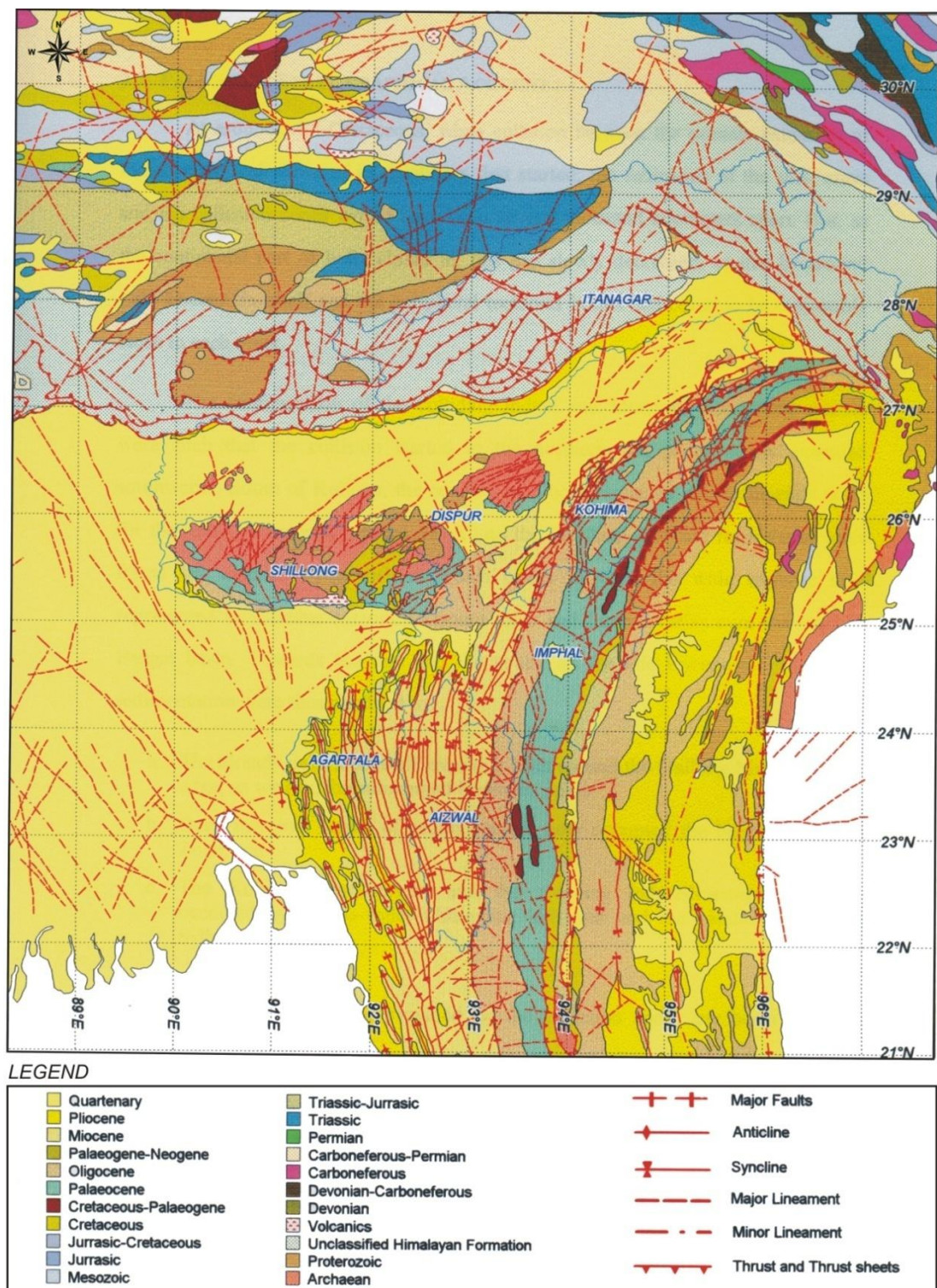
Fig. 2.3: Tectonic map of NE India (after Nandy, 1999)

LEGEND

Quartenary	Triassic-Jurrasic		Major Faults
Pliocene	Triassic		Anticline
Miocene	Permian		Syncline
Palaeogene-Neogene	Carboneferous-Permian		Major Lineament
Oligocene	Carboneferous		Minor Lineament
Palaeocene	Devonian-Carboneferous		Thrust and Thrust sheets
Cretaceous-Palaeogene	Devonian		
Cretaceous	Volcanics		
Jurrasic-Cretaceous	Unclassified Himalayan Formation		
Jurrasic	Proterozoic		
Mesozoic	Archaean		

recognized two other major structural units in the region including the Patkai and Kohima synclinoria.

2.3.1 Patkai Synclinorium

It covers an extensive area in the intermediate hill ranges of Nagaland (Fig 2.2). The highest ground of the Patkai Synclinorium comprises synclines with Barail rocks and the relatively open synclines are separated by faulted and overthrust Disang shale. The Disang are exposed on either side of this synclinorium. On the north-western fringe lie a number of thrust planes. The Disang Thrust is taken as the dividing line between the Patkai Synclinorium and the BoS.

2.3.2 Kohima Synclinorium

The Kohima Synclinorium occurs SSW of the Patkai Synclinorium and to the southwest of Kohima with a slight southerly pitch trending approximately N-S. The northern limb of this synclinorium forming the Barail Range of North Cachar extends south-westward of Haflong and then westward, fringing the eastern extension of the Meghalaya Plateau. The southern limb extends into west Manipur, east Cachar and east Mizoram. The younger Surma basin forms the core of this synclinorium. It is bound on the northwest by the Disang Thrust and in the south it merges into the eastern Surma valley. The younger group of rocks such as Barail, Surma, Tipam, etc., in this structural unit are encountered towards the Surma valley. The Surma valley folds represent immature first order topography and the area beyond the Kohima Synclinorium towards the northeast exhibits an inversion of topography (Dasgupta, 1977). The Barail of the southern limb exhibits intricate fold patterns but westward the Barail of the Khazawl range show first order topography in conformity with the fold range of Surma valley.

The regional structural trend is NE-SW while subordinate trends are NW-SE to WNW-ESE. Based on orientations of fold axes, three generations of folds are recorded in the litho-units which probably correspond to the first, second and third phases (F_1, F_2, F_3 respectively) of the Himalayan orogenies (DGM, 1978; Roy and Kacker, 1986; Rao and Samanta, 1987). Each generation is punctuated by an interval of comparative quiescence.

The first set of folds formed due to orthotectonic movements during Upper Cretaceous-Eocene is isoclinal with low plunges on either side and has N-S to NNE-

18

SSW axial trends. These are syn-collisional structural features (Roy and Kacker, 1986). Superimposition of later folds has resulted in the reversal of plunge. Recumbent folds reported from some places between Pfütsero and Chizami are, in all probability, related to the Alpine-Himalayan orogeny.

The second generation folds have NE-SW axial trends and steeply inclined axial surfaces. They show low to moderate plunges varying from 15°-30° towards NE or SW. The folds are moderately open with axial planes dipping steeply towards NW and SE. These are highly asymmetrical folds whose inter-limb angles vary from 90°-120°. The north-western limbs of the anticlines are much shorter than the south-eastern limbs. These folds are also called 'step folds' as they are step-like in distribution and orientation similar to the down-to-basin step faults. Most of such major folds are cut off longitudinally by NE thrust planes at or near their hinges. In combination with the first generation folds they control the topographic morphometry of the hills and valleys of Nagaland. The F_2 movement (Oligo-Miocene), which was a long-lived progressive deformational event, was initiated at the end of the Oligocene (post Barail) and continued up to the end of Miocene, and possibly early Pliocene (post Namsang). These folds probably correspond to the second phase of the Alpine-Himalayan Orogeny.

The third set of folds which began developing during the Pliocene (Dihing) and continues today has produced NW-SE and WNW-ESE trending cross-folds and ENE-WSW and NNE-SSW strike-slip faults with little positive or negative oblique slip components (Roy and Kacker, 1986). They are broad open folds with moderate to high plunges varying from 35°-60° towards NW and SE. The axial planes dip steeply (60°-70°) towards NE and SE. These folds are smaller in dimension and relatively less asymmetrical than the F_2 folds. These folds have broadly rounded hinges (domal type) as compared to the angular/sub-angular hinges of the F_2 folds. These are post thrusting in age and have affected the NE thrust planes with regular folds and swings around the NW and SE axes. Crenulation cleavages in basic schist and phyllite were developed during the generation of these folds. These folds might be linked to the Pleistocene movements of the Himalayas.

The three generations of folding is attributed to regional tectonism. The F_1 and F_2 folds are due to NW-SE compression whereas F_3 structures are formed by NE-SW strike-slip movements, acting favourably along or near the NE thrusts or fracture planes (Roy and Kacker, 1986). F_3 structural development is related to the Pliocene-

Quaternary plate convergence and northward movement of India. F_1 and F_2 are flexural-slip type.

The second order wrench movements took place along ENE and NNE shear planes producing reverse-cum-wrench and gravity-cum-wrench faults or shear zones. These faults or shear zones are of relatively small dimensions but have invariably developed in areas of influence of the F_3 folds of megascopic scale.

Two sets of distinctive faults have been reported (DGM, 1978). The earlier set trending NE-SW shows conformity with the regional trend of the early folds. The later set has a WNW-ESE trend. The two sets of faults interfere with each other resulting in the formation of large tectonic blocks.

The intricate tectonic setup of the region and the development of major and minor structural features are attributed to continental collision following an Early Cenozoic eastward subduction of the Indian plate to the north along the Himalayan thrusts as well as to the east along the Arakan-Yoma Thrust in the Indo-Myanmar range, which is a result of the anticlockwise rotation of the Indian plate subsequent to its first contact with the Eurasian continent (Roy and Kacker, 1986). Desikachar (1974), Nandy (1976) and Bhattacharjee (1991) have explained the evolution of major features of this area in terms of a plate tectonic model. According to them the Andaman-Arakan-Assam basin existed during the Mesozoic between the Burmese landmass and the Indian plate, extending from 5° to 27° N latitude. The Indian plate moved from the south to the north which resulted in the shallowing of the Tethys Sea and an arc-trench system was formed along the subduction zones giving rise to a long and narrow sedimentary trough. This is substantiated by paleomagnetic studies of the Indian rocks (McElhinny, 1973) and oceanic magnetic anomalies (McKenzie and Sclater, 1971). The eastern portion of the basin was the site of initial magmatic activity and emplacement of ophiolites whereas the western side was devoid of magmatic activity. This basin is marked by strong folding and overthrusting (Ghose and Singh, 1981). Naik (1994) elucidated the spatio-temporal evolution of the region with an 'oblique collision and tectonic wedging' model. The spatial distribution of earthquake epicenters in this region indicate eastward plunge of the subducting plate. The migrationary patterns of the high magnitude earthquake epicenters roughly represent the direction of movement of the overriding plate. However, controversy exists regarding location of the subduction line between the two plates. Desikachar (1974) and Nandy (1982) consider that the NHO belt of Nagaland and Manipur

20

exposed in the central axial zone of the Arakan-Yoma represents the suture zone whereas Mittchel and Mckerrow (1975) and Mittchel (1981) consider it further east of the Arakan-Yoma.

By the end of Eocene the Indian plate had already collided with the Tibetan plate in the north and Burmese plate in the east (Stoneley, 1974; Agrawal and Ghose, 1986). The Burmese volcanics may relate to subduction from Miocene to Quaternary (Mitchell and Mckerrow, 1975). The blue schist, melange, and ophiolitic association in the Naga Hills lend evidence of plate contact. Moreover, compressive deformations and the presence of an east dipping, active seismic belt and intermediate earthquakes in Myanmar and large negative isostatic anomalies suggest that the subduction processes are still continuing (Molnar and Tapponnier, 1975; Verma, *et al.*, 1976; Verma, 1985).

Chapter 3

METHODOLOGY

3.1 Petrography

Based on physical characters and distribution of rocks, representative Upper Disang sandstones and basalt are chosen for thin-section preparation. Rocks are sliced and polished to thicknesses of about 0.03 mm. Thin sections of fifteen basalt and twenty five Upper Disang sandstone are studied for their mineral assemblages, textures, alteration and effects of metamorphism.

The Gazzi-Dickinson point counting technique (Gazzi, 1966; Dickinson, 1970) is used for volumetric percentages and modal mineral compositions of the sandstone. Crystals and grains greater than 0.0625 mm within the lithic fragments are counted as monocrystalline grains (Ingersoll *et al*., 1984). Fourteen representative samples of Upper Disang sandstone with more than 400 framework counts per slide was considered for modal analysis.

The technique proposed by Folk (1980) is used for heavy mineral study. The samples are gently crushed, washed properly and subjected to alternate treatment with hydrogen peroxide, distilled water and dilute hydrochloric acid, and stannous chloride and zinc foil followed by boiling for about 5 to 10 minutes to remove authigenic clay, carbonate and ferruginous coatings on the grains. After thorough washing and drying 120 mesh fractions were separated through sieving using bromoform (sp. gr. 2.89). The heavy minerals separated are mounted on glass slides using Canada balsam. A total number of 20 grain mounts were prepared and studied under the microscope for identification of the heavy minerals.

3.2 Geochemistry

Representative samples of Upper Disang and basalt are crushed and ground to fine powder using an agate mortar and pestle to pass through a -200 ASTM mesh for the analyses.

3.2a   Major Oxides

Fifteen (15) sandstone and ten (10) shale samples of the Upper Disang and nineteen (19) basalt samples were chosen and analysed by XRF for determination of major oxides. Pressed pellets are employed for the analyses. The pressed pellets are prepared using collapsible aluminium cups that are filled with boric acid. About 1 gm of finely powdered rock sample is put over boric acid and hard-pressed under a hydraulic press at 20 tons of pressure to obtain pellets. For greater resilience some wax was added to the rock sample.

Basalt

A classification based on total alkali silica for volcanic rocks is plotted following after Le Bas *et al*. (1986) and Middlemost (1994). Al_2O_3 vs normative plagioclase composition and $Na_2O+K_2O-Fe_2O_3^T-MgO$ (AFM) plots of Irvine and Baragar (1971) are used for distinguishing tholeiitic rocks from the calc-alkaline series. K_2O+Na_2O vs $K_2O/(K_2O+Na_2O)x100$ of Hughes (1972) are used to evaluate post magmatic alteration in the volcanic rocks.

Upper Disang

Certain relationships of the oxides are used for various purposes. TiO_2/Al_2O_3 ratio is used for determination of palaeoclimate (Migdisov, 1960), provenance (Amajor, 1987) and chemical maturity (Spears and Sotiriou, 1976). K_2O/Na_2O ratio is useful for determining rock type (Kukal, 1968). The relation between Log K_2O/Al_2O_3 and Log MgO/Al_2O_3 following Roaldest (1978) is used to differentiate between marine and non-marine environments.

Log Fe_2O_3/K_2O vs SiO_2/Al_2O_3 and log (Na_2O/K_2O) vs SiO_2/Al_2O_3 ratios are plotted in the binary diagrams following Pettijohn *et al*. (1987), Herron (1988) and Creaser *et al*. (1997) for rock nomenclature. The percentages of quartz, feldspar and rock fragments are plotted in triangular diagrams following Dickinson and Suczek (1979).

For determination of extent of weathering at the provenance the Chemical Index of Alteration (CIA) is calculated using the formula of Nesbitt and Young (1982).

CIA = [Al$_2$O$_3$/(Al$_2$O$_3$ + CaO* + Na$_2$O + K$_2$O)] x100

where CaO* is the amount of CaO incorporated in the silicate fraction only. For the same purpose Al_2O_3, $(CaO+Na_2O)$ and K_2O are recalculated to 100 percent and plotted in triangular diagrams after Nesbitt *et al*. (1997).

The Chemical Index of Weathering (CIW) is determined using the equation given by Harnois (1988).

$$CIW = [Al_2O_3/(Al_2O_3 + CaO^* + Na_2O)] \times 100$$

Fedo *et al*. (1995) proposed the Plagioclase Index of Alteration (PIA) for monitoring the degree of plagioclase weathering which yields additional information for silicate weathering.

$$PIA = [(Al_2O_3-K_2O)/(Al_2O_3 + CaO^* + Na_2O-K_2O)]x\ 100$$

Chemical maturity of sediments has been expressed in terms of SiO_2 content/Chemical Maturity Index (CMI), and SiO_2/Al_2O_3 ratio following Potter (1978).

The total quartz/feldspar+rock fragment are plotted against polycrystalline quartz/feldspar+rock fragments and QFR ternary plots following Suttner and Dutta (1986) for determination of palaeoclimatic condition.

Na_2O+K_2O are plotted against SiO_2 for determination of provenance following Irvine and Baragar (1971). Following Amajor (1987) TiO_2 is plotted against Al_2O_3 for the same purpose. K_2O is plotted against SiO_2 in binary diagrams for determination of provenance following Le Maitre (1989). Sc vs Th and Y/Ni vs Cr/V binary plots have been used after Chakrabarti *et al*. (2009) and Mongelli *et al*. (2006) respectively for determination of provenance.

For determination of tectonic setting of the Upper Disang rocks, the ratio of K_2O/Na_2O vs SiO_2 is plotted following Roser and Korsch (1986) modified by Murphy (2000). Plots using SiO_2/Al_2O_3 ratio instead of SiO_2 after Maynard *et al*. (1982) has been used for the same purpose. The relationship amongst quartz, feldspar and lithic fragments are plotted in a ternary diagram following Dickinson and Suczek (1979), Dickinson *et al*. (1983) and Dickinson (1985) for discriminating tectonic setting.

The weight percentage of silica against that of the other major oxides, trace and rare earth elements is calculated for determination of the correlation coefficient of these elements. Coefficient correlation has been computed employing the Karl Pearson's formula. The coefficient of correlation is a numerical measure and is expressed numerically. The correlation coefficient is a ratio that is a unit-less number. Correlations range from +1 to -1. A correlation of +1 indicates a perfect direct

24

relationship between any two variables while -1 indicates that one variable changes inversely with relation to the other. The limit of correlation is between zero and +1 in positive correlation and zero and -1 in negative correlations. Relationships between them may be weak or strong depending on the correlation coefficient ratio and their relationship in scatter diagrams. The correlation coefficient between silica and the other elements are calculated using the formula $r = \Sigma dxdy/\sqrt{(\Sigma dx^2)(\Sigma dy^2)}$

where dx   - difference between x and x

dy   - difference between y and y

x and y are arithmetic mean of x and y values

3.2b   Trace and Rare Earth Elements

Nineteen (19) basalt samples for trace and five (5) for REE and fifteen (15) sandstone and ten (10) shale samples of Upper Disang for trace and REE are analysed by ICP-MS. The open acid digestion method is adopted. For analyses 50 mg of powdered samples are taken in a PTFE teflon beaker. Each sample is dampened with a few drops of water, then a mixture of 7 ml HF, 3 ml HNO_3 and 1 ml $HCIO_4/HCl$ is added to each beaker and sample is swirled till completely wetted. The beakers are then covered with lids and kept overnight for digestion. The beakers are then heated to 200±25ºC for about 1 hour after which the lids are removed and contents evaporated to dryness. The contents are then dissolved in 20 ml HNO_3+distilled H_2O (1:1) and heated for 20-30 minutes in an oven. After cooling, 5ml of rhodium is added. The volume of rhodium treated samples are increased to 250 ml by adding distilled water and stored in polythene reagent bottles (20-25 ml) till clear solutions are obtained. This gives a dilution of 1:1000. These solutions are used to determine the trace elements and REE. ICP-MS is best used for simultaneous multi-element determination of trace elements and REE in various geochemical materials. Trace elements and REE (ppm) are analysed using ICP-MS Model ELAN DRC II (Perkin-Elmer instrument, US). In order to smoothen out natural odd-even effects of the REE concentrations, REE abundances are divided by the corresponding chondrite values (Evensen et al., 1978). The Eu/Eu* (Eu anomaly) for determination of provenance following Taylor and McLennan (1985) is calculated by Eu/Eu* = $Eu_N/\sqrt{(Sm)_N(Gd)_N}$. Subscript $_N$ refers to chondrite-normalised ratios as recommended by Boynton (1983). Normalized data for the Upper Disang are plotted following Taylor and McLennan (1985) and Evensen et al. (1978). Basalt REE are normalised using N-MORB data

following after Sun and McDonough (1989). Cerium anomaly is calculated after Asiedu *et al.* (2004) by Ce/Ce*=Ce$_N$/(La$_N$×Nd$_N$)$^{0.5}$.

M (incompatible elements)/Yb are plotted against Nb/Yb following Pearce and Peate (1995) to determine crustal contamination related to dehydration of subducted slabs.

Various binary and ternary plots have been used to discriminate tectonic setting of the NHO basalt. These include Zr vs Zr/Y (Pearce and Norry, 1979), 2Nb-Zr/4-Y (Meschede, 1986) and V against Ti (after Shervais, 1982).

Cr/V ratios are calculated for determination of ventilation conditions in the depositional environment of Upper Disang rocks while Ni/Co ratios are calculated for determination of Eh conditions in the depositional basin and provenance of the Upper Disang sandstone and shale following Dypvik (1979). The V/Cr ratio has been used as an index of paleo-oxygenation in many studies (Ernst, 1970; Bjorlykke, 1974; Dill, 1986; Dill *et al.*, 1988).

La, Th and Sc are plotted in a ternary diagram for determination of provenance. For the same purpose Th/Sc is plotted against Zr/Sc in a binary diagram following McLennan *et al.* (1993).

3.3 Paleomagnetism

Paleomagnetic studies include collection of oriented samples followed by laboratory analyses to determine their susceptibility and natural remanence through thermal and alternating field demagnetization processes. The remanence is then examined for stability and possible age of components, thus defining the directions and intensity of geomagnetic field at certain specific periods. The methodology adopted and the instruments employed are briefly outlined below (Fig. 3.1).

3.3.1 Sampling and Orientation

Nineteen (19) oriented basalt block samples from the NHO were collected for paleomagnetic studies. Systematic and detailed fieldwork was carried out at Leshimi and Viswema villages to construct two vertical profile sections for magnetostratigraphic attributes. Oriented blocks are obtained using standard technique described by Butler (1998). Only siltstones, mudstones and fine grained sandstones were collected in order to obtain more reliable palaeomagnetic data from
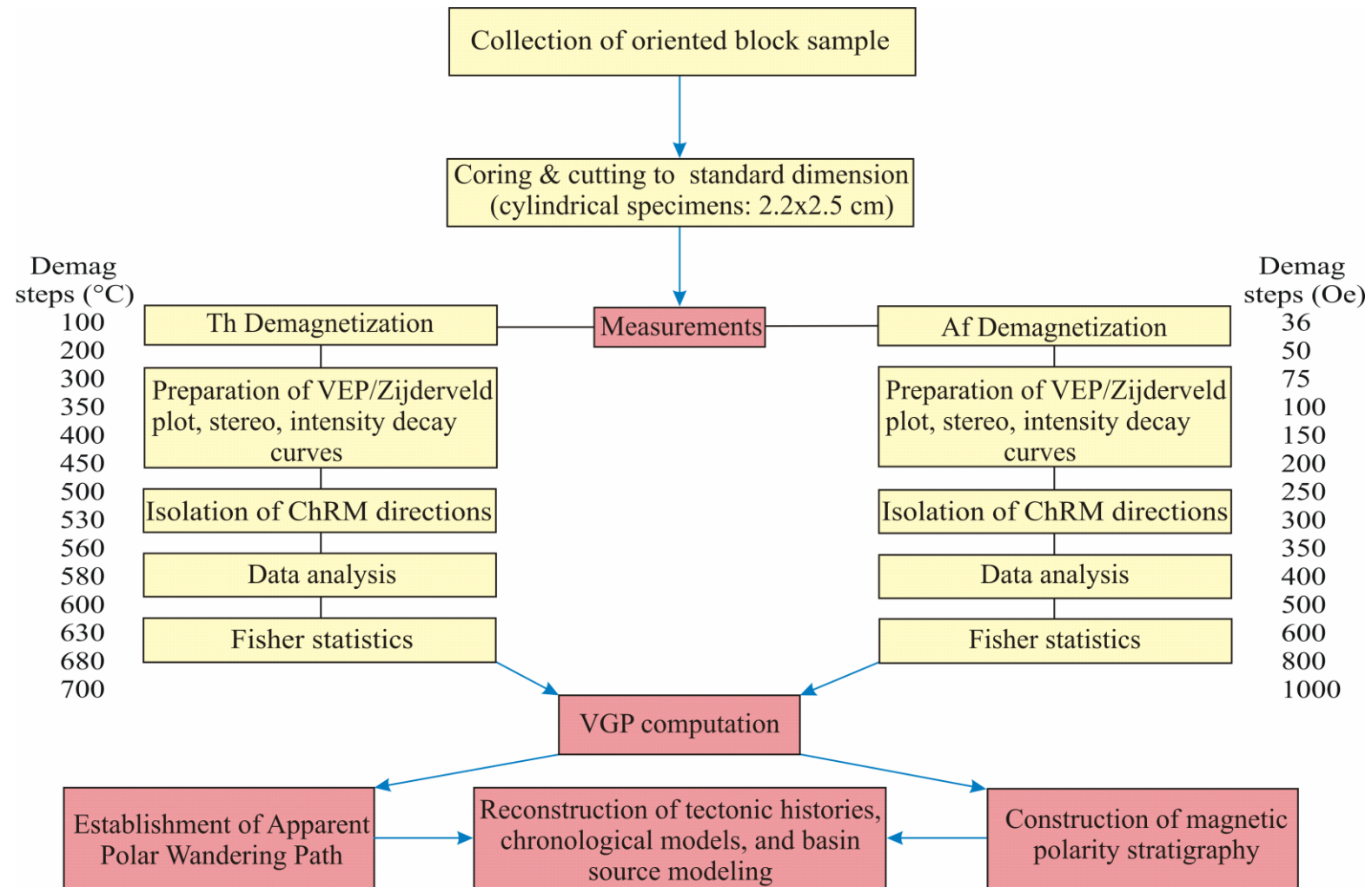
Fig. 3.1: Flow chart for methodology in paleomagnetism

stable single domain grains while avoiding zones of pedogenetically altered, sheared and disturbed beds.

The stratigraphic separation between paleomagnetic sites depends on the sedimentary environment and age of the section. According to Sadler (1981), sediment accumulation rates (SAR) for fluvial environments typically range from 10 to 100 m/Ma. With a polarity reversal rate of ~4 per Ma during the Neogene a typical polarity zone is expected to have a thickness of ~10 m. So a stratigraphic separation of 3 m between sites generally allows resolution of the polarity zonation. In pelagic environments SAR is generally <10 m/Ma and <0.5 m stratigraphic spacing of sites is recommended to allow resolution of important polarity zones. The uniqueness of correlation between an observed polarity zonation and the GPTS depends on the number and pattern of polarity zones. For typical SAR, a continental sedimentary sequence 100 m thick is generally required, but a pelagic sequence that is only a few meters thick may suffice (Butler, 1998). With lower rates of polarity reversals during Late Cretaceous-Paleogene, continental sedimentary sections of 500 m thickness and pelagic sequences of 100 m are vital for convincing correlation to the GPTS (Lowrie and Alvarez, 1977). In the present study area, the frequency of sampling was mainly controlled by availability of good exposures and lithofacies variation. An average of 8 m, with a minimum interval of 1 m and a maximum of 21 m for the Upper Disang sediments in Leshimi section and in the Viswema section, an average of 16 m with minimum and maximum intervals of 1 m and 101 m respectively was considered.

Fresh rock samples with dimensions of about 15x10x5 cm and flat surfaces that enable orientation while still in situ are collected using standard methods (Collinson, 1983). Horizontal lines are marked using a Brunton compass and magnetic north translated over the samples as fiducial lines. Attitudes of beds (strike and true dip) are recorded more than once at each sampling site so that the direction of magnetization can be related to the paleohorizontal (Tarling, 1971). After orientation the samples are detached from the outcrop using a hammer and a chisel.

A permanent arrow line is drawn on the side of the specimen and then cores are trimmed into standard length of ~2.2 cm. Site and specimen numbers are assigned on top of each specimen. Data are transformed from the sample coordinate system into geographic coordinates either graphically with a stereonet or with the help of software (Collinson, 1983).

3.3.2 Magnetic Susceptibility

Magnetic susceptibility is used as a first order measure of the amount of ferrimagnetic material in the rocks samples. It varies with composition (ferrimagnetic, antiferromagnetic, paramagnetic and diamagnetic), concentration and granulometry, e.g., Superparamagnetic (SP), Single domain (SD) and Multi domain (MD) of the magnetic minerals (Verosub and Robert, 1995; Han and Jiang, 1999; O'reilly, 1984).

The most frequent approach to establish magnetic concentration in samples involves measurement of magnetic susceptibility χ. Initial magnetic susceptibility has been measured on Bartington susceptibility meter (MS$_2$B) with a dual frequency sensor. The meter has two ranges of measurements, 1.0 and 0.1 with two dimensionless unit systems SI and CGS. The 0.1 range gives ten times the sensitivity, taking about ten times longer to make a reading. Since the samples are weakly magnetic, the readings have been taken in 0.1 range (SI unit).

This sensor is provided with a dual frequency system, i.e., low frequency and high frequency. The measurements made at two frequencies are used to detect the presence of ultrafine (<0.03 micron) SP ferromagnetic minerals occurring as crystals produced by bacteria or by chemical processes.

Low field magnetic susceptibility (χ_{lf}) is a fundamental room temperature parameter forming the ratio of induced magnetization to a weak applied field. It allows preliminary estimates of ferrimagnetic contents in a material and is proportionately affected by diamagnetic (silica and carbonates) and paramagnetic (clays, micas and feldspar) content (O'reilly, 1984; Thompson and Oldfield, 1986). The χ_{lf} is considered as a first order estimate of ferrimagnetic concentration but is an important decisive parameter when used as a ratio to other hysteresis parameters (Mullins, 1977; Maher, 1986; Singer and Fine, 1989; Evans and Heller, 2001).

Frequency dependence of susceptibility (χ_{fd}) is the variation of susceptibility between two frequencies. Magnetic susceptibility measured under different frequencies of applied field (0.465 KHz and 4.65 KHz) allow distinguishing and quantifying certain grain sizes, taking advantage of the phenomenon of magnetic viscosity (Stacey and Banerjee, 1974; O'reilly, 1984). SP material is that class of ferrimagnetic grain sizes which are characteristically viscous at room temperature and behaves differently in higher frequencies (Maher and Taylor, 1988; Zhou *et al*., 1990; Dearing *et al*., 1996; Dekkers, 1997). Thus, SP particles can be estimated simply by changing the frequency of the applied field (Thompson and Oldfield, 1986; Dearing *et*

al., 1996; Dekkers, 1997).

$$\chi_{fd}\% = \left(\frac{\chi_{\text{lf}} - \chi_{\text{hf}}}{\chi_{\text{lf}}}\right) \times 100$$

where χ_{lf} is the susceptibility at low frequency (0.465 kHz) of applied field and χ_{hf} is the high frequency (4.65 kHz) susceptibility.

3.3.3 NRM Measurements and Isolation of Primary Remanent Magnetization

The natural remanent magnetization (NRM) of a rock is assumed to have been acquired during rock formation and remained unaltered. NRM is usually made up of several components acquired at different times including sampling and preparation. Thus, an appropriate technique is crucial in order to recognize and eliminate undesirable secondary components and isolate the characteristic primary magnetization. This process is loosely called 'magnetic cleaning'. Demagnetization or magnetic cleaning is intended to

i)   understand the remanent component assemblage

ii)   study the changes in the vector direction during demagnetization and

iii)   monitor the intensity decay and change in the initial magnetic susceptibilities for identification of ChRM. Thus, using various instruments rock specimens are subjected to partial demagnetization experiments including thermal demagnetization (ThD) and alternating field demagnetization (AfD).

NRM has been measured using a SQUID cryogenic magnetometer for the Viswema samples and a JR6 magnetometer for the Leshimi samples. Prior to magnetic cleaning, initial NRM inclination (I), declination (D) and magnetic intensity (Int) values are measured for each specimen.

In order to understand the nature of the stable magnetic components of the samples and that of the magnetic minerals which carry the remnant magnetization, thermal and alternating field demagnetizations are applied for one pilot specimen representing each site. The main objective is to

a) determine characteristic demagnetization behavior,
b) establish the most efficient demagnetization temperature steps,
c) determine which lithology provides the best signal, and
d) localize stratigraphic intervals with potential paleomagnetic reversals.

This helps identify a more convenient method for the demagnetization processes (Renne *et al*., 1988). The results obtained are also used as guides to further select samples from key areas of the section at higher stratigraphic resolution. When results from a single sample at a sampling level are ambiguous, a second or third sample is processed and the best result taken to represent that sampling level.

3.3.3a Thermal Demagnetization

ThD is performed using a TDMD 800 thermal demagnetizer (Molspin). It is crucial to use both AF and Th techniques and compare results. Some specimens will be progressively demagnetized using the AF while other specimens using only the thermal technique. The overall objective is to reveal the NRM components which are carried by ferromagnetic grains within a particular interval of coercivity or blocking temperature spectra. Partial thermal demagnetization is carried out at temperatures of 100, 200, 300, 350, 400, 450, 500, 530, 560, 580, 600, 630, 680 and 700°C with continuous monitoring of magnetic susceptibility.

After each step of ThD the remanent magnetization is measured with a magnetometer. JR6 spinner magnetometer with a sensitivity of 2.4μ A/m works with a principle that defined shape and size rotates at a constant angular speed in the pickup unit inside a pair of coils. An AC voltage is induced in the coils whose amplitude and phase depend on the magnitude and direction of the magnetic remanence vector of the specimen. By Furier analysis the computer calculates two rectangular components of the projection of the remanence vector (D and I) in the plane perpendicular to the axis of rotation.

3.3.3b Alternating Field Demagnetization

Alternating field (Af) demagnetization involves application of a decaying alternating magnetic field to a sample. The waveform is sinusoidal with a linear decrease of magnitude with time. In the absence of external direct magnetic fields and significant distortion in the applied Af, the sample will be 'cleaned' of any remanent magnetization of coercivity less than the peak intensity of the applied Af. This cleaning is the result of randomizing the mobile magnetic domains along the axis of the applied field. The amplitude of each half-cycle of the applied Af is smaller than its predecessor. With each half-cycle the domains whose coercivities are less than the applied field align themselves with the field. During each half-cycle of the Af a small

percentage of the mobile domains will have coercivity greater than the following half-cycle and will therefore become fixed in direction. In this way equal numbers of domains will be magnetized in the positive and negative directions oriented along the axis of demagnetization, resulting in net zero remanent fields on the sample. Af demagnetization is often effective in removing secondary NRM and isolating ChRM in rocks with titano-magnetite as the dominant ferromagnetic mineral.

Twenty nine (29) pilot specimens representing each site from Leshimi section is demagnetized using AGICO LDA-3A and treated up to 90 mT with an incremental increase of 10 mT. These pilot specimens are chosen randomly from three to five specimens from each site. The same samples are also used for ThD treatment.

Thirty one (31) specimens from Viswema section are demagnetized using an AfD (Molspin) for pilot studies to determine their stable magnetic components and the magnetic minerals responsible for magnetic remanence. The specimens are treated in 14 incremental AfD steps (36, 50, 75, 100, 150, 200, 250, 300, 350, 400, 500, 600, 800 and 1000 Oersted). The same samples are also used for ThD treatment. The remaining specimens have been taken for blanket studies. Thermal pilot studies indicate the presence of secondary goethite component with an unblocking temperature of 150°C. To avoid possible contribution of a spurious goethite component which is difficult to demagnetize by AfD and also to avoid scatter caused by heating at high temperatures, the following measurement protocol was adopted for all the remaining specimens. NRM of each specimen is first measured and then heated to 150°C and re-measured. Subsequently, each specimen is subjected to 14 AfD steps as mentioned above. This treatment provides better results relative to thermal techniques for the Laisong sediments. Therefore, bulk of the specimens is subjected to AfD.

Remanent magnetization is measured after cooling down to room temperature using JR6 magnetometer for Leshimi samples and cryogenic SQUID magnetometer for Viswema samples. The AF technique is a rather fast cleaning procedure compared to the thermal demagnetization technique.

Demagnetization data is visualized and analyzed using Remasoft program (Chadima and Hrouda, 2006) which provides steronet plot, intensity decay curve and vector end (Zijderveld plot/vector migration curve) diagrams defining their directions and intensity. The primary and secondary magnetizations are identified and ChRM determined by principal component analysis (Kirschvink, 1980). ChRM directions are

calculated using a minimum of three to four consecutive steps decreasing towards the origin. Line fits were not anchored to the origin except for those samples exhibiting a progressive decrease in intensity upon demagnetization. Line fits with maximum angular deviation (MAD) above 30° are discarded.

Since the study area is a young active mobile belt represented by varying degrees of tilted beds, bedding tilt corrections have been necessitated to determine the actual ChRM direction with respect to the paleohorizontal. Structural attitudes of beds are determined during the course of fieldwork. Tectonic/tilt corrections are performed following the method described by Butler (1998).

After bedding correction, the mean values and related statistics are derived finally to determine the paleolatitudes of virtual geomagnetic pole (VGP) with the help of the equations. Finally, the zones of normal and reverse polarity are plotted along with stratigraphic heights to produce the local magnetic polarity, i.e., magnetic polarity times scale (MPTS) in order to identify the zones over the standard GPTS of Cande and Kent (1995).

3.4   Rock Magnetics

The measurement of induced magnetic remanent magnetizations, commonly isothermal remanent magnetization (IRM) and saturation IRM (SIRM) are routinely used in identifying certain components within bulk magnetic mineral assemblages.

IRM is the remanent magnetization acquired by deliberate exposure of a material to a steady field generally at room temperature (Robertson and France, 1994; Kruiver *et al*., 2001). IRM is imparted with a pulse magnetizer (MMPM 10) at intervals of 50, 100, 150, 200, 300, 600, 1000 mT. SIRM is induced at 1T and ultimately induced remanence is measured using a Molspin Spinner Magnetometer. Once saturated and SIRM measured the samples are exposed to a series of reverse or back fields (-10, -20, -30, -40, -50, -100, -300 mT) where the direction of the applied magnetic field is opposite the original saturating field. These induced IRMs are measured using a spinner magnetometer. S ratio is calculated using the definitions of Robinson (1986) and Bloemendal *et al*. (1992).

$$\text{S ratio\%} = (1\text{-}IRM_{-300mT}/IRM_{1T})/2*100$$

where IRM_{-300mT} is the magnetization at reverse applied field of 300 mT and IRM_{1T} represents the value of IRM at applied field of 1T (1000 mT). Low coercivity minerals get demagnetized at low fields (<-300 mT) and show negative S ratio while

high coercivity minerals require relatively higher back field to demagnetize (>-300 mT) show positive S ratio. Anisotropic magnetic susceptibility (AMS) is measured with a MFK1-FA Kappabridge (AGICO, Czech Republic) in manual mode into 15 directions.

The magnitude of fabric ellipsoid in the form of degree of AMS (Pj) and the shape parameter (T) are derived from the equations given by Jelinek (1981). Shape of the anisotropy ellipsoid (T) is used to infer prolate (-1<T<0), neutral (T=0) and oblate (0<T≤1) fabrics (Tarling and Hrouda, 1993). Degree of foliation (F) and lineation (L) are calculated following Stacey *et al*. (1960) and Balsley and Buddington (1960). The directions (declination and inclination) of principle susceptibility axes (K_1=maximum, K_2=intermediate and K_3=minimum) are computed in a computer program Anisoft 4, available with the KLY-2 Kappabridge using the formula:

$K = (K_1+K_2+K_3)/3$

Mean magnetic susceptibility (Nagata, 1961)

$P_j = exp\sqrt{\{2[(\eta_1-\eta_2)^2+(\eta_2-\eta)^2+(\eta_3-\eta)^2]\}}$

Corrected anisotropy degree (Jelinek, 1981)

$L = K_1/K_2$

Magnetic lineation (Balsley and Buddington, 1960)

$F = K_2/K_3$

Magnetic foliation (Stacey *et al*., 1960)

$T = 2(\eta_2-\eta_3)/(\eta_1-\eta_3)-1$

Ellipsoid shape (Jelinek, 1981)

SAR is computed by plotting the age of each reversal (in Ma) versus the stratigraphic thickness at which the reversal is preserved (in meters). This provides the rate in centimeters per thousand years (cm/Ka).

Chapter 4

PETROGRAPHY

4.1 Basalt

Fifteen representative basalt thin sections have been prepared for petrological studies. NHO basalts are very fine grained to aphanitic, olive green and greenish grey to brownish green (Plate 4.1), massive and compact with occasional pillow structures (Plate 4.2) and vesicles (Plate 4.3). They are often traversed by secondary quartz veins (Plate 4.4). The dominant minerals of the basalts are plagioclase (microlites as well as phenocryst), clinopyroxene and olivine. The secondary minerals include chlorite, epidote, calcite, serpentine and iron oxides that are products of alteration of pyroxene, plagioclase and olivine. Porphyritic texture is common. Intersertal, spherulitic and quenched textures are occasionally noted.

Plagioclase feldspars, often albitised, constitute the bulk volume of the rock. Plagioclase occurs as phenocrysts and as small tabular to elongated acicular microlites (Plate 4.5). The phenocrysts are euhedral to subhedral laths of variable sizes. Plagioclase crystals are often altered and clouded (Plate 4.5) and show undulose to inclined extinction. Lamellar to swallow tail twinning are also noted (Plate 4.6). Plagioclase phenocrysts are more altered than the microlites. Occasional spherulite (Plate 4.7) and variolitic textures (Plate 4.7) are also noted where plagioclase microlites are aligned along the flow direction.

Clinopyroxene is the predominant mineral after plagioclase. The phenocrysts occur as purplish brown anhedral crystals. The pyroxene crystals bear extinction inclined between 45° and 53° indicating augite composition. Pyroxene crystals are affected by chloritization. Green chlorite occurs along fractures and crystal rims. Partial alteration of augite to tremolite and actinolite is also noted, which impart a green colour to the rock (Plate 4.5).

Phenocrysts of olivine occur as anhedral crystals with polygonal outlines that have more or less corroded borders. Well rounded grains noted have probably been developed due to corrosion (Plate 4.8). Incipient alteration to serpentine is noticed. The larger crystals are somewhat fractured and display first and second order

Plate 4.1: Fine grained, greenish to brownish green basalt exposure along Sataza road, Phek district

Plate 4.2: Pillow lavas exposed 3.5 km east of Wazeho, Phek district
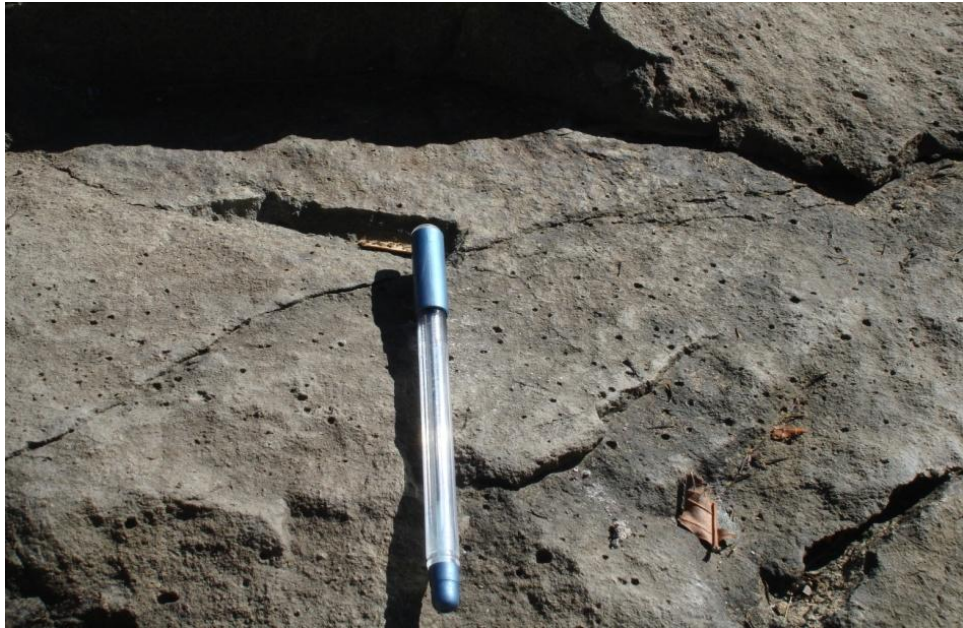
Plate 4.3: Pits and vesicles in NHO basalt

Plate 4.4: Displaced secondary quartz veins in basalt indicating sinistral movement

Plate 4.5: Phenocrysts of plagioclase, clinopyroxene and olivine in groundmass of acicular plagioclase microlites and dissolution of plagioclase to albite

Plate 4.6: Plagioclase feldspar showing undulose extinction and swallow tailed twinning
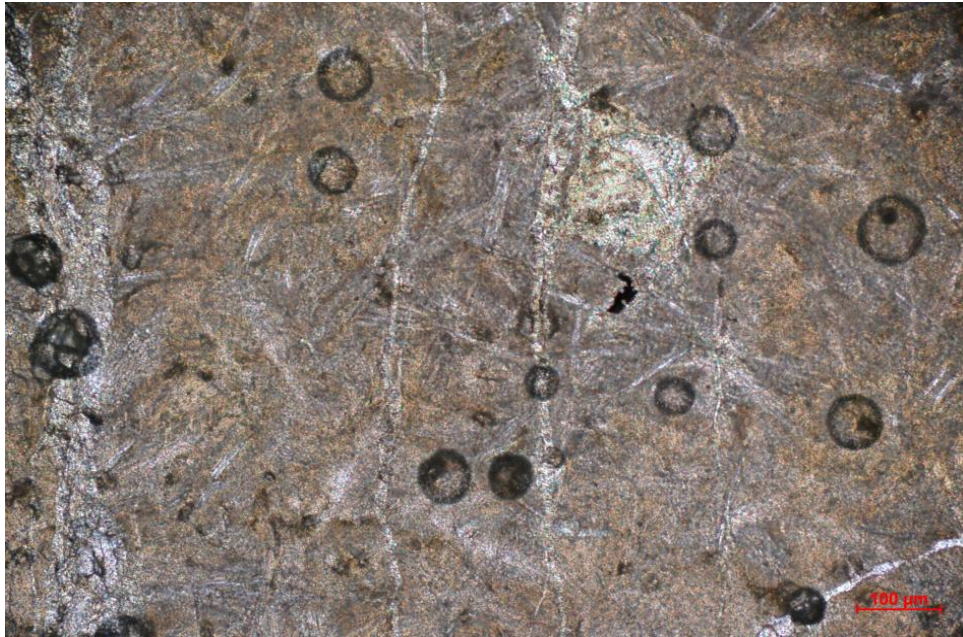
Plate 4.7: Photomicrograph of basalt showing spherulitic and variolitic textures
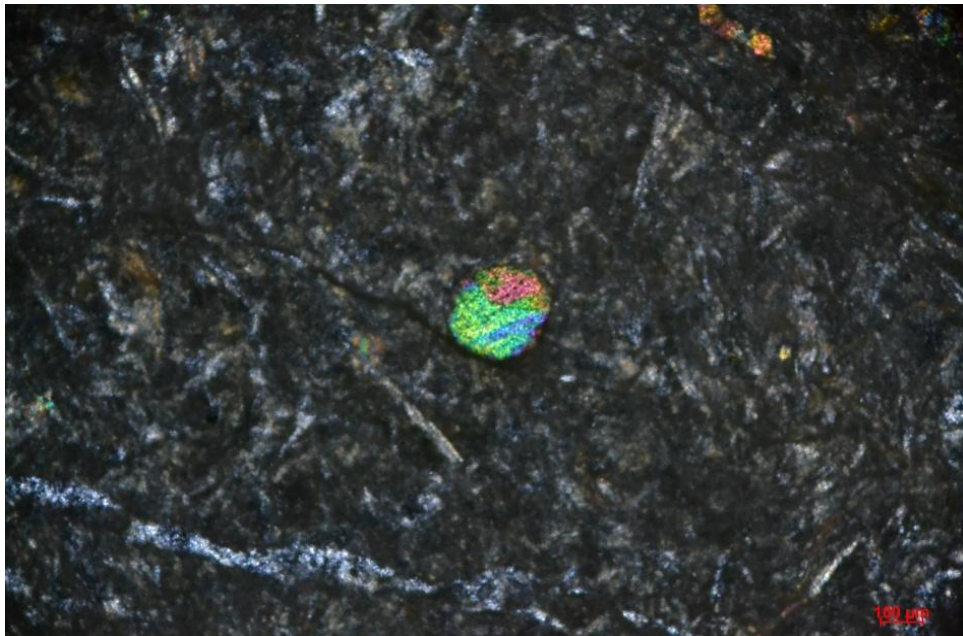
Plate 4.8: Quartz vein cutting through basalt and well rounded olivine phenocryst within groundmass of elongated plagioclase laths

interference colours. They commonly occur in a fine grained groundmass of pyroxene and plagioclase.

Iron oxides occur as anhedral crystals in the groundmass and along fractures. They are late magmatic minerals. A few late felsic veins of quartz cut across the basaltic flows.

4.2 Upper Disang

Mineralogy and texture of sedimentary rocks bear a direct relationship with provenance, transportation, depositional environment and diagenesis (Suttner, 1974; Pettijohn, 1984). Sandstone petrography aids in an understanding of the nature of climate and relief in the source area. It provides important evidences with which to draw satisfactory conclusions regarding the tectonic framework under which clastic rocks have been deposited (Mack, 1984). It also reflects the nature of lithification, cementation and the effect of pressure solution. Detrital minerals also carry a record about the area over which the debris from a given source is spread, the petrographic province. They also provide information about the tectonic conditions of deposition (Pettijohn 1984; Velbal, 1985). The geographic limit of the petrographic province, the information of mining of minerals from several sources and the changing of the suite from a given source because of progressive denudation may be determined from the study of detrital minerals. Petrographic studies also provide valuable information about the geographic history of the formation of sedimentary rocks, paleogeography and paleoclimate of the source area that prevailed during deposition (Suttner and Dutta, 1986).

4.2.1 Framework Constitution

More than 400 points are taken in each thin section to estimate the types and content of different framework grains of the Upper Disang sandstones (Table 4.1). A brief description of their petrographic features is summarized as follows:

4.2.1a Quartz

Broadly quartz can be classed under two main classes, monocrystalline and polycrystalline (Conolly, 1965; Blatt, 1967b).

Table 4.1: Modal composition of Upper Disang sandstone

Sample	Quartz Types				Q=(Qmt+Qpt)	Feldspar	Mica	Lithic Fragments	Matrix	Cement
	Monocrystalline Quartz			Polycrystalline Quartz (Qpt)						
	Non-undulose (Qmt_n)	Undulose Quartz (Qmt_u)	(Qmt)							
UD2	20.00	1.50	21.50	0.00	22.72	1.75	3.75	5.25	67.00	0.75
UD6	37.00	1.50	38.50	1.75	40.25	1.75	4.25	12.00	39.50	2.25
UD11	33.58	4.08	37.66	0.33	37.99	1.66	3.66	2.33	49.70	4.66
UD13	49.43	10.23	59.66	0.03	60.45	2.66	5.66	6.00	20.99	5.00
UD16	24.69	13.09	37.78	1.04	38.82	1.75	4.48	6.80	40.42	9.28
UD18	28.94	9.29	38.23	1.23	39.46	1.52	6.00	6.50	38.23	7.71
UD20	28.17	5.49	33.66	2.66	36.32	0.33	9.66	5.66	37.70	10.33
UD23	24.22	10.51	34.73	0.73	35.46	1.25	8.33	6.87	37.36	5.35
UD24	37.15	5.02	42.17	1.88	44.05	1.10	4.90	9.17	36.95	3.83
UD27	33.25	1.75	35.00	0.75	35.75	1.25	3.75	12.00	45.25	2.00
UD63	49.17	2.16	51.33	1.00	52.33	3.33	3.66	6.33	28.69	5.66
UD74	31.87	3.25	35.13	1.38	36.51	1.13	5.38	12.00	39.88	5.10
UD75	29.79	5.46	35.25	2.00	37.25	0.75	4.00	10.50	38.25	9.25
UD76	33.25	1.75	35.00	0.75	35.75	1.50	6.75	13.50	41.25	1.25

(i)   Monocrystalline Quartz

Monocrystalline quartz (Qmt) composed of a single unit boundary may be classified into three types.

Unit quartz / non-undulose quartz: It exhibits uniform extinction varying from 1° to 3° (Plate 4.9). The grains are mostly angular to sub-angular though a few grains are sub-rounded to rounded. Non-undulose quartz varies from 20.0 to 49.43% with an average of 32.89 in the Upper Disang sandstone.

Undulose quartz: It is identified by unit boundary and undulose extinction (Plate 4.9). To get complete extinction or release it requires more than 5° to rotate the microscopic stage (Basu *et al*., 1975). The grains are mostly angular to sub-rounded. Grain boundaries are straight sutures. Undulose quartz is thermodynamically less stable than non-undulose quartz and tends to break into small grains (Blatt *et al*., 1980). Unit undulose quartz varies from 1.5 to 10.55% with an average of 5.36 in these sandstones. Undulose extinction may be attributed to pre-depositional stress effects.

Vein quartz: The quartz grains exhibit parallel plane of weakness along which fluid, secondary quartz are present (Plate 4.10). Occurrence of vein quartz indicates the presence of some hydrothermal veins in the source rock.

(ii)   Polycrystalline Quartz

Polycrystalline quartz (Qpt) are single quartz grains composed of two or more optically different quartz crystal units (Plates 4.11, 4.12) but look like a single grain under polarized light (Conolly, 1965). It is an important tool for identification of source rock (Basu *et al*., 1975). Most polycrystalline quartz are larger than monocrystalline quartz. The average number of internal crystal units varies depending upon the nature of source rocks (Blatt *et al*., 1980; Basu *et al*., 1975). In the present study Qpt commonly exhibit two crystals per grain with straight to undulose extinction. Polycrystalline grains are generally made up of inequant individual crystals. The contact between sub-grains is straight. Qpt in the Upper Disang sandstones ranges from 0.33 to 2.66% with an average of 1.25.

Among quartz grains Qmt is dominant over Qpt. Qmt shows straight to slightly undulose extinction with rutile inclusions (Plate 4.11, 4.13).
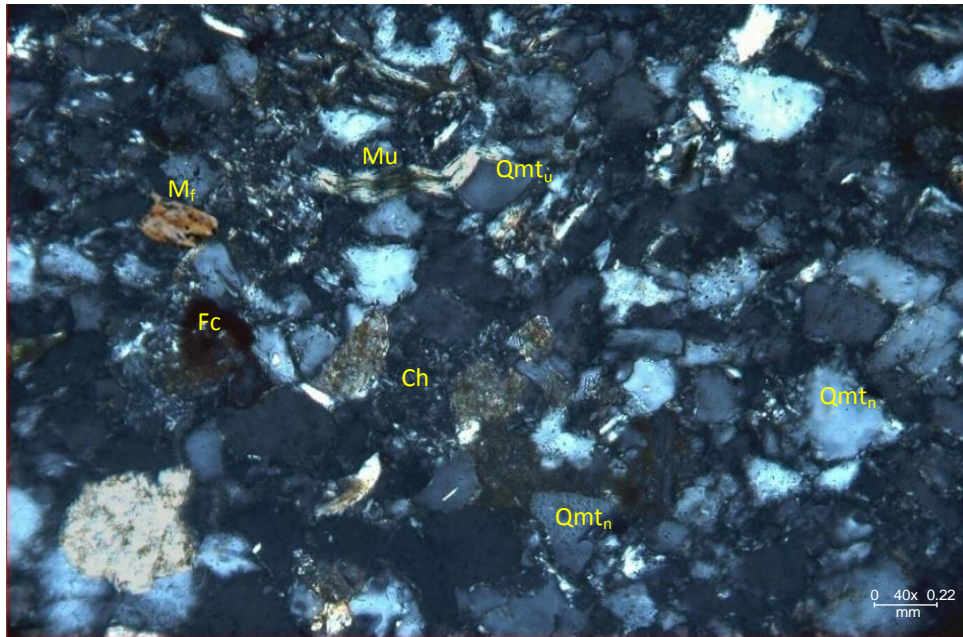
Plate 4.9: Photomicrograph showing non-undulose (Qmt_n), undulose monocrystalline quartz (Qmt_u), mica kinks (Mu), iron oxide (Fc), chert (Ch) and metamorphic rock fragments (M_f) (CN)
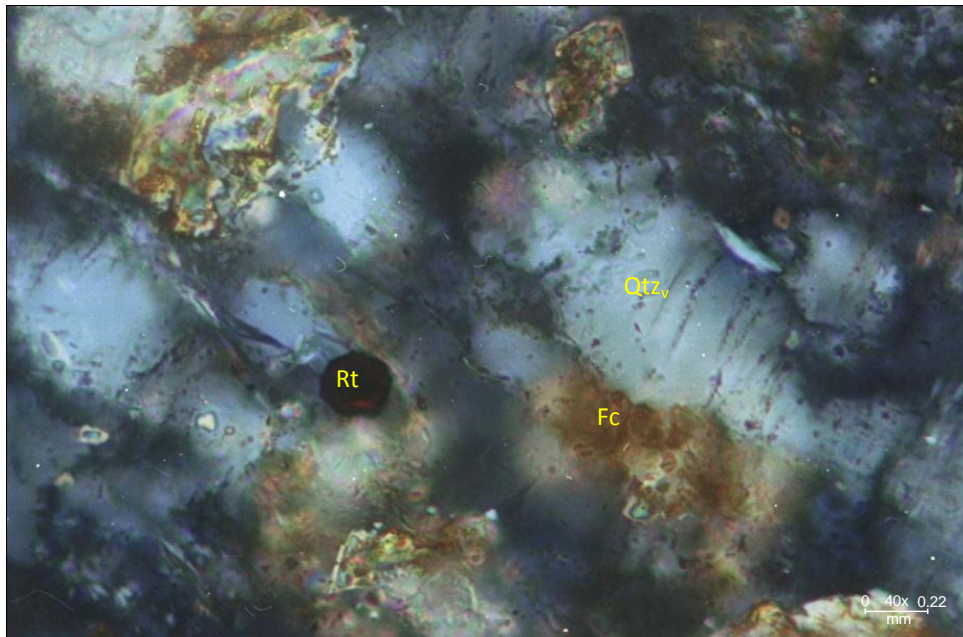
Plate 4.10: Vein quartz (Qtz_v) and inclusions of rutile (Rt) in monocrystalline quartz (CN)
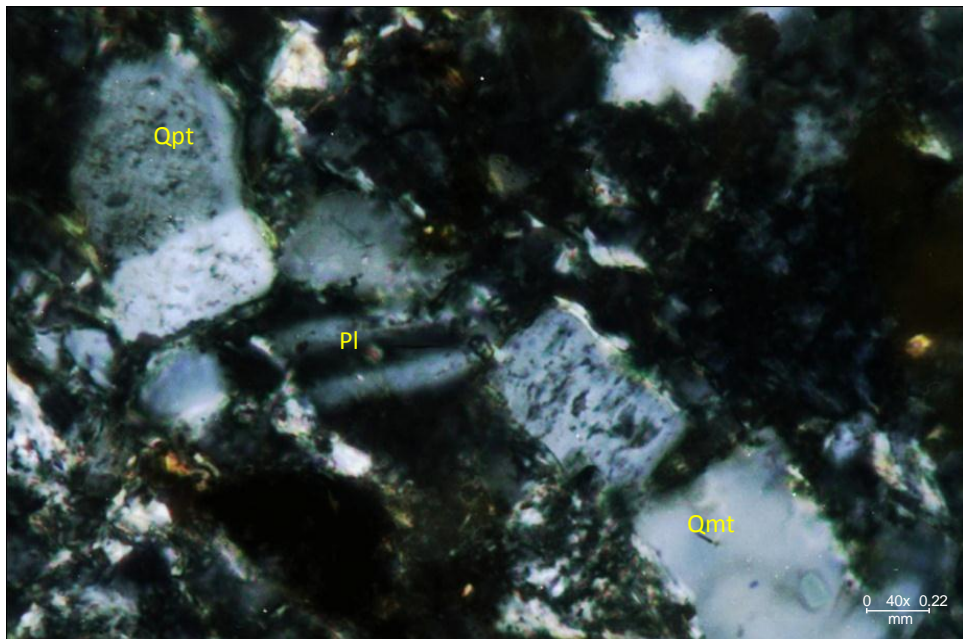
Plate 4.11: Polycrystalline quartz (Qpt) exhibiting two crystals per grain and plagioclase (Pl) (CN)
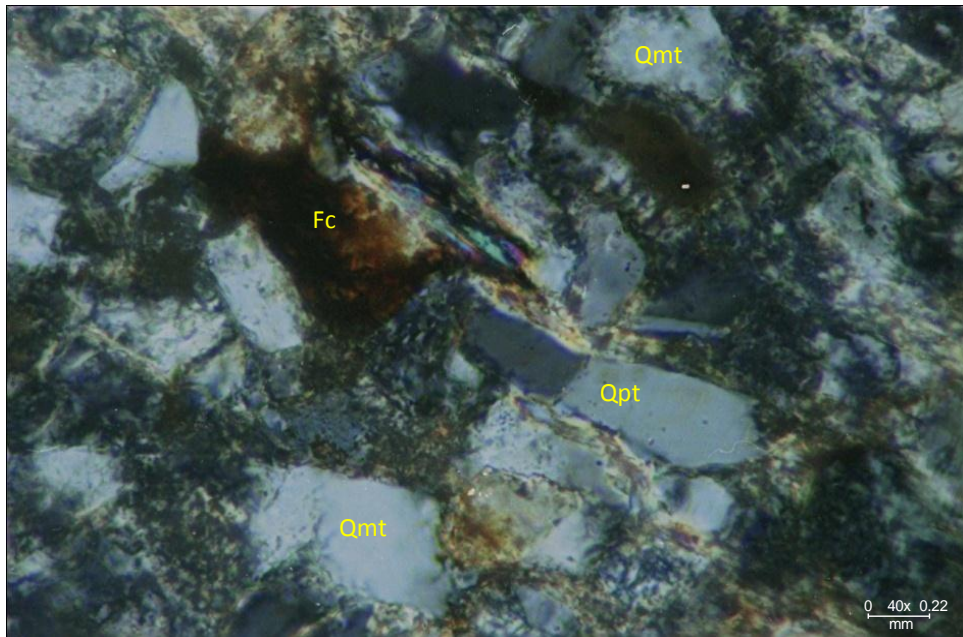
Plate 4.12: Polycrystalline quartz showing straight contact between sub-grains (CN)

4.2.1b Feldspar

All Disang sandstone samples contain minor amounts of feldspar, 1.55% on the average. In the present study K-feldspar (Plate 4.13) is less abundant than plagioclase. Feldspar grains are minute, subhedral and free of inclusions. Plagioclase grains exhibit well developed lamellar twinning (Plates 4.11, 4.13, 4.14, 4.15).

4.2.1c Mica

The Disang sandstones are generally rich in detrital mica flakes with an average of 5.3%. Muscovite occurs as elongated and flaky grains showing cleavage (Plate 4.15). The grains show parallel extinction and are generally colourless in ordinary light. Kink-bands of mica are common in these sandstones (Plates 4.9, 4.13). Bending and crumpling in the mica indicate post-depositional pressure effect on the grains.

4.2.1d Rock Fragments

The rock fragments include some chert (Plates 4.9), volcanic glass and some metamorphic rocks (Plate 4.9, 4.14). Compositionally, the most abundant type of rock fragments is argillaceous. The lithic fragments range from 2.33-13.5% with an average of 8.21% in these sandstones.

4.2.1e Matrix

Grains with 0.02 mm diameter or less were counted as matrix. The matrix content is significantly high with an average of 40.08% and comprise mainly of argillaceous material (detrital clay), silt and chert that are squeezed between framework grains. Large parts of the matrix are developed due to degradation of lithic grains (Cummins, 1962; Hawkins and Whetten, 1969). Detrital sandstones can be classified by their matrix and mineralogical content (Okada, 1971; Folk, 1980).

4.2.1f Cement

Iron oxides and silica are common cements in the Disang sandstone with an average value of 5.17%. Iron oxides occur mostly in the form of coatings around detrital grains, interstitial pore-filling and in patches (Plate 4.16). The precipitation of iron oxide from iron-saturated solutions is governed by Eh and pH of the depositional environment. Weathering and leaching during uplift has resulted in the disintegration
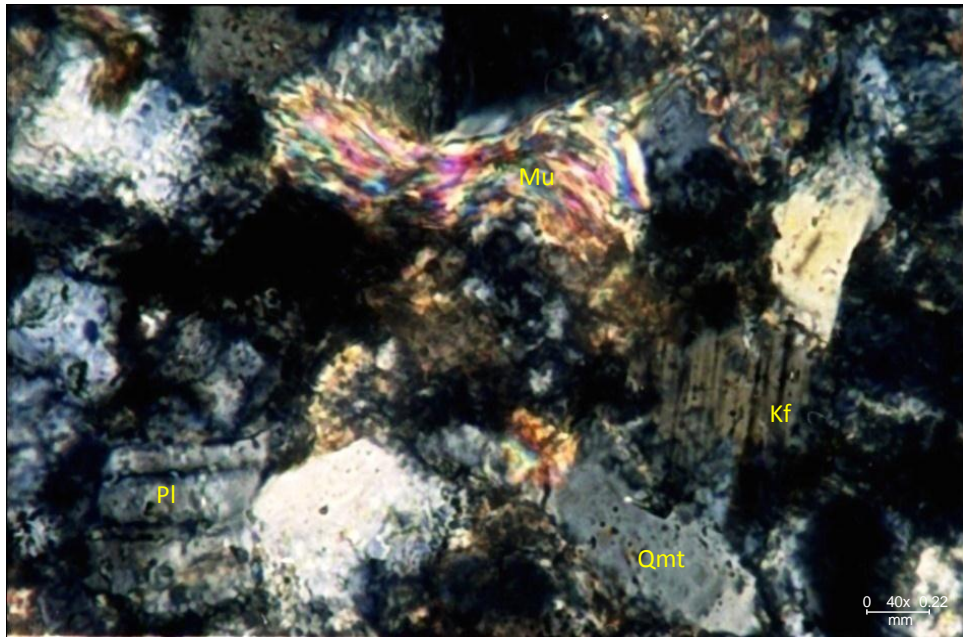
Plate 4.13: Mica kink (Mu), potash feldspar (Kf) and plagioclase feldspar (CN)
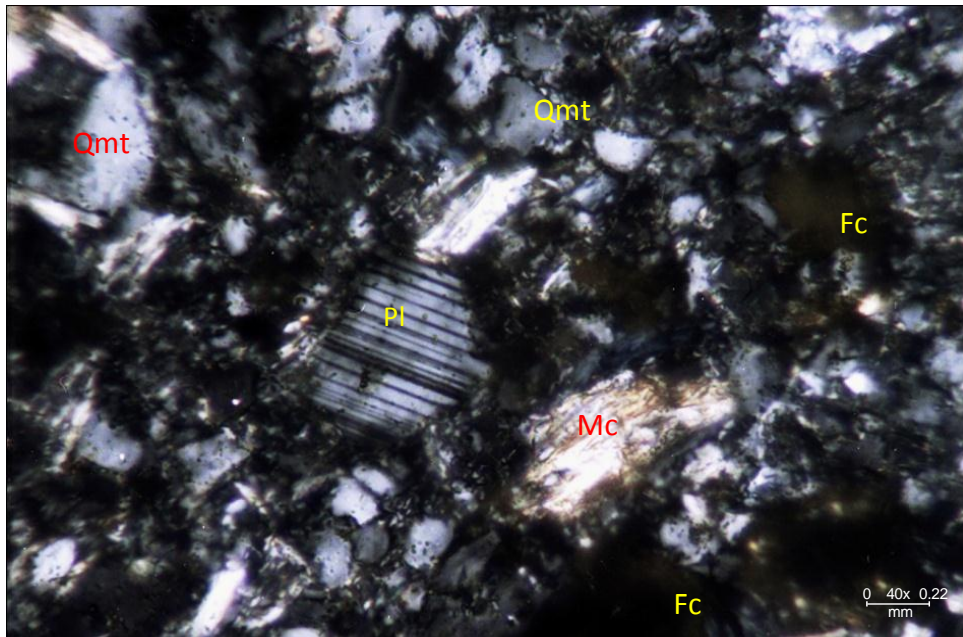
Plate 4.14: Plagioclase grains exhibiting well developed lamellar twinning (CN)
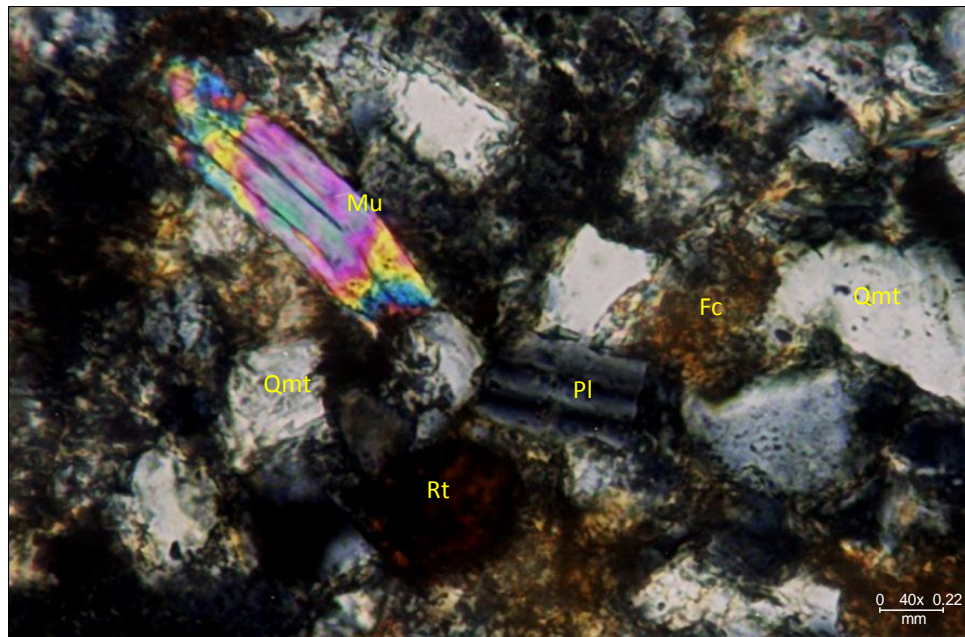
Plate 4.15: Muscovite with prominent cleavage (CN)
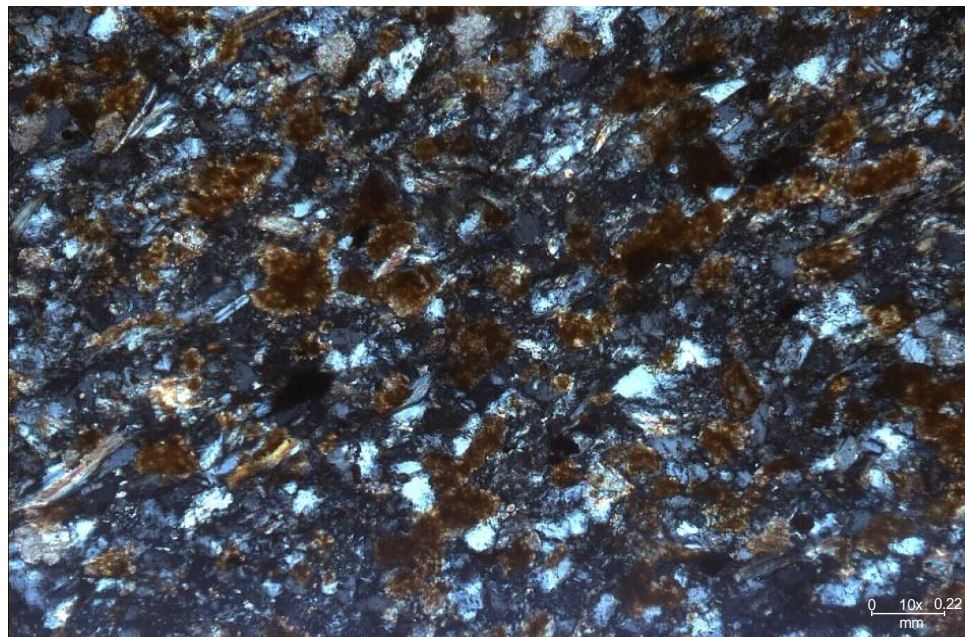
Plate 4.16: Iron oxide patches (CN)

of unstable ferromagnesian minerals and subsequently releasing iron oxides around the detrital grains.

4.2.2 Heavy Minerals

In the sediments of the study area a number of mineral species have been recorded. The common heavy minerals of the Upper Disang sediments comprise tourmaline, zircon, rutile, garnet, scapolite, wollastonite, corundum, opaques, etc.

4.2.2a Zircon

Zircon occurs as colourless, short, prismatic, euhedral to subhedral grains with or without pyramidal faces (Plate 4.17a-f). In shape they vary from anhedral (Plate 4.17m-n), sub-rounded (Plate 4.17k-l) to rounded (Plate 4.17g-j) with high relief and dark outlines. The majority of the grains are colourless but some of them are pale pink to straw yellow and pale brown. The prismatic grains show parallel extinction and strong birefringence.

4.2.2b Garnet

Garnet grains are sub-rounded, angular to sub-angular and isotropic (Plate 4.17o-t). Garnets are pale purple to almost colourless while some are pink to pinkish yellow with high relief.

4.2.2c Rutile

Rutile is either blood red or dark brown in colour and feebly pleochroic (Plate 4.18a-f). The grains are angular to sub-rounded with thick dark outlines and high relief. The prismatic grains exhibit straight extinction.

4.2.2d Wollastonite

Wollastonite occurs as colourless to pale purple grains (Plate 4.18g). The grains are subhedral with fairly high relief. Birefringence is rather weak.

4.2.2e Tourmaline

Elbaite (alkali tourmaline) is observed in the Disang sediments. The grains are colourless or pale and are colour-zoned under crossed nicols (Plate 4.18h-i). They are
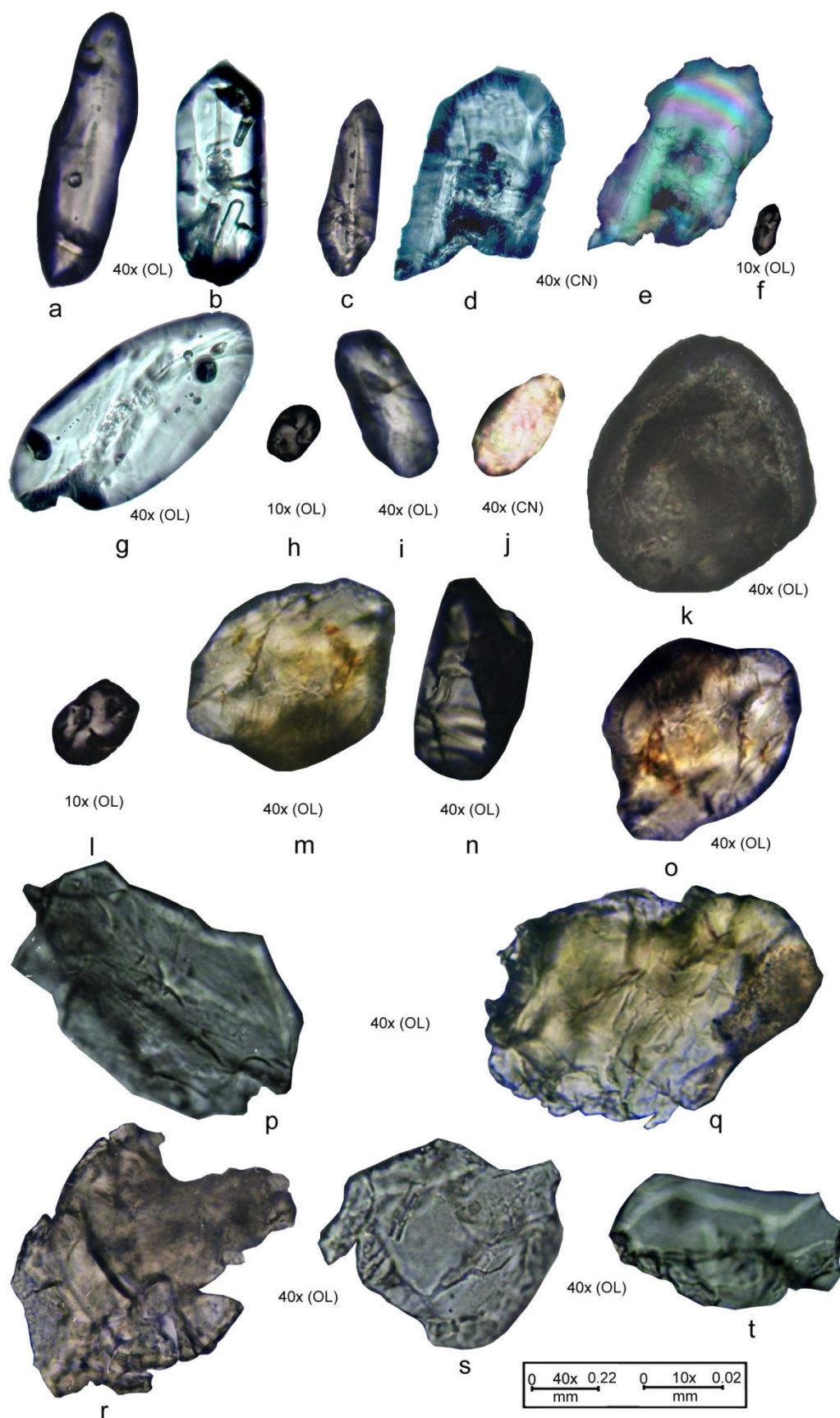
Plate 4.17: Heavy minerals in Upper Disang sandstone (a-f: euhedral zircon, g-j: rounded zircon, k-l: sub-rounded zircon, m-n: anhedral zircon, o-t: garnet)
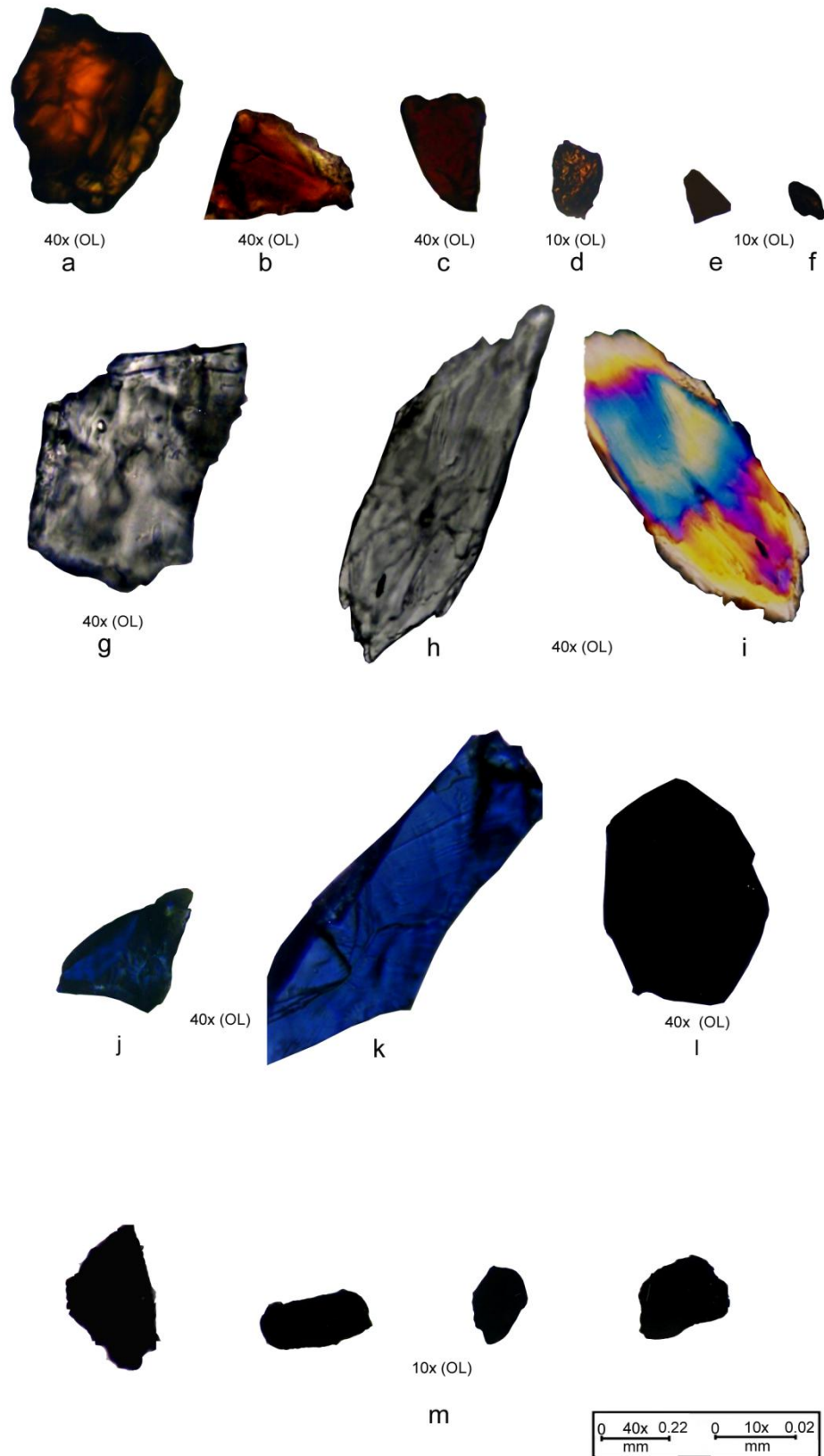
Plate 4.18: Heavy minerals in Upper Disang sandstone (a-f: rutile, g: wollastonite, h-i: tourmaline (elbaite), j-k: corundum, l- m: opaque)

prismatic, sub-angular and elongated. The mineral exhibits moderate to high relief and moderate birefringence with straight extinction.

4.2.2f Corundum

Corundum grains exhibit deep blue colour with weak birefringence (Plate 4.18j-k). The extinction is straight / symmetrical to the crystal outline and relief is very high relative to Canada balsam.

4.2.2g Scapolite

Scapolite occurs as columnar aggregates and is colourless (Plate 4.19a-j). It shows low to fair relief with strong birefringence and exhibits straight extinction.

4.2.2h Opaques

A considerable part of the heavy minerals are represented by opaques. The opaques are irregular in shape and size with broken surfaces (Plate 4.18l-m). They are usually black to brownish black in colour. They are mostly oxides of iron such as magnetite, ilmenite, pyrite and pyrrhotite.
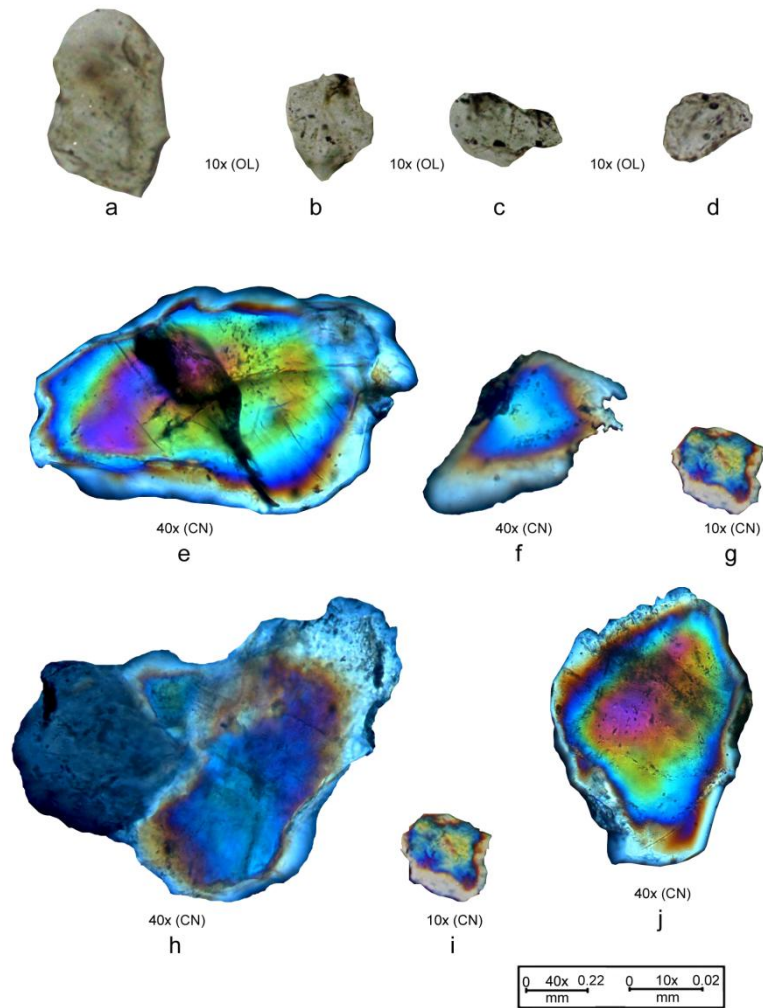
Plate 4.19: Heavy minerals in Upper Disang sandstone (a-j: scapolite)

Chapter 5

GEOCHEMISTRY

5.1   Basalt

Whole rock geochemistry of basalt aids in identification of the magmatic processes such as partial melting, crystallisation, magma mixing, assimilation, etc. It also serves as a potential tool on a quantitative basis in discriminating protolith evolution and tectonic setting.

Trace element distribution is a reliable guide in understanding the original nature of the rocks even when they are intensely metamorphosed. Goldschmidt (1937, 1954) and Wager *et al*. (1951) studied the behaviour of trace elements during fractional crystallisation of basic magma and opine that the entry of trace elements into a mineral is a function of their availability, chemical nature, ionic charge and ionic radius. Elements such as Co, Cr, Nb, Y, Zn, Zr and REE that are slightly mobile or immobile have been effectively used to determine the effect of alteration and low grade metamorphism (Cann, 1970; Thompson, 1973; Hart *et al*., 1974; Wood *et al*., 1976; Coish, 1977). Other trace elements including B, Ba, Cs, Cu, Ga, Li, Ni, Pb, Rb, Sr and V show minor to major variation with increasing metamorphism (Garcia, 1978).

Studies of origin of volcanic rocks using trace elements have been attempted by various workers. Jakes and Gill (1970) and Jakes and White (1972) compiled trace element data to characterise abyssal tholeiites as well as tholeiitic, calc-alkaline and shoshomitic rocks of island arcs. Pearce and Cann (1973) demonstrated the effectiveness of plots of Ti vs Zr and Y/Nb for discriminating magma types in recent basalts.

5.1.1   Major Elements

Major element oxides (wt %) of the NHO basalts (Table 5.1) indicate that they are saturated in SiO_2 (<52%) ranging from 46.27 to 51.87 (avg. 49.2%). The study area (Fig. 5.1) is characterised by intermediate to low Ti basalts (<2% TiO_2). P_2O_5 ranges from 0.05 to 0.21% (avg. 0.12%). The negative correlation of TiO_2 and P_2O_5 with MgO (r= -0.05 and r= -0.09 respectively) indicate enrichment of both oxides

Table 5.1: Major oxides of NHO basalt

Sample	Bs1	Bs2	Bs3	Bs4	Bs5	Bs6	Bs7	Bs8	Bs9	Bs10	Bs11	Bs12	Bs13	Bs14	Bs15	Bs16	Bs17	Bs18	Bs19
SiO_2	50.56	48.30	49.14	47.81	47.25	51.87	50.50	48.35	47.23	49.62	48.84	46.27	50.48	49.26	50.65	51.76	48.27	49.93	48.33
TiO_2	0.87	1.41	1.30	1.42	1.44	0.78	1.32	1.57	1.31	1.21	1.45	1.32	0.74	1.21	1.10	1.46	1.65	1.36	1.45
Al_2O_3	10.76	12.10	13.88	13.69	14.04	12.16	12.11	13.52	14.32	12.81	11.48	14.42	9.98	13.25	11.67	12.78	12.42	11.57	13.13
$Fe_2O_3{}^T$	9.12	11.30	12.78	11.12	12.28	10.62	11.57	12.33	12.22	10.21	9.87	11.72	8.65	11.86	9.95	11.16	11.42	11.29	12.21
FeO	6.98	8.66	9.77	8.50	9.37	8.12	8.85	9.43	9.35	7.81	7.55	8.96	6.62	9.07	7.61	8.54	8.73	8.63	9.34
$Fe_2O_3{}^*$	1.23	1.53	1.72	1.50	1.66	1.43	1.56	1.66	1.65	1.38	1.33	1.58	1.17	1.60	1.34	1.51	1.54	1.52	1.65
MnO	0.17	0.15	0.17	0.15	0.18	0.16	0.14	0.17	0.18	0.18	0.19	0.15	0.15	0.17	0.15	0.16	0.18	0.14	0.15
MgO	14.79	10.80	7.12	10.31	11.46	10.15	5.90	12.22	13.04	9.14	13.59	4.45	12.92	14.53	10.48	9.21	14.32	11.52	12.49
CaO	9.15	11.80	10.27	11.14	8.81	8.72	7.78	6.36	7.37	10.56	9.45	14.32	8.97	4.54	10.32	7.74	6.57	8.72	6.29
Na_2O	3.54	2.11	3.43	2.16	3.76	3.87	3.29	4.11	3.25	3.16	4.12	3.47	4.01	4.65	3.47	4.42	3.12	4.65	4.87
K_2O	0.89	0.76	1.12	0.34	0.50	0.27	1.25	0.25	0.55	0.67	0.31	0.19	0.14	0.32	0.87	0.61	0.28	0.35	0.58
P_2O_5	0.09	0.13	0.10	0.12	0.14	0.21	0.17	0.19	0.10	0.05	0.09	0.10	0.18	0.10	0.19	0.09	0.10	0.12	0.07

Total iron as $Fe_2O_3{}^T$

Recalculated iron as $Fe_2O_3{}^*$
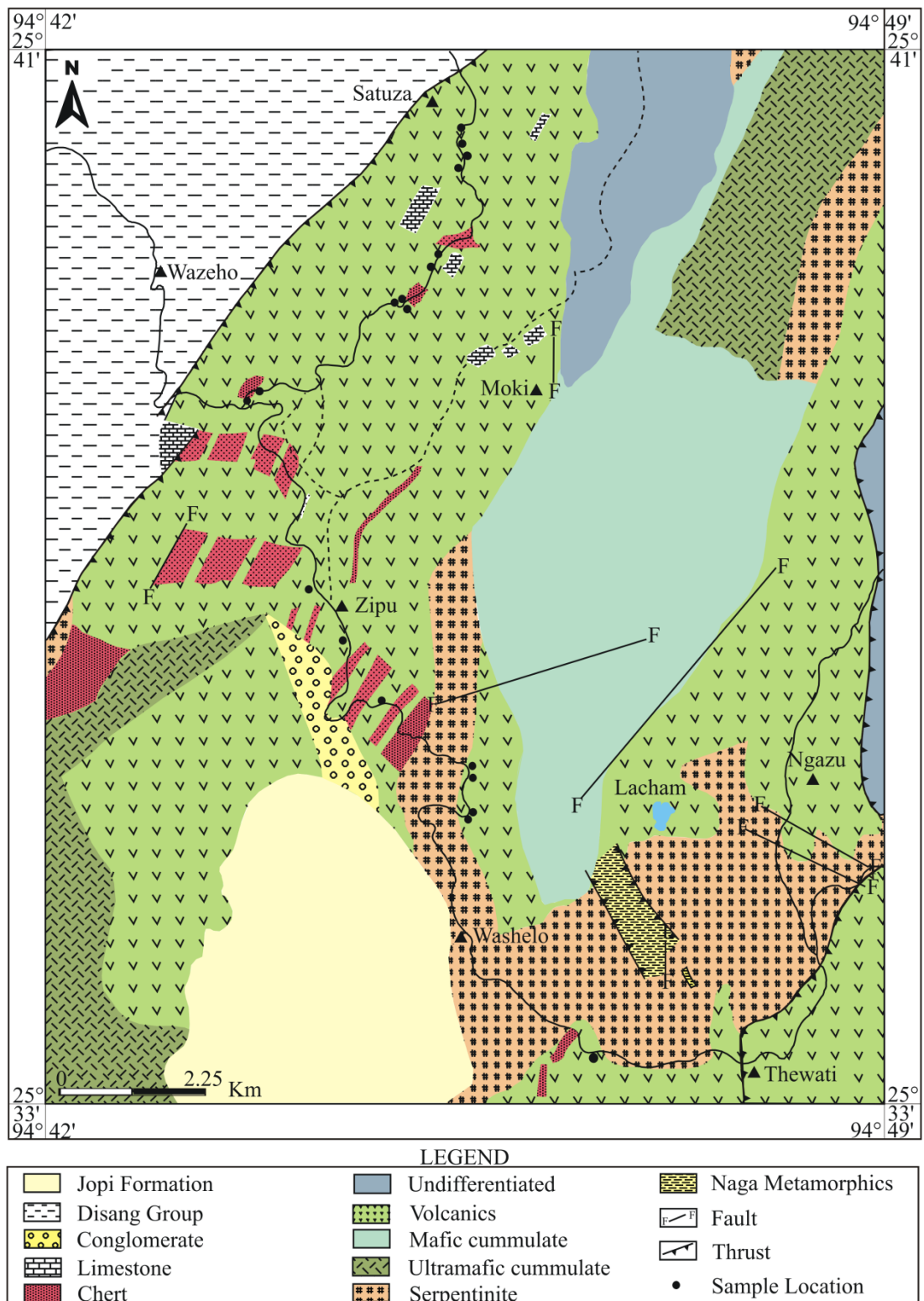
Fig. 5.1: Geological map of Zipu and adjoining areas with geochemical sample locations, Phek district (modified after GSI, 1986)

with decreasing MgO contents (Table 5.2). Al_2O_3 contents vary from 9.98 to 14.42 with an average of 12.63%. $Fe_2O_3{}^T$ values range from 8.65 to 12.78 (avg. 11.14%), CaO from 4.54 to 14.32 (avg. 8.88%) and MnO from 0.14 to 0.19 (avg. 0.16%). Both Mg rich (>10% MgO) as well as Mg poor (<10% MgO) basalts are noted in the NHO belt. MgO shows variable values ranging from 4.45 to 14.79 (avg. 10.96%) resulting in Mg numbers ($Mg_\# = 100 \times MgO/FeO + MgO$) from 33.18 to 66.12 (avg. 54). The NHO basalts have Na_2O and K_2O averages of 3.65% and 0.54% respectively. The total $Na_2O + K_2O$ values are very similar throughout the samples amounting to 4.20% on average. The average value of Na_2O/K_2O ratio is 9.80, reflecting their sodic affinity. The Al_2O_3/TiO_2 ratio average of 10.19% indicates basic affinity of the rock.

For nomenclature and identification of the basaltic magma series, total alkali and silica diagrams are plotted after Le Bas *et al*. (1986) (Fig. 5.2) and Middlemost (1994) (Fig. 5.3). The alkali content of the NHO basalt varies from 2.5 to 4.45 with an average of 4.19%.

Al_2O_3 abundance versus normative anorthite content in the plagioclase of NHO basalts are plotted (Fig. 5.4) after Irvine and Baragar (1971) in order to distinguish rocks of the tholeiitic and calc-alkaline series. The rationale behind this classification is that for any given normative plagioclase composition, calc-alkaline series rocks should have higher Al_2O_3 concentration than tholeiitic rocks. Data from NHO basalt shows lower Al_2O_3 values suggesting a tholeiitic composition of the basalt with an exception of a few samples evolving into the calc-alkaline field. Similarly, the tholeiitic nature is observed in the ternary $Na_2O + K_2O - Fe_2O_3{}^T - MgO$ (AFM) plots (Fig. 5.5) after Irvine and Baragar (1971). The NHO basalt shows a linear trend of progressive enrichment of iron which may be attributed to the early fractionation of magnesian olivine and other MgO-rich mafic minerals.

In order to examine the chemical behavior during the evolution of the basaltic magma of the NHO basalts, major oxides are plotted against SiO_2 (Fig. 5.6). SiO_2 contents bear negative correlation with Al_2O_3 ($r = -0.7$), Fe_2O_3 ($r = -0.52$), CaO ($r = -0.23$), MgO ($r = -0.03$) and TiO_2 ($r = -0.56$) which indicate the possibility of fractional crystallization of ferromagnesian minerals such as olivine and clinopyroxene in the magmatic evolution (Table 5.2).

SiO_2, TiO_2, Al_2O_3, FeO^T, CaO and P_2O_5 are plotted against MgO (Fig. 5.7). The negative correlation between MgO and CaO ($r = -0.59$) indicates depletion of Mg

41

Table 5.2: Correlation coefficient matrix (*r*)

r	SiO$_2$	MgO	Zr	MgO/FeO^T
SiO$_2$	1	0.031	0.037	-
TiO$_2$	-0.558	-0.056	-0.032	-
Al$_2$O$_3$	-0.659	-0.356	-0.193	-
Fe$_2$O$_3$	-0.526	-0.272	-0.296	-
MnO	-0.234	0.435	0.309	-
MgO	0.031	1.000	0.232	-
CaO	-0.226	-0.595	0.065	-
Na$_2$O	0.296	0.259	-0.392	-
K$_2$O	0.267	-0.355	-0.039	-
P$_2$O$_5$	0.319	-0.090	-0.277	-
Sc	0.031	0.084	0.035	0.190
V	-0.534	0.013	0.185	-0.100
Cr	0.046	0.811	0.081	0.755
Co	-0.298	0.333	0.239	0.273
Ni	-0.119	-0.045	0.207	0.060
Cu	-0.040	0.385	-0.109	-
Zn	-0.295	0.055	-0.306	-
Rb	-0.255	-0.059	0.301	-
Sr	0.122	0.091	0.326	-
Y	0.155	-0.055	0.486	-
Zr	0.037	0.232	1.000	-
Nb	-0.070	0.193	-0.252	-
Cs	-0.400	0.294	0.070	-
Ba	-0.353	-0.013	0.244	-
Hf	-0.441	0.273	0.384	-
Ta	0.172	0.241	0.103	-
Pb	0.016	0.064	0.196	-
Th	-0.032	0.131	-0.063	-
U	0.242	-0.055	-0.242	-
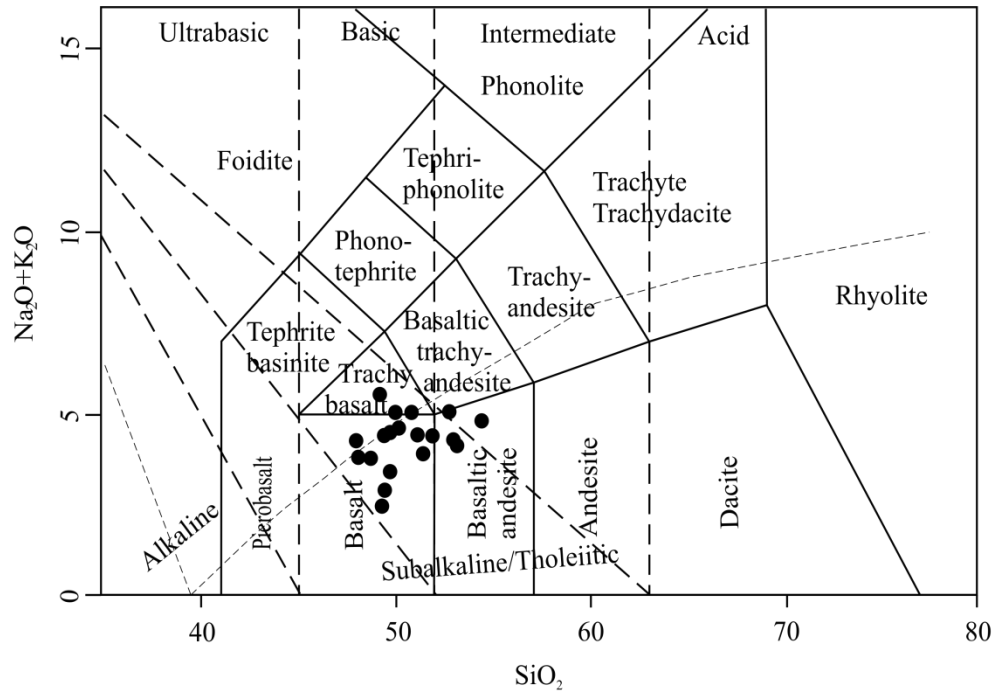
Fig. 5.2: Total alkali-silica classification of NHO basalt (after Le Bas *et al.*,
1986)
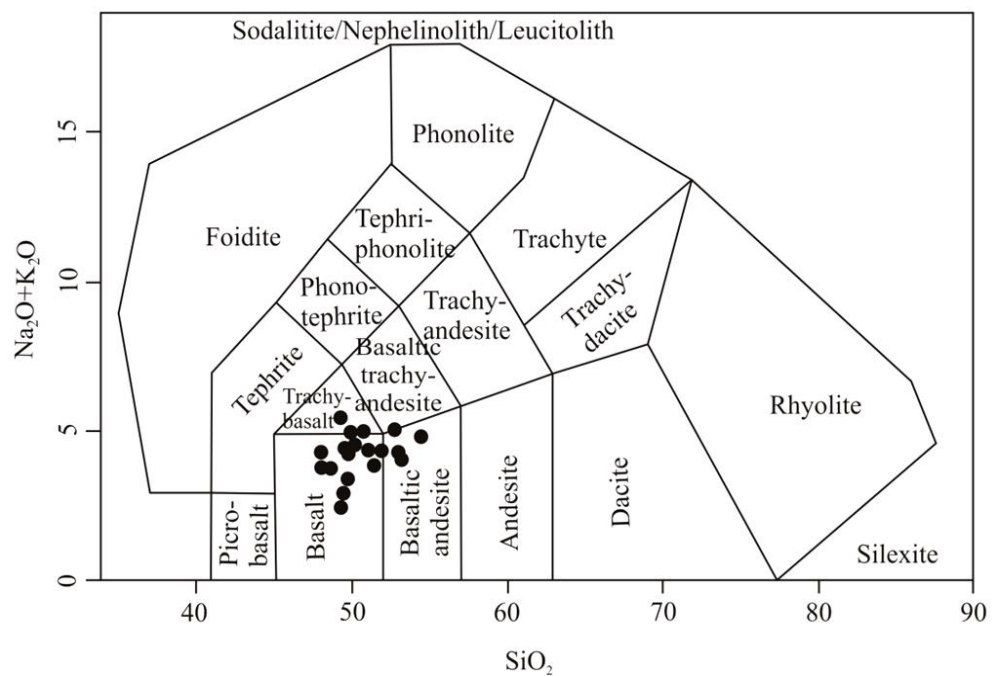
Fig. 5.3: Total alkali-silica classification of NHO basalt (after Middlemost,
1994)
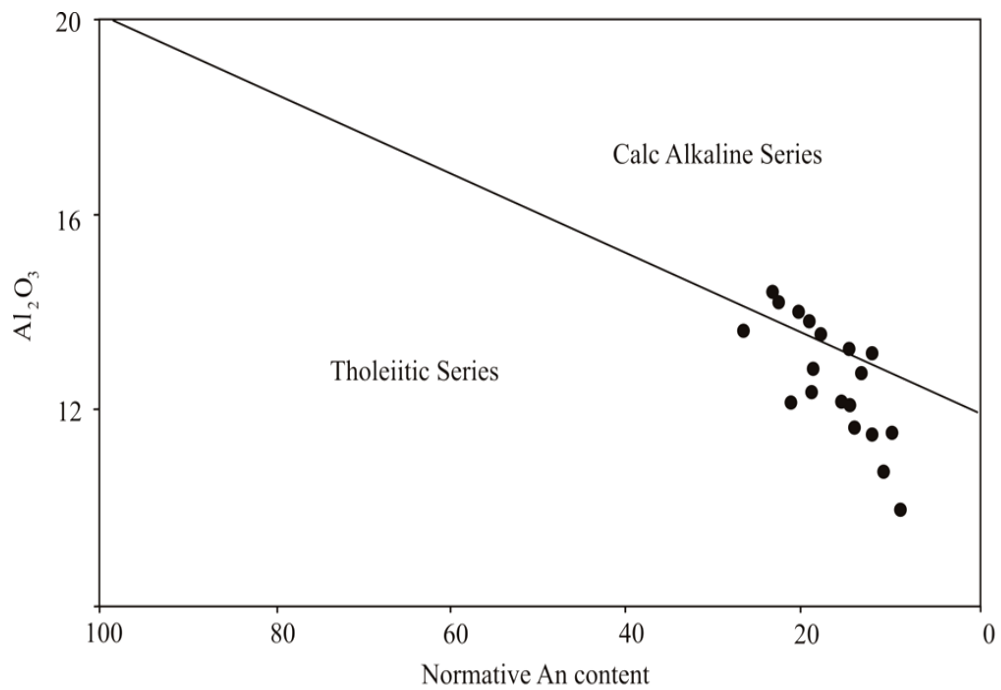
Fig. 5.4: Al$_2$O$_3$ vs normative anorthite in plagioclase of NHO basalt (after Irvine and Baragar, 1971)
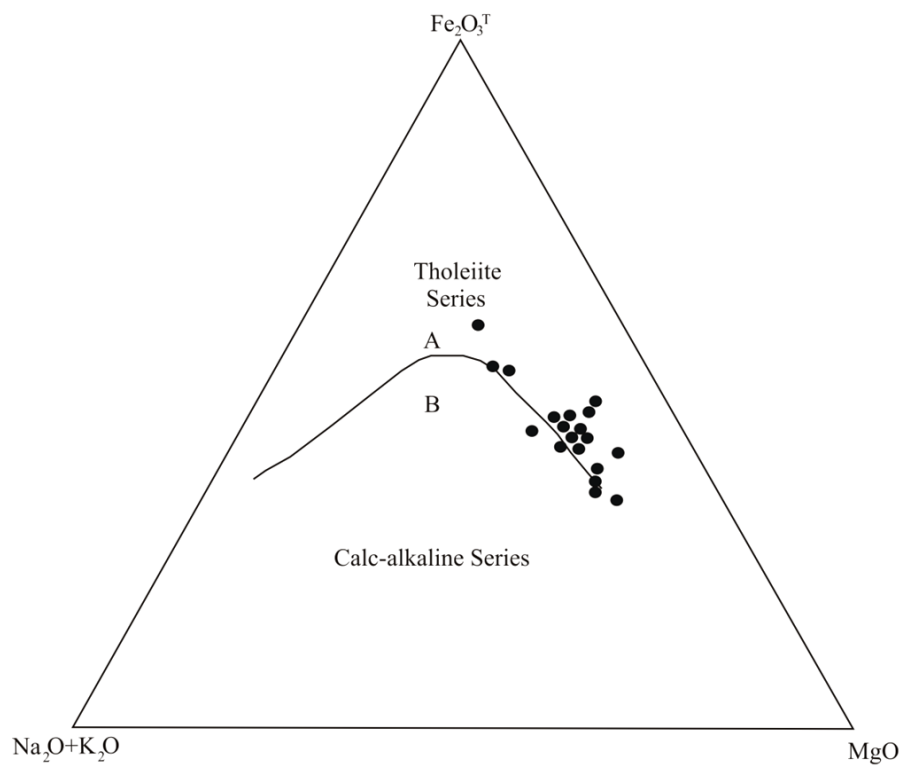
Fig. 5.5: Na$_2$O+K$_2$O-Fe$_2$O$_3^T$-MgO diagram of NHO basalts (after Irvine and Baragar, 1971)
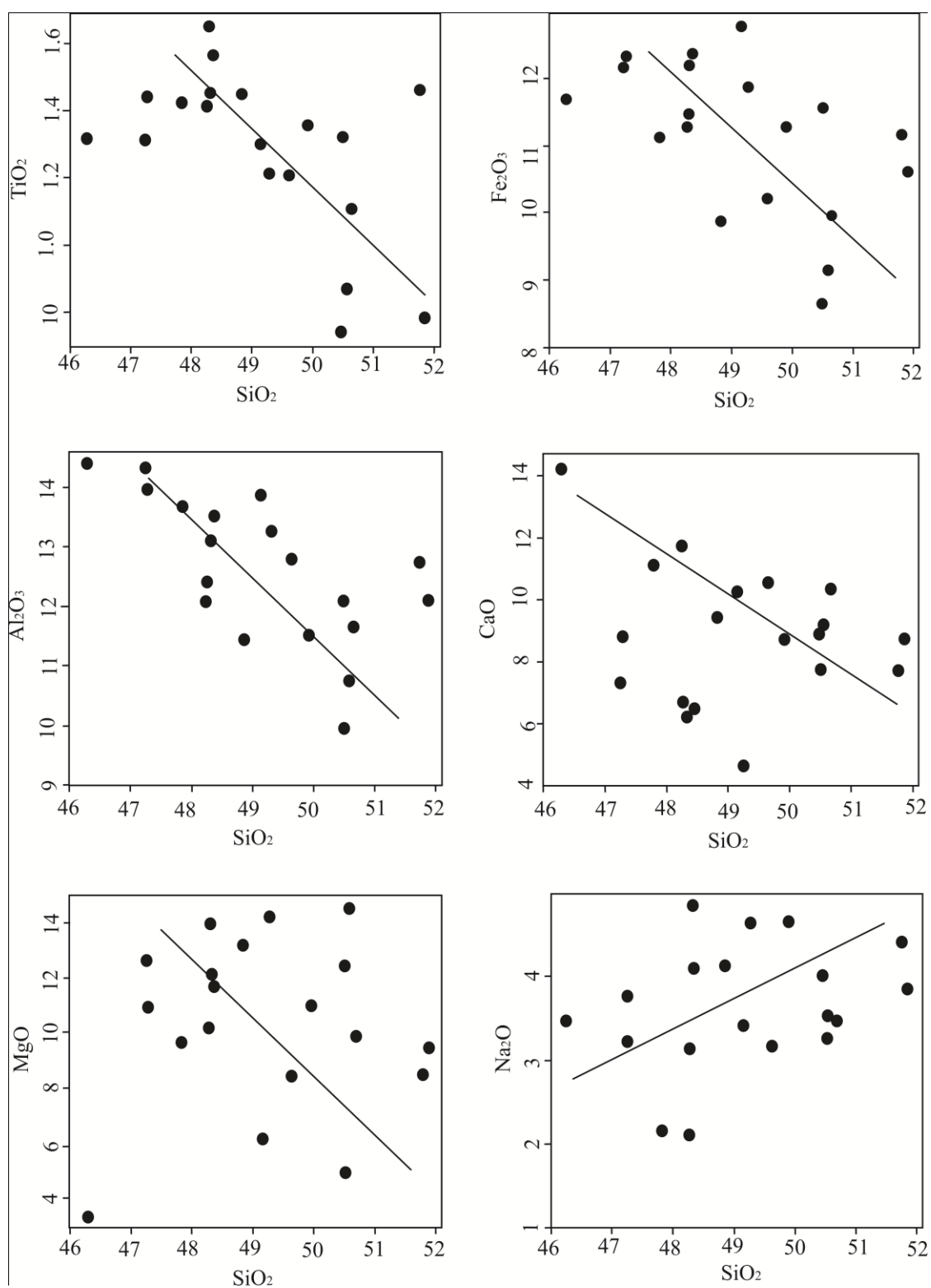
Fig. 5.6: Harker variation diagrams of SiO_2 vs major oxides
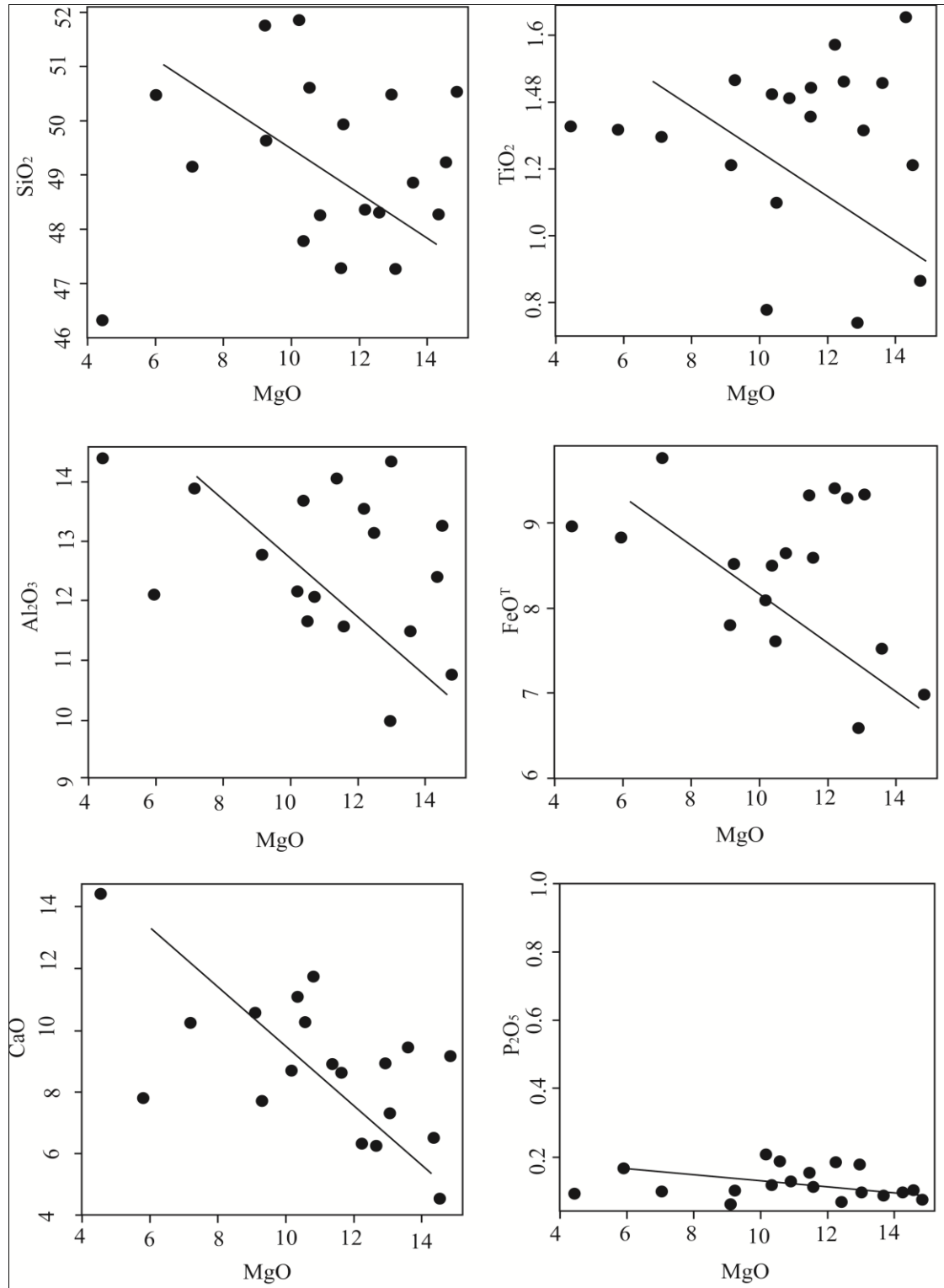
Fig. 5.7: Harker variation diagrams of MgO vs major oxides

in clinopyroxene with stability of Ca content (Sofy, 2003). The inverse correlation of P_2O_5 with MgO ($r= -0.09$) is related to the presence of apatite which is crystallized at a late stage from the magma differentiation process. There exists a negative correlation between MgO and TiO_2 and FeO^T. According to Reichow et $al.$ (2005) such relationships mean magnetite or titano-magnetite were not major fractionating phases. The NHO basalts show low FeO^T/MgO ratio (0.60-0.96, avg. 0.83) except for five samples (Bs 3, 7, 10, 12 and 16; 1.0 - 2.4, avg. 1.6); such high values according to Miyashiro (1974) and Miyashiro and Shido (1975) are a precursor of advanced fractional crystallisation.

Values of major oxides like SiO_2, TiO_2 and Al_2O_3 and Na_2O/K_2O ratios of NHO basalts resemble ocean floor basalts (OFB) rather than those of oceanic island basalts (OIB) (Table 5.3). Comparison of the major oxides of NHO basalts with that of N-MORB, E-MORB and OIB suggest that the NHO basalts coincide with values of E-MORB (Table 5.4). Most abyssal tholeiites show a FeO/MgO ratio of <1.7 whereas the majority of volcanic rocks in island arcs and continental margins have ratios of >1.7 (Miyashiro, 1974). In the NHO basalts these ratios vary from 0.3 to 1.5 (avg. 0.8) with an exception of Bs 12 (2.01) which is suggestive of abyssal tholeiites.

5.1.2 Trace Elements

The behaviour of trace elements during the evolution of magmas may be considered in terms of their partitioning between crystalline and liquid phases. Elements that are preferentially concentrated in the liquid phase are termed *incompatible* while those preferentially retained in the mineral phase are *compatible*. Trace element partition and preference for the liquid or melt phase vary widely, which helps identify the magmatic processes. Accordingly, an attempt is made to study trace elements characteristics and evaluate petrogenetic models.

Analytical results of trace element (ppm) of the NHO basalts (Table 5.5) show variation of Sc from 33-47 (avg. 38.7), Cr from 85-303 (avg. 208), Co from 46-94 (avg. 70.68), Ni from 33-140 (avg. 77), Rb from 1.5-53.4 (avg. 18.32), Y from 16.2-37.6 (avg. 28.53), Zr from 37.2-75.1 (avg. 52.6), Hf from 0.8-2.2 (avg. 1.57), Nb from 1.2-13.9 (avg. 5.33), Pb from 2.4-5.9 (avg. 3.2), Ba from 17-160 (avg. 67.5), Th from 0.1-1.2 (avg. 0.44) and U from 0.1-0.3 (avg. 0.15). Pearce and Cann (1973) opine that Y/Nb ratio <1 indicate alkali magmas while Y/Nb >1 are typical of calc-alkaline and

Table 5.3: Comparison of major oxides of NHO Basalt with island arc tholeiites and ocean floor tholeiites

Major oxides (wt %)	Island Arc Tholeiites (IAT)	Ocean Floor Tholeiites (OFT)	NHOB
SiO_2	45 - 70 (avg. 53)	47 - 62 (avg. 49)	46.27-51.87 (avg. 49.20)
TiO_2	0.3 - 1.2	0.3 - 2.5	0.74-1.65 (avg. 1.28)
Al_2O_3	14 - 19	14 - 19	9.98-14.42 (avg.12.63)
Na_2O/K_2O	4 - 6	10 - 15	2.63-28.64 (avg. 9.82)

Table 5.4: Comparison of major oxides of NHO basalt with N-MORB, E-MORB and OIB

Oxides	NHOB			N-MORB	E-MORB	OIB
	Minimum	Maximum	Average	Average	Average	Average
SiO_2	46.27	51.87	49.2	50.53	49.98	48.07
TiO_2	0.74	1.65	1.28	1.56	1.99	3.12
Al_2O_3	9.98	14.42	12.63	15.27	15.11	16.87
FeO	6.62	9.77	8.52	10.46	11.04	11.18
MnO	0.14	0.19	0.16	-	-	-
MgO	4.45	14.79	10.96	7.47	6.87	5.69
CaO	4.54	14.32	8.89	11. 49	11.25	10.22
Na_2O	2.11	4.87	3.65	2.62	2.81	3.46
K_2O	0.14	1.25	0.54	0.18	0.47	1.39
P_2O_5	0.05	0.21	0.12	0.13	0.32	-

Table 5.5: Trace elements (ppm) of NHO basalt

Sample	Sc	V	Cr	Co	Ni	Cu	Zn	Rb	Sr	Y	Zr	Nb	Cs	Ba	Hf	Ta	Pb	Th	U
Bs1	41	156	303	88	43	131	101	10.3	333	16.2	62.8	3.5	0.1	33	1.5	1.1	4.4	0.1	0.2
Bs2	45	275	218	72	120	78	156	53.4	91	29.9	56.2	6.2	2.6	112	1.9	2.1	5.9	0.2	0.2
Bs3	35	321	172	68	76	123	109	9.5	156	35.4	64.1	6.6	0.1	160	1.8	0.9	3.2	0.1	0.2
Bs4	33	325	198	51	66	58	113	15.3	495	37.2	62.5	4.1	1.5	126	1.9	1.8	3.4	1.2	0.1
Bs5	33	345	249	70	46	88	127	21.2	87	23.6	39.7	1.6	0.6	128	1.5	0.7	2.7	0.3	0.1
Bs6	33	221	212	46	54	111	113	8.5	260	18.1	43.8	5.8	0.3	20	0.8	2.3	2.7	0.3	0.2
Bs7	34	237	127	56	62	72	104	24.6	93	24.8	37.2	3.3	0.1	41	0.8	0.9	4.2	0.2	0.2
Bs8	33	265	221	65	77	83	120	22.0	35	27.6	55.3	4.0	0.7	34	2.1	0.8	4.2	0.5	0.2
Bs9	37	255	254	93	63	141	115	8.6	23	19.7	52.7	7.3	2.1	18	1.2	2.6	2.6	0.4	0.1
Bs10	41	247	175	90	118	38	111	13.2	71	37.6	72.3	5.5	0.5	83	1.8	0.9	2.9	0.4	0.1
Bs11	37	234	182	76	123	99	131	3.2	72	24.4	46.7	3.3	1.1	55	1.5	1.1	2.6	1.2	0.1
Bs12	44	312	85	68	88	71	174	22.1	57	19.5	39.5	3.7	0.5	50	1.6	1.2	2.5	0.2	0.1
Bs13	46	347	243	60	110	99	160	16.8	92	34.7	69.4	1.2	1.2	20	1.6	2.4	3.8	0.1	0.1
Bs14	44	324	272	62	47	86	178	3.2	121	29.9	38.8	13.6	1.1	147	2.1	1.1	3.5	0.2	0.1
Bs15	41	272	258	72	72	83	132	1.5	40	34.2	41.2	3.5	0.4	17	1.1	2.6	2.4	1.2	0.2
Bs16	42	198	112	66	33	51	125	26.8	102	35.7	55.2	4.8	0.4	44	1.6	1.4	2.4	0.5	0.1
Bs17	35	382	212	78	78	76	121	50.3	175	35.5	75.1	3.2	0.5	133	1.8	2.4	2.6	0.5	0.1
Bs18	35	235	219	68	140	91	130	12.4	49	32.8	42.6	6.2	1.1	44	1.2	2.8	2.5	0.5	0.2
Bs19	47	272	234	94	47	122	151	25.3	48	25.3	45.3	13.9	0.5	19	2.2	1.2	2.5	0.3	0.3

tholeiitic basalts. In the present study Y/Nb ratios for all the samples are >1 (1.8-28.9; avg. 7.6), which are characteristics of calc-alkaline and tholeiitic basalts.

Harker variation diagrams of selected trace elements (Sr, Ba, Nb, Th, Rb and Zr) are plotted against SiO_2 (Fig. 5.8). Elements such as Ba (r= -0.35), Th (r= -0.03), Rb (r= -0.25) and Nb (r= -0.07) show negative correlation with SiO_2 while Sr (r= 0.12) and Zr (r= 0.03) show low positive correlation (Table 5.2). Scattering of data may be attributed to metamorphism and/or secondary alteration of the samples.

Based on field evidences and petrographic studies the NHO basalts have undergone low-grade metamorphism or late hydrothermal alterations. Thus the large ion lithophile elements (LILE) such as Rb, Cs, Ba, Sr, K, etc., may be mobile (Pearce and Cann, 1971, 1973; Rollinson, 1993). Accordingly Zr which is considered to be relatively immobile has been correlated with major and trace elements to determine their degree of remobilization and fractionation. With differentiation, that is, with increasing Zr, TiO_2, CaO and K_2O increase while Na_2O, MgO and P_2O_5 decrease (Fig. 5.9) suggesting primary fractionation of plagioclase and pyroxene during magma evolution. This is further corroborated by low SiO_2, high MgO (>7%) for most of the samples except for Bs 3, 7, 10, 12 and 16 and ΣFeO (>11%) which are distinctive criteria for the slightly fractionated nature of the NHO basalt (Table 5.1). The positive correlation of compatible elements such as Ni, Cr, Co and V with MgO/FeO^T ratios (Fig. 5.10) may be related to fractional crystallization of olivine and clinopyroxene.

Geochemical plots of Zr/Ti vs Nb/Y after Pearce (1996) indicate that the volcanics from the study area are mostly basalt (Fig. 5.11). The basalts exhibit a predominantly sub-alkaline character in the SiO_2 vs Zr/TiO_2 plots (Fig. 5.12) following Winchester and Floyd (1977). Values of trace elements substantiate the tholeiitic character of these basalts as indicated by the TiO_2 vs $Zr/P_2O_5 \times 10^4$ diagram (Fig. 5.13) of Winchester and Floyd (1976). A few samples fall in the alkaline field, which may be due to seawater alteration as these samples have unusually high Na_2O contents (Table 5.1).

The five (5) REE and their corresponding trace elements are normalized to the primitive mantle composition (Sun and McDonough, 1989) to understand the degree of evolution relative to the mantle. The primitive mantle-normalized spider diagram (Fig. 5.14) of the basalts is plotted from left to right in order of increasing compatibility. The diagram shows variable and selective incompatible-element

43
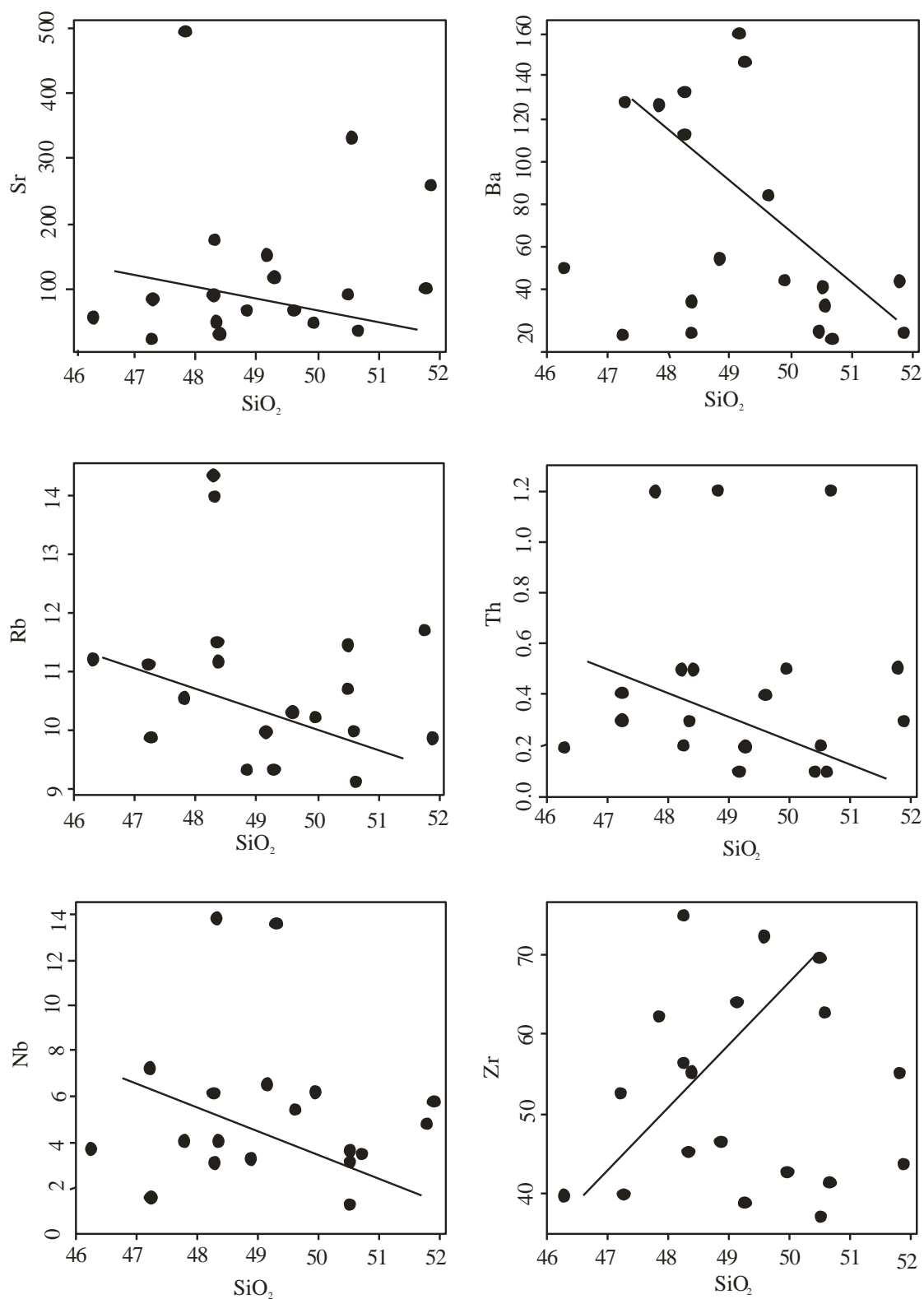
Fig. 5.8: Harker variation diagram of SiO_2 vs trace elements
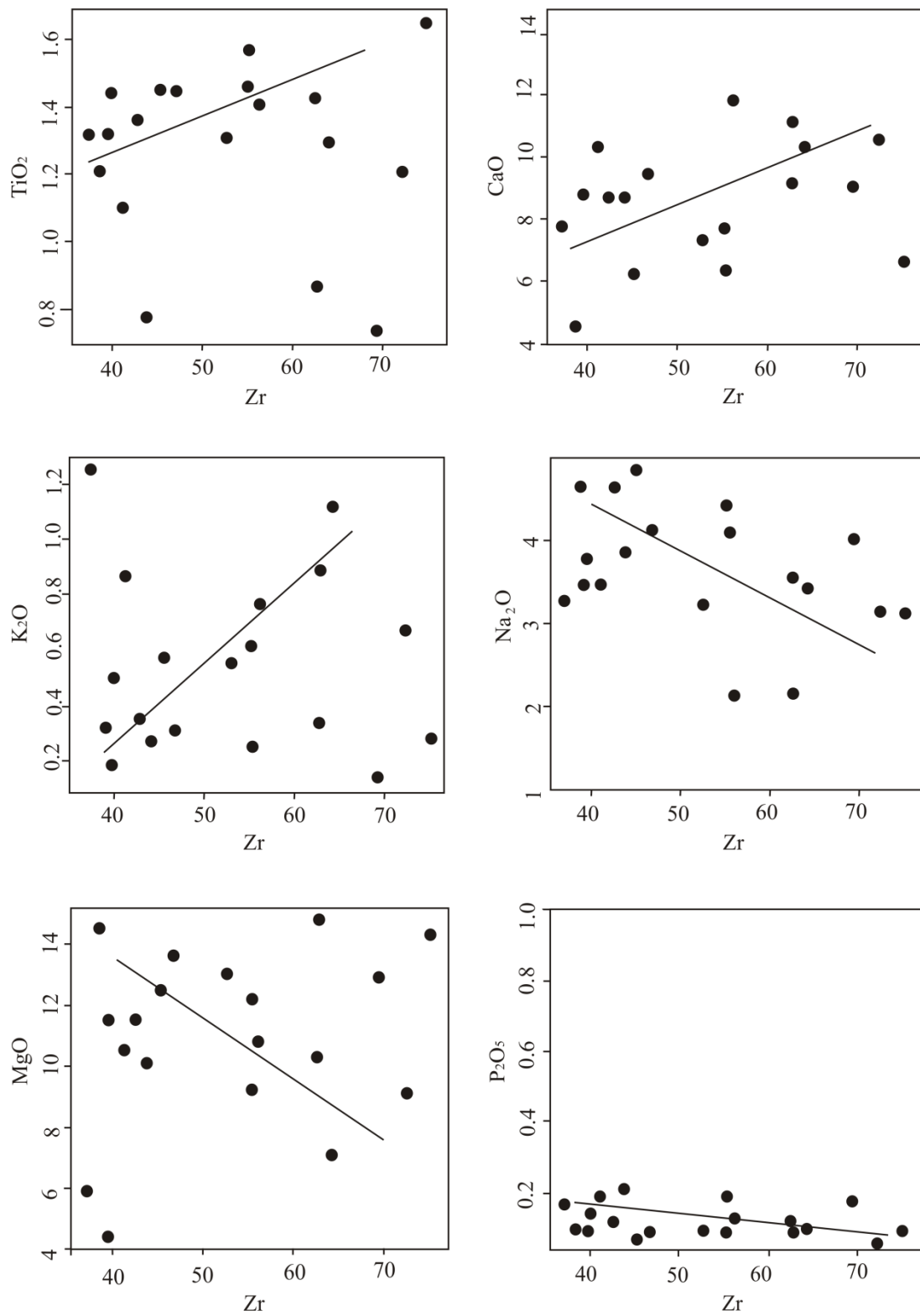
Fig. 5.9: Harker variation diagrams of Zr vs major oxides
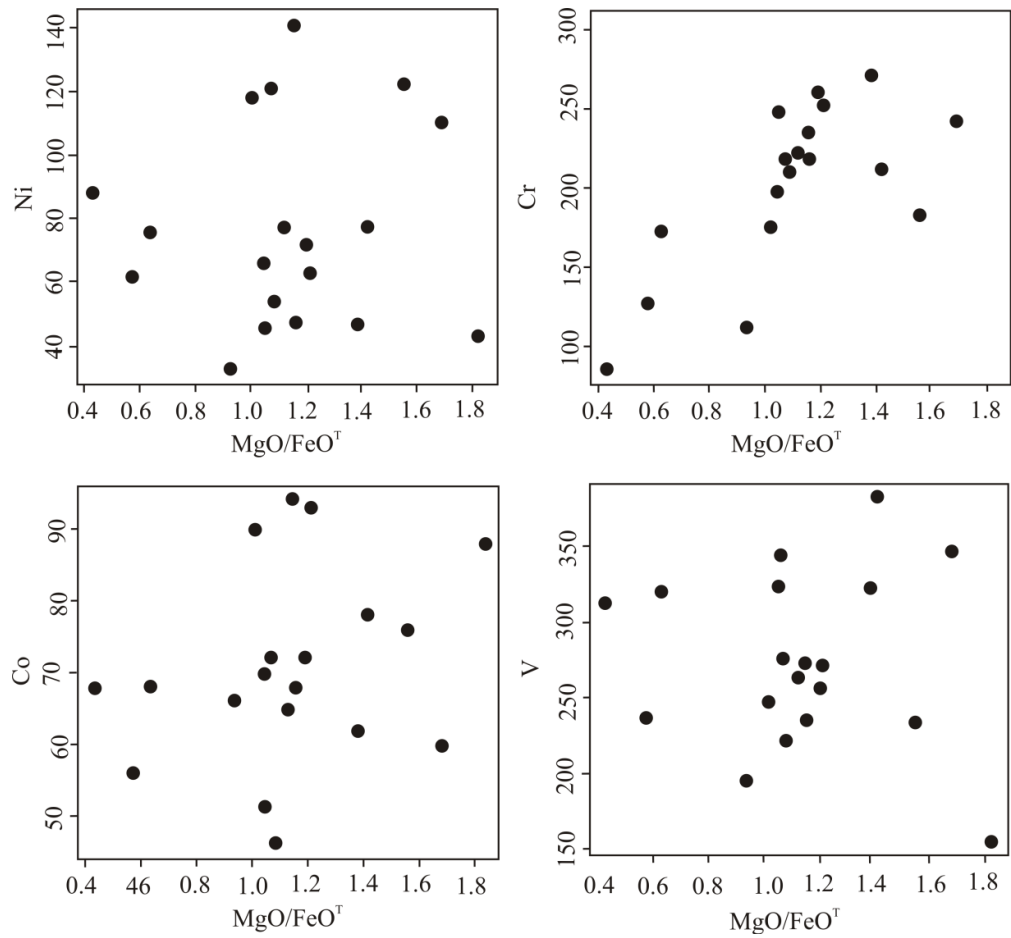
Fig. 5.10: Harker variation diagrams of MgO/FeO^T vs compatible elements
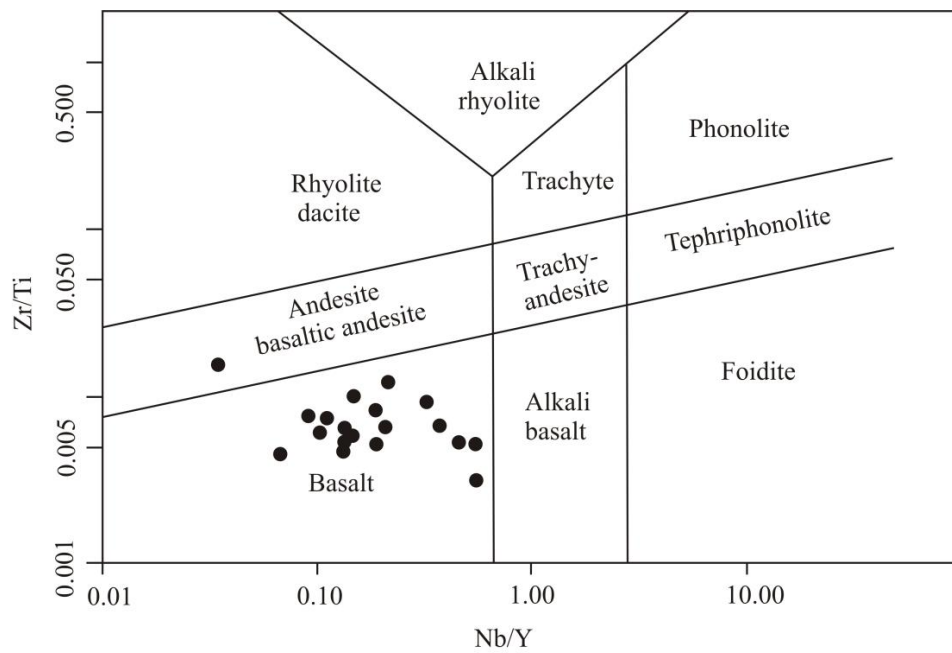
Fig. 5.11: Zr/Ti vs Nb/Y chemical classification plot (after Pearce, 1996)
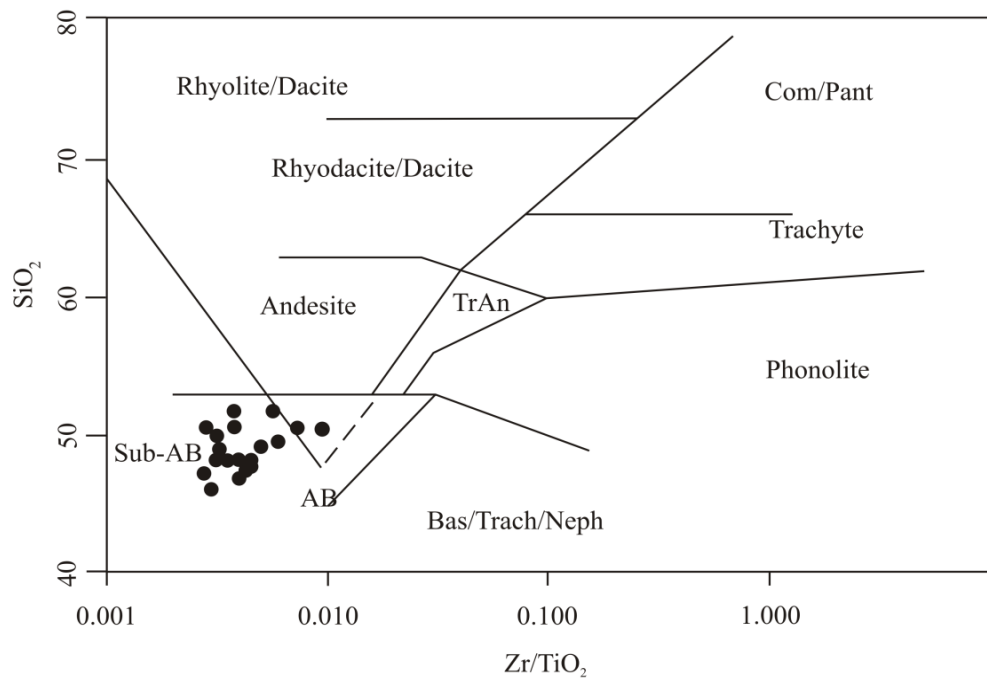
Fig. 5.12: Zr/TiO$_2$ vs SiO$_2$ bivariate plot of NHO basalt (after Winchester and Floyd, 1997)
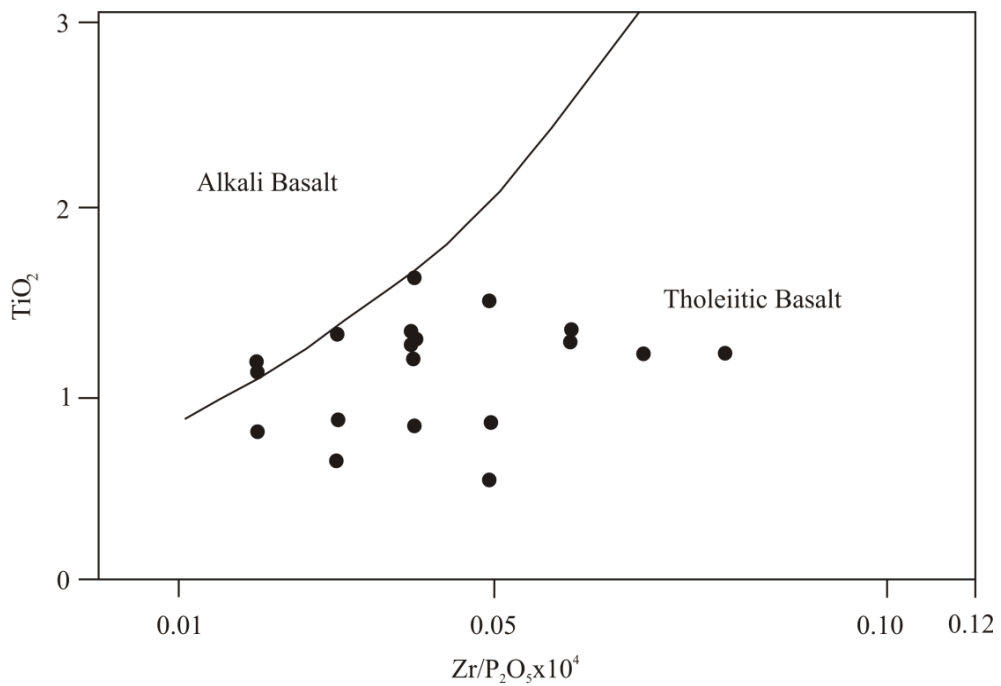
Fig. 5.13: Zr/P$_2$O$_5$x10^4 vs TiO$_2$ composition plot of NHO basalt (after Winchester and Floyd, 1976)

enrichment, particularly of LILE. The basalts also show higher concentrations of Cs, Rb, Ba and Sr. A distinctive spiked pattern for K and Pb and pronounced trough at Th, Nb, La and Ce are noted. The REE and trace element plots (Fig. 5.15) of the same basalt samples normalized to N-MORB (Sun and McDonough, 1989) show enrichment of LILE relative to high-field-strength elements (HFSE).

Most of the NHO basalts show enrichment of Ba, Th, Nb, Sr and Zr relative to N-MORB, suggesting derivation of a parental melt of these basalts from an enriched mantle source similar to E-MORB or a source which has experienced a small degree of melting (Table 5.6).

Ti and V behave like pseudo-incompatible elements, their contents increasing with greater fractional crystallisation. Similarly, Sr is higher in more evolved volcanic magmas. Sr contents vary from 23-495 (avg. 126.3 ppm) which is relatively higher than N-MORB (90 ppm).

5.1.3   Rare Earth Elements

The naturally occurring REE have similar chemical and physical properties and are regarded as the least soluble trace elements that are relatively immobile during low-grade metamorphism, weathering and hydrothermal alteration. The behaviour of REE is controlled by a number of petrogenetic processes which can cause them to fractionate relative to each other. Samples analysed are used to infer the role of minerals during magmatic evolution.

The total REE content of the NHO basalts (Table. 5.7) varies from 36.1-54.9 with an average of 45.5 ppm. Fractionation ratio of LREE/HREE varies from 1.07-1.84 (avg. 1.52). Chondrite normalised $(La/Yb)_N$ ratios vary from 1.07-2.32 (avg. 1.70), $(La/Sm)_N$ from 0.83-3.16 (avg. 1.76), $(Gd/Yb)_N$ from 0.85-1.36 (avg. 1.10), $(La/Ce)_N$ from 0.63-2.64 (avg. 1.23) and $(Ce/Yb)_N$ from 0.83-2.07 (avg. 1.47).

Ophiolites are generated in different oceanic environments such as MORB, back-arc and fore-arc basins, leaky transform faults and immature island arcs (Shervais, 2001). The evolution of ophiolites in different oceanic environments gives rise to considerable geochemical and petrological complexities due to mantle heterogeneities, magma mixing, contamination, fractional processes, etc. Considering these features REE abundances are normalized to N-MORB (Sun and McDonough, 1989) and plotted (Fig. 5.16). The distribution pattern displays slight LREE enrichment and almost flat middle and heavy REE patterns with nominal Eu-anomaly.

Table 5.6: Comparison of NHO basalt with island arc tholeiite and ocean floor tholeiite

Trace elements	Island arc tholeiite (ppm)	Ocean floor tholeiite (ppm)	NHO basalt (ppm)
Rb	3.00 - 10.00	0.20 - 5.00	1.5 - 53.4 (avg. 18.33)
Sr	100.00 - 200.00	70.00 -150.00	23 - 495 (avg. 126.32)
Ba	50.00 - 150.00	6.00 - 30.00	17 - 160 (avg. 67.58)
Pb	2.00 - 4.00	0.50	2.4 - 5.9 (avg.3.21)
Cs	0.10	0.05	0.1 - 2.6 (avg.0.81)
Th	0.50	0.15	0.1 - 1.2 (avg. 0.44)
U	0.30	0.10	0.1 - 0.3 (avg.0.15)
Ni	0.00 - 30.00	30 - 200	33 - 140 (avg.77.0)
Cr	0.00 - 150.00	100 - 500	85 - 303 (avg. 207.68)
La	1.00 - 6.00	2.00 - 8.00	3.1 - 5.7 (avg. 4.26)

Table 5.7: Rare earth elements of NHO basalt (ppm)

Sample	Bs2	Bs8	Bs11	Bs16	Bs17
La	5.70	3.50	3.10	4.80	4.20
Ce	12.90	8.50	8.00	11.80	9.90
Pr	1.90	1.20	1.10	1.70	1.50
Nd	10.30	7.30	6.80	9.40	7.90
Sm	3.40	2.40	2.30	3.20	2.60
Eu	1.40	1.00	0.90	1.30	1.10
Gd	4.90	3.70	3.30	4.30	4.20
Tb	0.90	0.70	0.60	0.80	0.80
Dy	4.90	4.20	3.90	5.20	5.20
Ho	1.10	0.80	0.70	1.00	0.90
Er	3.10	3.10	2.40	3.30	3.20
Tm	0.60	0.50	0.40	0.60	0.50
Yb	3.10	2.70	2.20	2.90	3.10
Lu	0.70	0.50	0.40	0.80	0.60
ΣREE	54.90	40.10	36.10	51.10	45.70
Eu*	1.04	1.02	0.99	1.06	1.01
LREE/HREE	1.65	1.33	1.44	1.53	1.33
$(La/Yb)_N$	2.24	1.58	1.72	2.02	1.65
$(La/Sm)_N$	1.76	1.53	1.42	1.58	1.70
$(Gd/Yb)_N$	1.31	1.14	1.24	1.23	1.12
$(La/Ce)_N$	1.32	1.23	1.16	1.22	1.27
$(Ce/Yb)_N$	1.69	1.28	1.47	1.65	1.29
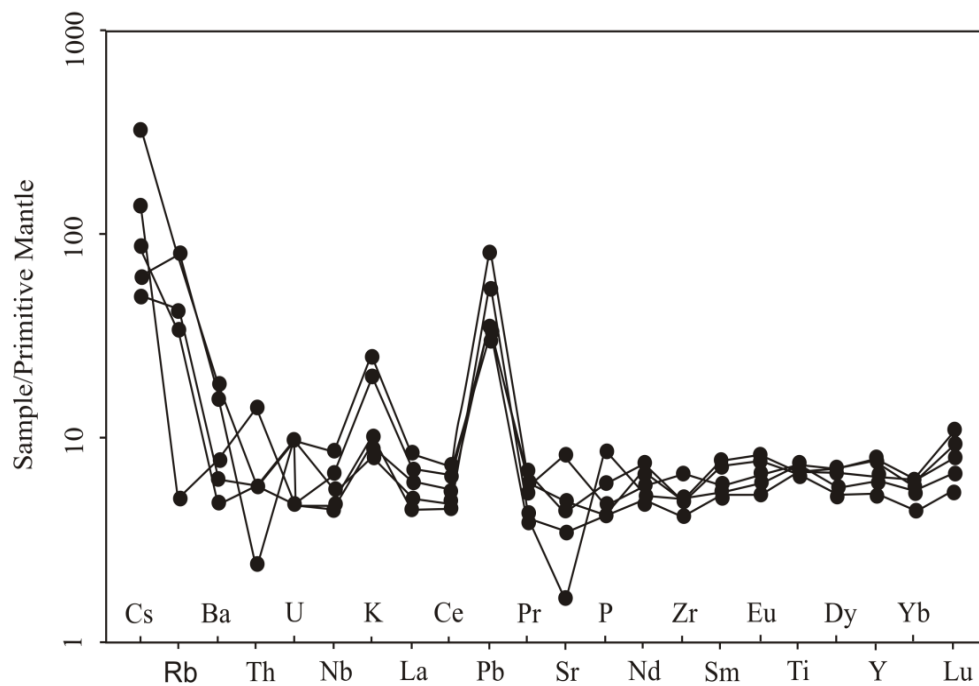
Fig. 5.14: Primitive mantle normalised spidegram of NHO basalt (after Sun and McDonough, 1989)

Fig. 5.15: N-MORB normalised spidergram of NHO basalt (after Sun and McDonough, 1989)
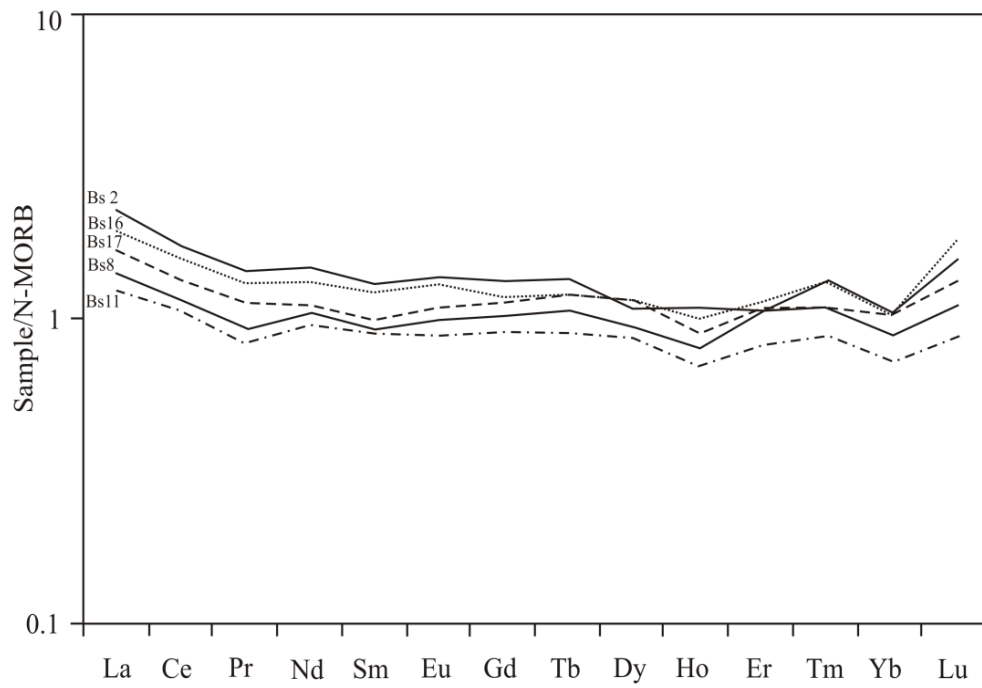
Fig. 5.16: N-MORB normalised REE diagram of NHO basalt (after Sun and McDonough, 1989)

The REE are compared with those of N-MORB, E-MORB and OIB; resemblance is noted with that of MORB, particularly E-MORB (Table 5.8).

5.2 Upper Disang

Large-scale chemical and mechanical fractionation give rise to sediments that are chemically homogenous products. Complex interaction of variables such as provenance, weathering, transportation and diagenesis give terrigenous sedimentary rocks a definite geochemical composition. Besides, geochemical studies also give an idea of the redistribution of the elements during and after deposition (Bhatia, 1983). Crook (1974), Schwab (1975) and Dickinson and Suczek (1979) showed strong relationships amongst sediments, provenance type and tectonic setting of sedimentary basins. Their composition therefore helps understand their evolution and the associated geochemical processes (Pettijohn, 1984; McLennan and Taylor, 1991). (Kukal, 1968) has identified excellent chemical indicators for petrographic composition of sandstones that include TiO_2, Al_2O_3, Fe_2O_3, Na_2O and K_2O.

Argast and Donnelly (1987) defined tectonic and sedimentary environments through geochemical studies. Bhatt and Ghosh (2001) used sediment geochemistry to determine compositions of source rocks. Nesbitt and Young (1982) and Fedo *et al*. (1995) used the same to evaluate the weathering processes and paleoclimate at the provenance. Bhatia (1983), Bhatia and Crook (1986), Naqvi *et al*. (1988) and Banerjee and Bhattacharya (1994) reconstructed tectonic setting of depositional basins while McLennan *et al*. (1993) used geochemical data to understand sorting and diagenesis. Condie (1993) and McLennan and Taylor (1980) opine that geochemistry aids in determination of the composition and evolution of the continental crust. Geochemical approaches are also more advantageous because they are applicable to both coarse and fine grained rocks and those mineralogically altered but where bulk chemistry was not substantially affected. Hence, geochemical data are used to determine provenance, tectonic setup, depositional conditions and weathering intensity prevailing in the detrital system.

5.2.1 Major Elements

Major element compositions are effectively used to make inferences on the original detrital constituents though post depositional processes may have altered the

Table 5.8: Comparison of trace and rare earth elements of NHO basalt (ppm) with N-MORB, E-MORB and OIB

Elements	NHOB			N-MORB	E-MORB	OIB
	Minimum	Maximum	Average	Average	Average	Average
Rb	1.50	53.4	18.33	0.60	5.00	31.0
Ba	170	160	67.58	6.30	57.00	350
Th	0.10	1.2	0.44	0.10	0.60	4.00
V	156	382.0	274.89	0.50	0.20	1.00
Nb	1.20	13.9	5.33	2.30	8.30	48.00
Ta	0.70	2.80	1.59	0.10	0.50	2.70
La	3.10	5.70	4.26	2.50	6.30	37.00
Ce	8.00	12.90	10.22	7.50	15.00	80.00
Sr	23.00	495.0	126.31	90.00	155.00	660.00
Nd	6.80	10.30	8.34	7.30	9.00	38.50
Sm	2.30	3.40	2.78	2.60	2.60	10.00
Zr	37.20	75.10	52.65	74.00	73.00	280.00
Hf	0.80	2.20	1.58	2.10	2.00	7.80
Eu	0.90	1.40	1.14	1.00	0.90	3.00
Gd	3.30	4.90	4.08	3.70	3.00	7.60
Y	16.20	37.60	28.53	28.00	22.00	29.00
Lu	0.40	0.80	0.60	0.60	0.40	0.30
∑REE	36.90	54.90	45.58	39.10	49.10	199.00

rock. Bulk chemical compositions are useful in understanding paleoclimate and chemical maturity of rocks (Potter, 1978; Suttner and Dutta, 1986). Various ratios of the detrital fractions help understand provenance. Geochemical studies of the Upper Disang rocks have been carried out from Pfutsero and its adjoining area (Fig. 5.17).

Major element data (Table 5.9a,b) indicate that the Upper Disang sandstone and shale are enriched in SiO_2 relative to PAAS showing overlapping abundances ranging from 62.70 to 75.89 with an average of 66.01%. Al_2O_3 contents of sandstone range from 11.42 to 15.62 whereas shale shows higher concentrations with an average of 17.10%. Major elements (average) normalized to PAAS values after Taylor and McLennan (1985) and plotted in a multi-element diagram (Fig. 5.18) indicate enrichment of Fe_2O_3 and MgO with slight enrichment in SiO_2 and depletion of TiO_2, Na_2O, CaO and K_2O suggesting a mixed provenance and intense weathering at the source.

Progressive increase in K_2O/Na_2O ratio from shale to sandstone depicts sorting of the sediments (Table 5.10a,b). The negative correlation coefficient of Al_2O_3 and Na_2O in the shale ($r=$ -0.92) suggests that the distribution of sodium is not controlled by a mineral phase such as plagioclase while sandstone (Table 5.11a,b) shows a positive correlation ($r=0.77$). There exists a moderate negative correlation between SiO_2 and CaO ($r=$ -0.77 and -0.19 for sandstone and shale respectively). Such values, according to Feng and Kerrich (1990), suggest that the detrital grains and matrix in all the samples are primary rather than secondary.

K_2O/Al_2O_3 ratios of sediments can be used as indicators of the original composition of source rocks. K_2O/Al_2O_3 ratios for clay minerals and feldspars are different (0.0-0.3 and 0.3-0.9 respectively) according to Cox *et al.* (1995). In the present study K_2O/Al_2O_3 ratio ranges from 0.01 to 0.22 (Table 5.10a,b) which suggests that illite is the dominant clay mineral. Al_2O_3-K_2O plots show that all samples lie close to the illite line (Fig. 5.19) suggesting that major K_2O and Al_2O_3 bearing minerals in the samples are illite. The high positive correlation coefficient between Al_2O_3 and K_2O in the sandstone ($r=$ 0.77) also attest to clay mineral control over the major element composition while negative correlation ($r=$ -0.06) in shale may be due to other factors. The positive correlation between Al_2O_3 and TiO_2 in the sandstone and shale ($r=$ 0.2 and 0.89 respectively) suggest that Ti is mainly contained in phyllosilicates (Condie *et al.*, 1992; Asiedu *et al.*, 2000). Al_2O_3/K_2O ratios range from 6.58 to 15.61 which suggest that considerable Ti-bearing mafic phases such as

Table 5.9a: Major elements of Upper Disang sandstone

Sample	UD29	UD32	UD36	UD37	UD38	UD39	UD40	UD44	UD46	UD52	UD54	UD56	UD57	UD61	UD76
SiO_2	67.64	69.24	75.22	74.55	74.89	67.64	64.27	66.10	65.33	63.08	63.24	63.16	66.93	66.27	75.89
Al_2O_3	14.93	13.88	11.74	12.05	11.90	11.98	13.50	13.55	14.55	15.06	15.62	15.34	13.74	14.55	11.42
Fe_2O_3	8.94	8.69	6.81	7.09	6.95	7.02	10.77	10.32	8.86	9.09	9.06	9.08	9.61	9.66	6.52
MnO	0.09	0.07	0.04	0.05	0.05	0.04	0.35	0.23	0.14	0.10	0.10	0.10	0.10	0.20	0.03
MgO	2.62	2.56	1.54	1.66	1.60	1.65	3.12	3.10	4.05	4.49	4.38	4.44	3.71	1.70	1.42
CaO	0.43	0.37	0.35	0.42	0.39	0.36	3.31	1.55	1.22	2.15	2.18	2.17	1.09	2.26	0.27
Na_2O	1.32	1.28	0.87	0.88	0.88	0.91	1.17	1.32	1.50	1.29	1.22	1.26	1.37	0.98	0.85
K_2O	1.59	1.43	1.17	1.17	1.17	1.19	1.15	1.09	1.44	1.82	1.86	1.84	0.88	1.64	1.16
TiO_2	0.81	0.77	0.76	0.74	0.75	0.76	0.13	0.70	0.87	0.84	0.83	0.84	0.63	0.86	0.78
P_2O_5	0.15	0.14	0.13	0.12	0.13	0.13	0.13	0.19	0.13	0.16	0.12	0.14	0.16	0.14	0.13
CIA	81.72	81.84	83.09	82.99	82.98	82.96	70.57	77.38	77.77	74.11	74.81	74.43	80.44	74.88	83.36
CIW	89.51	89.39	90.59	90.26	90.36	90.42	75.08	82.52	84.25	81.41	82.12	81.73	84.81	81.79	91.07
PIA	88.40	88.30	89.65	89.33	89.42	89.47	73.38	81.28	82.82	79.38	80.19	79.74	83.94	79.94	90.16

Table 5.9b: Major elements of Upper Disang shale

Sample	UD43	UD45	UD47	UD48	UD55	UD58	UD60	UD64	UD70	UD73
SiO_2	65.55	65.71	63.20	62.70	63.00	62.89	62.91	64.19	64.23	63.57
Al_2O_3	16.04	16.07	18.84	18.85	17.18	16.37	16.34	16.89	16.94	17.25
Fe_2O_3	7.85	7.86	9.05	9.07	8.90	8.85	8.79	8.44	8.47	9.07
MnO	0.12	0.10	0.08	0.07	0.11	0.12	0.13	0.07	0.09	0.13
MgO	2.85	2.97	1.40	1.42	2.81	3.52	3.51	3.58	3.68	3.05
CaO	0.95	0.99	0.27	0.29	1.41	1.98	1.98	0.56	0.59	0.55
Na_2O	1.27	1.29	0.95	0.91	1.11	1.21	1.18	1.03	1.08	1.03
K_2O	2.32	2.36	2.25	2.26	2.19	2.14	2.17	2.75	2.78	2.62
TiO_2	0.94	0.92	1.14	1.16	0.94	0.80	0.89	0.95	0.90	0.97
P_2O_5	0.15	0.13	0.17	0.17	0.14	0.13	0.12	0.12	0.11	0.10
CIA	77.94	77.60	84.45	84.49	78.49	75.44	75.40	79.56	79.20	80.42
CIW	87.84	87.57	93.92	94.01	87.20	83.69	83.79	91.40	91.03	91.61
PIA	86.07	85.74	93.15	93.25	85.6	81.69	81.77	89.89	89.45	90.25

Table 5.10a: Major oxide ratios of the Upper Disang sandstone

Sample	K_2O/Na_2O	K_2O/Al_2O_3	Al_2O_3/K_2O	MgO/Al_2O_3	TiO_2/Al_2O_3	Al_2O_3/TiO_2	Na_2O/K_2O	SiO_2/Al_2O_3	Na/Al	Na_2O+K_2O
UD 29	1.20	0.11	9.39	0.18	0.05	18.43	0.83	4.53	0.12	2.91
UD 32	1.12	0.10	9.71	0.18	0.06	18.03	0.90	0.64	0.13	2.71
UD 36	1.34	0.10	10.03	0.13	0.06	15.45	0.74	6.41	0.10	2.04
UD 37	1.33	0.10	10.30	0.14	0.06	16.28	0.75	6.19	0.10	2.05
UD 38	1.33	0.10	10.17	0.13	0.06	15.87	0.75	6.29	0.10	2.05
UD 39	1.31	0.10	10.07	0.14	0.06	15.76	0.76	5.65	0.11	2.10
UD 40	0.98	0.09	11.74	0.23	0.05	18.49	1.02	4.76	0.12	2.32
UD 44	0.83	0.08	12.43	0.23	0.05	19.36	1.21	4.88	0.14	2.41
UD 46	0.96	0.10	10.10	0.28	0.06	16.72	1.04	4.49	0.15	2.94
UD 52	1.41	0.12	8.27	0.30	0.06	17.93	0.71	4.19	0.12	3.11
UD 54	1.52	0.12	8.40	0.28	0.05	18.82	0.66	4.05	0.11	3.08
UD 56	1.46	0.12	8.34	0.29	0.05	18.26	0.68	4.12	0.12	3.10
UD 57	0.64	0.06	15.61	0.27	0.05	21.81	1.56	4.87	0.14	2.25
UD 61	1.67	0.11	8.87	0.12	0.06	16.92	0.60	4.55	0.09	2.62
UD 76	1.36	0.10	9.84	0.12	0.07	14.64	0.73	6.65	0.11	2.01
Average	**1.23**	**0.10**	**10.22**	**0.20**	**0.06**	**17.52**	**0.86**	**4.82**	**0.12**	**2.51**

Table 5.10b: Ratios of some major oxides of the Upper Disang shale

Sample	K_2O/Na_2O	K_2O/Al_2O_3	Al_2O_3/K_2O	MgO/Al_2O_3	TiO_2/Al_2O_3	Al_2O_3/TiO_2	Na_2O/K_2O	SiO_2/Al_2O_3	Na/Al	Na_2O+K_2O
UD 43	1.83	0.14	6.91	0.18	0.06	17.06	0.55	4.09	0.11	3.59
UD 45	1.83	0.15	6.81	0.18	0.06	17.47	0.55	4.09	0.11	3.65
UD 47	2.37	0.12	8.37	0.07	0.06	16.53	0.42	3.35	0.07	3.20
UD 48	2.48	0.12	8.34	0.08	0.06	16.25	0.40	3.33	0.07	3.17
UD 55	1.96	0.13	7.86	0.16	0.05	18.22	0.51	3.67	0.09	3.30
UD 58	1.77	0.13	7.65	0.22	0.05	20.46	0.57	3.84	0.10	3.35
UD 60	1.84	0.13	7.53	0.21	0.05	18.36	0.54	3.85	0.10	3.35
UD 64	2.67	0.16	6.14	0.21	0.06	17.78	0.37	3.80	0.09	3.78
UD 70	2.57	0.16	6.09	0.22	0.05	18.82	0.39	3.79	0.09	3.86
UD 73	2.54	0.15	6.58	0.18	0.06	17.78	0.39	3.69	0.08	3.65
Average	**2.19**	**0.14**	**7.23**	**0.17**	**0.06**	**17.87**	**0.47**	**3.75**	**0.09**	**3.49**

Fig. 5.11a: Coefficient correlation (*r*) of Upper Disang sandstone

r	Al$_2$O$_3$	Fe$_2$O$_3$	MnO	MgO	CaO	Na$_2$O	K$_2$O	TiO$_2$	Zr	Y
SiO$_2$	-0.86	-0.81	-0.56	-0.82	-0.77	-0.74	-0.56	0.09	-0.09	-0.69
Al$_2$O$_3$	1.00	0.72	0.34	0.82	0.62	0.77	0.77	0.20	0.30	0.71
Rb	0.81	0.49	0.09	0.71	0.54	0.52	0.65	0.24	-0.01	0.92
Cs	0.76	0.47	0.12	0.75	0.61	0.46	0.62	0.15	-0.14	0.94
Th	0.73	0.53	0.16	0.72	0.60	0.60	0.54	0.26	-0.28	0.99
Ba	0.67	0.52	0.24	0.69	0.68	0.40	0.50	-0.02	-0.21	0.90
U	0.70	0.47	0.11	0.69	0.68	0.40	0.54	0.26	-0.31	1.00
Sr	0.73	0.53	0.18	0.78	0.62	0.53	0.52	-0.01	-0.10	0.88
Sc	0.75	0.53	0.17	0.69	0.62	0.44	0.58	0.23	-0.22	0.98
V	0.72	0.72	0.49	0.69	0.61	0.41	0.57	0.20	-0.25	0.99
Ni	0.73	0.48	0.11	0.84	0.60	0.53	0.54	0.16	-0.28	0.96
Co	0.80	0.57	0.20	0.70	0.62	0.49	0.61	0.19	-0.01	0.94
Cr	0.77	0.50	0.15	0.88	0.56	0.66	0.54	0.25	-0.26	0.88
Cu	0.88	0.56	0.13	0.82	0.53	0.68	0.65	0.32	-0.01	0.91
Hf	0.73	0.63	0.29	0.49	0.38	0.66	0.64	0.34	0.53	0.47
Yb	0.73	0.50	0.15	0.73	0.61	0.45	0.56	0.26	-0.30	0.99
∑ LREE	0.75	0.52	0.16	0.73	0.60	0.48	0.57	0.29	-0.28	0.98
∑ HREE	0.74	0.50	0.16	0.75	0.63	0.46	0.58	0.25	-0.30	0.99
(La/Yb)$_N$	-0.48	-0.55	-0.49	-0.56	-0.74	-0.30	-0.26	0.19	0.44	-0.69
(Gd/Yb)$_N$	-0.77	-0.69	-0.38	-0.76	-0.68	-0.61	-0.47	-0.16	0.26	-0.91

Fig. 5.11b: Coefficient correlation (*r*) of Upper Disang shale

r	Al$_2$O$_3$	Fe$_2$O$_3$	MnO	MgO	CaO	Na$_2$O	K$_2$O	TiO$_2$	Zr	Y
SiO$_2$	-0.56	-0.94	0.02	0.25	-0.19	0.59	0.37	-0.23	0.30	-0.29
Al$_2$O$_3$	1.00	0.69	-0.61	-0.83	-0.64	-0.92	-0.06	0.89	-0.86	-0.19
Rb	0.44	0.41	-0.32	0.00	-0.67	-0.71	0.78	0.31	-0.05	0.61
Cs	0.37	0.36	-0.14	0.12	-0.61	-0.66	0.78	0.26	0.13	0.74
Th	-0.10	0.40	0.35	0.50	0.01	0.01	0.54	-0.30	0.53	0.98
Ba	0.07	0.33	0.08	0.36	-0.32	-0.39	0.76	-0.09	0.36	0.88
U	-0.20	0.34	0.40	0.60	-0.32	-0.13	0.53	-0.41	0.61	1.00
Sr	-0.12	0.24	0.65	0.13	0.04	0.03	0.11	-0.09	0.36	0.65
Sc	-0.19	0.46	0.44	0.61	0.29	-0.11	0.35	-0.47	0.60	0.98
V	-0.13	-0.13	0.37	0.56	0.03	-0.21	0.59	-0.35	0.56	0.99
Ni	-0.09	-0.10	-0.08	0.39	-0.38	-0.23	0.83	-0.01	0.30	0.55
Co	-0.17	-0.06	0.25	0.35	-0.35	-0.07	0.74	-0.15	0.46	0.70
Cr	-0.09	0.01	-0.13	0.52	-0.37	-0.26	0.95	-0.20	0.42	0.72
Cu	-0.10	0.18	0.05	0.56	-0.21	-0.26	0.83	-0.27	0.49	0.88
Hf	-0.18	0.04	0.63	0.66	0.77	0.50	-0.18	-0.77	0.68	0.55
Yb	-0.18	0.39	0.41	0.59	0.15	-0.14	0.48	-0.42	0.60	1.00
∑ LREE	0.09	0.43	0.39	0.47	0.04	-0.21	0.49	-0.30	0.52	0.99
∑ HREE	0.16	0.40	0.41	0.56	0.13	-0.15	0.48	-0.39	0.58	1.00
(La/Yb)$_N$	0.31	-0.33	-0.34	-0.75	-0.45	0.00	-0.31	0.62	-0.67	-0.85
(Gd/Yb)$_N$	0.30	-0.34	-0.34	-0.74	-0.42	0.01	-0.33	0.61	-0.67	-0.87
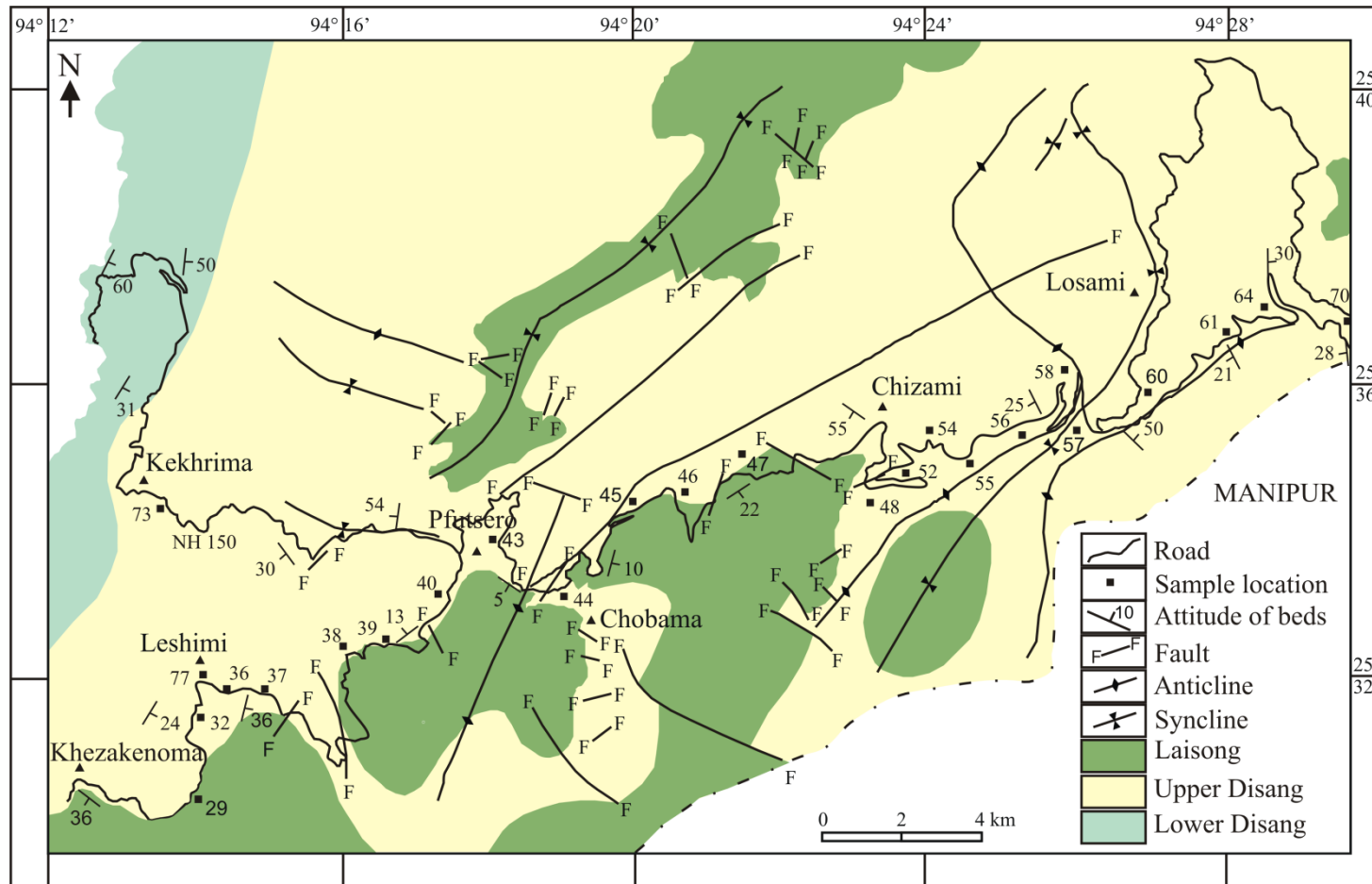
Fig. 5.17: Geological map of Pfütsero and adjoining areas, Phek district with sample locations for petrographic and geochemical study (modified after Agarwal and Madhav, 1988)
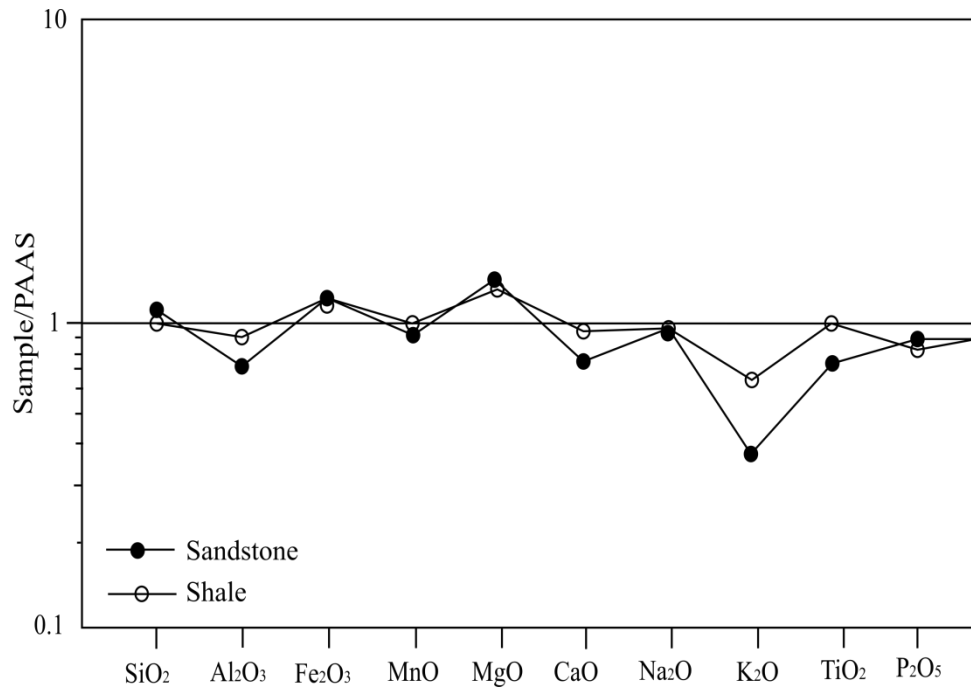
Fig. 5.18: PAAS normalized major oxide spider diagram (after Taylor and McLennan, 1985)
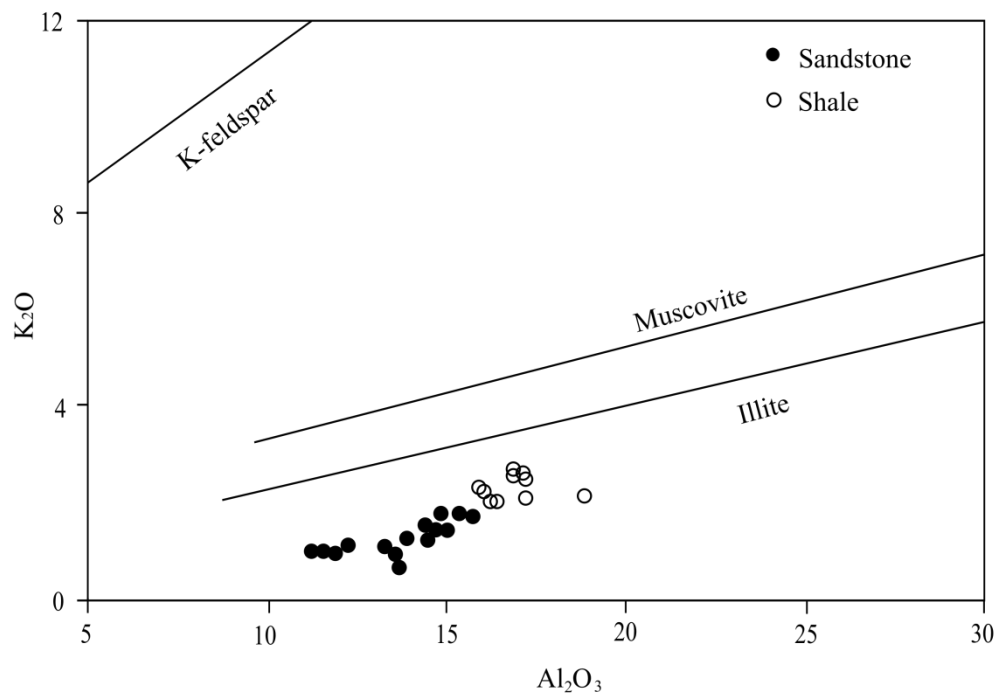
Fig. 5.19: Al$_2$O$_3$ vs K$_2$O plots showing samples lying in illite field (after Sinha *et al.*, 2007)

biotite, chlorite and illmenite are derived from basic rocks. The positive correlation between Al_2O_3 and Fe and Ti also may reflect the occurrence of some Fe and Ti oxides such as rutile, hematite, etc. associated with the clays.

Fe_2O_3/K_2O ratios discriminate sands more clearly than do Na_2O/K_2O ratios (Vital and Statteger, 2000). Hence, following Herron (1988) for Upper Disang sandstone, litharenite is indicated (Fig. 5.20). In the geochemical plots of Pettijohn *et al*. (1987) and Creaser *et al*. (1997) they scatter in the fields of litharenite and greywacke (Fig. 5.21). Okada (1971) classified detrital sandstone by their matrix and mineralogical contents. Low Na/Al and Na/K ratios (Pettijohn, 1984) such as those of the Disang indicate greywacke.

The major elements are mobile during weathering, transportation and post depositional processes making them useful for determining degree of maturity of sediments (McLennan *et al*., 1993). The SiO_2/Al_2O_3 ratio is sensitive to sediment recycling and weathering and hence, can be used as a signal of sediment maturity, increasing as quartz survives preferentially to feldspar, mafic minerals and lithic grains (Roser and Korsch, 1986; Pettijohn *et al*., 1987). Average values in unaltered igneous rocks range from ~3.0 (basic) to ~5.0 (acid); values >5.0-6.0 in sediments indicate progressive maturity (Roser *et al*., 1996). The majority of the Upper Disang sediments show SiO_2/Al_2O_3 ratios between 3.33 to 4.88 except for five sandstone samples with values >5, indicating that the Upper Disang sediments are chemically immature. Low Na_2O/K_2O ratios with average of 0.86 also attest to sediment immaturity. The TiO_2/Al_2O_3 ratios of these sediments are lower than those of continental rocks (Spears and Sotiriou, 1976), which denote chemical immaturity of the sediments.

5.2.2 Trace Elements

Trace element concentrations result from the influence of provenance, weathering, diagenesis, sediment sorting and the aqueous geochemistry of individual elements (Rollinson, 1993). Factors controlling the presence of trace elements in sediments include pressure and temperature, physical and chemical properties of the elements and the chemical environment. Due to remarkably high concentrations of trace elements in clay-rich sediments most geochemical studies have concentrated on these lithologies. Trace elements of fine-grained clastics have been widely used to determine provenance. Certain trace elements in sedimentary rocks indicate their

47
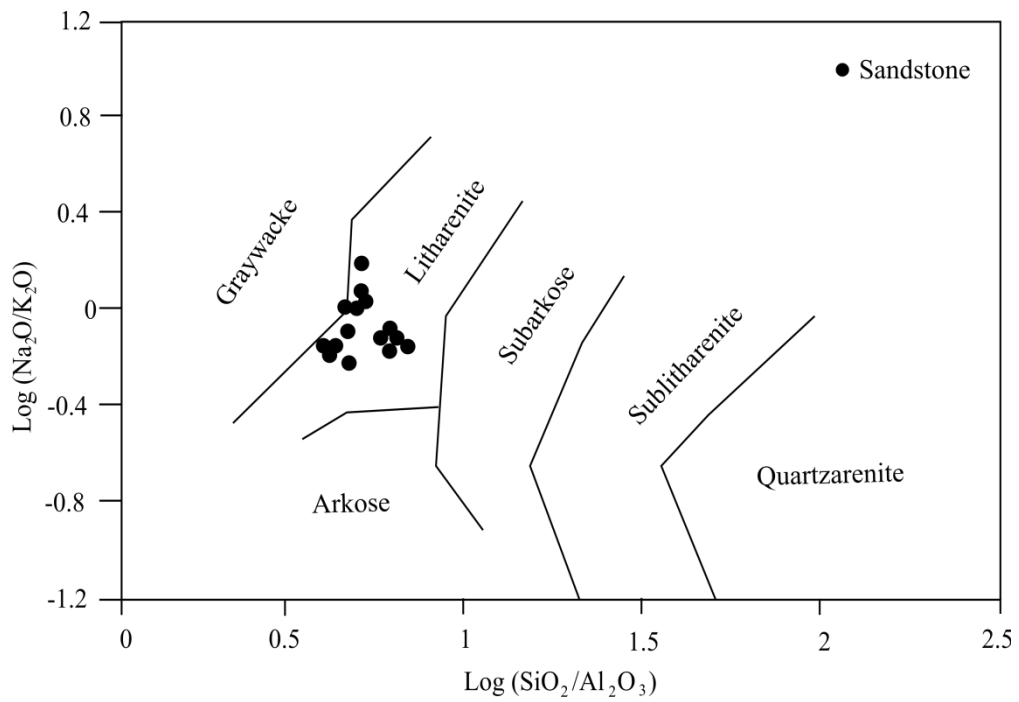
Fig. 5.20: Geochemical plots of Upper Disang sandstone (after Herron, 1988)
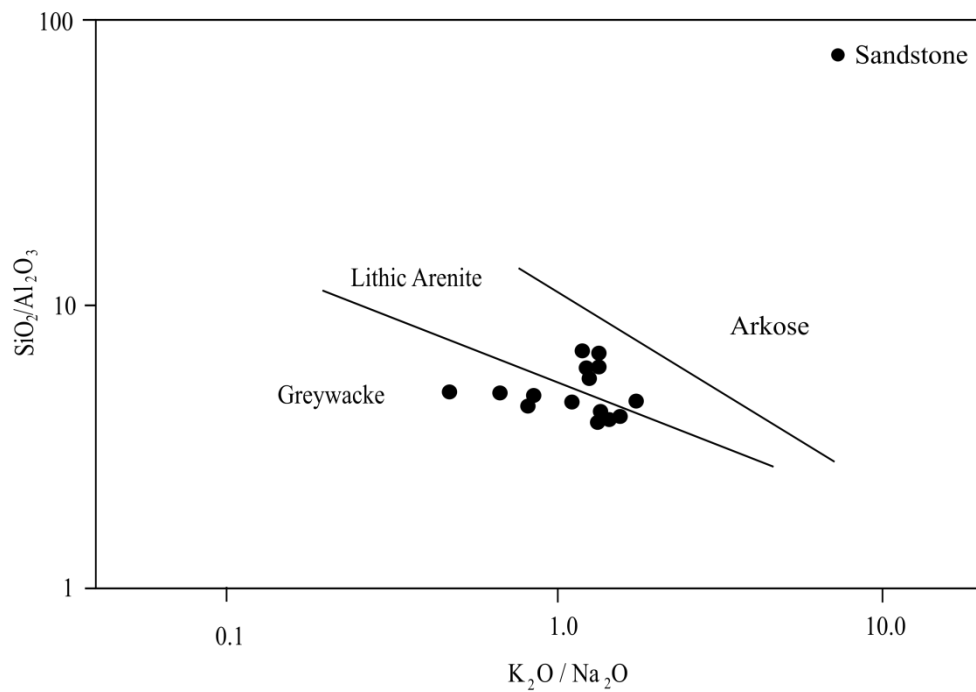
Fig. 5.21: Geochemical plots showing ranges in composition of Upper Disang sandstones (after Pettijohn *et al*., 1987 and Creaser *et al*., 1997)

mode of formation and environment of deposition (Majumder *et al.*, 1980). Chromium and nickel concentrations in Phanerozoic shale have pointed to ultramafic sources, presumably ophiolites in tectonic highlands (Garver and Scott, 1995).

Trace elements are widely used to facilitate studies of complex processes involved in rock formation including average composition of the provenance, weathering, transportation, diagenesis and metamorphism. Some elements are highly mobile during sedimentary processes; hence, their abundances in sedimentary rocks do not represent the composition of their source rocks. Many other elements however, are less mobile and have low residence time in seawater (Holland, 1978). The abundance of such elements strongly represents the composition of source rocks.

Trace element composition of the Disang sediments are shown in Table 5.12a,b.

Large-Ion Lithophile Elements

Upper Disang sediments are enriched in most of the trace elements (Fig. 5.22) relative to PAAS (Taylor and McLennan, 1985). Relative enrichment of LILE is noted in shale samples while the associated sandstones show depletion in Rb, Sr and Ba. A positive correlation between LILE-K_2O (Table 5.11a,b) suggests a strong link to illite (Dokuz and Tanyolu, 2006). High positive correlation of Rb with K ($r= 0.65$ and 0.78 for sandstone and shale respectively) suggests its association with illitic phases as Rb is preferentially retained in weathered illite with respect to K (Garrels and Christ, l965). This is in agreement with studies by Nesbitt *et al.* (1980), Wronkiewicz and Condie (1987) and Condie (1993) in which it was concluded that small cations such as Na, Ca and Sr are selectively leached and removed from weathering profiles whereas cations with relatively larger ionic radii such as K, Cs, Rb and Ba may be fixed by preferential exchange and adsorption onto clays. However Rb, Cs and Ba exhibit moderate to high positive correlation coefficients with Al_2O_3 (Table 5.11a,b) suggesting that their distributions may also be controlled by kaolinite and montmorillonite phases. The presence of clay minerals such as illite and chlorite with minor concentrations of kaolinite and montmorillonite in the sediments inferred from geochemical data is consistent with earlier clay mineral studies by Baruah (2003).

Table 5.12a: Trace elements of Upper Disang sandstone

Sample	UD29	UD32	UD36	UD37	UD38	UD39	UD40	UD44	UD46	UD52	UD54	UD56	UD57	UD61	UD76
							Sandstone (n=15)								
Sc	24.84	24.87	17.52	19.20	22.15	25.42	25.78	27.94	30.41	56.48	56.30	56.39	56.12	55.58	17.32
V	158.92	159.12	112.15	114.12	120.35	193.16	194.12	168.86	209.94	511.38	509.77	510.58	508.16	461.6	111.21
Cr	54.33	54.77	42.03	45.02	47.89	61.28	62.32	67.03	131.97	135.83	133.36	134.59	130.89	92.38	41.52
Co	28.22	28.56	22.45	23.45	24.62	27.91	28.14	25.66	29.48	38.54	38.58	38.56	38.62	38.85	21.87
Ni	123.25	124.30	97.12	99.25	102.86	158.17	158.56	144.08	194.90	342.41	332.15	337.28	321.89	203.62	96.74
Cu	56.03	56.37	36.87	37.15	39.77	40.36	43.25	48.91	68.45	82.24	81.21	81.73	80.18	71.36	36.66
Zn	61.63	62.07	39.65	40.15	43.15	56.23	54.12	53.09	68.66	101.76	102.10	101.91	102.37	104.05	39.50
Ga	26.05	26.52	18.42	25.18	26.03	26.17	28.15	37.91	41.62	134.93	132.44	133.68	129.94	113.3	18.19
Rb	113.78	114.23	66.57	68.37	69.54	94.22	94.56	63.72	119.18	181.19	180.38	180.78	179.57	168.28	66.34
Sr	146.04	146.23	97.23	99.15	102.54	178.44	179.54	113.59	150.00	239.99	239.235	239.61	238.48	169.38	95.86
Y	36.73	37.24	25.13	26.47	28.32	47.94	48.54	85.83	61.10	226.46	225.51	225.98	224.56	169.53	23.56
Zr	293.17	294.12	178.22	179.56	181.25	194.97	196.47	180.52	199.57	198.18	176.18	187.18	154.17	205.81	176.17
Nb	15.05	15.52	10.24	10.56	10.78	11.89	12.58	21.09	19.66	45.93	46.09	46.01	46.25	47.45	9.67
Cs	9.67	9.87	6.56	7.26	8.57	10.19	11.26	5.91	11.88	20.34	19.46	19.91	18.59	16.01	5.82
Ba	312.57	314.16	214.23	220.87	225.45	528.17	528.19	255.93	372.27	718.34	715.46	716.90	712.58	593.96	213.71
Hf	8.48	9.22	5.87	5.89	5.95	6.14	6.45	7.67	8.56	8.48	7.83	8.15	7.17	9.81	5.08
Ta	1.07	1.12	0.87	0.84	0.73	0.77	0.87	3.94	2.21	9.58	8.72	9.15	7.85	5.36	0.81
Pb	12.79	10.66	8.78	9.12	10.56	12.02	13.15	17.54	19.85	47.59	46.79	47.19	45.98	37.15	8.55
Th	13.69	12.58	9.23	9.45	9.58	10.74	11.65	31.53	20.69	57.99	56.61	57.30	55.23	49.18	8.57
U	2.09	1.78	1.30	1.36	1.39	1.55	2.16	12.19	8.74	44.08	43.48	43.78	42.87	35.78	1.26

Table 5.12b: Trace elements of Upper Disang shale

Sample	UD43	UD45	UD47	UD48	UD55	UD58	UD60	UD64	UD70	UD73
				Shale (*n=10*)						

Sample	UD43	UD45	UD47	UD48	UD55	UD58	UD60	UD64	UD70	UD73
Sc	23.90	24.70	26.58	26.69	36.72	41.69	41.89	38.94	40.35	51.25
V	230.20	173.09	195.56	235.21	252.46	287.54	285.56	332.62	333.69	450.68
Cr	114.65	85.12	95.00	114.25	125.64	133.25	132.50	156.98	145.65	212.30
Co	33.20	33.30	28.54	30.46	29.53	30.07	29.97	34.55	36.89	44.87
Ni	154.22	156.68	130.54	132.12	127.81	22.087	230.80	289.24	290.80	284.62
Cu	65.87	68.20	66.98	68.97	74.67	77.53	79.50	102.92	105.79	112.58
Zn	87.50	87.75	70.55	71.78	79.30	82.46	84.89	94.11	95.18	120.52
Ga	23.87	26.22	29.45	30.91	46.93	54.58	56.75	62.33	63.72	107.87
Rb	130.25	132.08	168.55	172.65	146.53	134.58	136.46	194.87	195.45	219.21
Sr	145.85	147.62	138.02	138.27	145.18	140.55	156.96	133.86	134.61	197.55
Y	15.88	17.28	16.59	18.67	38.04	47.82	49.70	50.44	51.09	84.21
Zr	176.32	177.11	89.59	96.93	184.28	189.98	183.27	175.22	188.84	195.20
Nb	12.85	14.25	14.98	16.19	17.89	17.89	20.79	24.55	26.35	40.22
Cs	8.52	10.82	12.98	13..61	10.88	8.69	10.96	16.45	17.34	23.22
Ba	360.57	365.97	420.66	426.43	438.53	445.29	449.64	634.87	636.53	838.21
Hf	3.27	4.70	2.19	2.76	4.23	6.87	5.62	4.54	3.05	5.22
Ta	0.38	0.51	1.12	1.16	2.08	2.45	2.68	2.58	2.87	4.24
Pb	15.22	17.94	18.52	18.79	18.93	18.5	19.76	24.59	26.78	42.15
Th	12.27	12.85	12.89	15.27	19.15	21.82	22.74	24.15	26.01	39.25
U	1.54	1.72	1.32	1.65	7.87	10.86	11.44	13.1	13.14	24.15

High-Field-Strength Elements

Disang sediments are enriched in HFSE (Zr, Hf, Y, Nb, Ta, Th and U) relative to PAAS (Taylor and McLennan, 1985). Y bears a strong positive correlation with Yb (Table 5.11a,b) and HREE, which seem to reflect that the HREE are controlled mainly by mafic minerals (Dokuz and Tanyolu, 2006). Zr and Hf behave similarly during magmatic differentiation and show positive correlation coefficient with sandstone and shale (r= 0.53, 0.68 respectively). In addition, the negative correlation between Y and SiO_2 in sandstone and shale suggests association with clay minerals rather than quartz dominant rock (r= -0.69, -0.29).

Transition Trace Elements

The TTE (Cr, Co, Ni, Cu, Sc and V) contents of the sandstone and shale are also enriched relative to PAAS with an exception of Cu in the sandstone samples (Fig. 5.22). The high concentrations of TTE in all Disang sediments suggest significant contribution from mafic and ultramafic rocks (Taylor and McLennan, 1985; Wronkiewicz and Condie, 1987). The Cr/Th ratio, a good indicator for provenance (Condie and Wronkiewicz, 1990) has an average value of 8.69. All TTE of the sandstones are positively correlated with TiO_2 and Al_2O_3 (Table 5.11a,b) which, according to Fedo *et al.* (1996) suggests that these elements may be bound in clay minerals and concentrated during weathering. In contrast, negative correlation between TTE and TiO_2 and Al_2O_3 in the shale suggests additional factors contributing to their distribution (Dokuz and Tanyolu, 2006). The enrichment of Cr and Ni in clay-rich samples is due to adsorption or substitution of these metals on to clay-sized particles during weathering and deposition (Wronkiewicz and Condie, l987).

5.2.3 Rare Earth Elements

The REE comprise the lanthanides (lanthanum to lutetium) and yttrium. Yttrium resembles dysprosium and holmium and is typically included with the heavy rare earths (HREE) gadolinium to lutetium (yttrium earths). The light rare earth elements (LREE), lanthanum to samarium are the cerium earths (Fairbridge, 1972). A characteristic feature of the rare earths including yttrium is their trivalent state and similar ionic sizes that give them similar physical and chemical properties. Cerium and europium behave differently under specific conditions, which make them environment sensitive. Under reducing conditions, europium may exist in the divalent

state whereas Ce^{3+} maybe oxidized to Ce^{4+}. Apart from these anomalies the REE behave as an unusually coherent group. As no internal fractionation takes place within the REE during metamorphism or the sedimentary processes it is possible to make inferences on the evolution of sedimentary rocks (Wildeman and Haskin, 1973).

REE are good indicators of igneous processes. There exists a slight decrease in ionic radii from LREE to HREE, *lanthanide contraction*, which results in LREE enrichment through crustal differentiation. Hence, REE in shale is effectively used in provenance studies because of bulk transfer of these elements in sedimentary systems, low natural abundance and relative immobility in seawater and during diagenesis and metamorphism (Taylor and McLennan, 1985; McLennan, 1989). Because of near quantitative transfer of REE from a source region to the depositional site, terrigenous sediments reflect the average composition of source rocks. Some studies have documented feeble mobility of REE during diagenesis. Nesbitt (1979) has shown that although REE may be locally remobilized in a weathering profile, there are no selective losses of REE during weathering and thus weathering probably does not produce Eu anomalies. The immobility of REE during fluvial transportation reflects stable tectonic conditions under which they evolved (Hariharan and Nambiar, 1998).

REE distributions help infer sediment derivation from various modern and ancient plate tectonic settings. Sediments derived from mature continental crusts are characterized by LREE enrichment. Old continental crusts lack Eu anomalies. During erosion and sedimentation the REE are carried largely as suspended loads and hence are transferred nearly in bulk from the source (Taylor and McLennan, 1985). Cratonic shales have uniform chondrite normalized REE distributions. Progressive weathering fractionates REE (Nesbitt, 1979; Suttner *et al*., 1981; Cullers *et al*., 1987; Cullers, 1988; Johnsson *et al*., 1988). Hydraulic sorting may also lead to REE fractionation (Gromet *et al*., 1984; Cullers *et al*., 1987; McLennan, 1989). Diagenetic and low-grade metamorphic effects on REE however, appear to be minimal in fine-grained sediments (Sholkovitz, 1978; Chaudhuri and Cullers, 1979; Elderfield and Sholkovitz, 1987). The relatively insensitive nature of REE to remobilization during alteration and metamorphism makes them useful for inference of tectonic setting and provenance type (Condie and Allen, 1984; Cullers *et al.*, 1987; Vance and Condie, 1987).

Disang sediments show large variation (133-936 ppm) in REE contents (Table 5.13a,b). Distribution patterns of the sediments normalized to chondrite values are plotted (Fig. 5.23, 5.24) following Evensen *et al*. (1978). The sandstone and shale

Table 5.13a: REE of Upper Disang sandstone

Sample	UD29	UD32	UD36	UD37	UD38	UD39	UD40	UD44	UD46	UD52	UD54	UD56	UD57	UD61	UD76
Sandstone (n=15)															
La	38.59	37.55	25.56	27.02	29.07	29.25	30.63	80.39	90.11	183.21	180.22	179.39	178.56	163.23	25.51
Ce	81.37	63.46	52.62	54.13	61.56	61.92	70.15	155.77	184.15	354.19	346.55	340.35	334.15	320.76	52.21
Pr	10.12	7.89	6.39	6.44	7.45	7.73	9.26	18.88	20.87	44.01	38.99	40.12	41.25	38.99	6.32
Nd	39.49	34.66	25.12	27.52	30.87	31.99	34.45	70.24	83.20	167.61	159.24	154.74	150.24	144.85	24.95
Sm	8.76	8.32	5.82	6.32	7.88	8.24	9.66	14.72	15.55	35.86	33.55	33.22	32.89	29.30	5.62
Eu	2.07	1.89	1.52	1.56	2.42	2.44	2.54	2.93	2.96	7.22	6.84	6.595	6.35	5.69	1.33
Gd	8.09	6.87	5.46	6.32	8.56	8.68	9.36	14.71	16.88	34.96	32.42	30.98	29.54	27.43	5.24
Tb	1.32	0.97	0.92	1.22	1.54	1.58	1.72	2.52	3.02	6.42	5.26	5.475	5.69	4.85	0.83
Dy	7.78	6.83	5.32	6.87	8.57	9.53	10.33	15.46	18.65	40.86	38.53	36.00	33.47	31.07	5.06
Ho	1.23	0.96	0.86	1.02	1.47	1.53	1.65	2.75	2.98	7.21	7.25	6.55	5.85	5.48	0.78
Er	3.62	3.25	2.46	3.07	4.12	4.16	4.36	8.37	9.57	22.85	21.58	20.06	18.54	17.41	2.26
Tm	0.42	0.32	0.34	0.39	0.43	0.48	0.75	1.09	1.17	2.99	2.78	2.67	2.56	2.42	0.24
Yb	3.27	2.65	2.02	2.12	3.27	3.48	4.08	9.04	9.39	25.17	23.67	23.05	22.43	20.13	1.91
Lu	0.37	0.29	0.35	0.35	0.36	0.38	0.69	1.20	1.28	3.38	3.18	3.10	3.02	2.74	0.23
∑REE	206.50	175.91	134.76	144.35	167.57	171.39	189.63	398.07	459.78	935.94	900.06	882.30	864.54	814.35	132.49
LREE/HREE	6.33	6.32	6.00	5.30	4.45	4.31	4.34	5.86	5.98	5.20	5.36	5.56	5.78	5.95	6.41
Eu /Eu*	0.75	0.76	0.82	0.75	0.90	0.88	0.82	0.61	0.56	0.62	0.63	0.63	0.62	0.61	0.75
Ce/Ce*	1.11	0.94	1.11	1.06	1.10	1.08	1.15	1.11	1.13	1.08	1.09	1.09	1.09	1.11	1.10
$(La/Yb)_N$	7.96	9.57	8.54	8.60	6.00	5.67	5.07	6.00	6.48	4.91	5.14	5.25	5.37	5.47	9.01
$(Gd/Yb)_N$	2.00	2.10	2.18	2.41	2.12	2.02	1.85	1.32	1.45	1.12	1.11	1.09	1.06	1.10	2.22
$(La/Sm)_N$	2.77	2.84	2.77	2.69	2.32	2.23	2.00	3.44	3.65	3.22	3.38	3.40	3.42	3.51	2.86
$(La/Y)_N$	4.30	4.12	4.16	4.17	4.20	2.49	2.58	3.83	6.03	3.31	3.27	3.25	3.25	3.94	4.43
$(Ce/Yb)_N$	6.44	6.20	6.74	6.61	4.87	4.60	4.45	4.46	5.08	3.64	3.79	3.82	3.86	4.12	7.07

Table 5.13b: REEs of Upper Disang shale

Sample	UD43	UD45	UD47	UD48	UD55	UD58	UD60	UD64	UD70	UD73
					Shale (n=10)					
La	37.88	39.39	42.92	44.55	64.63	74.59	76.37	82.25	82.92	141.25
Ce	74.83	75.17	85.11	86.17	119.58	136.45	137.19	145.51	145.99	241.87
Pr	8.66	9.04	10.55	10.69	15.06	17.24	17.39	17.22	18.27	31.22
Nd	32.56	34.03	38.11	39.14	55.33	63.55	64.33	65.55	67.5	113.54
Sm	4.85	6.83	6.79	7.85	11.25	13.25	13.71	14.12	14.32	23.07
Eu	1.50	1.54	1.63	1.67	2.36	2.70	2.76	2.78	2.84	4.44
Gd	4.88	5.11	5.54	5.79	8.70	9.84	10.73	10.89	11.04	18.21
Tb	0.76	0.83	0.84	0.86	1.55	1.89	1.92	1.88	1.96	3.45
Dy	3.80	3.91	4.22	4.31	8.3	10.25	10.43	10.78	10.84	17.56
Ho	0.55	0.69	0.72	0.74	1.53	1.92	1.94	1.88	2.00	3.33
Er	1.77	1.85	2.08	2.11	4.26	5.30	5.41	5.64	5.76	9.50
Tm	0.22	0.25	0.25	0.30	0.63	0.75	0.90	0.53	0.95	1.62
Yb	1.61	1.69	1.86	1.92	4.72	6.12	6.17	6.54	6.56	11.12
Lu	0.20	0.25	0.26	0.28	0.71	0.88	0.98	1.02	1.03	1.88
$\sum$REE	174.07	180.58	200.88	206.38	298.61	344.73	350.23	366.59	371.98	622.06
LREE/HREE	10.38	10.20	10.54	10.48	8.12	7.69	7.49	7.74	7.65	7.75
Eu /Eu*	0.94	0.80	0.81	0.76	0.73	0.72	0.70	0.69	0.69	0.66
Ce/Ce*	1.14	1.10	1.12	1.10	1.07	1.06	1.04	1.06	1.04	1.02
$(La/Yb)_N$	15.88	15.73	15.57	15.66	9.24	8.23	8.35	8.49	8.53	8.57
$(Gd/Yb)_N$	2.45	2.44	2.41	2.44	1.49	1.30	1.41	1.35	1.36	1.32
$(La/Sm)_N$	4.92	3.63	3.98	3.57	3.62	3.54	3.51	3.67	3.65	3.85
$(La/Y)_N$	9.75	9.32	10.58	9.76	6.95	6.38	6.28	6.67	6.64	6.86
$(Ce/Yb)_N$	12.03	11.51	11.84	11.61	6.56	5.77	5.76	5.76	5.76	5.63
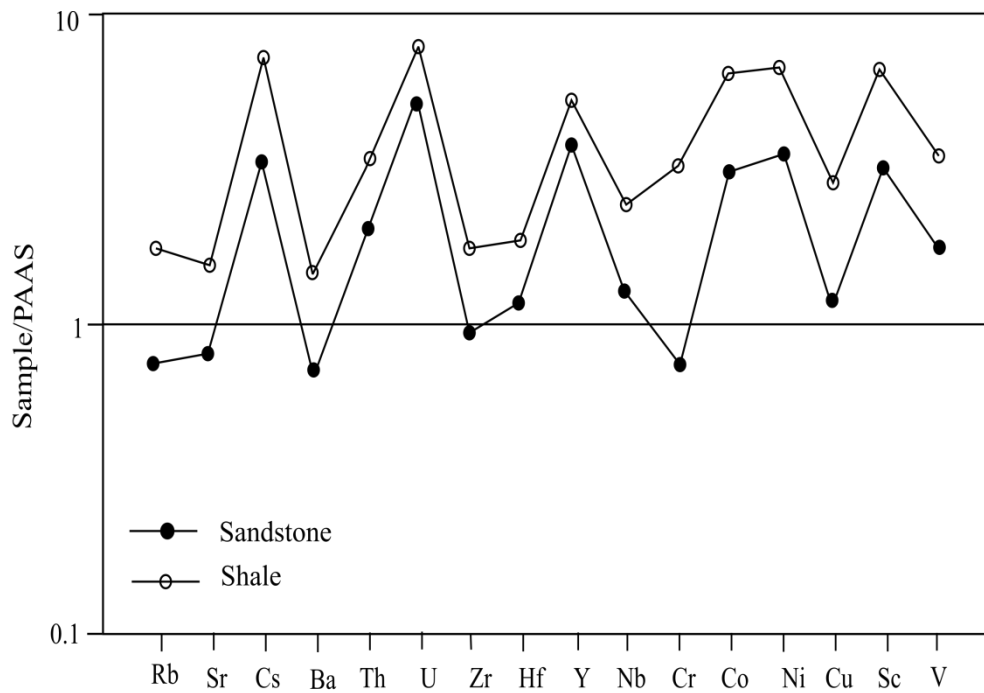
Fig. 5.22: PAAS-normalized trace element spider diagram (after Taylor and McLennan, 1985)
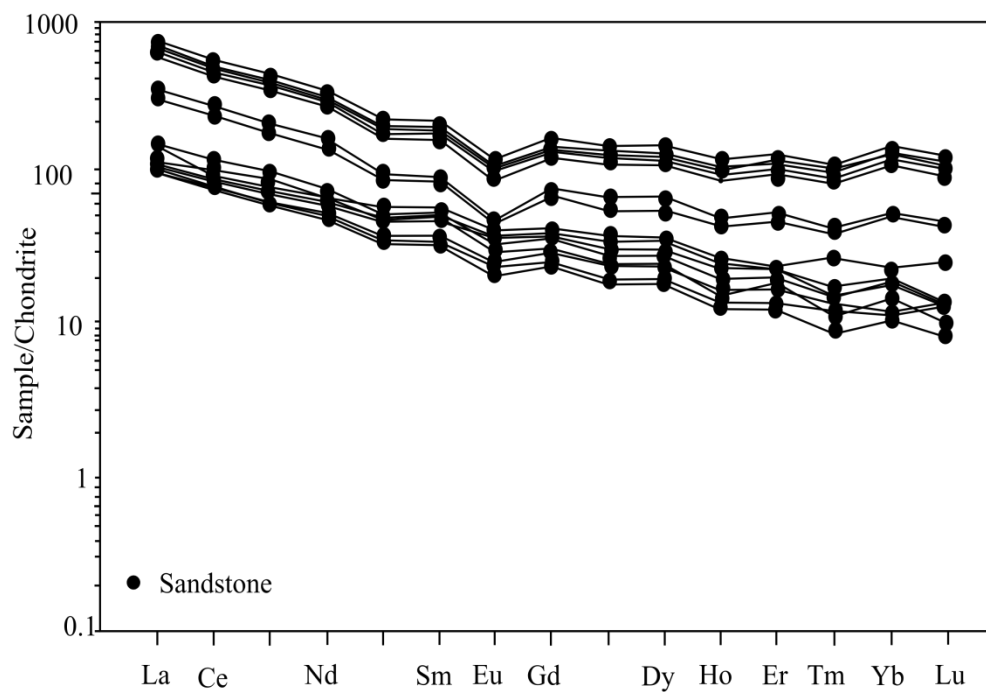
Fig. 5.23: Chondrite-normalized REE patterns of Upper Disang sandstones (after Evensen *et al*., 1978)
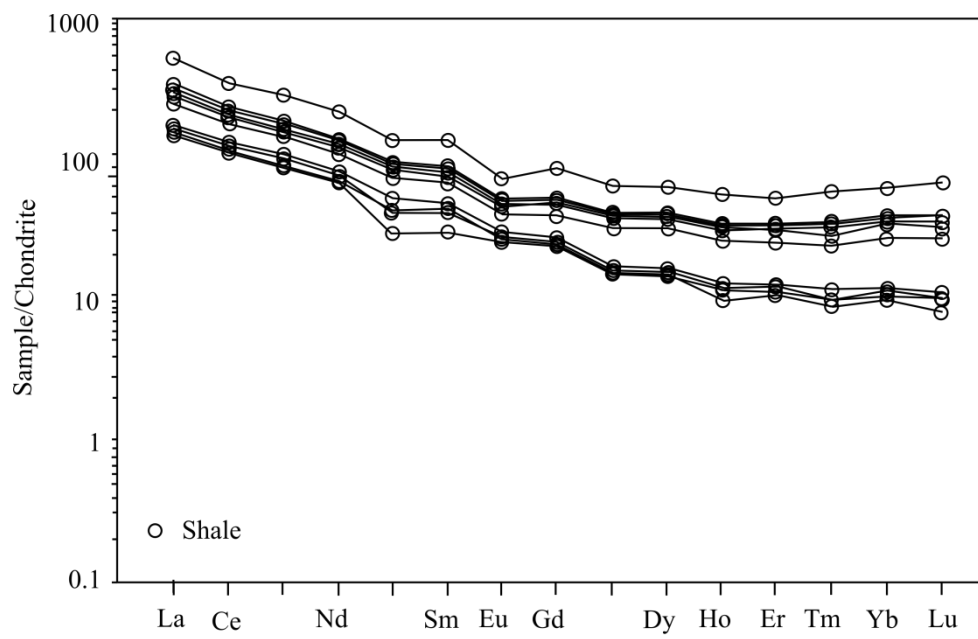
Fig. 5.24: Chondrite-normalized REE patterns of Upper Disang shale (after Evensen *et al.*, 1978)

show broadly similar patterns with slight LREE enrichment and flat HREE with negative Eu anomalies. $(Gd/Yb)_N$ ratios of sandstone and shale (1.7 and 1.8 respectively) are less than 2, which suggest that they were derived from less HREE depleted source rocks. LREE/HREE, $(Ce/Yb)_N$ and $(La/Yb)_N$ values are higher in shale (8.8, 1.2 and 11.43 respectively) than in sandstone (5.7, 0.04 and 6.6 respectively) (Table 5.13) indicating that REE in shale are more fractionated than in sandstone. However, higher REE content in the sandstone, according to Cullers *et al.* (1979) and Taylor and McLennan (1985) may be due to dominance of fine to very fine sand, silt and clay fractions as well as concentration of zircon in the heavy fraction. A strong positive correlation between Al_2O_3 with LREE and HREE ($r = 0.75$, 0.74) and negative correlation with SiO_2 ($r = -0.83$) in the sandstone suggest association with phyllosilicates. The moderately negative coefficient correlation between Zr and (Gd_N/Yb_N) in the shale indicate that HREE fractionation is not controlled by zircon in REE content whereas positive correlation in sandstone indicate the influence of zircon. This study is in agreement with the conclusions of Condie (1991) that probably very fine grains of zircon and heavy minerals resting on fine clay particles may help REE concentrate. REE patterns exhibit pronounced Ce anomaly with an average of 1.09 and 1.08 for sandstone and shale respectively. This feature may be attributed to the chemistry of seawater with no precipitation of carbonate during their deposition. Y in the sandstone and shale show strong positive correlation with Yb, LREE and HREE, which may be due to REE control by abundant hornblende.

Chapter 6

PALEOMAGNETISM

Introduction

Ever since its formation the earth was surrounded by its own magnetic field. Rocks get magnetized at the time of their formation and serve as records of the geomagnetic field over geologic time. The study of this geomagnetism to determine the intensity and direction of the earth's magnetic field of the geologic past is paleomagnetism. This magnetic information is used to understand the evolution of tectonic regions through geologic time (Athavale *et al*., 1963; Klootwijk, 1976, 1979) and establishment of a magnetic time scale.

Paleomagnetism is an important technique used to determine the changing geographical distribution of continents over geologic time. The ability of rocks to record ambient magnetic field during their deposition and retain this record over geological time provides the basis for paleomagnetism.

6.1   Magnetic Mineralogy

Rock magnetic studies have been taken up to assess magnetic mineralogy and assess the reliability of data for paleomagnetic studies. Magnetic susceptibility (χ), frequency dependence of susceptibility ($\chi fd\%$), $F_{300\%}$ and rock magnetic ratios such as S-ratio are computed to validate the concentration and composition of magnetic mineralogy.

Magnetic susceptibility, a measure of the magnetizability of a material, enlightens about Fe bearing minerals in soils, rocks, dust and sediments (Thompson and Oldfield, 1986). Magnetic susceptibility values suggest the presence of ferrimagnetic mineral concentrations (Currie and Bornhold, 1983; Thompson and Oldfield, 1986; Dunlop and Ozdemir, 1997). The spatial and temporal distribution of 'χ' is a function of the concentration and mineralogy of the ferrimagnetic (magnetite, maghemite, Fe-sulphides) minerals present, but can also depend on the strength of the applied magnetic field and the particle size distribution of the magnetic grains. In the absence of ferrimagnetic minerals, χ may be ascribed to antiferromagnetic (hematite, goethite), paramagnetic or diamagnetic minerals such as quartz, feldspar, carbonates

and clays (Bareille *et al*., 1994). Magnetic susceptibility is also dependent on the dimensions of the samples. Therefore, it is customary to present susceptibility as mass normalized susceptibility (Mooney *et al*., 2002). The χlf is considered as a first order estimate of ferrimagnetic concentration and an important decisive parameter when used in conjunction with other hysteresis parameters (Mullins, 1977; Maher, 1986; Singer and Fine, 1989; Evans and Heller, 2001).

χlf for two basalt samples, Spl_2 and Spl_4, show relatively high values (avg. 690 and 180 $x10^{-5}$ SI units respectively). The other samples show very low values ranging from 5.3 to 112 $x10^{-5}$ SI with an average of 28.0 $x10^{-5}$ SI units.

χlf of Upper Disang rocks range from 10.54 to 25.14 x 10^{-5} SI (avg. $12.96x10^{-5}$ SI) while it varies from 0.23 to 8.43 x 10^{-5} SI with an average of 3.55 x 10^{-5} SI in the Laisong (Table 6.1, 6.2). These values suggest that the sediments are weakly magnetic; the Laisong being relatively weaker than the Upper Disang sediments.

Frequency dependence of susceptibility (χfd) is a non-destructive method used in studying magnetic enhancement and also for detection of SP, ferrimagnetic (magnetite or maghemite) grains of >0.02 μm (Mullins and Tite, 1973; Bloemendal *et al*., 1985; Thompson and Oldfield, 1986; Maher, 1988; Dearing *et al*., 1996). χfd is the variation of susceptibility between two frequencies. Magnetic susceptibility measured under different frequencies of applied field (0.465 kHz and 4.65 kHz) allows distinguishing and quantifying certain grain sizes taking advantage of magnetic viscosity (Stacey and Banerjee, 1974; O'reilly, 1984). SP material is that class of ferromagnetic grain sizes which are characteristically viscous at room temperature and behaves differently in higher frequencies (Maher and Taylor, 1988; Zhou *et al*., 1990; Dearing *et al*., 1996; Dekkers, 1997).

According to Dearing *et al*. (1996) and Dekkers (1997) SP particle can be estimated simply by changing the frequency of the applied field. Since the relaxation time of SP particles is short, SP particles behaves as SD while measuring at higher frequencies and thus the susceptibility is lowered (Dearing *et al*., 1996; Dekkers, 1997). Therefore, the differences of susceptibility at low and high frequencies are directly proportionate to the amounts of SP particles present in the substance. Large values of this parameter ($χfd_{\%}$ >5) indicate the presence of ferromagnetic grains lying at the stable SD / SP boundary (~0.03 um) (Maher and Taylor, 1988; Dearing *et al*., 1996; Dekkers, 1997). χfd% ranges from 0.2 to 22 (avg. 2.63±4.96) in the Upper

Table 6.1: Rock magnetic parameters from Leshimi section

	χ*lf*	χ**fd%**	*S*$_{-300}$ *ratio*	*SIRM*	*SIRM/*χ*lf*	*F*$_{300\%}$
Mean	12.96	2.63	97.56	6.69	0.55	96.61
Standard Error	0.78	1.17	1.07	0.62	0.06	1.03
Median	11.78	1.12	98.82	7.24	0.58	98.00
SD	3.31	4.96	4.54	2.63	0.24	4.38
Kurtosis	11.89	14.98	13.21	-1.05	-0.88	13.77
Skewness	3.23	3.77	-3.47	-0.57	-0.35	-3.55
Range	14.60	21.55	19.96	7.98	0.79	19.00
Minimum	10.54	0.20	80.46	1.78	0.07	80.00
Maximum	25.14	21.75	99.80	9.76	0.86	99.00
Count	18.00	18.00	18.00	18.00	18.00	18.00

Table 6.2: Rock magnetic parameters from Viswema section

	χ*lf*	χ**fd%**	*S*$_{-300}$ *ratio*	*SIRM*	*SIRM/*χ*lf*	*F*$_{300\%}$
Mean	3.55	10.59	80.50	59.96	22.42	94.31
Standard Error	0.36	2.26	1.33	5.03	3.73	0.70
Median	3.31	5.77	83.33	54.95	17.03	93.54
SD	2.01	12.58	7.43	27.97	20.78	3.86
Kurtosis	-0.18	4.17	0.82	0.62	19.50	-0.92
Skewness	0.60	1.88	-1.29	0.99	4.15	0.15
Range	8.19	54.84	28.24	115.42	115.14	13.83
Minimum	0.23	0.00	61.60	20.74	8.09	86.00
Maximum	8.43	54.84	89.84	136.16	123.23	99.00
Count	31.00	31.00	31.00	31.00	31.00	31.00

Disang sediments and from 0.01 to 55 (avg. 11±12.48) in Laisong sediments (Table 6.1, 6.2). Considerable numbers of samples show values >5 suggesting stable ferromagnetic grains suitable for paleomagnetic studies.

IRM is studied to gain insight into magnetic mineralogy. IRM is acquired by a sample after exposure to, and removal from a steady direct current magnetic field. IRM is a function of strength of the applied field, magnetic mineralogy and grain size. IRM is often used as an indicator for ferrimagnetic minerals. Antiferromagnetic minerals such as hematite and goethite are also capable of acquiring IRM (Mooney *et al*., 2002). Ferrimagnetic minerals are usually saturated in the field at less than 300 mT, while canted antiferromagnetic minerals require more than 2 T to be saturated (Butler, 1992). Although monoclinic pyrrhotite is a ferrimagnetic mineral, SD or pseudo-SD pyrrhotite generally shows a continuous increase in IRM intensity at relatively high fields (0.3-2.7 T) (Rochette *et al*., 2001). IRM acquisition curves representing Upper Disang sediments from Leshimi section reveals that IRM saturates between 150~200 mT (Fig. 6.1a). According to Alva-Valdivia *et al*. (2003), such IRM saturation at low to moderate fields of 150~200 mT indicate the ferrimagnetic phase corresponding to titano-magnetites. Samples from Viswema section shows that IRM saturates at 300 mT indicating the predominance of magnetite as the main magnetic remanence carrier (Zhu *et al*., 2000; Tian *et al*., 2002). However, saturation is not obtained at fields under 1T, indicating the presence of antiferromagnetic minerals like goethite and hematite (Fig. 6.1b). IRM saturates at 300°C for basalt suggesting magnetite as the magnetic carrier (Fig. 6.2). Magnetic susceptibility vs temperature curves of the basalt samples indicate that it contains magnetite as the susceptibility drop around 580°C (Fig. 6.3a,b). The incremental increase in susceptibility with temperature till 550°C (Fig. 6.3c) may be ascribed to diagenesis or low grade metamorphism, but it may be noted that susceptibility drops suddenly after 580°C indicating the presence of magnetite.

Remanent coercivities are the amount of backfield IRM to reduce the saturation isothermal remanence to zero. Soft magnetic minerals (ferrimagnetic) require less applied field (<50 mT) whereas antiferromagnetic minerals need comparatively higher backfield of IRM (>300 mT) to reduce the SIRM to zero. The low values (<50 mT) are indicative of low-coercivity minerals such as magnetite, titanomagnetite and maghemite, and also depends on their grain sizes. The higher values (>100 mT) are characteristic of high coercivity minerals (hematite and
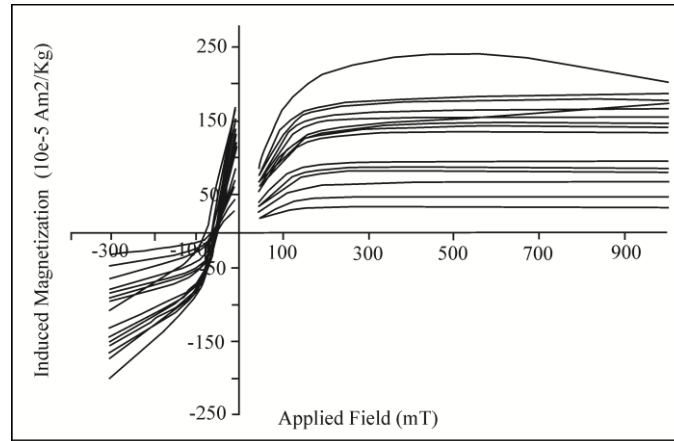
Fig. 6.1a: Representative IRM acquisition curves from Leshimi section, Phek district
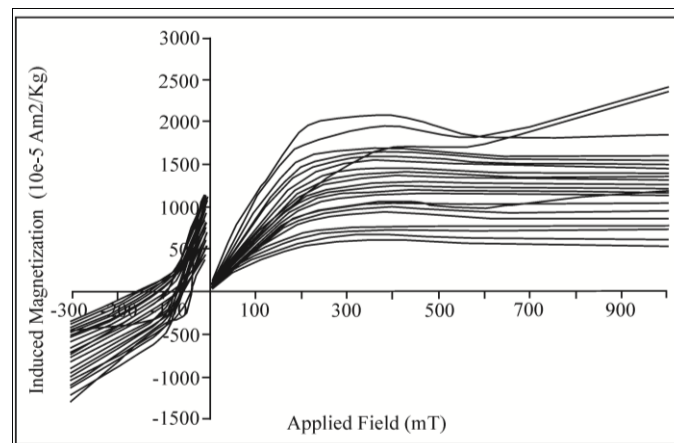
Fig. 6.1b: IRM acquisition curves from Viswema section, Kohima district
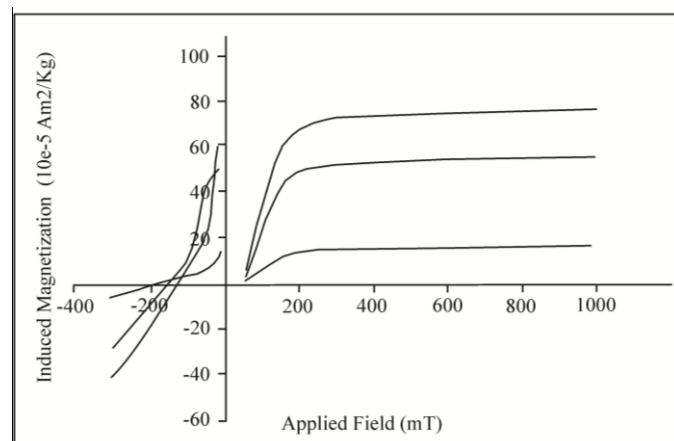
Fig. 6.2: IRM acquisition curves of representative basalt samples from NHO
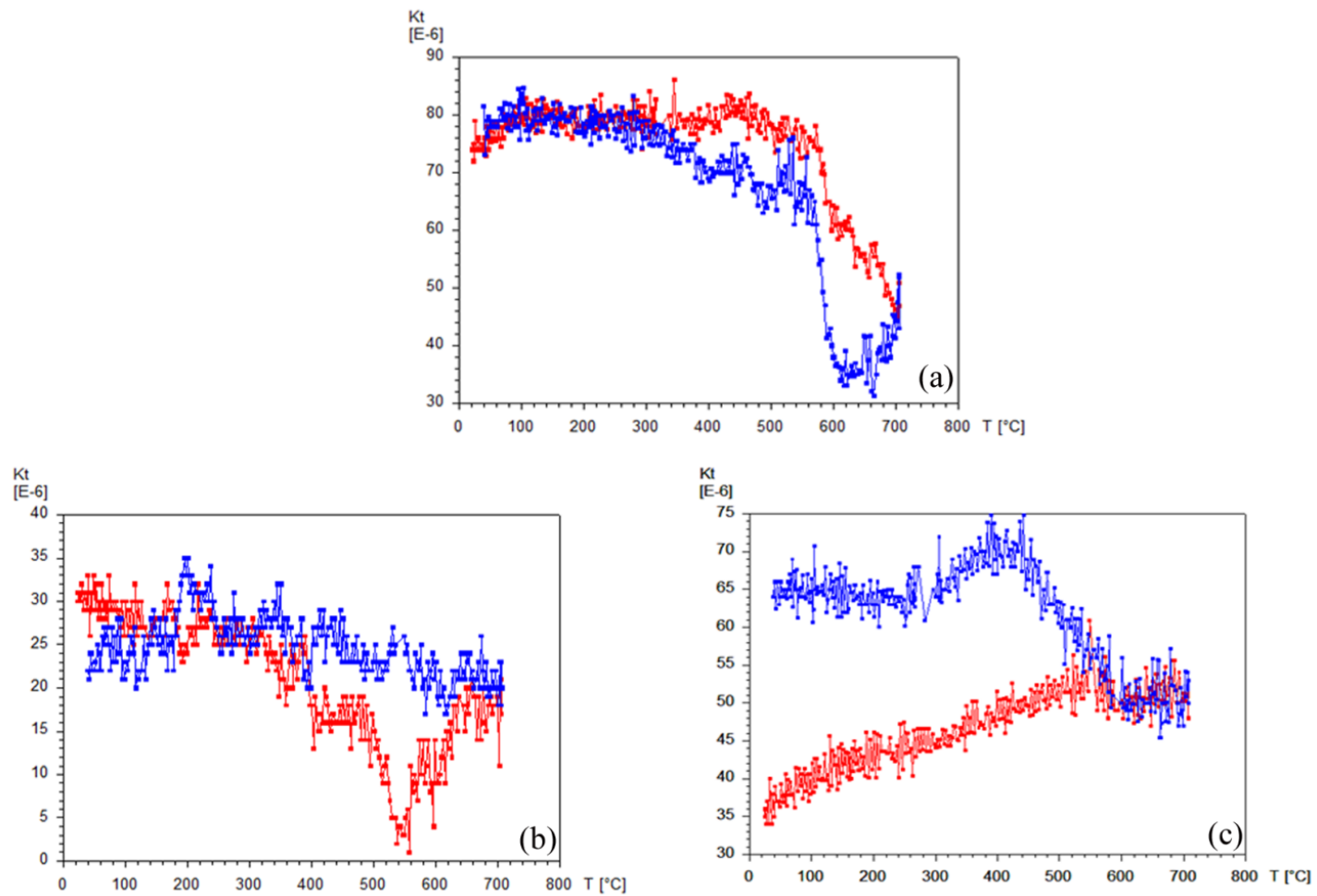
Fig. 6.3: Magnetic susceptibility vs temperature curves of representative basalt samples from NHO

goethite). Goethite is the one of the most hard coercivity mineral (>>400 mT). Remanent coercivities in Upper Disang range between 30-40 mT. These values indicate low coercivity magnetic minerals, mainly magnetite (Dunlop and Ozden, 1997; Vigliotti, 1997; Zhu *et al*., 2000; Tian *et al*., 2002). However, Hcr from Viswema section is higher relative to Disang sediments, varying between 40-70 mT, indicating probable admixture of ferri and antiferromagnetic minerals in varying proportions.

F_{300} (IRM$_{300mT}$÷SIRM) is computed to determine the relative proportions of ferrimagnetic minerals such as magnetite and anti-ferromagnetic minerals such as hematite and goethite (Weiguo and Lizhong, 2003). This ratio decreases with increased contribution from antiferromagnetic minerals. It ranges from 80 to 99% in the Upper Disang with an average of 96.6 ±4.38%, whereas it varies from 86.09 to 99.92% (avg. 94.3±3.85%) in the Laisong sediments (Table 6.1, 6.2). This ratio suggests that IRM obtained by the sediments is nearly saturated in a field of 300 mT. Laisong rocks indicate that only 94.30±3.85% IRM is saturated at 300 mT; nearly all IRM obtained by Upper Disang sediments gets saturated at 300 mT. This attests to the fact that the Upper Disang sediments are predominantly ferrimagnetic. S ratio indicates the proportion of SIRM carried by low coercivity components. This ratio estimated following Robinson (1986) and Bloemendal *et al*. (1992), varies from 80.46 to 99.00 (avg. 97.56±4.54) in the Leshimi section and from 61.60 to 89.84% (avg. 80.50±7.43%) in the Viswema section (Table 6.1, 6.2). The higher S ratio in the Upper Disang sediments relative to the Laisong indicates greater ferrimagnetic minerals concentrations, especially magnetite.

6.2   Basalt Paleomagnetism

Preliminary paleomagnetic studies were carried out on the basalts of parts of the NHO (Appendix I). Out of 19 oriented block samples collected only two sites SE of Wazeho, Phek district have shown statistically acceptable results. ChRM directions in the magnetite grains were successfully isolated between 550° and 580° using progressive ThD. The overall mean normal polarity direction for the basalt is calculated as declination (D) = 330.8°, inclination (I) = 25.2° (α_{95}=7.84; k=130.08). The paleopole of basalt is plotted in a synthetic apparent polar wandering path for India (APWP) following Vandamme *et al*. (1991) for determination of age of the rocks.

6.3 Magnetostratigraphy

The geomagnetic field of the earth has been arbitrarily switching its polarity in the geologic past resulting in alternating periods of normal and reverse polarity. Geomagnetic polarity reversal is a global event that provides markers for correlation and is the basis for chronostratigraphy. Magnetic polarity stratigraphy helps in determination of age and precise temporal correlation between series of sediments (Butler and Opdyke, 1979; Channel *et al*., 1984; Ogg and Lowrie, 1986; Heller *et al*., 1988; McNeill *et al*., 1988; Aissaoui *et al*., 1990; King and Channell, 1991). Magnetostratigraphy aids in correlating normal and reversed polarity zones of a rock succession to magnetic anomalies of the standard geomagnetic polarity time scales (Cande and Kent, 1992) by tie points from independently dated benchmarks and iterative matching of reversal patterns to GPTS. With the aid of radiometric geochronologic techniques, magnetostratigraphy permits assignment of a 'quasi-continuous' age to sedimentary strata based on correlation of local magnetostratigraphic columns with local polarity time scales (Gradstein *et al*., 2004). Magnetic polarity is independent of lithogenic constraints such as lateral litho-facies variations, thereby permitting good correlation amongst Cenozoic successions (Tauxe and Opdyke, 1982; Tandon *et al*., 1984; Johnson *et al*., 1985; Raynold and Johnson, 1985; Appel *et al*., 1991; Tandon, 1991; Rao, 1993; Burbank *et al*., 1996; Sangode *et al*., 1996, 1999; Brozovik and Burbank, 2000; Kotlia, *et al*., 2002; Sangode and Kumar, 2003; Sangode and Bloemendal, 2004). Consequently magnetostratigraphy can give very high resolution within this order of time (Alva-Valdivia *et al*., 2002).

A combination of rugged terrain, dense and impenetrable forest cover, dearth of good exposures and complex structural configuration have permitted the construction of only two vertical profile sections, one at Leshimi and the other at Viswema, for magnetostratigraphic attributes (Fig. 6.4). These two sections provide the only continuous, well-exposed and structurally undisturbed sections in the study area. The splintery nature of the Disang shale has also been a constraint in obtaining standard cores / cubic samples.

A total litho-column thickness of 234 m at Leshimi and a 483 m thick column at Viswema have been systematically measured and logged and from where oriented samples have been collected at suitable intervals based on lithofacies variation. Lithologs for these two sections have been prepared based on various
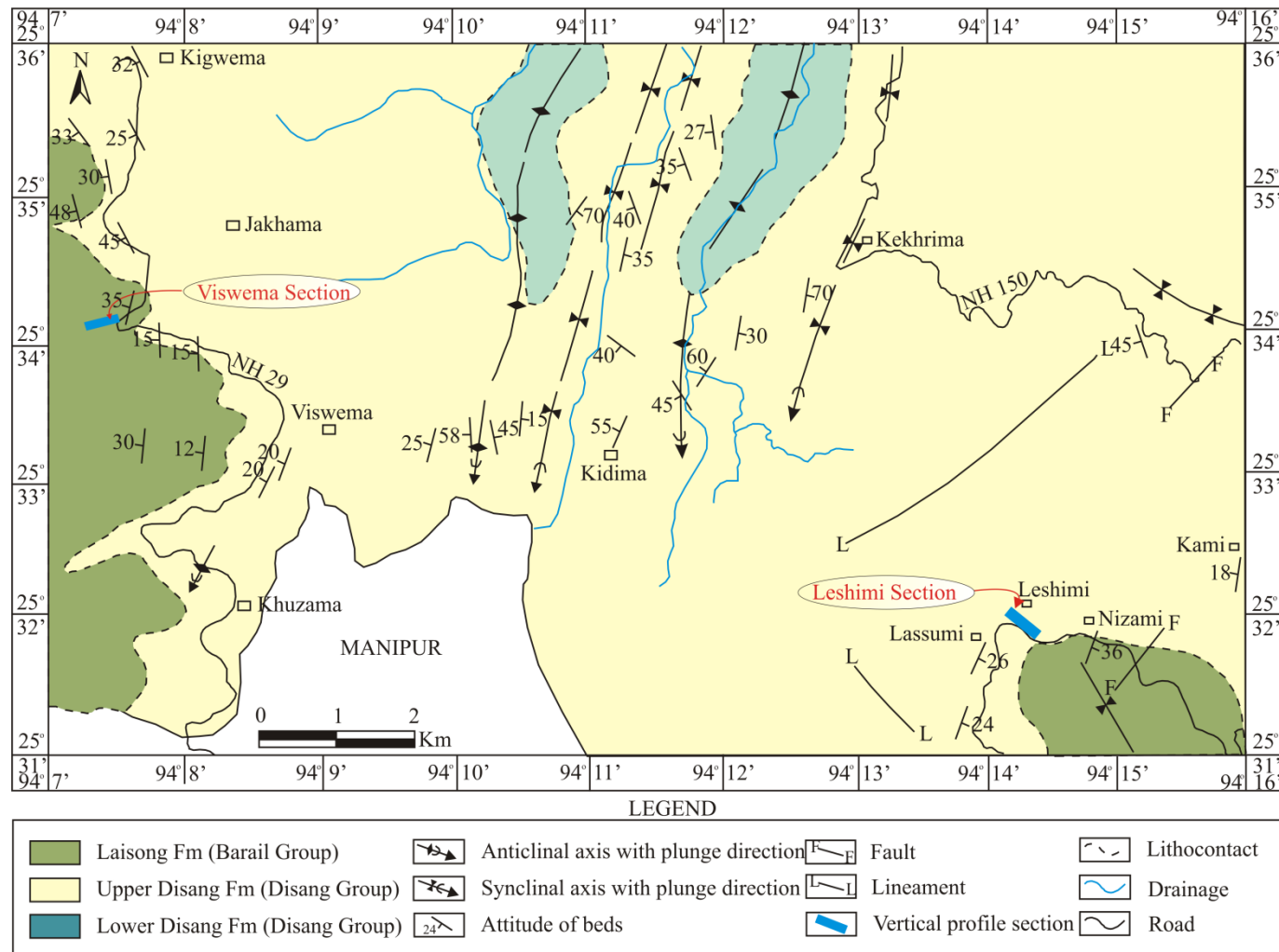
Fig. 6.4: Geological map showing Leshimi and Viswema sections (after Jayaram *et al.*, 1987)

sedimentological observations including grain size, color and upper and lower contact relationship. A lithological description of individual section is described below.

6.3.1 Leshimi Section

The Leshimi section mainly exposes heteroliths of Upper Disang sediments (Fig. 6.5; Plate 6.1). The beds strike NE-SW, dipping at angles varying from 14-30° due SE. This section is characterized by overall fining upward cycle. The lowermost 24 meters of the section is comparatively more argillaceous with interbeds of silty shale and siltstone. The thickness of siltstone varies from 3 to 10 cm. Shales are carbonaceous, dark gray and silty.

The basal shale-siltstone sequence is overlain by medium to coarse grained, gray, indurated, laminated sandstone with shale intercalations. This sequence of rocks is named Unit 1 (24 m to 61 m). The upper part of this unit is represented by a 24 m thick sequence of predominantly dark gray carbonaceous shale interbedded with minor siltstone. Siltstone is gray, laminated and micaceous.

The overlying Unit 2 (62 m to 104 m) is characterized by coarse grained sandstone with shale intercalations at the basal part. The upper part is overlain by interbeds of sandstone, carbonaceous shale and siltstone with a sharp contact. Thickness of shale varies from 2 to 3.5 cm, while it is 1 to 2.5 cm for siltstone. The sandstone is gray and fine grained with thicknesses varying from a few to about 13 cm.

The basal part of Unit 3 (105 m to 158 m) is represented by gray, coarse grained sandstone about 6 m thick with occasional shale partings. Interbeds of sandstone and shale overlie the basal coarse grained sandstone. Sandstones are medium to coarse grained. Shale is dark gray and splintery in nature. The thickness of individual sandstone beds range from 20 to 34 cm whereas that of shale ranges from 2 to 3 cm. The overall sequence of this sandstone exhibit gradual decrease in size from coarse to fine. The uppermost part of this unit is predominantly argillaceous, mainly dark gray carbonaceous shale with flaggy sandstones. The thickness of sandstones varies from 2 to 5 cm. Nodules and concretions of varying sizes are widespread in this argillaceous sequence.

Unit 4 (159 m to 204 m) is predominantly argillaceous with negligible sandstone. Shale is predominantly carbonaceous, silty and splintery. It is highly jointed and on collapse produces splinters/needles. Nodules and concretions of

57
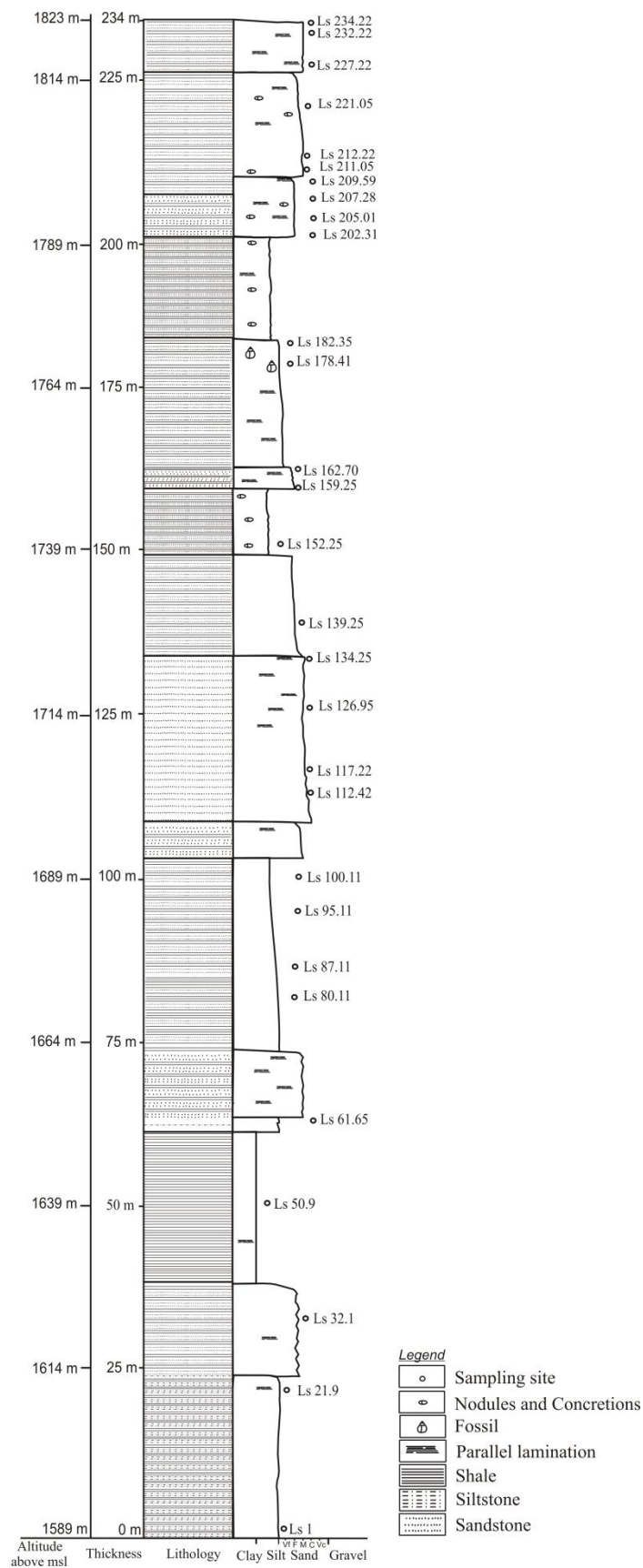
Fig. 6.5: Composite litholog of Leshimi section with paleomagnetic sampling sites, Phek district

varying sizes are widespread in this unit as well. In shape they vary from sub-rounded to elliptical and are random in distribution. However, some nodules show crude orientation along the bedding plane. They are mainly clayey concretions. This nodular and concretionary argillaceous unit is fossiliferous. The sandstones are hard, indurated and laminated, and vary in thickness from 2 to 5 cm. The thickness of sandstone beds gradually diminishes upward.

Grain size of Unit 5 (205 m to 234 m) is comparatively coarser than that of the lower units. The sandstone is essentially coarse grained, gray, hard and laminated at the base with gradual fining upwards. Intercalations of thin shale partings are common. The proportion of shale is comparatively lower than the underlying units.

The intensity of initial remnant magnetization in this section ranges from 4.69×10^{-5} to 2.56×10^{-4} A/m (avg. 7.22×10^{-4} A/m). Orthogonal vector plots of both ThD and AfD of representative samples are constructed (Fig. 6.6, 6.7 respectively). Results indicate that both treatments provide consistent results and allow clear identification of ChRM. AfD above 70 mT or ThD above 400°C is successful in obtaining ChRM directions for these samples. A secondary component, probably of viscous origin, is removed above 400°C or 70 mT. The greater part of remanent magnetization is removed at temperatures between 500 and ∼600°C, which points to (titano) magnetite as the remanence carrier.

6.3.1a Thermal Demagnetization

Most specimens exhibit a gradual drop in intensities with temperature increase up to 600°C. A linear decay towards the origin has been obtained in most of the samples (Fig. 6.6c,d,j,k) indicating a single magnetic component. Orthogonal vector plots of these samples reveal that 90% of the initial intensity decays till 500°C of demagnetization. The remaining intensity decays between 550°C to 580°C after which a slight increase in intensity may be observed. The step between 500°C to 600°C has been considered for ChRM which corresponds to the blocking temperature of magnetite (580°C).

A convex shape in intensity decay curve at temperature 400°C (Fig. 6.6i) indicates production of new magnetic minerals induced by thermal alteration. A rapid increase in bulk magnetic susceptibility above 550°C indicates alteration of magnetic mineralogy, that is, probably oxidation of magnetite due to heating (Fig. 6.6b,f,g,h,k).
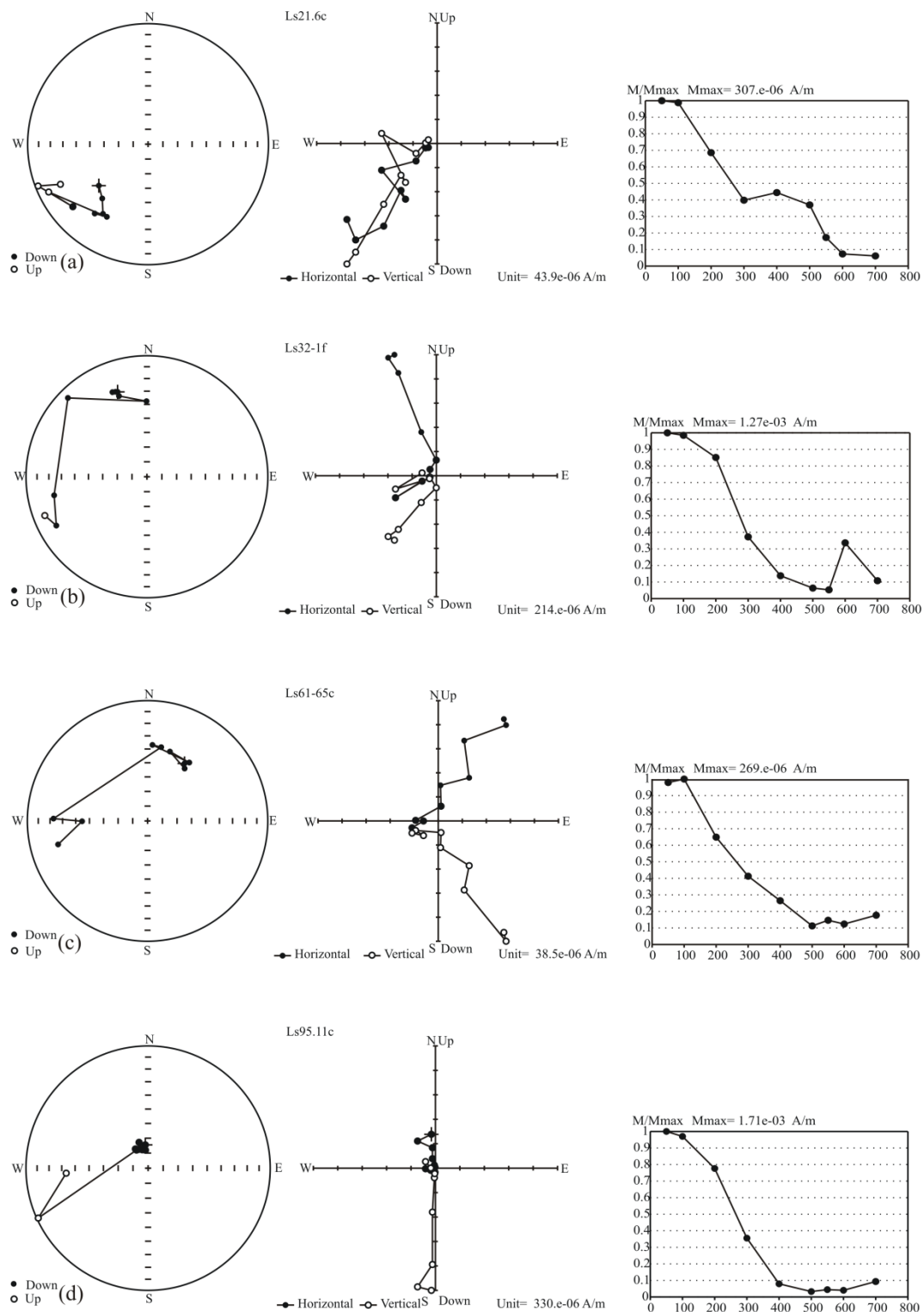
Fig. 6.6: Orthogonal vector plot and corresponding normalized intensity decay curves of thermal demagnetization of representative samples from Leshimi section, Phek district
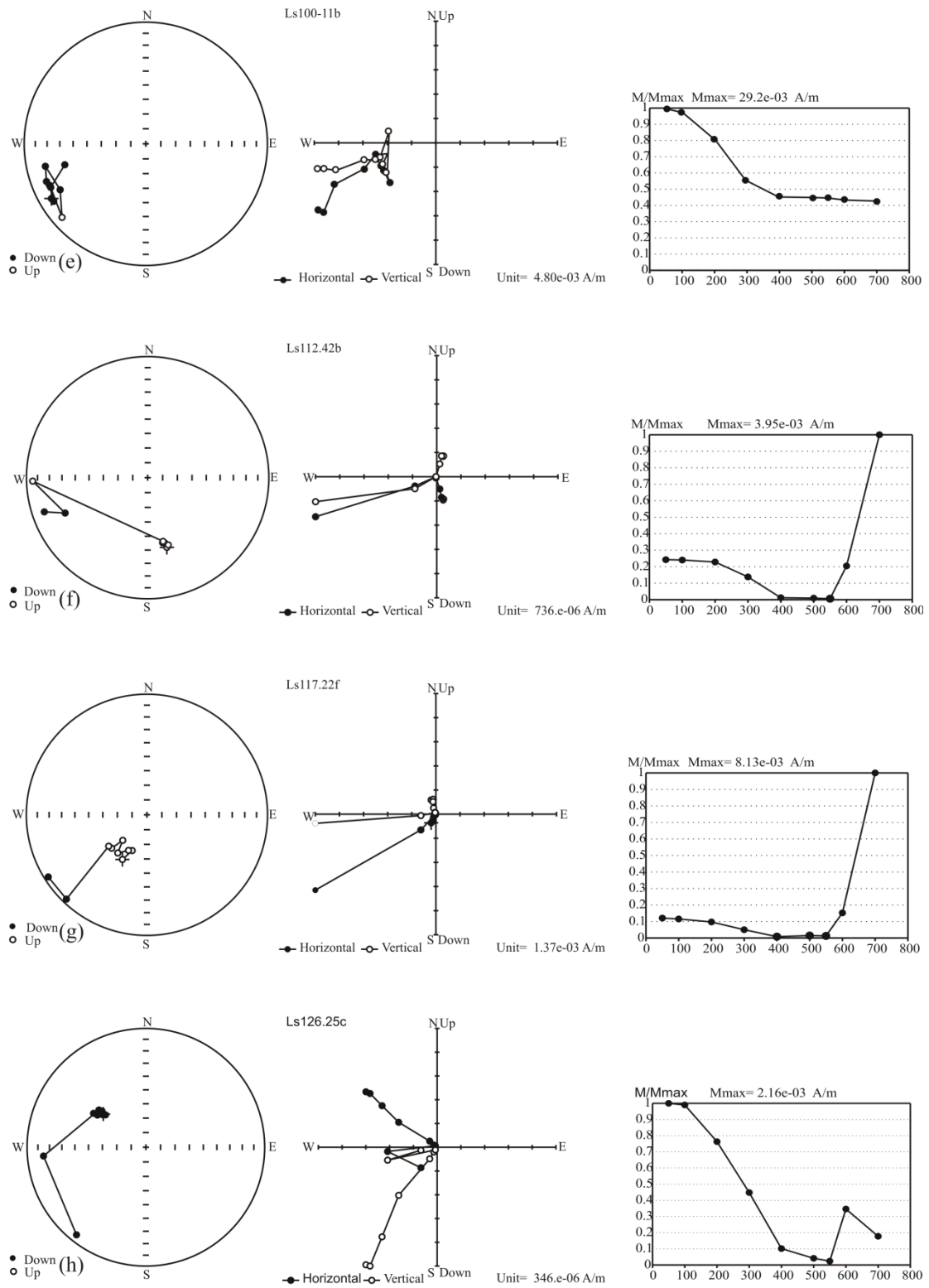
Fig. 6.6 (Cont'd): Orthogonal vector plot and corresponding intensity decay curves of thermal demagnetization from Leshimi section, Phek district
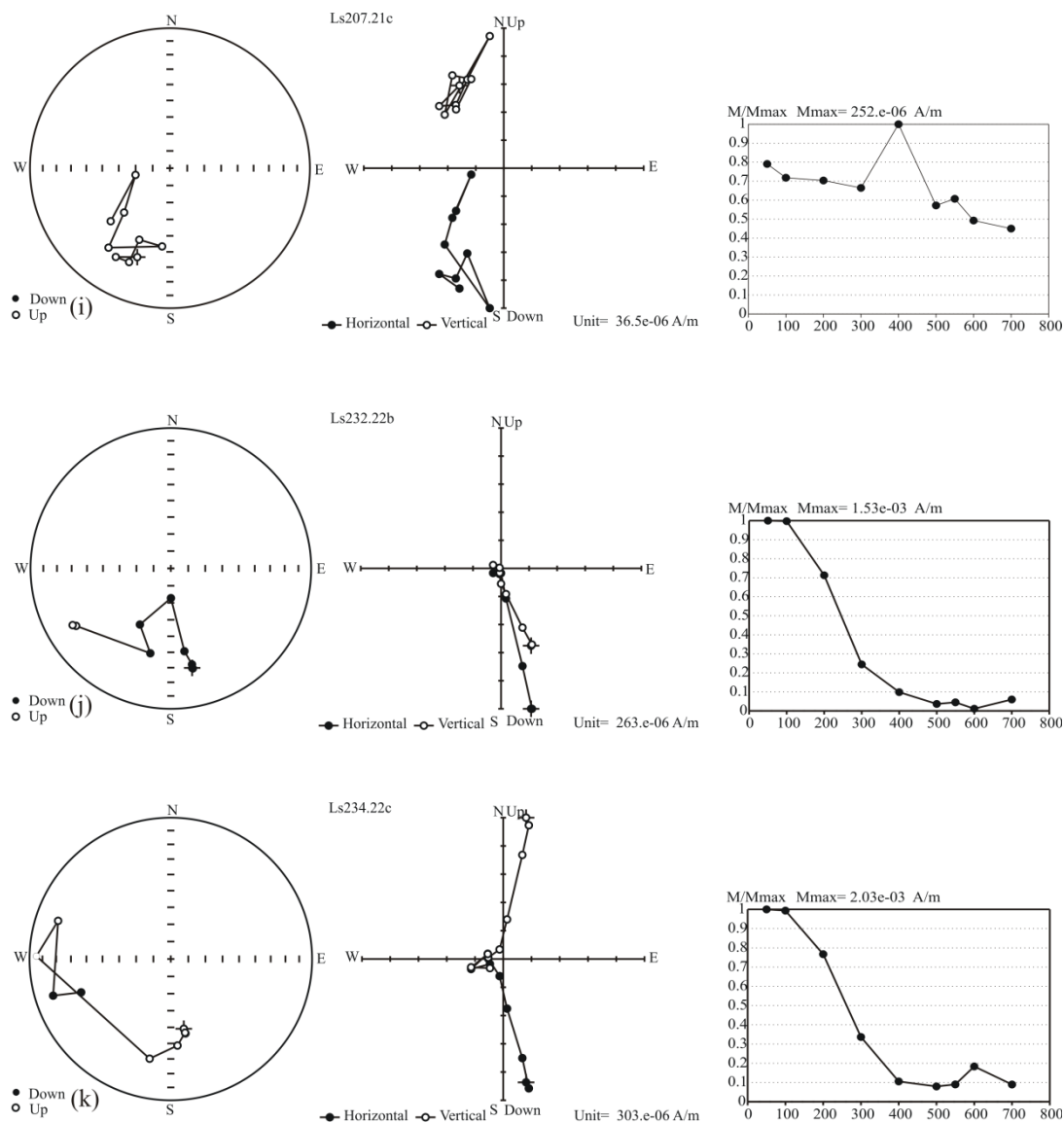
Fig. 6.6 (Cont'd): Orthogonal vector plot and corresponding intensity decay curves of thermal demagnetization from Leshimi section, Phek district
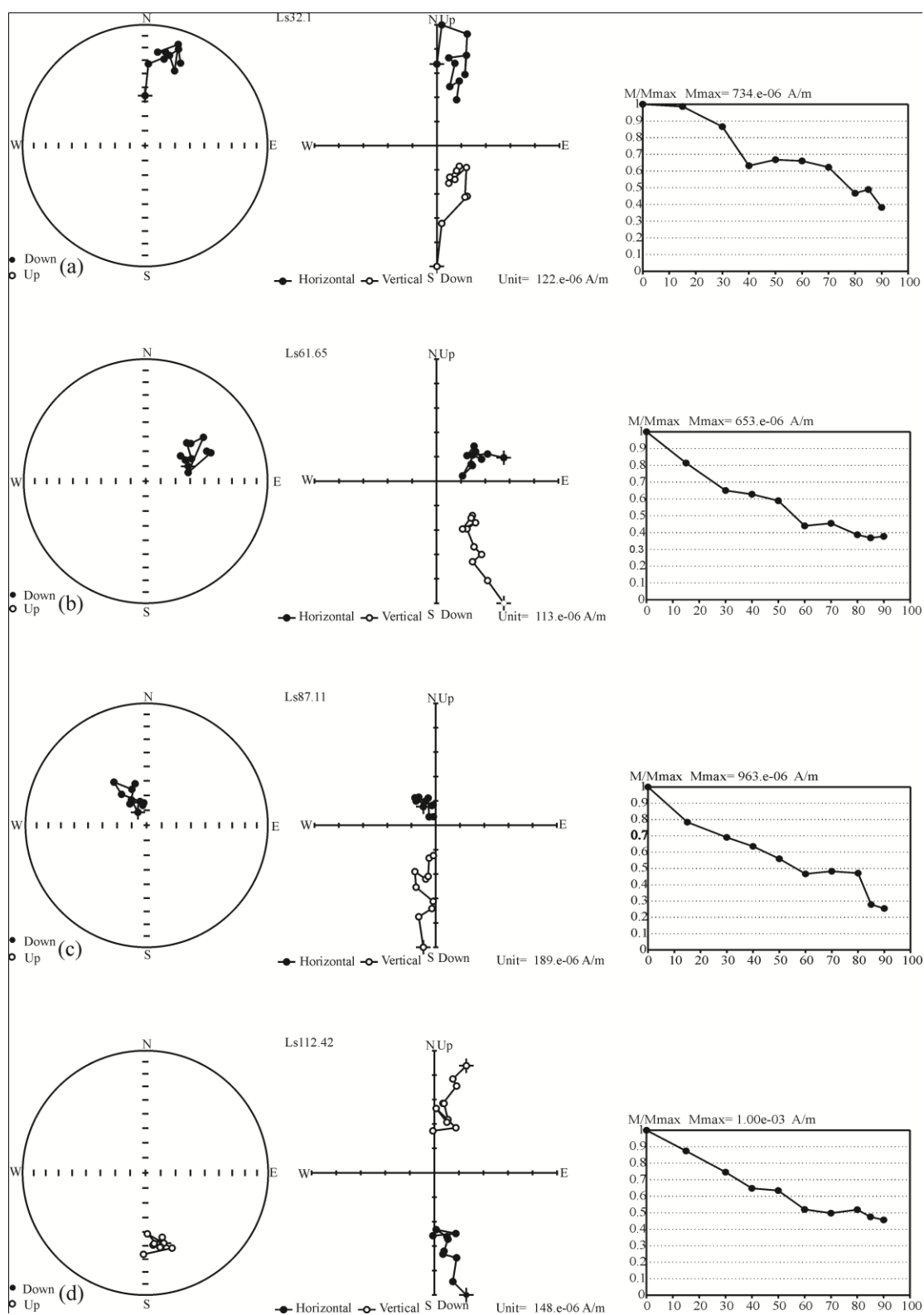
Fig. 6.7: Vector end point diagrams and normalized intensity decay curves illustrating AfD of representative samples from Upper Disang Leshimi section, Phek district
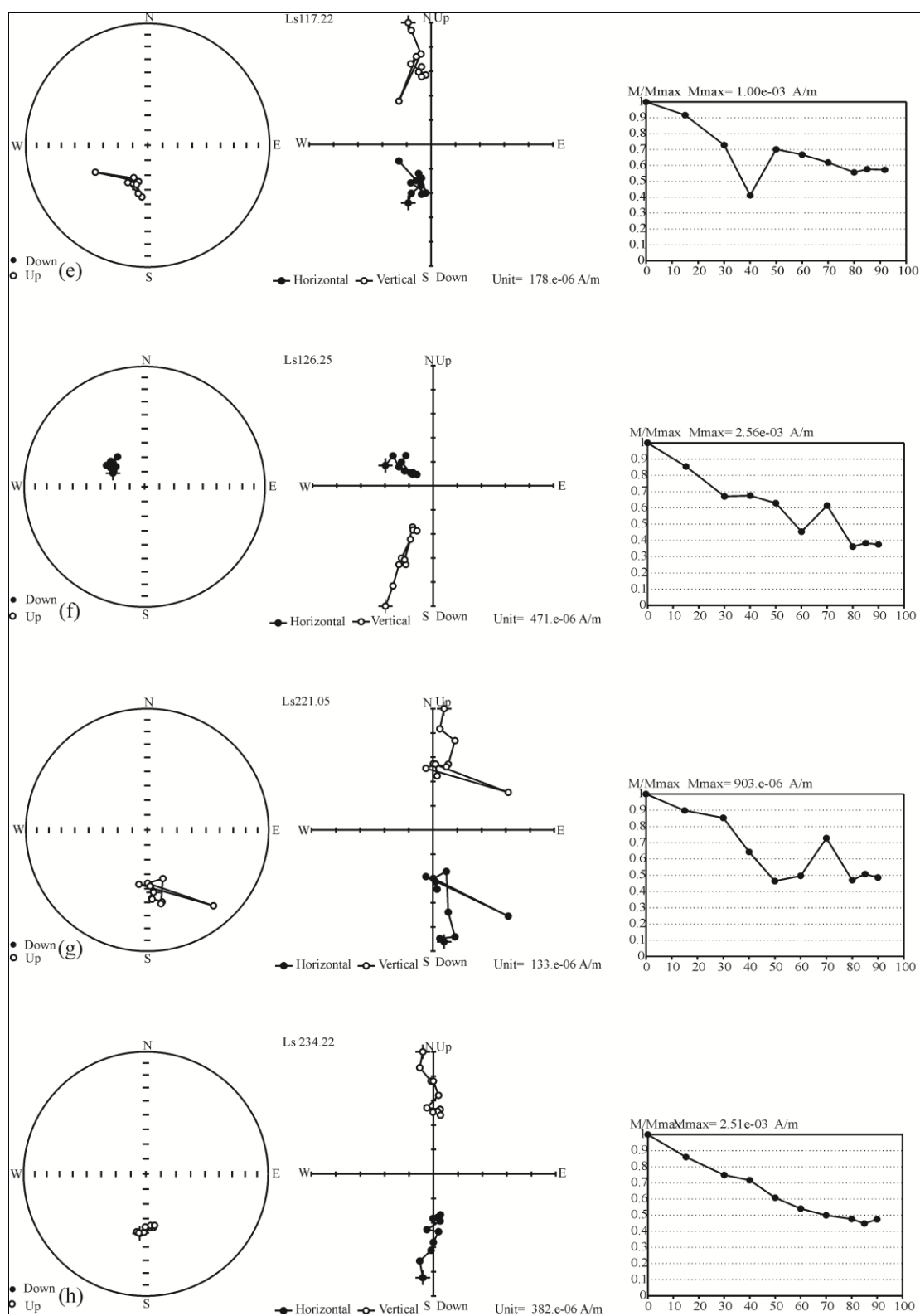
Fig. 6.7 (Cont'd): Vector end point diagrams and normalized intensity decay curves illustrating AfD of representative samples from Upper Disang Leshimi section, Phek district

Leshimi section (Table 6.3) a total of 2 normal and three reverse polarities are delineated in the Upper Disang (Table 6.4).

6.3.2   Viswema Section

This section representing the Laisong Formation (Plate 6.2) shows an overall coarsening upwards cycle (Fig. 6.8). The general attitude of the bed varies from N-S to NNW dipping at angle of 25° to 60° due west. The lower part of the section (<75 m) is characterized by interbeds of shale, sandstone and siltstone. Shale is dark gray, laminated, splintery and slightly silty. Sandstones are well bedded, gray, fine to medium grained and laminated. Thickness of sandstone beds range from 2-30 cm, their thickness increasing upwards in the litho column. Load cast and coal streaks are widespread at the base of these sandstone beds. Indurated, massive sandstone unit (∼4 m) with symmetrical ripples intermittently occur between shale-sandstone-siltstone interbeds.

A variation in lithology relative to the lower unit is noted from 75 m till 270 m. They are intercalations of fine grained sandstone, siltstone and shale. The proportion of sand ratio is greater relative to the lower lithounits. Besides bedding, this unit is devoid of other primary sedimentary structures. Grain size gradually increases from fine to medium grained towards the top of this unit. Load structures are common in the medium grained sandstone.

This is overlain by medium to coarse grained sandstone with subordinate siltstone and shale. Sandstone are gray to buff coloured, medium to thick bedded with widespread ichnofossils particularly Ophiomorpha *nodusa* and loadcasts. Symmetrical ripples are also noted particularly between 340-340 m. Occasional occurrence of clayey nodules with iron coatings are observed between 360-380 m.

The intensity of NRM in this section ranges from 4.11×10^{-8} to 1.11×10^{-6} A/m with an average of 6.07×10^{-7} A/m. ThD and AfD of representative samples are plotted (Fig. 6.9, 6.10 respectively). Pilot studies indicate that AfD provides better results in identification of a ChRM than ThD. AfD above 60 mT (600 Oe) or the ThD above 500^oC is successful in obtaining the ChRM directions for these samples. A secondary component probably has been removed prior to 500^oC or 60 mT (600 Oe). Thermally demagnetized samples suggest that the greater part of remanent magnetization was removed at temperatures between ~550 and ~680^oC, indicating predominance of

Table 6.3: Paleomagnetic results for the Upper Disang sediments from Leshimi section, Phek district

Site	Height (m)	Latitude (N)	Longitude (E)	Bedding attitude		In situ		Tilt Corrected		VGP		Polarity
				Dip Az.	Dip	Dec.	Inc.	Dec.	Inc.	Latitude	Longitude	
L$_S$1	1.00	25°31'39.00"	94°13'57.30"	110	23	202	-28	213	-25	-57	20	R
L$_S$21.9	21.90	25°31'38.82"	94°13'58.26"	120	10	239	-16	241	-11	-29	12	R
L$_S$32.1	32.10	25°31'38.56"	94°13'58.70"	130	20	273	23	355	38	83	323	N
L$_S$50.9	50.90	25°31'38.82"	94°13'59.13"	110	21	21	36	35	33	57	190	N
L$_S$61.65	61.65	25°31'38.82"	94°13'59.31"	70	22	343	81	48	66	46	140	N
L$_S$80.11	80.11	25°31'38.82"	94°13'59.31"	130	16	327	31	332	46	65	15	N
L$_S$87.11	87.11	25°31'38.82"	94°13'59.48"	130	16	7	57	330	63	59	50	N
L$_S$95.11	95.11	25°31'38.65"	94°13'59.92"	120	26	307	44	315	70	46	57	N
L$_S$100.11	100.11	25°31'38.73"	94°14'0.18"	130	14	232	11	229	13	-33	31	R
L$_S$112.42	112.42	25°31'38.82"	94°13'0.53"	140	14	164	-27	168	-40	-78	173	R
L$_S$117.22	117.22	25°31'38.73"	94°13'0.61"	133	22	196	-46	221	-52	-54	343	R
L$_S$126.95	126.95	25°31'38.91"	94°13'1.23"	120	24	302	33	303	57	41	33	N
L$_S$134.25	134.25	25°31'38.91"	94°13'1.58"	115	30	238	-37	250	-18	-22	4	R
L$_S$139.25	139.25	25°31'38.91"	94°13'1.76"	125	23	230	-28	240	-20	-31	8	R
L$_S$152.25	152.25	25°31'38.82"	94°13'2,46"	115	21	21	-26	12	-23	-50	256	R
L$_S$159.25	159.25	25°31'38.82"	94°13'2.37"	105	19	47	-23	215	38	-32	55	R
L$_S$162.70	162.70	25°31'38.82"	94°13'2.54"	110	50	265	36	205	70	-8	80	R
L$_S$178.41	178.41	25°31'39.08"	94°13'3.07"	115	50	135	24	135	-23	-46	175	R
L$_S$182.35	182.35	25°31'39.07"	94°13'3.51"	133	36	226	-34	247	-25	-26	361	R
L$_S$202.31	202.31	25°31'39.00"	94°13'4.03"	130	26	235	-33	248	-23	-25	362	R
L$_S$205.01	205.01	25°31'39.35"	94°13'4.12"	125	32	238	-49	260	-30	-16	354	R
L$_S$207.28	207.28	25°31'39.26"	94°13'4.21"	137	38	197	-27	221	-39	-52	360	R
L$_S$209.59	209.59	25°31'39.43"	94°13'4,29"	130	38	248	-40	265	-16	-8	359	R
L$_S$211.05	211.05	25°31'39.43"	94°13'4.38"	130	31	213	-23	227	-23	-44	12	R
L$_S$212.22	212.22	25°31'39.17"	94°13'4.38"	125	35	225	-32	242	-20	-30	7	R
L$_S$221.05	221.05	25°31'39.43"	94°13'5.08"	150	24	168	-28	175	-50	-83	235	R
L$_S$227.05	227.05	25°31'39.26"	94°13'5.34"	70	25	237	-40	240	-15	-30	10	R
L$_S$232.22	232.22	25°31'39.26"	94°13'5.52"	105	24	199	-36	215	-31	-56	12	R
L$_S$234.22	234.22	25°31'39.17"	94°13'5.78"	93	34	140	-30	165	-48	-76	202	R

Plate 6.1: Leshimi section

Plate 6.2: Viswema section
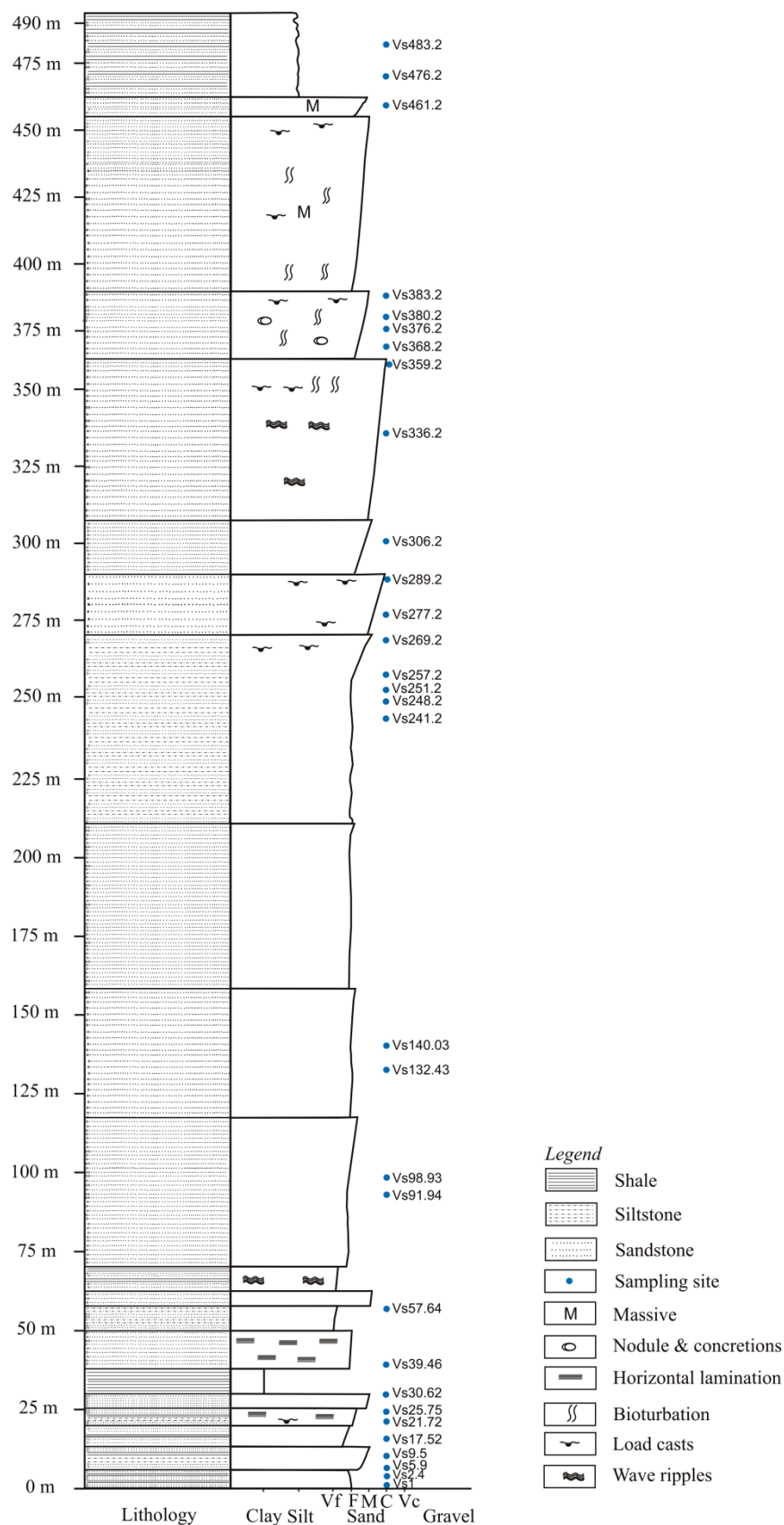
Fig. 6.8: Composite litholog of Viswema section, southern Kohima with paleomagnetic sampling sites

magnetite as the main remanence carrier. However, a minor remanence by hematite and goethite cannot be ruled out.

6.3.2a Thermal Demagnetization

Thermal pilot study did not provide satisfactory result as compared to AfD. It may be noted that fall in intensity by 50-60% at 200°C in all the specimens suggests a strong secondary magnetic component of secondary origin probably goethite.

Two viscous magnetic components of secondary origin is evident (Fig. 6.9a); first, a linear intensity decay till 300°C with PCA 309/57/5.8 and second, from 350°C to 530°C (PCA 331/66/13) with a slight increase at 350°C. Blocking temperatures have been considered between 560° and 580°C with >90% intensity decay showing PCA 314/60/11 which corresponds to magnetite as remanence carrier. Abrupt rise in intensity after 600°C may possibly be attributed to oxidation of magnetite to hematite.

A strong steady secondary component decays by about 70% till 300°C with PCA 306/62/4.1 (Fig. 6.9b). Another secondary component is obvious at 350°C to 400°C showing PCA 315/54/6.7 with intensity decay by 90%, and thereafter a component between 560°C and 580°C with PCA 338/12/4 have been assigned as characteristic direction.

6.3.2b Alternating Field Demagnetization

Smooth logarithmic decay in intensity with remarkably straight single component approaching the origin indicate monomineralic stable vector component (Fig. 6.10l,m,n,o). Most samples contain a low stability overprint that had unblocking temperatures between 100 to 125°C portraying an abrupt drop in intensity, an indication of mineral alteration and weathering of goethite (McElhinny and McFadden, 2000). ThD and AfD techniques yield agreeable results; stable ChRM directions between 500°C and 580°C indicate magnetite as the dominant ferromagnetic mineral in these rocks.

Increase in susceptibility after attaining a stable magnetic state that is noted (Fig. 6.10c,e,f,k,l) may probably be attributed to laboratory oxidation of poorly crystalline iron oxides, those not affecting the primary remanence.

A slight drop in intensity by about 5% after 150°C (Fig. 6.10a) suggests the probable presence of small amounts of goethite showing PCA directions of 314/38/3.9. Furthermore, two secondary imprints are evident from the orthogonal
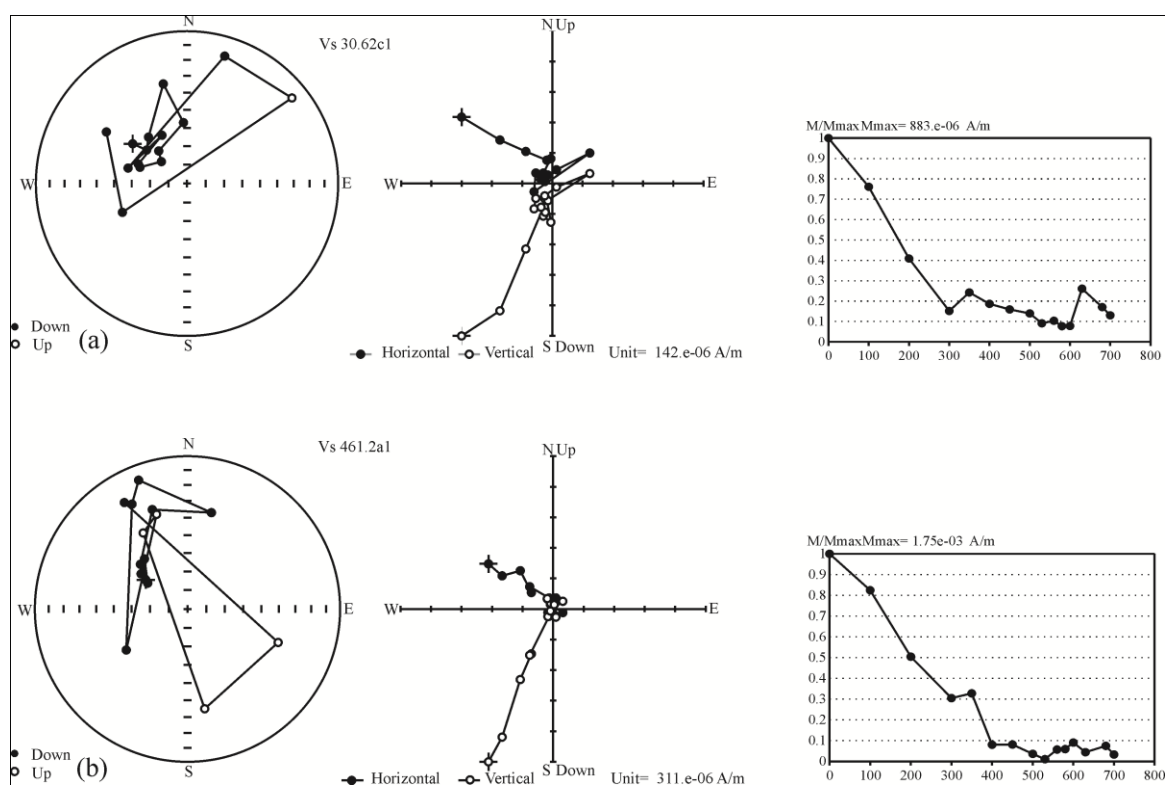
Fig. 6.9: Orthogonal vector plots and corresponding normalized intensity decay curves illustrating ThD of Viswema section, southern Kohima

vector end plot and intensity decay curve; first between 36 and 200 Oe, and second between 250 to 500 Oe. Intensity gradually drops to about 55% from 36 Oe till 200 Oe showing PCA of 309/31/2.4. With a minor fluctuation the intensity decays to 85% at 500 Oe. The vector linear path retains its original course after a slight rise at 600 Oe. Magnetic vectors of 320/11/1.0 between 600 and 1000 Oe is deemed as ChRM direction.

The presence of goethite is indicated by an abrupt fall in intensity by about 13% on heating to 150°C with PCA 310/51/3.4 (Fig. 6.10b). Gradually, intensity decreases by about 70% till 200 Oe maintaining its original path with PCA vectors of 308/45/3.2; a secondary magnetic component. This is followed by a slight rise in intensity at 250 Oe with steady decay till 500 Oe. Demagnetization steps 500-800 Oe with 90% intensity decay showing PCA 291/46/11 have been considered for ChRM direction.

About 60% of intensity decays till 200 Oe with some fluctuations (PCA 256/4/8.7) suggesting the presence of a strong secondary magnetic overprint (Fig. 6.10c). Vector end point plots suggest another secondary component between 200-600 Oe characterized by arbitrary vector and intensity fluctuations (PCA, 237/02/19). The magnetic vector retains its original path and >90% of intensity decays after 600 Oe with no variations in intensity till 800 Oe. The magnetic direction between 600-800 Oe with PCA of 261/-8/4.1 is deemed as characteristic vector.

Goethite present in minor concentrations is magnetically cleaned at 150°C (Fig. 6.10d). Progressive demagnetization till 300 Oe reduces intensity by >30% and removes a strong secondary component showing PCA vector 291/39/6. Another component probably of secondary origin with PCA 294/33/10 is noted between 300-500 Oe. Vector end point diagram (VEP) indicates sole variations in intensity with a constant magnetic vector. Logarithmic decay in intensity by 80% between 600-1000 Oe demagnetization steps reflects characteristic magnetic direction for this sample.

Two secondary components are apparent in the VEP plot (Fig. 6.10e). The first component with PCA 278/29/1 direction is removed by heating at 150°C where intensity rapidly drops by 10% and second component portrays a linear decay in intensity by >70% till 350 Oe with PCA vectors of 286/35/11. Further, with a slight rise in intensity at 400 Oe it retains a straight linear decay till 600 Oe where intensity drops by >95%. These demagnetization steps with PCA 290/34/15 have been assigned characteristic magnetic directions.

Small amount of goethite is also evident in the Zijderveld plots (Fig. 6.10f) which suggest that about 60% of intensity decays till 300 Oe with PCA directions of 301/33/3.6. With some fluctuations it retains its original path with linear decay till 800 Oe where intensity falls by >75%. Demagnetization steps between 500 and 800 Oe with PCA 294/42/9.3 is considered for ChRM direction.

A plateau-like rise in intensity (Fig. 6.10g) may be ascribed to alteration from low to high coercivity magnetic minerals. A strong secondary component precedes mineral alteration with linear intensity decay by 60% till 300 Oe (Fig. 6.10g,h). This component portrays PCA directions of 313/28/7.1. The presence of goethite in minor amounts cannot be ruled out. VEP plots as well as normalized intensity curves suggest demagnetization steps between 600-1000 Oe as a plausible ChRM direction with PCA 342/21/3.6.

Two strong components probably of secondary origin (Fig. 6.10i,j) are apparent. The first component is cleaned after heating to 150°C; alterations of this magnetic component seem to be relatively higher in Fig. 6.10i than in Fig. 6.10j as suggested by the normalized intensity decay curve. The second component shows a logarithmic decay till 400 Oe, though with some fluctuations. Thereafter, with a slight rise in intensity it retains a linear path from 600 Oe till origin and thereby attains its stable state with characteristic directions of PCA 306/75/12 and 332/59/1 respectively.

Progressive demagnetization to 150°C reduces initial intensity by 10% showing PCA direction of 277/40/2.8, thereby suggesting a viscous secondary component (Fig. 6.10k). Another secondary component is removed after 200 Oe, which reduces the intensity by about 60%. This is followed by some noise in intensity till 500 Oe, which again retain its original path providing stable state of magnetization from 500-800 Oe with PCA 261/43/8.7. A similar pattern with a smoother intensity decay curve is apparent in Fig. 6.10l.

Removal of viscous component at 150°C and the linear vector trajectories that decayed towards the origin (Fig. 6.10m,n,o) indicates predominance of a single component. About 20-30% of the initial intensity is decayed by removal of this viscous component portraying magnetic imprint with PCA direction 321/44/2.9. Intensity decay curve (Fig. 6.10o) shows a slight rise in intensity at 350 Oe. However, the smooth logarithmic linear path from VEP plots suggests presence of only one

component. This fluctuation in intensity may be attributed to spurious laboratory induced magnetization during measurements.

Two secondary components are evident in Fig. 6.10p; the first component probably of viscous nature is removed after 100 Oe and the second component at 350 Oe. It depicts a smooth logarithmic decay till origin. However, the presence of two components is unmistakably apparent from the VEP / Zijderveld diagram. The removal of secondary components is followed by a linear decay in intensity where initial intensity reduces to >90%. Demagnetization after 350 Oe yields stable magnetic directions (PCA, 316/32/5.5) which is consistent with the directions obtained by ThD, unblocked between 500-580°C.

A VGP is calculated for each characteristic component from stable end point directions after bedding tilt corrections. The latitude of the specimen VGP with respect to the overall mean north paleomagnetic pole is used to delineate the magnetic polarity stratigraphy after Lowrie and Alvarez (1977) and Kent *et al.* (1995). VGP relative latitudes approaching +90° and -90° are interpreted as normal and reverse polarity respectively.

The site-mean directions (before and after tilt correction), resultant vector (R), VGP latitude and longitude for the Viswema section is summarized in Table 6.5. Mean directions depict improved clustering after tilt corrections. The VGP latitude for each site is plotted against the litholog to reconstruct the local magnetic reversal pattern. A total of 2 normal and one reverse magnetozones have been obtained from this section (Table 6.6).

6.4   Sediment Accumulation Rate

SAR in the Leshimi section varies from 4.92 cm/ka to 25.81 cm/ka with an average of ~13.94 cm/ka (Table 6.7). There is a gradual increase in SAR from 9.02 cm/ka (36.341 Ma) to 10.82 cm/ka (35.685 Ma) and 15.09 cm/ka at around 35.526 Ma. Drop in SAR to 4.92 cm/ka can be seen after 35.526 Ma which gradually attains 25.81 cm/ka at around 35.94 Ma. Drop in SAR from 15.09 to 4.92 cm/ka is noted after 35.526 Ma. Average SAR for this section is 13.94 cm/ka.

SAR in the Viswema section varies from 11.53 cm/ka to 54 cm/ka with an average of 25.66 cm/ka (Table 6.8). Sedimentation rate at the base of the section is moderate (32.28 cm/ka) which gradually decreases to 11.53 cm/ka after 34.655 Ma. Rapid increase in SAR to 54 cm/ka is noted after 33.545 Ma. Average SAR for this

Table 6.4: Magnetic polarity events (Normal and Reversal) from Leshimi section, Phek district

Sl. No	GPTS Events	Duration (Ma)	Stratigraphic level (m)	Magnetic polarity
1	C16r	36.618 - 36.341 (0.277)	0-25	R1
2	C16n.2n	36.341 - 35.685 (0.656)	26-96	N1
3	C16n.1r	35.685 - 35.526 (0.159)	97-120	R2
4	C16n.1n	35.526 - 35.343 (0.183)	121-129	N2
5	C15r	35.343 - 34.940 (0.403)	130-234	R3

Table 6.6: Magnetic polarity events (Normal and Reversal) from Viswema section, southern Kohima

Sl. No	GPTS Events	Duration (Ma)	Stratigraphic level (m)	Magnetic Polarity
1	15n	34.940-34.655 (0.285)	0-92	N1
2	13r	34.655-33.545 (1.110)	93-220	R1
3	13n	33.545-33.058 (0.487)	221-483	N2

Table 6.7: Estimate of sedimentation rate using magnetostratigraphic ages from Leshimi section, Phek district

Sl. No	GPTS Events	Duration (Ma)	Stratigraphic level (m)	Magnetic polarity	Thickness (m)	Sedimentation rate (cm/ka)
1	C17n.1n-C16n.2n	36.618 - 36.341 (0.277)	0-25	R1	25	9.02
2	C16n.2n	36.341 - 35.685 (0.656)	26-96	N1	71	10.82
3	C16n.2n - C16n.1n	35.685 - 35.526 (0.159)	97-120	R2	24	15.09
4	C16n.1n	35.526 - 35.343 (0.183)	121-129	N2	09	4.92
5	C16n.1n - C15r	35.343 - 34.940 (0.403)	130-234	R3	104	25.81

Table 6.5: Paleomagnetic results from Viswema section, southern Kohima

Site	Height (m)	Latitude (N)	Longitude (E)	Bedding		In situ		Tilt corrected		VGP		Polarity
				Dip	Dip	Dec. (°)	Inc. (°)	Dec. (°)	Inc. (°)	Latitude	Longitude	
Vs1	1.00	25°34'13.11"	94°7'22.94"	281	45	319	60	300	20	31	360	N
Vs2.4	2.40	25°34'12.73"	94°7'22.37"	281	40	349	49	323	25	53	351	N
Vs5.9	5.90	25°34'12.54"	94°7'22.28"	250	34	285	-1	291	-28	12	341	N
Vs9.5	9.50	25°34'12.36"	94°7'22.09"	270	40	28	63	315	55	50	29	N
Vs17.52	17.52	25°34'12.26"	94°7'21.80"	328	42	328	42	299	25	32	4	N
Vs21.72	21.72	25°34'12.07"	94°7'21.52"	266	48	266	12	266	-36	-12	348	R
Vs25.75	25.75	25°34'11.88"	94°7'21.52"	238	42	343	32	315	33	48	363	N
Vs30.62	30.62	25°34'11.79"	94°7'21.42"	245	44	5	48	310	50	46	23	N
Vs39.46	39.46	25°34'11.60"	94°7'21.23"	281	46	9	70	308	40	43	12	N
Vs57.4	57.40	25°34'11.69"	94°7'20.76"	271	48	16	64	307	43	42	16	N
Vs91.94	91.94	25°34'11.50"	94°7'20.38"	218	52	351	2	336	34	67	352	N
Vs98.93	98.93	25°34'11.31"	94°7'19.91"	282	55	284	33	284	-22	7	348	N
Vs132.43	132.43	25°34'11.22"	94°7'20.00"	245	37	256	7	257	-29	-18	355	R
Vs140.03	140.03	25°34'10.84"	94°7'20.10"	245	60	147	36	185	23	-52	86	R
Vs241.2	241.20	25°34'9.80"	94°7'19.72"	235	50	341	38	301	34	35	10	N
Vs248.2	248.20	25°34'9.89"	94°7'19.24"	250	74	11	34	309	34	43	7	N
Vs251.2	251.20	25°34'10.08"	94°7'18.96"	237	54	19	14	350	50	77	37	N
Vs257.2	257.20	25°34'10.27"	94°7'18.87"	235	54	330	10	320	10	47	343	N
Vs269.2	269.20	25°34'10.08"	94°7'18.49"	245	52	358	77	261	42	3	30	N
Vs277.2	277.20	25°34'10.18"	94°7'18.20"	243	52	349	43	303	35	37	10	N
Vs289.2	289.20	25°34'9.99"	94°7'18.01"	227	37	295	31	282	13	14	5	N
Vs306.2	306.20	25°34'9.99"	94°7'17.16"	254	42	324	71	277	39	15	22	N
Vs336.2	336.20	25°34'9.89"	94°7'16.59"	227	65	336	57	264	31	2	22	N
Vs359.2	359.20	25°34'9.80"	94°7'15.55"	235	28	317	41	297	32	31	10	N
Vs368.2	368.20	25°34'8.00"	94°7'11.86"	320	34	330	19	330	-15	46	319	N
Vs376.2	376.20	25°34'9.13"	94°7'14.70"	230	42	346	28	318	38	51	7	N
Vs380.2	380.20	25°34'8.76"	94°7'13.28"	218	41	339	46	289	51	28	28	N
Vs383.2	383.20	25°34'8.28"	94°7'12.42"	225	31	328	25	312	28	44	360	N
Vs461.2	461.20	25°34'5.91"	94°7'8.82"	240	35	357	52	312	52	48	25	N
Vs476.2	476.20	25°34'5.53"	94°7'8.07"	245	39	346	34	319	19	48	349	N
Vs483.2	483.20	25°34'4.68"	94°7'7.12"	250	45	350	38	316	32	48	361	N

Table 6.8: Estimate of sedimentation rate using magnetostratigraphic ages from Viswema section, southern Kohima

Sl. No	GPTS Events	Duration (Ma)	Stratigraphic level (m)	Magnetic Polarity	Thickness (m)	Sedimentation Rate (cm/Ka)
1	15n	34.940-34.655 (0.285)	0-92	N1	92	32.28
2	13r	34.655-33.545 (1.11)	93-220	R1	128	11.53
3	13n	33.545-33.058 (0.487)	221-483	N2	263	54.00

Table 6.9: Comparison of SAR in the studied sections

Sl. No		Leshimi section	Viswema section
1	Average rate of sedimentation	13.94 cm/ka	25.66 cm/ka
2	Peak of sedimentation	25.81 cm/ka	54.00 cm/ka
3	Lowest rate of sedimentation	4.92 cm/ka	11.53 cm/ka
4	Thickness of sedimentation	234.00 m	483.00 m
5	Duration of sedimentation	1.67 Ma	1.88 Ma

Fig. 6.10: Orthogonal vector plot and corresponding normalized intensity decay curves illustrating AfD of Viswema section, southern Kohima

Fig. 6.10 (Cont'd): Orthogonal vector plot and corresponding normalized intensity decay curves illustrating AfD of Viswema section, southern Kohima

Fig. 6.10 (Cont'd): Orthogonal vector plot and corresponding normalized intensity decay curves illustrating AfD of Viswema section, southern Kohima

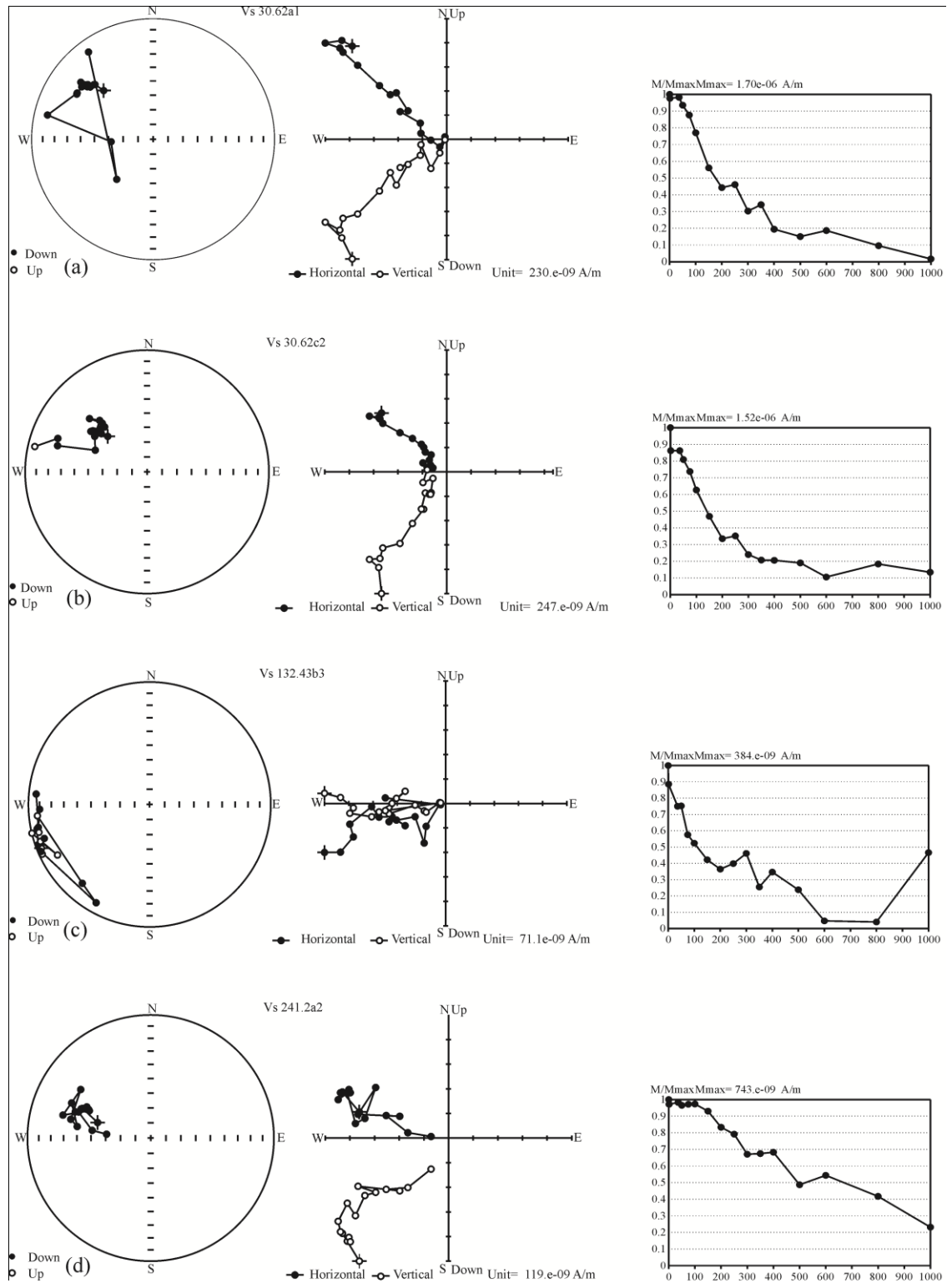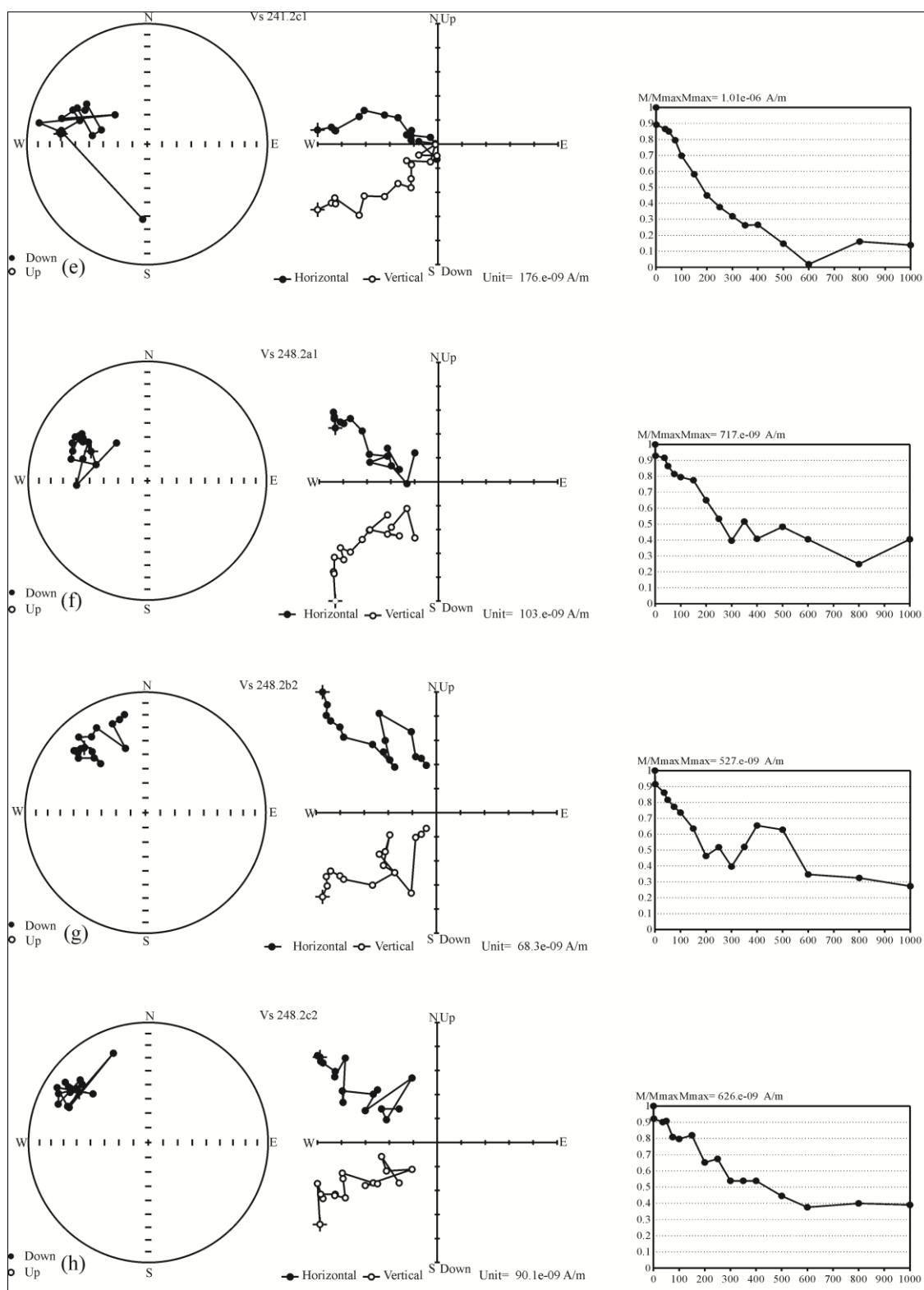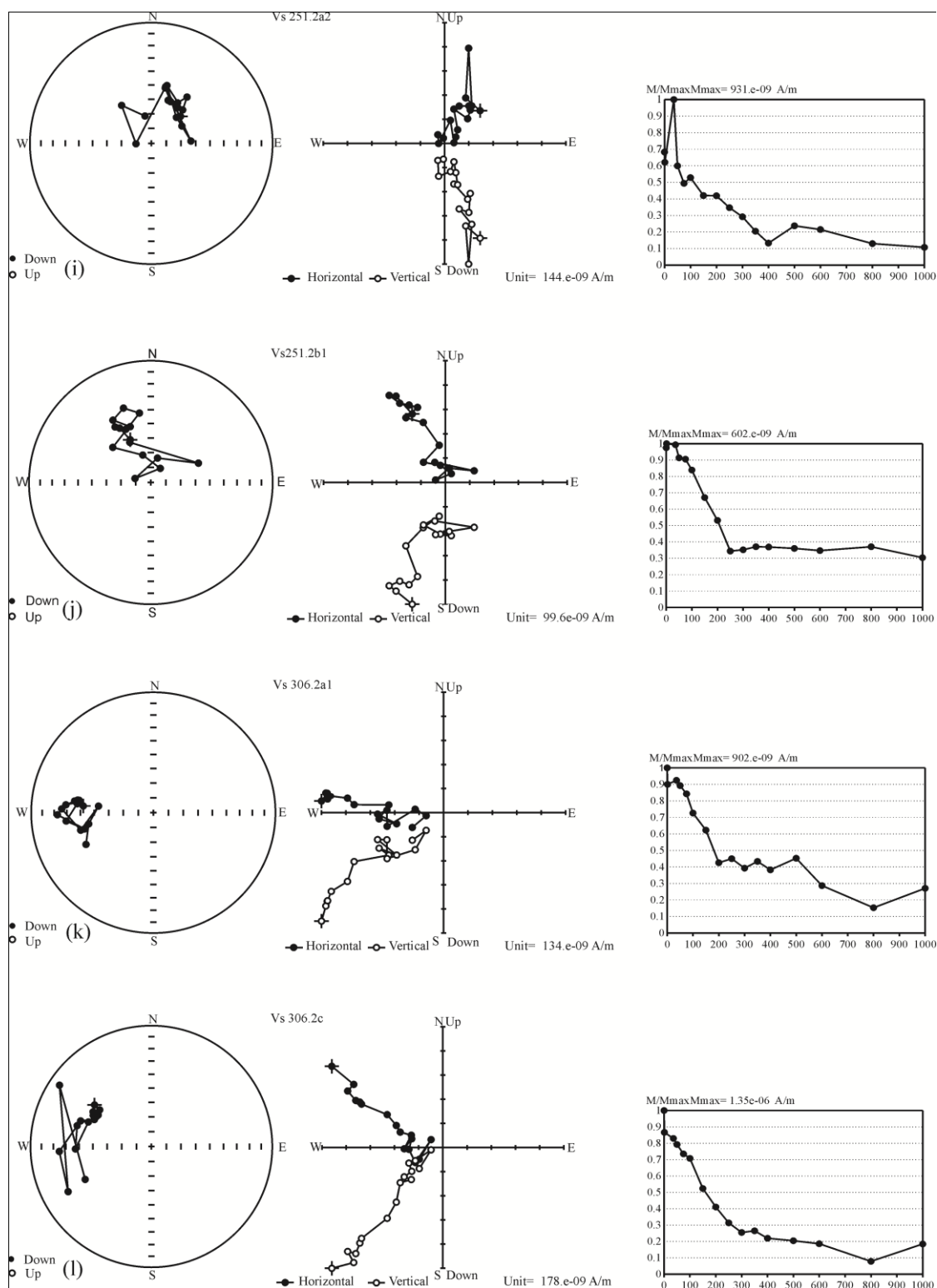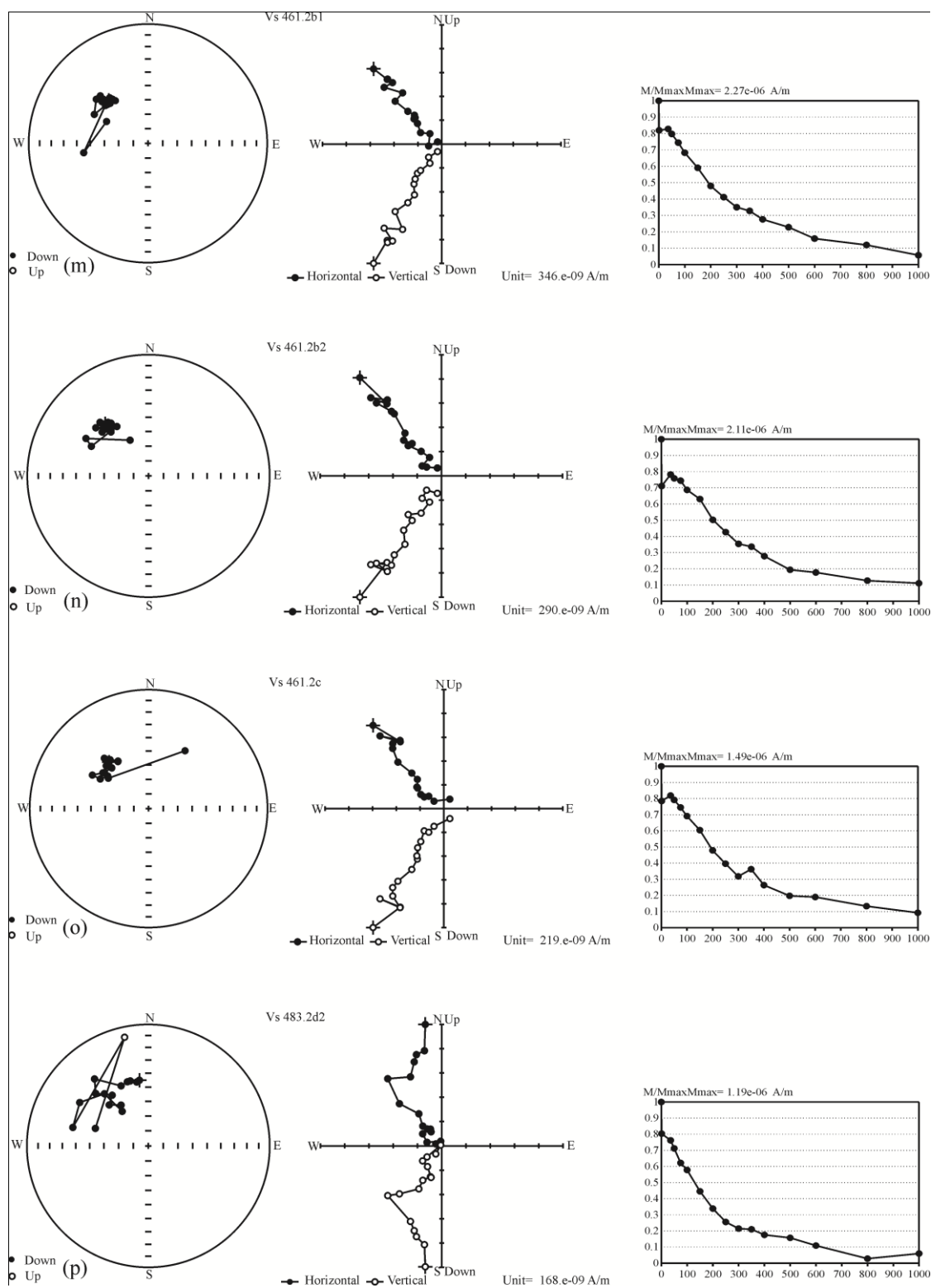**Figure 6.10 (Cont'd):** Orthogonal vector plot and corresponding normalized intensity decay curves illustrating AfD of Viswema section, southern Kohima

section is 25.66 cm/ka. SAR of Laisong sediments are relatively higher than that of Upper Disang sediments (Table 6.9).

6.5   Magnetic Rock Fabrics

Magnetic anisotropy studies have recently come to the forefront as accurate, fast and inexpensive in the investigation of rock fabrics. All materials acquire magnetization in a magnetic field, that is, magnetic susceptibility. This susceptibility is not always isotropic and varies with orientations of rocks (Ising, 1942). This spatial susceptibility variation is defined as the anisotropy of magnetic susceptibility (AMS) and reflects the preferred orientation of magnetic minerals in rocks or unconsolidated sediments (Hrouda, 1982; Tarling and Hrouda, 1993). According to Borradaile and Henry (1997) magnetic fabrics in the form of magnitude, shape and orientation of ellipsoids are indispensable for strain determinations in weakly deformed rocks.

The different parameters of AMS are combinations of the corresponding eigen values of the three principal susceptibility axes (Jelinek, 1981; Tarling and Hrouda, 1993). The shape of the susceptibility ellipsoid is characterized by the shape parameter T ($-1 \geq T \geq 1$). $T < 0$ refers to a prolate ellipsoid and $T > 0$ to an oblate ellipsoid. The eccentricity of the ellipsoid is measured by P' ($1 \geq P' \geq$ infinity), which is related to its degree of sphericity. The parameter showing the mean susceptibility is K_m ($=K_1+K_2+K_3/3$). The other important parameters include magnetic lineation $L = K_1/K_2$, magnetic foliation $F = K_2/K_3$ and T (shape parameter). Only the lower part of the Viswema section (upto 140 m) has been taken up for AMS studies.

Tarling and Hrouda (1993) proposed an ellipsoid shape parameter (T) to infer prolate ($-1< T< 0$), neutral ($T = 0$) and oblate ($0< T \leq 1$) fabrics. In the present study 27 (47%) samples out of the 58 show T value >0.1; the other 31 (53%) samples show strongly prolate fabric (Fig. 6.11), that is, $T<-0.1$ (Table 6.10). Pj vs T plots show the distribution of oblate and prolate AMS ellipsoids (Fig. 6.12). The orientation of K_{max} is significant towards NE-SW and NW-SE.
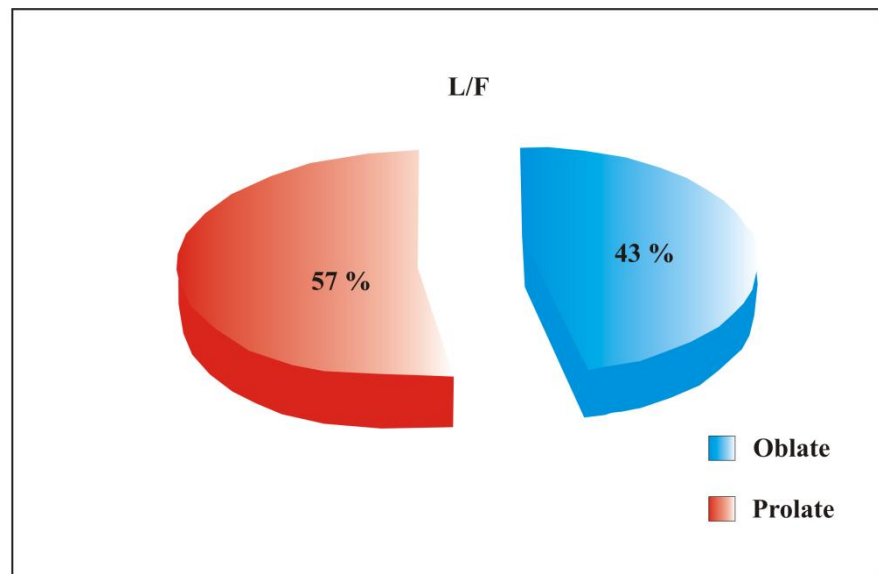
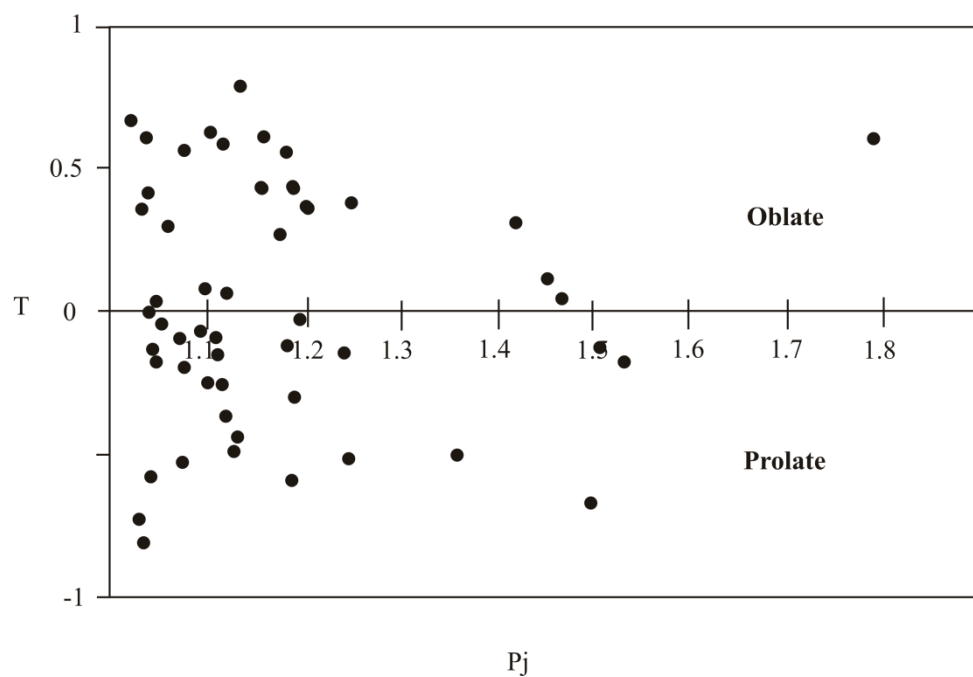**Fig. 6.11:** Pie chart showing distribution of oblate and prolate AMS ellipsoids

Fig.6.12: Jelinek shape plot showing eccentricity of magnetic ellipsoids with degree of anisotropy (Pj)

Table 6.10: Different magnetic fabric parameters of the rocks from Viswema section, southern Kohima

Sample	K_m	L	F	P_j	T
Vs1$_{b1}$	24.28892	1.116	1.553	1.789	0.602
Vs1$_{b2}$	14.10612	1.570	6.676	12.107	0.616
Vs1$_{c1}$	27.76307	1.125	1.256	1.421	0.319
Vs1$_{c2}$	29.44024	1.037	1.133	1.184	0.554
Vs1$_{d2}$	26.92448	1.174	1.054	1.249	-0.504
Vs1$_{d3}$	31.29712	1.059	1.132	1.204	0.367
Vs1$_{e3}$	24.64831	1.050	1.130	1.192	0.432
Vs2.4$_{c1}$	130.9132	1.004	1.018	1.023	0.667
Vs2.4$_{d}$	123.3055	1.025	1.004	1.032	-0.715
Vs2.4$_{e1}$	99.88354	1.012	1.026	1.039	0.373
Vs2.4$_{e2}$	86.2858	1.025	1.019	1.046	-0.133
Vs21.72$_{a1}$	52.14228	1.045	1.053	1.101	0.079
Vs21.72$_{a2}$	43.15726	1.028	1.120	1.161	0.606
Vs21.72$_{b1}$	65.79958	1.021	1.021	1.043	0.006
Vs21.72$_{b2}$	53.16058	1.077	1.045	1.126	-0.258
Vs21.72$_{b3}$	48.18886	1.054	1.017	1.075	-0.515
Vs21.72$_{c2}$	43.39686	1.029	1.027	1.056	-0.027
Vs25.75$_{a3}$	34.352	1.051	1.045	1.098	-0.067
Vs25.75$_{b1}$	31.53672	1.060	1.050	1.112	-0.089
Vs25.75$_{b2}$	35.37029	1.099	1.078	1.186	-0.113
Vs25.75$_{c1}$	38.42517	1.133	1.098	1.245	-0.141
Vs25.75$_{c2}$	115.3983	1.023	1.024	1.047	0.023
Vs25.75$_{c3}$	48.00916	1.022	1.087	1.118	0.584
Vs25.75$_{c4}$	30.63824	1.369	1.067	1.499	-0.657
Vs25.75$_{d1}$	33.75300	1.092	1.035	1.134	-0.437
Vs25.75$_{d2}$	39.74297	1.031	1.008	1.042	-0.571
Vs30.62$_{a1}$	118.8128	1.079	1.037	1.121	-0.358
Vs30.62$_{a2}$	112.1036	1.055	1.063	1.122	0.060
Vs30.6$_{a3}$	122.7663	1.062	1.038	1.104	-0.235
Vs30.62$_{b2}$	127.1393	1.016	1.058	1.079	0.552
Vs30.6$_{c2}$	126.5402	1.031	1.003	1.038	-0.795
Vs30.62$_{c3}$	130.9132	1.118	1.063	1.192	-0.292
Vs57.4$_{a3}$	76.94118	1.071	1.042	1.117	-0.247

	K_m	L	F	P_j	T
Vs57.4a4	53.99918	1.091	1.032	1.131	-0.471
Vs57.4b2	51.24377	1.111	1.024	1.147	-0.630
Vs57.4b3	74.96444	1.041	1.109	1.159	0.436
Vs57.4b4	66.09914	1.203	1.222	1.469	0.041
Vs57.4c3	65.79960	1.070	1.163	1.250	0.381
Vs57.4d1	59.62982	1.060	1.108	1.178	0.274
Vs57.4d3	67.17735	1.282	1.194	1.533	-0.167
Vs91.94a2	39.32367	1.012	1.110	1.137	0.789
Vs91.94a3	42.85776	1.097	1.094	1.200	-0.012
Vs91.94b1	41.48009	1.276	1.363	1.741	0.120
Vs91.92b2	46.39186	1.139	1.035	1.189	-0.585
Vs91.94c1	47.94926	1.046	1.031	1.078	-0.190
Vs91.94c2	43.81616	1.064	1.048	1.115	-0.141
Vs91.94c4	57.47343	1.258	1.197	1.507	-0.121
Vs132.43b1	116.0572	1.028	1.020	1.049	-0.165
Vs132.43b2	127.3190	1.049	1.104	1.162	0.343
Vs132.43b3	134.2079	1.052	1.055	1.109	0.030
Vs140.03d1	114.2002	1.007	1.027	1.036	0.608
Vs140.03d2	114.9790	1.023	1.025	1.048	0.032

K_m = mean susceptibility

L = lineation

F = foliation

P_j = degree of magnetic anisotropy

T = shape parameter

Chapter 7

DISCUSSION AND CONCLUSIONS

7.1   Basalt

The volcanic complex is one of the major units of the NHO belt, next in abundance to the serpentinite. These volcanics are confined to the northern, central and eastern parts of the belt, their contacts with other rocks suite being tectonic. Basalts occur in association with minor basaltic andesites, hyaloclastites and pyroclastics (volcanic breccia, tuff, ash and glass). These volcanics are exposed along the boundary thrusts of the ophiolite with the Disang and Nimi Formations. Important volcanic sections are exposed in and around Zipu. The volcanics are mixed with pelagic sediments such as chert and crystalline limestone. Spilitization is very common and intense in the volcanics between Wazeho and Zipu. It could indicate a state of extensive hydration of the parental magma through rock seawater interaction. However, the degree of spilitization varies from place to place. Basalt is found as sheet flows and pillow lavas that are affected by alteration/metasomatism and metamorphosed at places (Roy, 1989).

a) Sheet flows

These are well exposed along the road section between Waziho and Zipu. Individual flows vary from 3 to 6 m in thickness. They are intimately interbedded with chert and grey and white limestone. They are olive green to greenish grey rocks exhibit round/elliptical vesicles that are 2 mm to 1 cm in size. These vesicles are ordinarily filled with chalcedony, zeolite, calcite and epidote. The rocks display intergranular textures, which are locally subophitic. The mafic and felsic minerals show different stages of low grade alteration. The common secondary minerals are palagonite, chlorite, quartz, calcite and tremolite.

b) Pillow Lavas

The pillow lavas occur with round/elliptical outlines with bulbous tops. In cross-section at least 3 zones are recognized: an outer chilled glassy margin (1-3 cm) followed inward by a zone rich in vesicles and a massive portion with very few

vesicles at the centre. Textural and structural variations from centre to margin have been recorded. The pillow structures are stretched and aligned in a preferred orientation.

7.1.1 Petrogenesis

The presence of plagioclase phenocrysts may be attributed to fractional crystallisation (Roy *et al*., 1997). The high contents of clinopyroxene and olivine as phenocryst in the basalt may be due to higher MgO content. The prevalence of phenocrysts has significant petrogenetic implications for they demonstrate the rareness of superheated magmas (Cox *et al*., 1979). Swallow-tailed plagioclase is also observed. Such features, according to Best and Bothner (1971) are due to disequilibrium within the melt. Quench textures are also noted in these basalts. Knight (1971) opines that the formation of quenched crystals is due short unsteady periods of super cooling immediately following the initial nucleation event.

Geochemically the NHO volcanics are predominantly basaltic (Fig. 5.2, 5.3), evolving to basaltic andesite and trachy basalt and showing affinity with subalkaline / tholeiitic magmas. AFM ternary plots (Fig. 5.5) indicate that NHO basalts have a distinct tholeiitic trend. The tholeiitic trend suggests that oxygen fugacity of the magma chamber was low, as high oxygen fugacity would produce a calc-alkaline trend (Coleman *et al*., 1990; Wang *et al*., 2002).

High Mg numbers (Mg#) indicate primitive mantle source (Reichow *et al*., 2005). Intermediate Mg# of NHO basalts varying from 33.18 to 66.12 (avg. 54) suggest slightly evolved magmatic source. This is corroborated by slightly higher content of Cr and Ni. Binary plots of Ce/Yb vs Zr/Nb after Bagci (2013) suggest that smaller degrees of partial melting and/or differentiation play a more important role in the petrogenesis of these basalts (Fig. 7.1).

Melting experiments suggest that high-alumina basaltic liquids are not a product of low-pressure fractionation (Ringwood, 1976). Lower content of Al_2O_3 (9.9-14.4; avg. 12.6) of NHO basalts relative to N-MORB (15.27) suggest fractionation at relatively higher pressure. This further implies that these basalts were emplaced from a shallower magma source.

Zr/Nb ratios of NHO tholeiite ranging from 3.25 to 24.8 (avg. 11.9), with an exception of sample B13 (57), are relatively lower than N-MORB (>30) suggesting enrichment in the mantle. The $(La/Sm)_N$ ratio, an index of mantle enrichment that is

slightly higher in the NHO basalts (1.07-2.32; avg. 1.79) also suggest an enriched mantle source. This is further attested by higher ratios of Ta/Nb (0.08-2.0; avg. 0.42) as compared to 0.06 of most N-MORB (Sun and McDonough, 1989).

Primitive mantle-normalized spider diagrams show variable and selective incompatible element enrichment, particularly in LILE. Primitive mantle and N-MORB normalized spidergrams of NHO basalts are characterized by enrichment in LILE such as Cs, Ba, Rb and K relative to REE and HFSE. LILE enrichment may have been due to different processes. As these elements are very mobile they could have been enriched by remobilization during seafloor alteration or metamorphism related to obduction or collision. Alternatively, their enrichment could also suggest that the mantle source of these rocks had been previously and selectively metasomatized in a supra-subduction zone (SSZ) setting (Tatsumi *et al*., 1986).

Wood *et al*. (1979) opines that the negative Nb and Ta anomalies are characteristic of arc volcanic rocks. In the present study both elements are enriched relative to N-MORB values except for two samples with negative Nb anomaly. Subduction related mobile elements such as Ba and Pb are enriched relative to REE; such pattern according to Bezos *et al*. (2009) suggests that garnet had no influence. The overall flat REE pattern suggests poor fractionation of the parent magma with very limited negative Eu anomaly. The positive Eu anomaly relative to neighboring elements reflects the substitution of Eu for Ca in the Ca-rich plagioclase (Rollinson, 1993).

In various spidergrams selective enrichment of certain elements (Sr, Ba and U) and the relative lack of others (Zr, Y and Hf) are noted. Such patterns and the HFSE variations exhibited by tholeiitic rocks are characteristic of a SSZ (Pearce *et al*., 1984; Resimic-Saric *et al*., 2004). To evaluate the nature of the sediment component in modulating the composition of the lavas, the mobile nature of Ba and immobility of Th and Nb have been used effectively. Low Th/Nb is considered to have been derived from sources with less sediment addition. Th/Nb ratio of NHO tholeiitic lavas vary from 0.02 to 0.36 (avg. 0.1). This average value is significantly higher than N-MORB composition (0.05) suggesting contamination by the subducting slab. Low Zr/Nb ratios (3.25 to 24.8) may imply chemical modification due to addition of a subduction component (Ray *et al*., 2012).

M (incompatible elements)/Yb vs Nb/Yb plots following Pearce and Peate (1995) characterizes mantle source regions of the NHO basalts (Fig. 7.2a,b,c,d). For
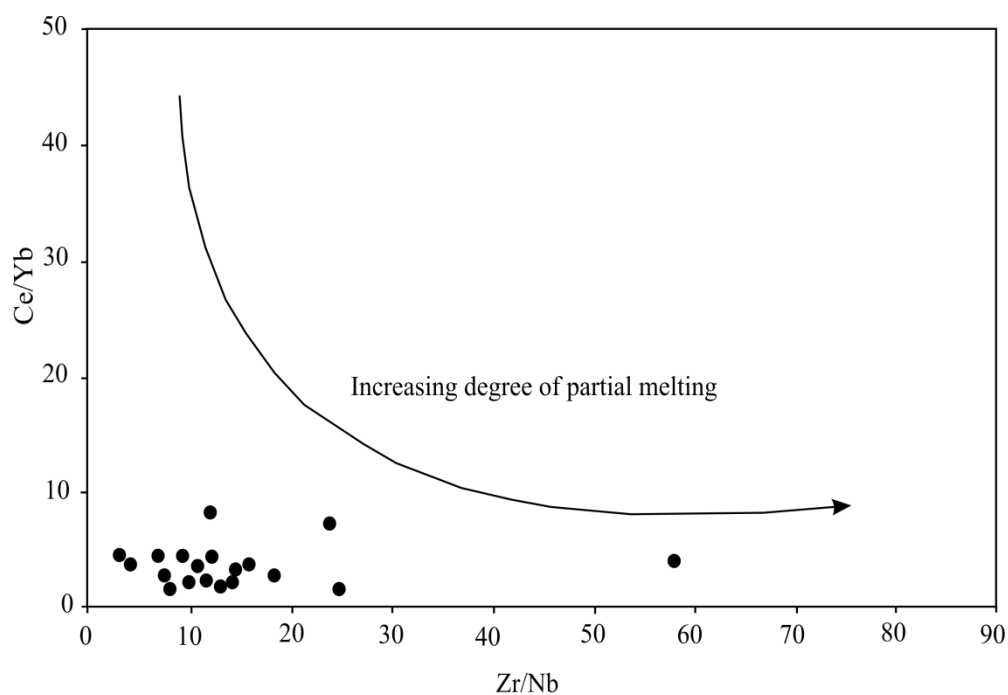
Fig. 7.1: Binary plot of Ce/Yb vs Zr/Nb (after Bagci, 2013)
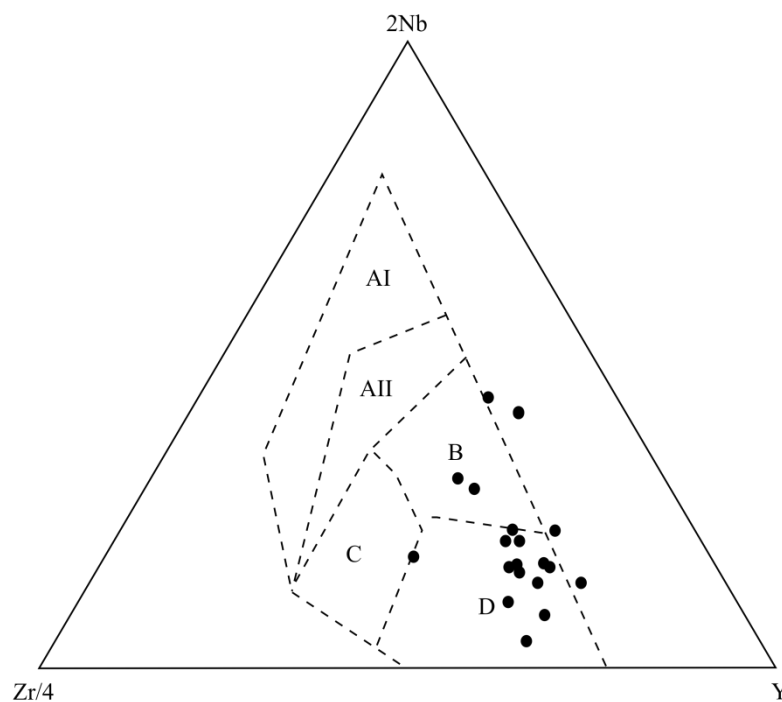
Fig. 7.3: Nb-Zr-Y tectonic discrimination plot (after Meschede, 1986) of NHO basalt (AI-AII: Plate alkaline basalt; AII-C: Plate tholeiite; B: P-type mid-ocean ridge basalt; D: N-type mid-ocean ridge basalt; C-D: Volcanic arc basalt)
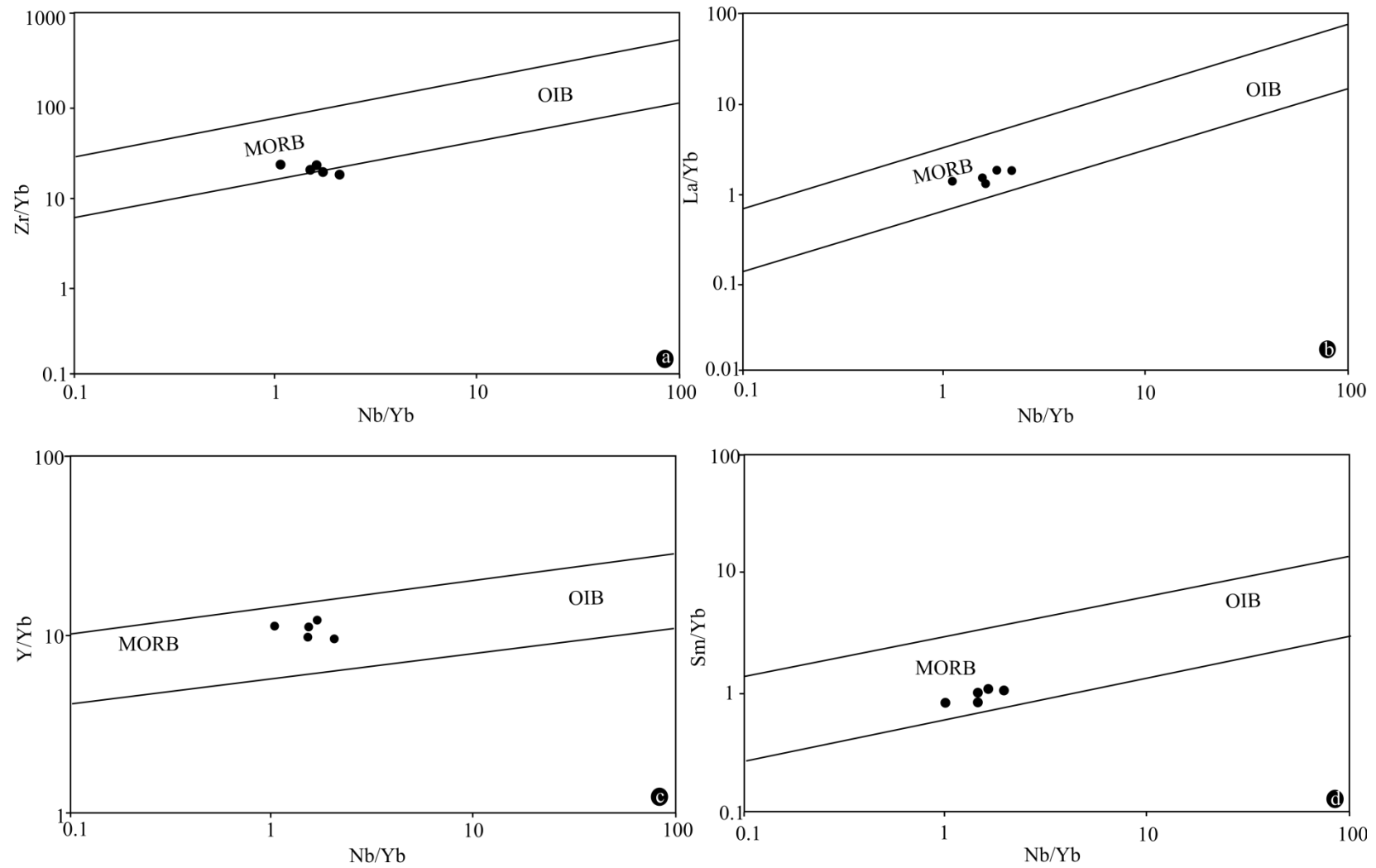
Fig. 7.2: M/Yb vs Nb/Yb plots (after Pearce and Peate, 1995)
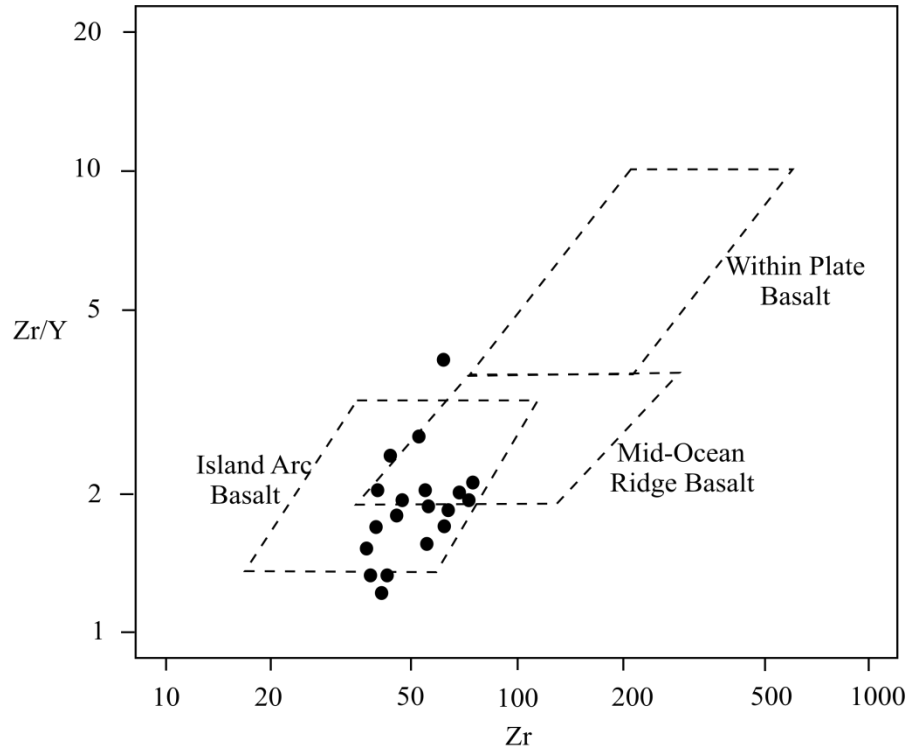
Fig. 7.4: Zr vs Zr/Y tectonic discrimination plot of NHO basalt (after Pearce and Norry, 1979)
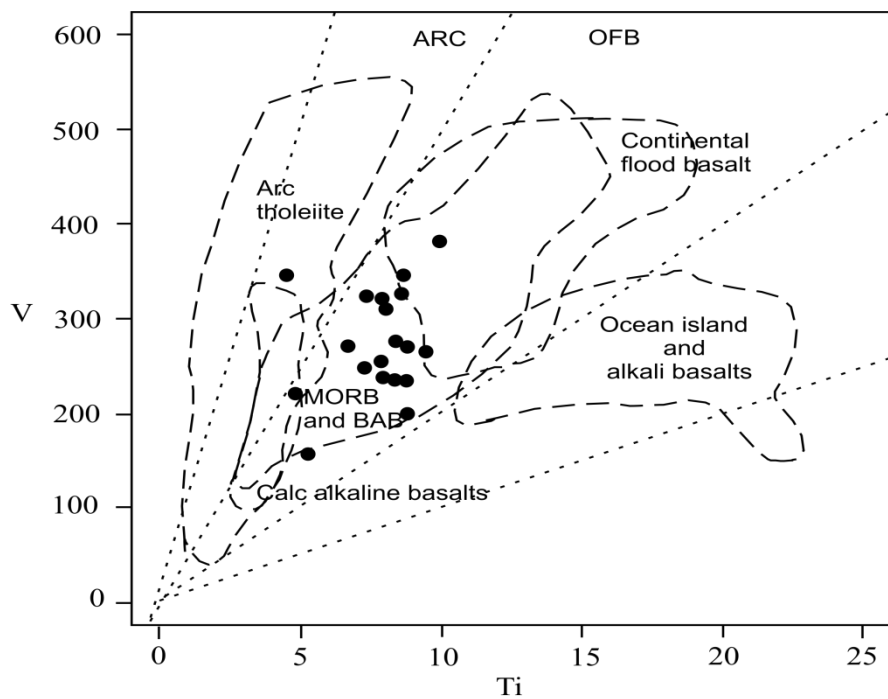
Fig. 7.5: V vs Ti discrimination diagram (after Shervais, 1982) for NHO basalt (MORB: mid-ocean ridge basalt, BABB: back arc basin basalt, OFB: ocean floor basalt)

Fig. 7.6: K_2O+Na_2O vs $K_2O/(K_2O+Na_2O)x100$ plots (after Hughes, 1972)

primitive mantle normalized spider plots showing enrichment of most trace elements probably suggest alteration by secondary processes. The negative Sr peak may also be attributed to removal of Sr with Ca during seafloor weathering. Mineralogical and chemical alteration of volcanic sequences of ophiolite by submarine hydrothermal alteration processes is well known (Pearce and Cann, 1973; Smewing and Po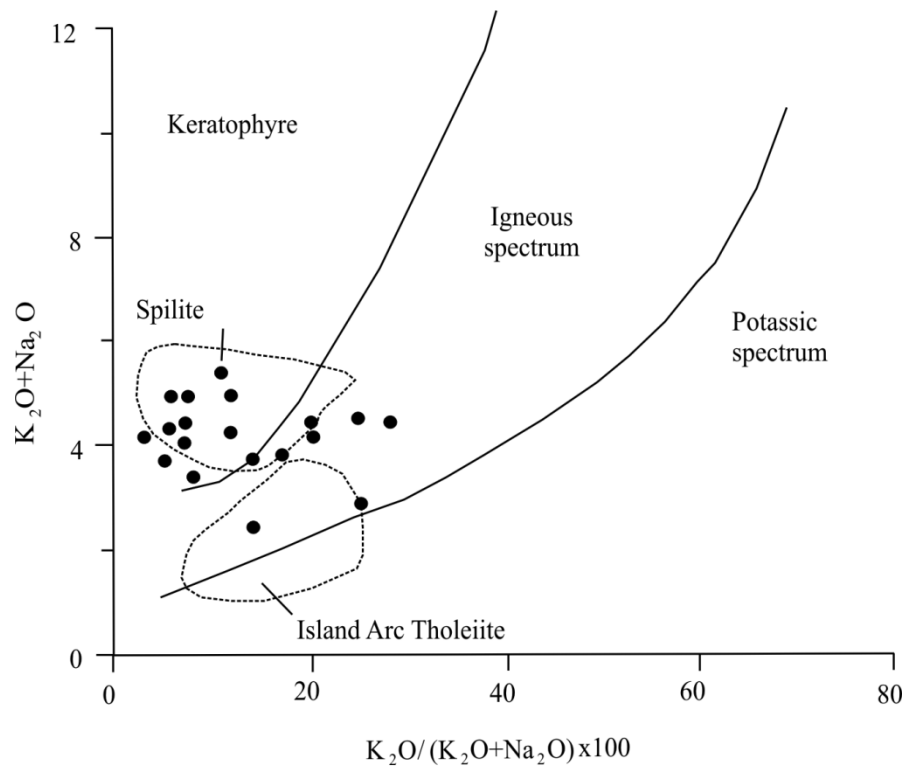tts, 1976; Spooner and Fyfe, 1973). Thus, data scatter in most of the bivariate plots may be attributed to hydrothermal alteration and / or metamorphism. Moderate negative correlation between MgO and CaO ($r=$ -0.59) indicates seafloor weathering / alteration (Seifert and Brunotte, 1996). The variation of Cu from 38 to 141 ppm may account for the high mobility of this element during hydrothermal alteration.

7.2   Upper Disang

7.2.1   Paleoweathering at Provenance

The degree of weathering is chiefly a function of climate and rates of tectonic uplift (Wronkiewicz and Condie, 1987). Increased intensity may reflect the decrease in tectonic activity and/or change of climate towards warm and humid conditions in the source region (Jacobson *et al.*, 2003). The alteration of minerals due to chemical weathering depends on the intensity and duration of weathering. Degradation of feldspar into clay minerals is the dominant chemical weathering process in the upper crust. Taylor and McLennan (1985) opine that feldspar degradation increases the mobility of many elements through clays. During chemical weathering Ca, Na and K are removed from feldspar (Nesbitt *et al*., 1980). The amount of these chemical elements surviving in the sediments derived from them is a sensitive index of the intensity of weathering. Thus, the prevalence of easily removable elements serves as an index of chemical weathering. The relative enrichment of Fe_2O_3, MgO and SiO_2 and depletion of TiO_2, Na_2O, CaO and K_2O in this study points to chemical weathering of the source rocks. There exists a positive correlation between Al_2O_3 and TiO_2 in the sandstone ($r=$ 0.2) and shale ($r=$ 0.89). Saxena and Pandit (2012) opine that such relationships are due to intense chemical weathering of source rocks, increasing values denoting increasing intensity. Feldspars are among abundant labile minerals that are significantly altered during weathering. Hence, the proportion of alumina to alkali typically increases in the weathered product. The average K_2O/Na_2O ratio of the sandstone and shale is 1.23 and 2.18 respectively, which is much lower

than that of the North American Shale Composite (NASC) (3.5). Ranjan and Banerjee (2009) opine that low ratios are due to the predominance of plagioclase over K feldspar.

Weathering indices of sedimentary rocks provide useful information on tectonic activity and climatic conditions of source areas. Nesbitt and Young (1982) proposed the Chemical Index of Alteration (CIA) which is an estimation of the degree of weathering of continental rocks. According to this scheme, greater alteration is reflected by higher CIA values. The CIA index is estimated using molar proportions:

$$CIA = [Al_2O_3/(Al_2O_3+CaO*+Na_2O+K_2O)] \times 100$$

where CaO* represents the amount of CaO incorporated in silicate phases. Unweathered source rocks possess CIA values of <50. Average shales have values between 70 and 75 which indicate muscovite, illite and smectite due to moderate weathering. Values from 76 to 100 indicate intense weathering. Under such conditions residual clays enriched in kaolinite and Al oxi-hydroxides are produced. CIA values of the sandstones of the study area range from 70.57 to 83.36 (avg. 78.89) whereas those of the shale range from 75.40 to 84.49 (avg. 79.23) pointing more or less to intense weathering of the source rocks. Al/Na vs CIA scatter plots of these rocks after Selvaraj and Chen (2006) indicate moderately high to high intensities of weathering (Fig. 7.7). Negative correlation matrix of SiO_2 with MnO, MgO and CaO indicate chemical weathering at the source area that has resulted in the relative concentration of residual elements. This is also attested by the positive correlation between Al_2O_3 and TiO_2. Dokuz and Tanyolu (2006) opine that chemical weathering of source rocks produce such values. In the A-CN-K diagram (Nesbitt and Young, 1982, 1984) all samples plot in the 'A' corner near illite, above the average PAAS suggesting marked loss in Na and Ca due to intense chemical weathering at the source (Fig. 7.8).

CIA becomes insensitive to the degree of weathering when K is reintroduced to the system so Harnois (1988) proposed the Chemical Index of Weathering (CIW). This index is not sensitive to post depositional K enrichment and is based on the presumption that Al remains in the system and accumulates in the residue while Ca and Na are leached out. Potassium metasomatic enrichment in sediments and sedimentary rocks brings about mineralogical changes which alter the earlier composition (Nesbitt and Young, 1989; Condie, 1993). K-metasomatism involves
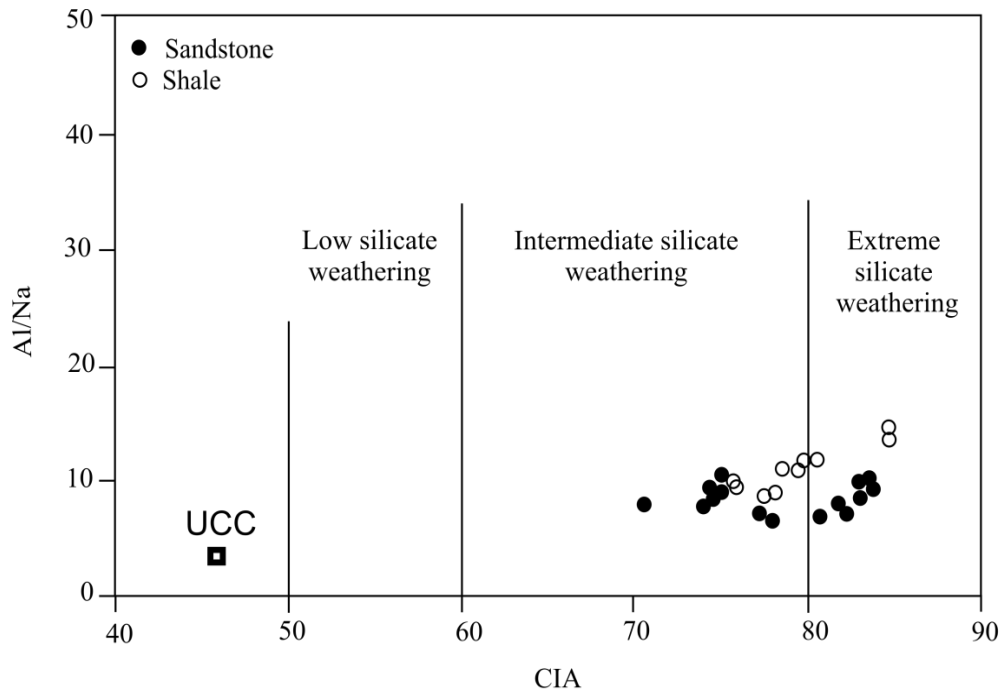
Fig. 7.7: Scatter plots of Al/Na ratio vs CIA reflecting silicate weathering intensity (after Selvaraj and Chen, 2006)
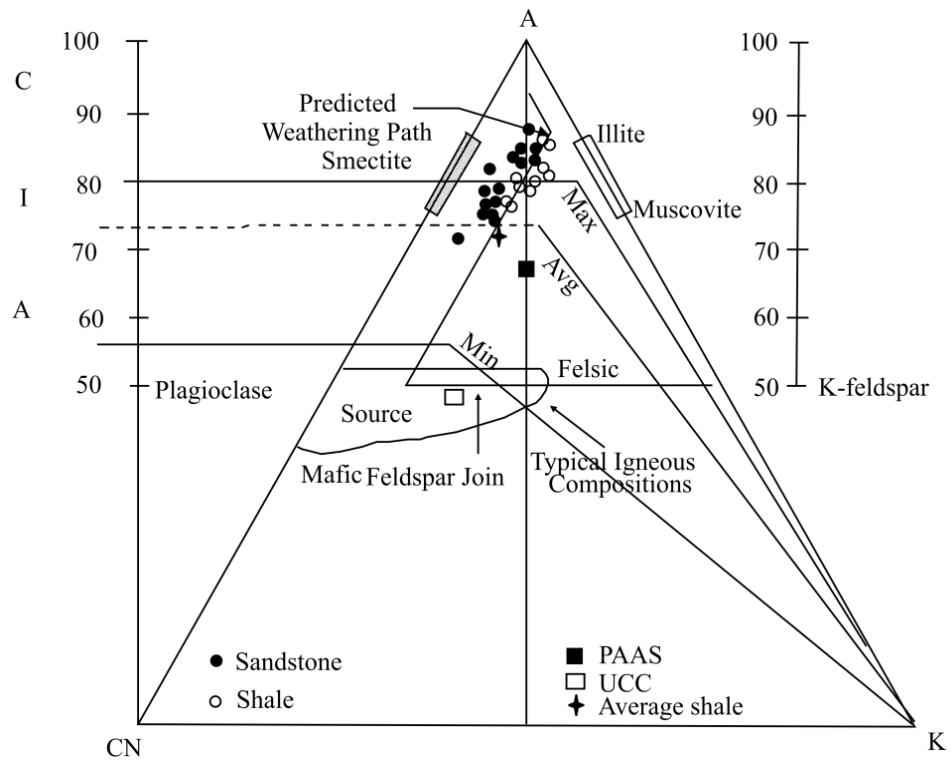

Fig. 7.8: A-CN-K plots of Upper Disang sediments showing weathering trend compared to UCC, PAAS and average shale (after Nesbitt and Young, 1984)

conversion of kaolin to illite by reaction with potassium bearing pore waters (Fedo *et al*., 1995). In sandstone, K-metasomatism can occur in two ways:

(i) Aluminous clay minerals (kaolinite) are converted to illite, and

(ii) Conversion of plagioclase to K-feldspar

These processes lead to K_2O enrichment in sedimentary rocks. Both these processes bring about chemical changes in the composition of sedimentary rocks.

The intense chemical weathering may be associated with high rainfall and relatively higher mean annual temperature, which accelerates the destructive processes during the time of deposition of the sandstones (Suttner and Dutta, 1986). CIW is determined using

$$CIW = [Al_2O_3/(Al_2O_3+CaO*+Na_2O)]x100$$

Phanerozoic shale values are close to 85, higher values indicating intense weathering. Average CIW values of the Upper Disang sandstones (85.69) and that of the shale (89.21) indicate intense weathering at the source. ACN plots after Harnois (1988) support intense weathering (Fig. 7.9).

Fedo *et al*. (1995) used the Plagioclase Index of Alteration (PIA) to monitor the degree of plagioclase weathering to supplement silicate weathering of sedimentary rocks.

$$PIA = [(Al_2O_3-K_2O)/(Al_2O_3+CaO*+Na_2O-K_2O)]x100$$

Unweathered plagioclase shows PIA values of 50 while that of PAAS is 79. The Upper Disang sediments, with the exception of sandstone sample UD40 (PIA=73), show very high PIA values (avg. sandstone 85.14; shale 87.69) indicating high intensity of weathering at the source (Fig. 7.10). High values, according to Mongelli *et al*. (2006), develop when much plagioclase is converted to clay minerals. However, high PIA values may also be attributed to subsequent weathering of the sediments.

In the AKF diagram (Fig. 7.11) plots lie in the field of residual clays and NASC indicating intense weathering in the source area substantiating CIA indices and A-CN-K plots (Wronkiewicz and Condie, 1987). McLennan (1993) considers Rb/Sr ratios of sediments (UCC 0.32; PAAS 0.8) as a monitor of the degree of source rock weathering. Disang sandstones and shales show average values of 0.71 and 1.11 respectively, implying moderately high to intense weathering of the source rocks.

The average TiO_2/Al_2O_3 ratios of both sandstone and shale are 0.06. Such low values, according to Migdisove (1960), indicate semi-humid to humid paleoclimatic
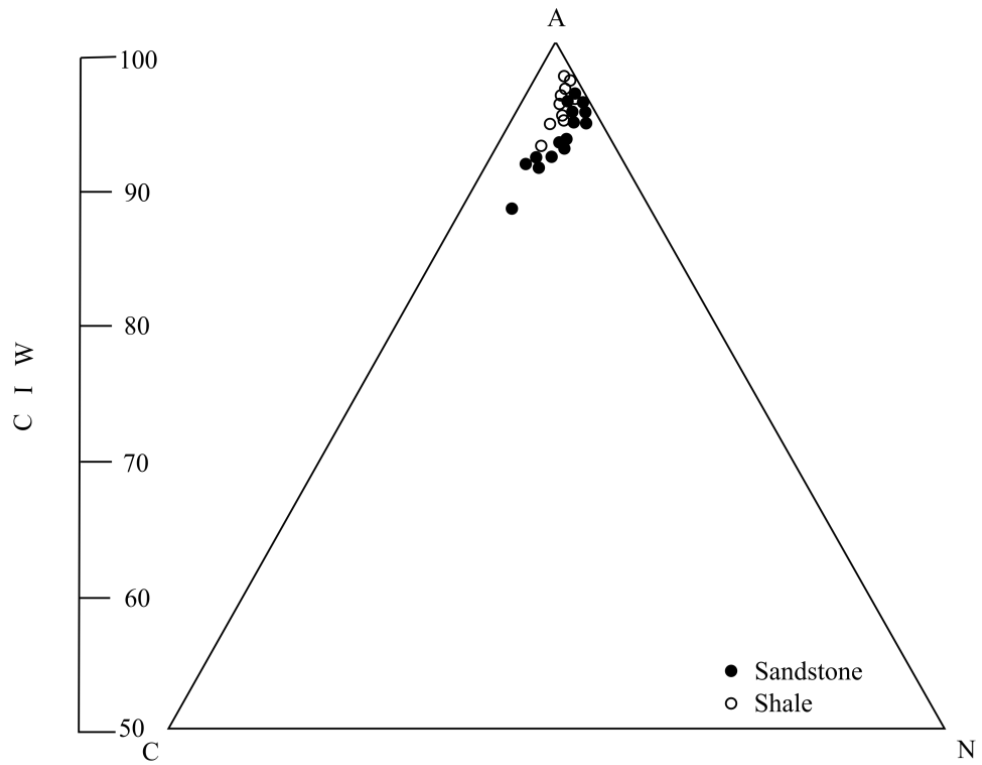
Fig. 7.9: A-C-N plots of Upper Disang sediments indicating intensity of weathering (after Harnois,1988)
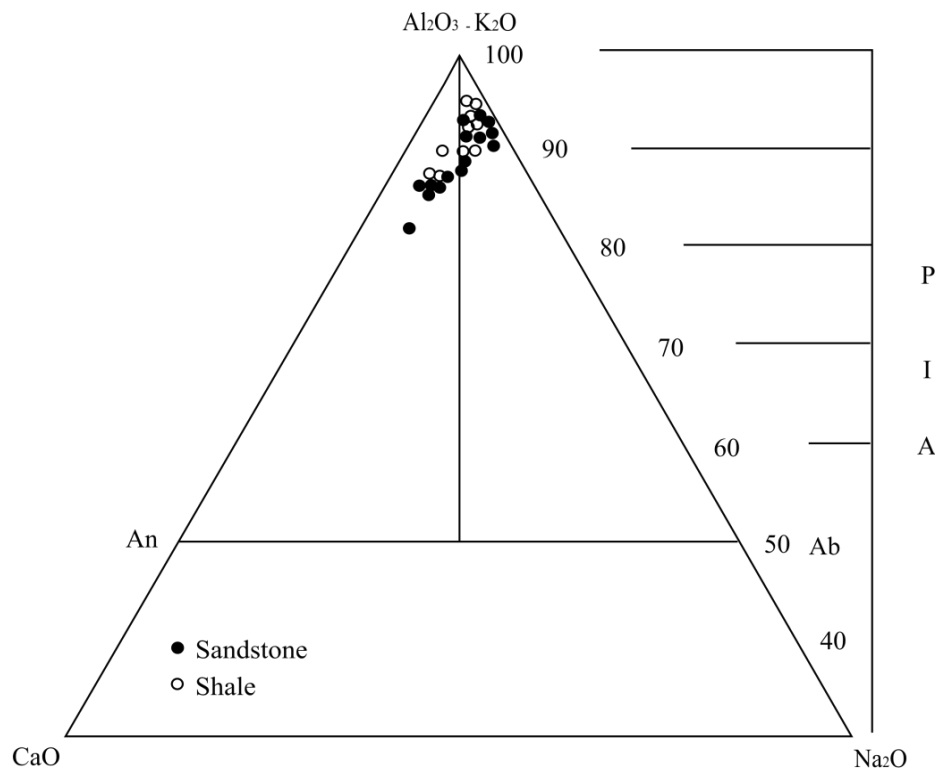

Fig. 7.10: Scatter plots of Upper Disang sediments indicating intensity of weathering (after Fedo *et al*., 1995)

conditions. Total quartz/feldspar+rock fragments are plotted against polycrystalline quartz/feldspar+rock fragments following Suttner and Dutta (1986), which indicate semi-humid paleoclimate at the source area (Fig. 7.12). This is corroborated by plots in the QFL ternary diagram (Fig. 7.13) of Dickinson and Suczek (1979) where illite is indicated; this (Prothero and Schwab, 2003) is ascribed to chemical weathering of feldspars and micas under humid temperate climate.

Early Cenozoic is known for tropical climates, the period recorded as the warmest of the era. The extreme case is the Early Eocene Climatic Optimum and the more transient Mid Eocene Climatic Optimum, when CO_2 concentrations and global temperatures reached a long term maximum. Warming has been attributed to increased atmospheric CO_2 due to volcanic emissions, which were particularly high during parts of Paleocene and Eocene (Zachos *et al*., 2008). These conditions would have greatly enhanced chemical weathering and erosion of rocks, particularly those at lower mid-latitudes near sea levels where temperature and humidity would be high. The rise of the ophiolite above sea level most likely began during this period. The crystalline complex situated along similar latitudes on the west of the study area would also have been affected by the same extreme conditions.

7.2.2 Tectonic Setup

The geochemistry of sedimentary rocks has been widely used to discriminate tectonic setting of the sedimentary basin (Bhatia, 1983, 1985a,b; Roser and Korsch, 1986; Argast and Donnelly, 1987; Floyd and Leveridge, 1987; McLennan *et al*., 1990; McLennan and Taylor, 1991; Garver and Scott, 1995). Several workers have shown the relationship between framework mineralogy of sandstones, provenance and tectonic setting of sedimentary basins (Crook, 1974; Schwab, 1975; Dickinson and Suczek, 1979). Tectonism is advocated as the primary control over sedimentary rock composition (Blatt *et al*., 1980). However, framework grains fail to reveal the true crustal setting due to obliteration of the grains, destruction by post depositional modification or due to inherent difficulties in correct identification of grains. Geochemical indices frequently used in the interpretation of ancient depositional environments and the parameters that represent more reliable geochemical paleo-oxygenation indices have been discussed by Jones and Manning (1994). Crook (1974) employed bulk elements to discriminate the different tectonic setting of sedimentary rocks. The nature and proportion of the detrital components and bulk composition
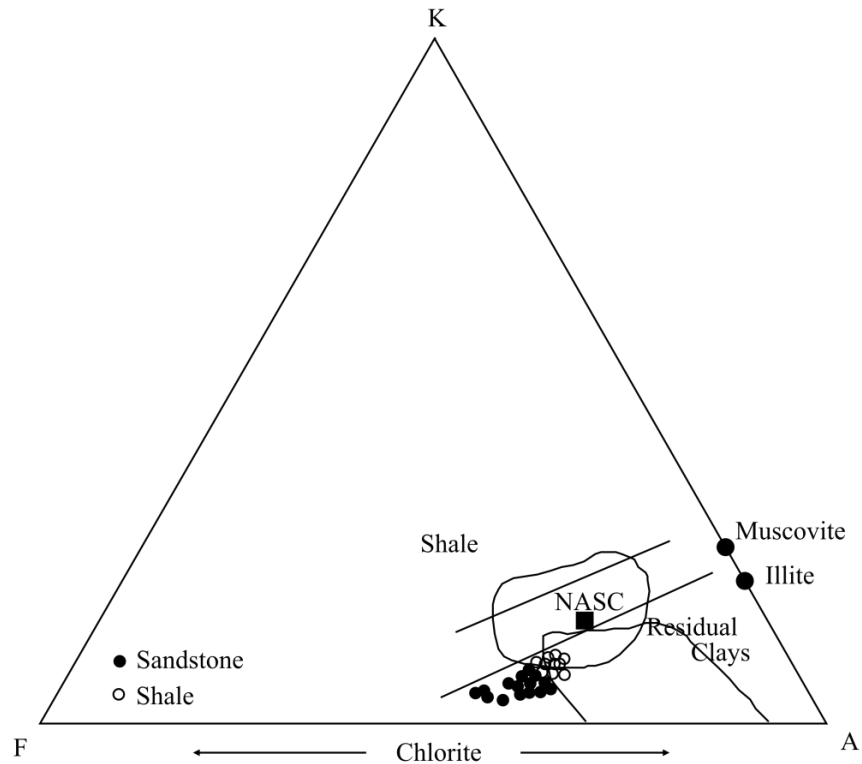
Fig. 7.11: K$_2$O-Fe$_2$O$_3$-Al$_2$O$_3$ plots of Upper Disang sediments (after Wronkiewich and Condie, 1987)
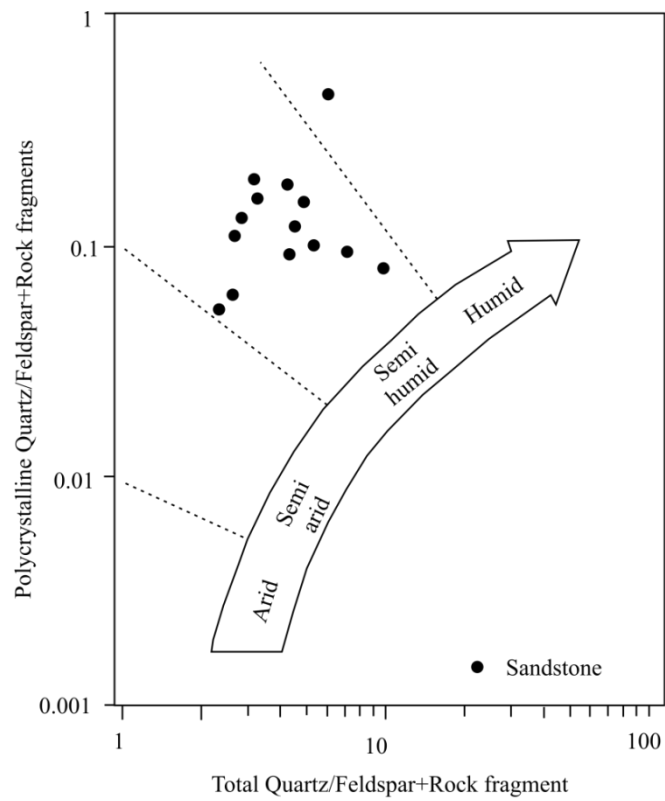

Fig. 7.12: Log total QFR vs Log polycrystalline QFR plots of Upper Disang sediments (after Suttner and Dutta, 1986)

reflect the tectonic setting of sedimentary basins (Seiver, 1979; Roser and Korsch, 1986). Bhatia and Taylor (1981) and Bhatia (1983) also used composition and tectonic setting. Plots of K_2O/Na_2O vs SiO_2/Al_2O_3 (Fig. 7.14) after Maynard *et al*. (1982) discriminates sediments of various settings. K_2O/Na_2O vs SiO_2 plots (Fig. 7.15) after Murphy (2000) provide tectonic setting for sandstone-mudstone suites. In both diagrams an active continental margin (ACM) is indicated, suggesting an unstable continental setting. Such a setting should produce mineralogical, chemically and texturally immature sediments. This is further corroborated by the tectonic discrimination plot (Fig. 7.16) of Bhatia (1983). Compared to the average $(La/Sm)_N$ values (4.26) of PAAS (Dampare *et al*., 2004) the Disang sandstone and shale have relatively lower values of 2.0-3.65 (avg. 2.97) and 3.51-4.92 (avg. 3.79) respectively but higher Eu/Eu* ratios of 0.56-0.90 (avg. 0.71±0.11) and 0.66-0.94 (avg. 0.75±0.08) respectively (avg. PAAS 0.65) which is possibly due to their deposition along an active continental margin. This was a confined and rapidly closing turbidite basin representing a closed wedge of an accretionary complex.

7.2.3 Sorting and Recycling of Sediments

Major oxides, trace elements and REE geochemistry help decipher sediment sorting, recycling, and concentration of accessory minerals, particularly of coarser rocks (McLennan *et al*., 1993; Cullers, 1994, 2000). Modal and chemical compositions of sedimentary rocks are strongly controlled by grain size (Roser and Korsch, 1985). As mean grain size decreases from sandstone to argillite, modal quartz, feldspar and lithic fragments decline in abundance with the corresponding increase of modal matrix and phyllosilicate. This in turn affects the bulk chemistry of sediments. SiO_2 and Na_2O gradually decrease from sandstone to argillite with a regular increase of K_2O thereby producing a progressive rise in K_2O/Na_2O ratios. The Upper Disang shale samples exhibit higher K_2O/Na_2O ratios (avg. 2.2) than sandstone (avg. 1.2). SiO_2/Al_2O_3 ratios representing proportions of quartz to clay thus decrease with decreasing grain size.

McLennan *et al*. (1993) opine that the Th/Sc ratio is a good indicator of the igneous chemical differentiation process as Th is incompatible whereas Sc is compatible to igneous systems. A useful index of sediment recycling is the Zr/Sc ratio, which allows evaluation of Zr enrichment during sorting (Hassan *et al*., 1999). Since Zr is concentrated in the dense mineral zircon, the Zr/Sc ratio provides a

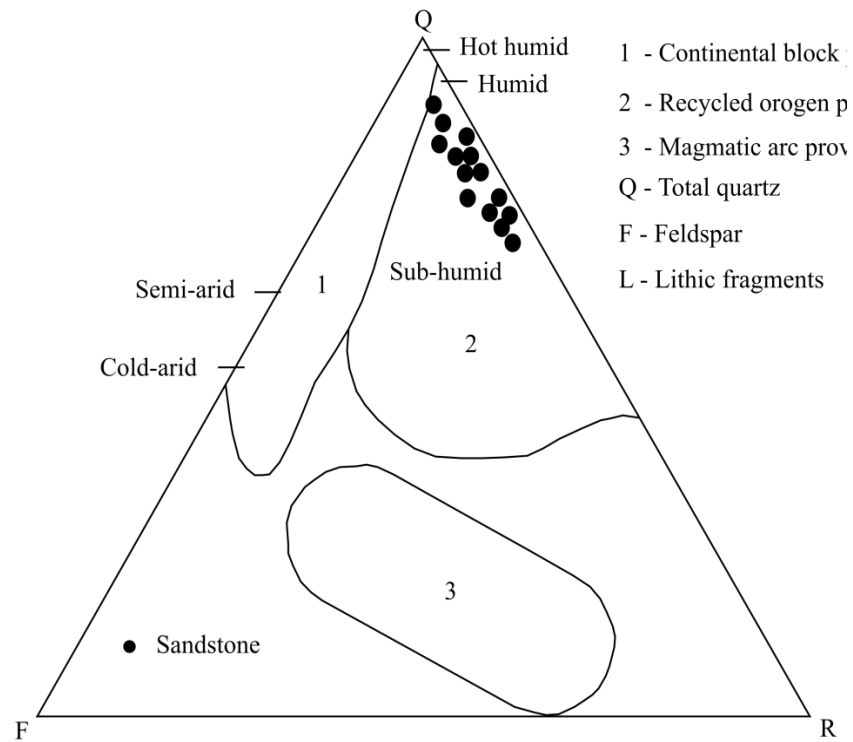**Fig. 7.13:** QFL diagram of Upper Disang sandstones (after Dickinson and Suczek, 1979)
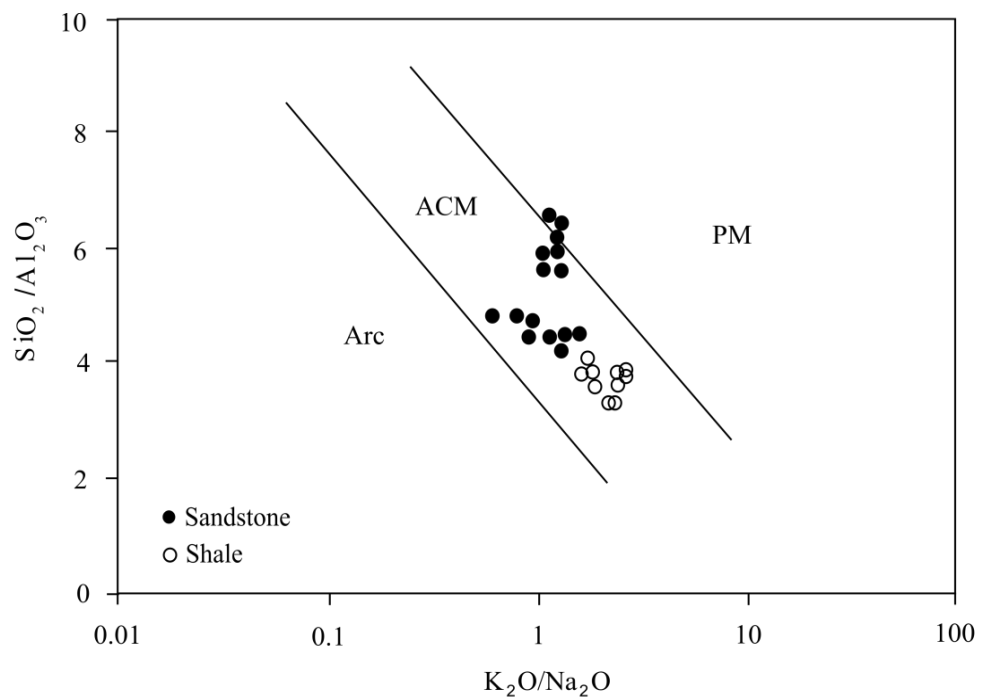
Fig. 7.14: SiO$_2$ vs K$_2$O/Na$_2$O tectonic discrimination plots (after Maynard *et al.*,1982)
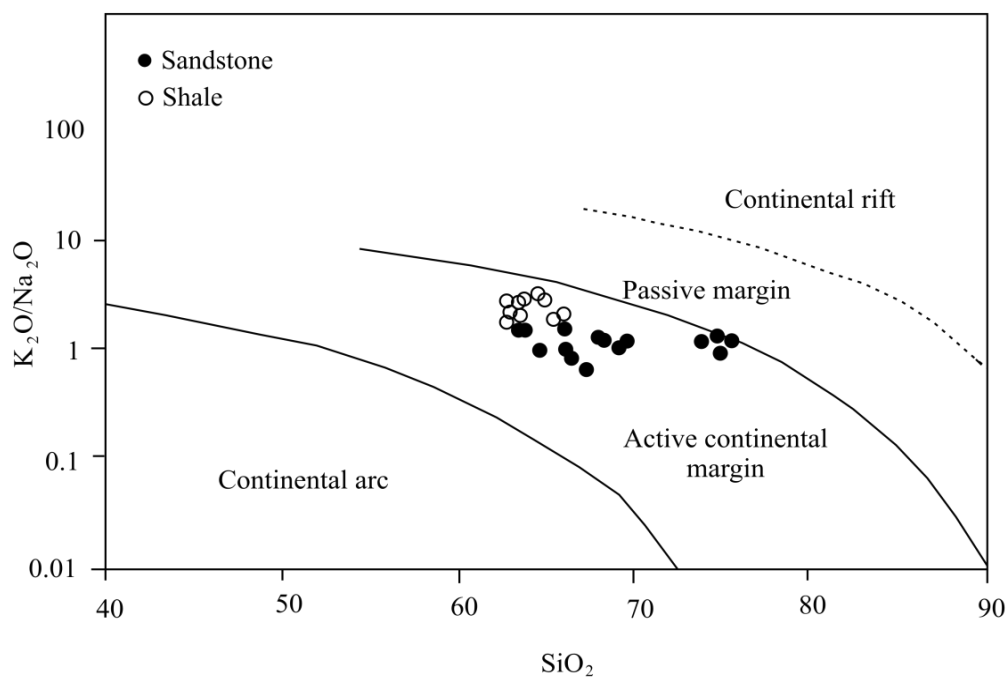
Fig. 7.15: Tectonic setting discrimination diagram for Upper Disang sediments (after Murphy, 2000)
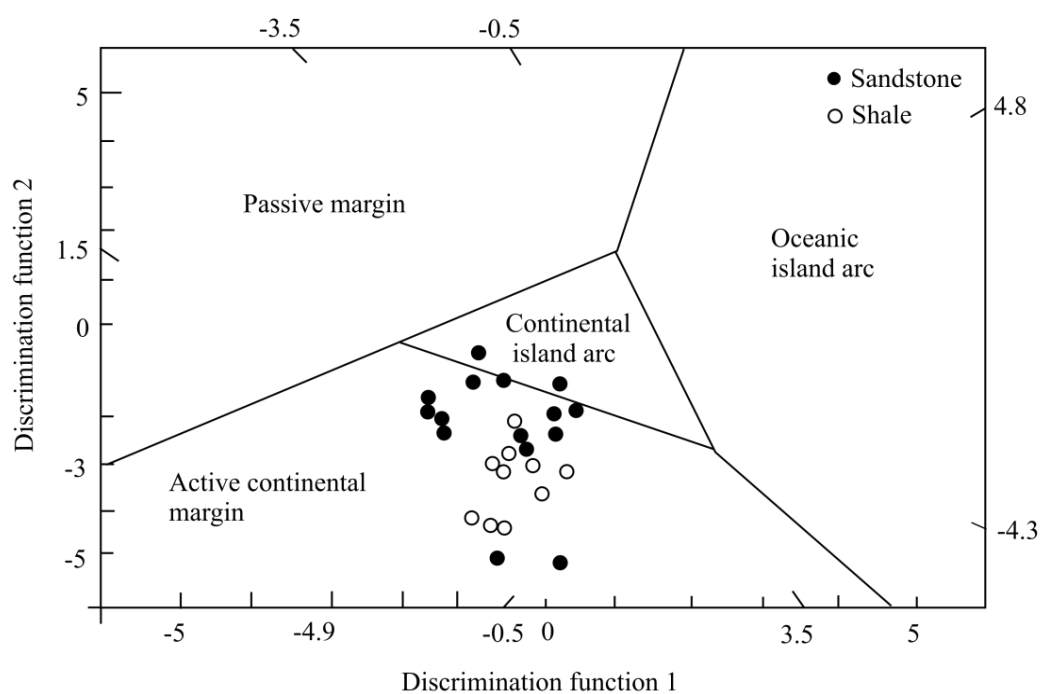

Fig. 7.16: Tectonic discrimination diagram for Upper Disang sediments (after Bhatia, 1983)

measure of sedimentary recycling and sorting (Basu, 1976). Zr is enriched in the Upper Disang sandstone (avg. 345.12) as compared to the shale (avg. 165.70). This reflects on the preferable concentration of zircon in coarser, silica-rich sandstones relative to the finer grained associated shales. Th/Sc and Zr/Sc plots indicate slight addition of zircon in some of the sandstone samples, suggesting recycling and continuous reworking of the sediments (Fig. 7.17). Most grains of zircon (Plate 4.7) and some rutile (Plate 4.10) are rounded to well-rounded which point to a polycyclic origin or continuous reworking. The relationship amongst quartz, feldspar and lithic fragments is brought out in the diagrams of Dickinson and Suczek (1979) and Dickinson *et al*. (1983), which indicate a recycled orogen (Fig. 7.18, 7.19). This is corroborated by plots (Fig. 7.20) in the Qt-F-Rt ternary diagram of Dickinson (1985). The dominance of monocrystalline quartz over polycrystalline quartz in association with a small amount of feldspar in the sandstone suggests reworking of the sediments (Omar and Khan, 2005). This suggests that the provenance of the first generation sediments most probably was the granite gneiss of Karbi Anglong. The sediments were initially deposited in front of the foreland spur in a shallow marine basin where they were continuously reworked by oceanic currents. Continued piling of sediments and buckling and eastward slanting of the cratonic floor caused bottom currents to transport these sediments to the depositional site near the subduction zone. The paucity of heavy minerals in these sandstones also may be due to continued reworking of the sediments. Quartz-rich sediments, according to Cullers *et al*. (1979) have low values of ΣREE and La/Yb_N (UCC - 146.39 and 9.21 respectively). The Disang sediments however, possess high values of ΣREE (sandstone 438.51; shale 311.61). The shales also have higher values of La/Yb_N (11.43). Such results suggest that the Disang sandstones have suffered the "quartz-dilution effect" (Thong and Rao, 2006). The lower values of La/Yb_N (6.6) in the sandstone may be due to poor fractionation of the sediments. Quartz overgrowths are lacking in these sandstones which may be due to reworking rather than recycling of the sediments. This may be attributed to the presence of illite in the matrix. According to Heald and Laresse (1974) illite acts as a barrier that prevents silica solutions from reaching quartz detritals.

7.2.4   Depositional Environment

Various views on the paleo-depositional environment of the Disang have been proposed. Mathur and Evans (1964) consider these rocks as a deepwater facies while

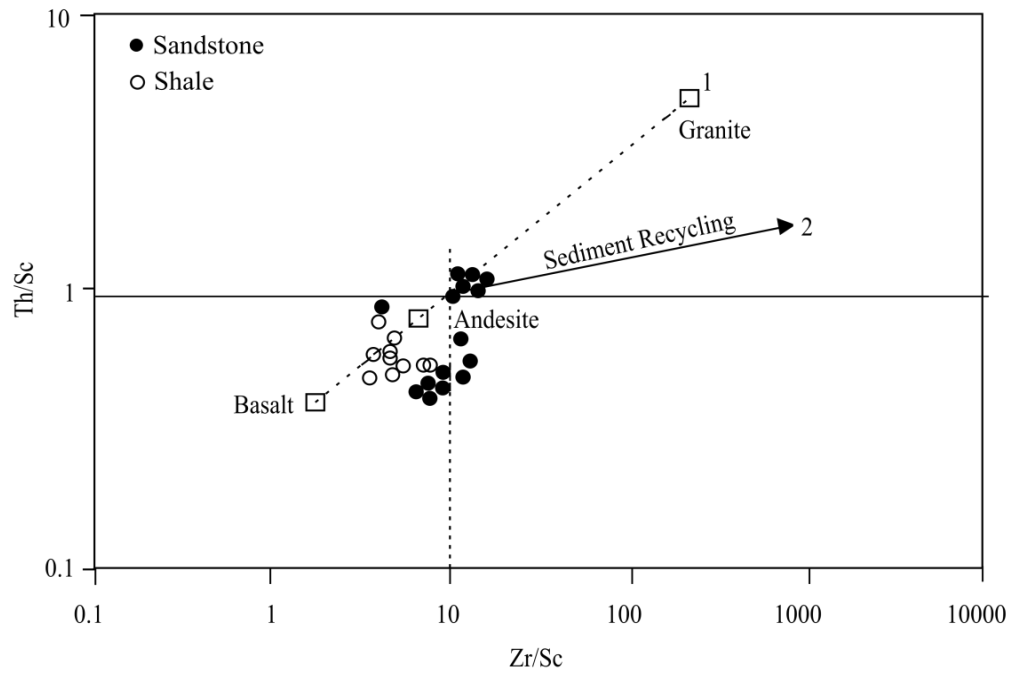**Fig. 7.17:** Th/Sc vs Zr/Sc plots of Upper Disang sediments indicating recycling of sediment (after McLennan *et al*., 1993)
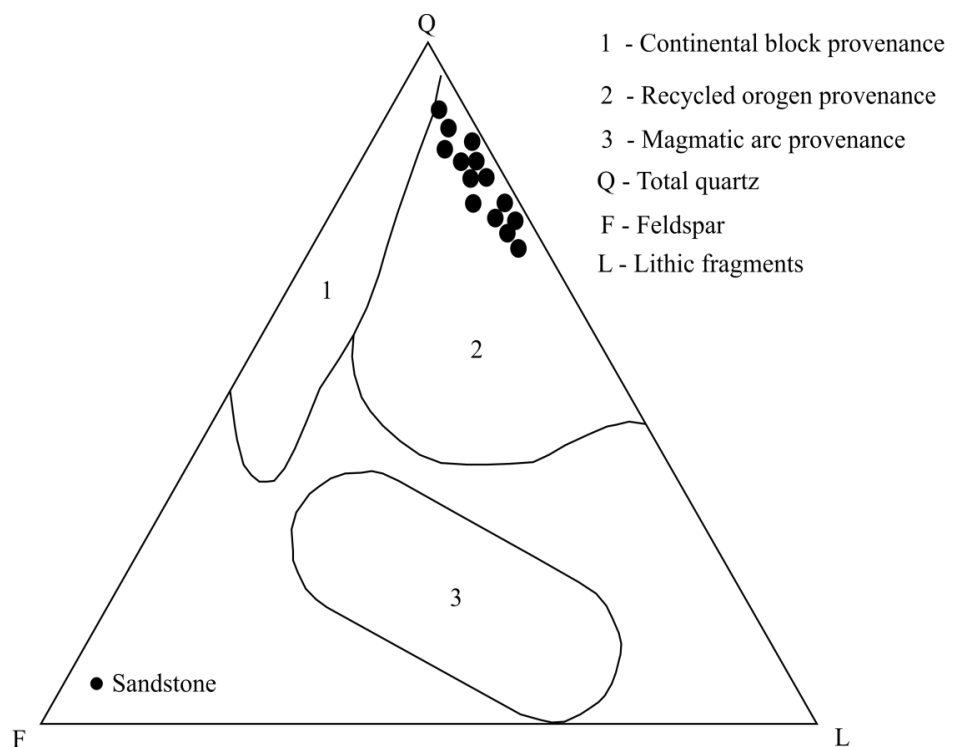

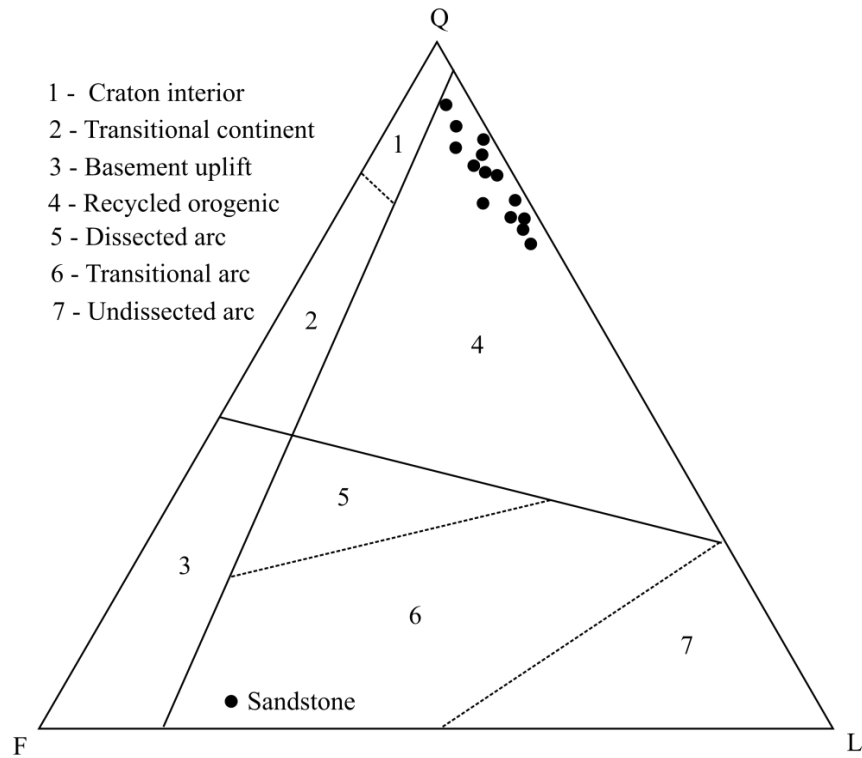**Fig. 7.18:** QFL plots of Upper Disang sandstones (after Dickinson and Suczek, 1979)

Fig. 7.19: QFL plots of Upper Disang sandstones (after Dickinson *et al*.,1983)
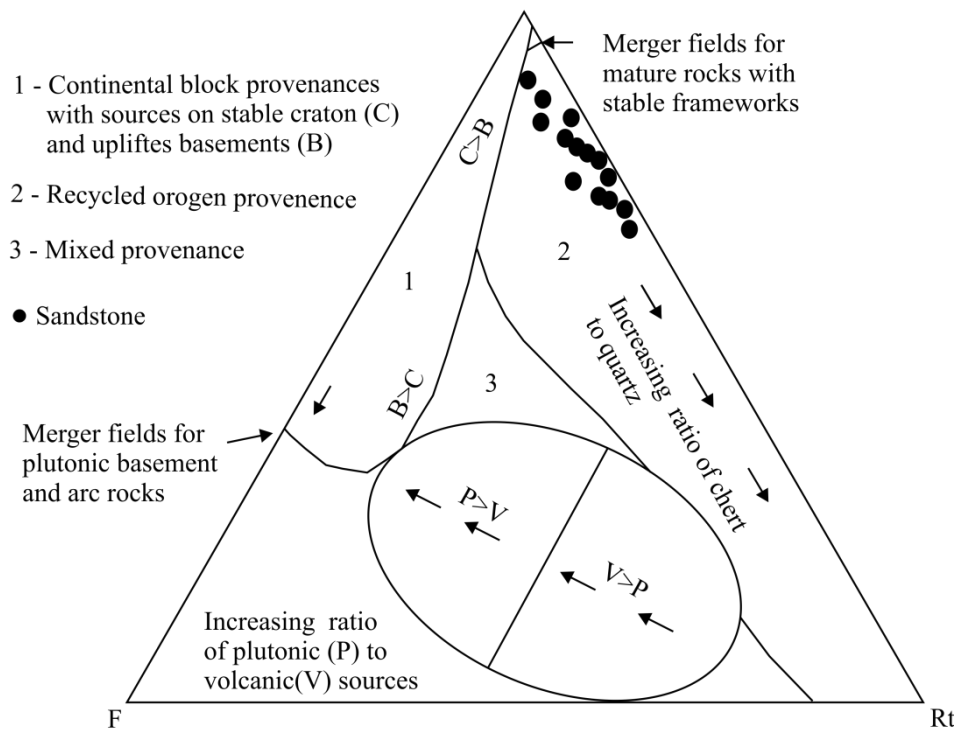
Fig. 7.20: Qt-F-Rt plots for tectonic setting discrimination of Upper Disang sandstones (after Dickinson, 1985)

Rao (1983) and Acharyya *et al.* (1986) favour a shallow distal shelf to deltaic facies. Studies of the Disang and Barail sandstones of Kohima near the BoS (Sarmah, 1983) indicate that the depositional basin was a near shore, shallow water lagoon.

The presence of certain trace elements in the rocks indicates their mode of formation and environment of deposition. In the present study V content of sandstone (avg. 270 ppm) and shale (avg. 278 ppm) is much higher than that of PAAS (150 ppm), NASC (130 ppm) and UCC (60 ppm). Such enrichment according to Ernst (1970) occurs in a marine setup. The relation between K_2O/Al_2O_3 and MgO/Al_2O_3 was used by Roaldest (1978) to differentiate between marine and non-marine clays. Values of Upper Disang sediments depict a marine setup (Fig. 7.21). Drever (1977) and Mason and Moore (1982) believe that illite is one of the most stable and common clay minerals in the marine environment. Illite is favoured by an alkaline environment and presence of potash.

7.2.5 Paleo-Oxygenation Conditions

The V/Cr ratio has been used as an index of paleo-oxygenation in many studies (Ernst, 1970; Bjorlykke, 1974; Dill, 1986; Dill *et al.*, 1988). Ratios above 2 indicate anoxic conditions whereas values below 2 suggest more oxidizing conditions (Jones and Manning, 1994). In the sediments of the study area, average values of 3.1 and 2.1 are noted for the sandstone and shale respectively, which indicate anoxic depositional conditions. Hallberg (1976) opines that high Cu/Zn ratios indicate reducing depositional milieu, while low Cu/Zn ratios suggest oxidizing conditions. High Cu/Zn ratios in the Upper Disang sandstone (avg. 0.86) and shale (0.94) suggest anoxic depositional condition. This is further substantiated by higher Ni/Co ratios that are >5 (avg. 5.7); such values, according to Dypvik (1984), Dill (1986) and Jones and Manning (1994) are due to anoxic conditions. Lokho and Kumar (2008) have reported well preserved Uvigerinid foraminifers in this area which indicate deposition in the deeper parts of a shallow marine anoxic environment. Negative Eu* values of the Disang sediments also indicate anoxic marine conditions as proposed by Freyer (1977). Pyrite crystals are fairly common in these Disang sediments, which also point to anoxic conditions in the depositional environment.

V/(V+Ni) ratios aid the determination of Eh and pH conditions and sulphide activity in the depositional environment (Lewan and Maynard, 1982; Lewan, 1984; Breit and Wanty, 1991; Hatch and Leventhal, 1992; Tribovillard *et al.*, 1994).

Bellanca *et al*. (1996) are of the opinion that the solubility of V in natural waters, its extraction from seawater and absorption onto sediments are influenced to a great extent by redox conditions. Dissolved V is readily bound to high molecular metallo-organic complexes (Lewan and Maynard, 1982) or absorbed by biogenic material (Prange and Kremling, 1985). During early diagenesis of sediments under oxic environments V is mobilized from biogenic material; however, its mobilization is restricted under anoxic conditions (Shaw *et al*., 1990). Organic-rich sediments are enriched in Ni, Cu and Cr as these metals are easily trapped in organic matter (Leventhal and Hosterman, 1982; Gilkson *et al*., 1985). In reducing environments where sulphate reduction is more efficient V accumulates preferentially over Ni (Lewan and Maynard, 1982; Odermatt and Curiale, 1991; Huerta-Diaz and Morse, 1992). The normal marine system shows an average V/(V+Ni) value of ≤ 0.5 (Lewan, 1984) while ratios >0.8 indicate the presence of significant dissolved H_2S in highly reducing bottom waters of a marine setup (Hatch and Leventhal, 1992). Values of the Upper Disang sandstone (0.57) and shale (0.62) suggest that the Disang sediments were deposited under anoxic conditions with moderate frequencies in the redox state of the depositional environment.

7.2.6   Provenance

The Disang sandstones contain non-undulose, undulose and polycrystalline quartz in varying proportions (Table 4.1). Non-undulose quartz is considered as from an igneous source (Folk, 1968; Blatt *et al*., 1980). Undulose and polycrystalline quartz indicate metamorphic sources (Folk, 1960; Blatt and Christie, 1963; Blatt, 1967; Waugh, 1970).

Geochemical signatures of clastic sediments have long been used to identify their provenance (Madhavaraju and Ramasamy, 2002; Armstrong-Altrin *et al*., 2004). Cullers *et al*. (1988) opine that diagenesis and weathering affect chemical composition and therefore, less mobile elements under geologic conditions are most reliable. REE, Th, Sc, Cr and Co are used for provenance studies as they are less soluble and relatively immobile. These elements are more or less transported in the terrigenous component and therefore, reflect the chemistry of their source (Rollinson, 1993; Fedo *et al*., 1996; Cullers and Berendsen, 1998).

Composition of clastic rocks is mainly influenced by source rock characteristics, nature of sedimentary processes within the basin and the kind of

dispersal paths that link provenance to the basin (Dickinson and Suczek, 1979). Nesbitt *et al*. (1996) opine that the nature of a provenance can be inferred from the study of sedimentary rocks. The geochemical composition of terrigenous sediments is a function of intricate interplay of provenance, weathering, transportation and diagenesis. Vital *et al*. (1999) successfully utilized clay as well as heavy mineral fractions to deduce provenance.

The relative enrichment of Fe_2O_3, MgO and SiO_2 and depletion of TiO_2, Na_2O, CaO and K_2O in these sediments may be due to derivation from various sources. Al_2O_3/TiO_2 ratios of clastic rocks are commonly used to infer source rock compositions. Brooks (1973) and Spears and Sotiriou (1976) found that the Carboniferous sediments of England have high Al_2O_3/TiO_2 ratios reflecting a strong correlation to the ratios of the parent basalt. Al_2O_3/TiO_2 ratios range from 3 to 8 in mafic, 8 to 21 in intermediate and 21 to 70 in felsic igneous rocks and 15-25 in Precambrian sediments (Willis *et al*., 1988). Ratios of the Disang sandstones range from 14.64 to 21.81 (avg. 17.52) while that of the shales from 16.25 to 18.82 (avg. 17.87) pointing to intermediate source rocks. This may be due to thorough mixing of various source rocks due to turbidity currents to yield such values as much evidence indicates that the bulk of the material are from acid and basic sources. The total iron content (Fe_2O_3) of these rocks (avg. sandstone 8.56; shale 8.63) is much higher than that of the average UCC (5.0) which point to basaltic sources as basalts are enriched in Fe.

Th/Sc ratios are reliable indicators of provenance as these elements, according to Taylor and McLennan (1985) are easily fractionated during sedimentary processes. Th/Sc ratios near 0.6 belong to more mafic components while those >1 are typical of UCC. Th/Sc ratios of the Upper Disang sandstone range from 0.42 to 0.98 (avg. 0.58) except for four samples (UD44, UD52, UD54, and UD56) with ratios >1, while that for shale range from 0.48 to 0.77 (avg. 0.64). Values suggest an inclination towards mafic sources, however, with contribution from acid sources as well. The presence of muscovite flakes suggests contribution from basic sources. Al_2O_3/K_2O ratios suggest that considerable Ti-bearing mafic phases (biotite, chlorite and illmenite) are derived from basic rocks. Na_2O+K_2O values are plotted against SiO_2 in a binary diagram (Fig. 7.22) following Irvine and Baragar (1971). Plots indicate a sub-alkaline composition. K_2O plotted against SiO_2 in the binary diagram (Fig. 7.23) of Le Maitre (1989) indicate low to medium potash rocks. Such rocks are usually basaltic derivatives.
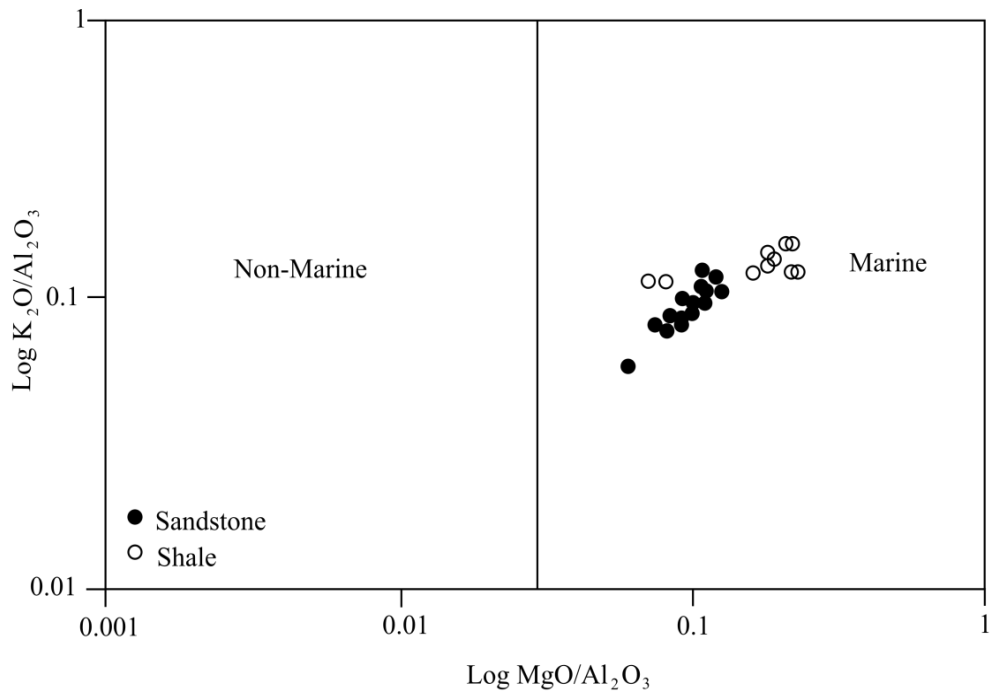
Fig. 7.21: Depositional environment dicrimination plots of Upper Disang sediments (after Roaldest, 1978)
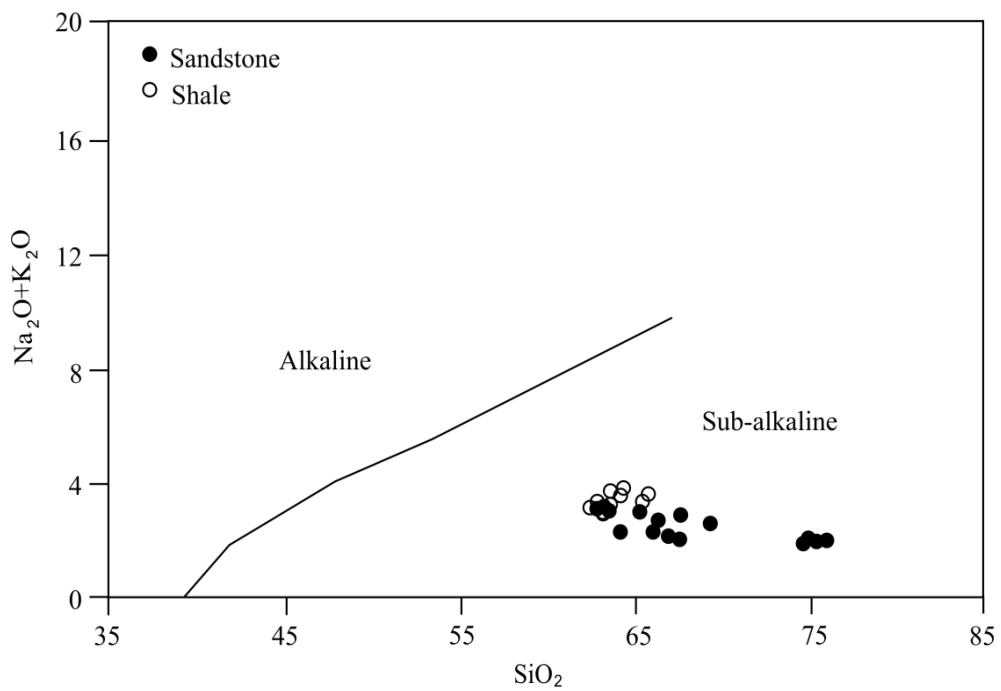

Fig. 7.22: Provenance of Upper Disang sediments (after Irvine and Baragar, 1971)

Amajor (1987) used the TiO_2 vs Al_2O_3 binary plot to distinguish between granitic and basaltic sources; most samples plot in the basalt-granite field (Fig. 7.24) indicating mixed sources. On the Sc vs Th plots most samples show mafic-rich signature (Fig. 7.25). The La-Th-Sc diagram of Bhatia and Crook (1986) and Cullers (1994) is used to discriminate felsic and basic provenance of fine grained sediments. Plots (Fig. 7.26) suggest a metabasic source. In the diagram plotted after Roser and Korsch (1988) indications are contribution of detritus mostly from mafic and intermediate igneous provenances (Fig. 7.27). Provenance discrimination plots after Bhatia (1983), however show some samples lying within the quartzose sedimentary field (Fig. 7.28). Based on the mixing curve between granite and ultramafic end members in the Y/Ni vs Cr/V diagram (Fig. 7.29) it is suggested that both mafic-ultramafic and felsic rocks have contributed significantly to the Disang.

Significant differences in Eu/Eu*, $(La/Yb)_N$, La/Sc, Th/Sc, Th/Co and Th/Cr ratios exist between mafic and felsic source rocks, particularly those that are more or less affected by recycling. Such ratios are good indicators of sediment provenance (Cullers *et al*., 1988; Cullers, 1994, Cullers and Podkovyrov, 2000). Wronkiewicz and Condie (1987) opine that these ratios exhibit some changes in recycled sediments. In the present study, these ratios are compared with those of sediments derived from felsic and basic rocks (fine fraction) as well as UCC, PAAS and rocks from the vicinity of the study area (Table 7.1). This comparison suggests probable sediment contribution from diversified sources. The lower Th/Sc and Th/Cr ratios in the Upper Disang shale suggest increased mafic components as compared to their sandstone counterpart. Low Th/Sc ratios (<1) probably also reflect input of a less evolved source to the Upper Disang sediments. Higher La/Sc and Th/Co ratios in the sandstones may indicate detrital contribution from felsic sources. Moreover, a slightly higher Eu/Eu* ratio in the Upper Disang shale reflects mafic detritus. Liu *et al*. (2007) are of the opinion that higher values are due to mafic detritus or additional plagioclase. Average values of La/Th ratios of the Upper Disang sandstone and shale are 3.06±0.4 and 3.28±0.17 respectively; such values according to Bhatia and Crook (1986) and McLennan *et al*. (1993) suggest influence of a magmatic arc in the hinterland.

The Cr/Th ratio is a sensitive indicator of provenance (Condie and Wronkiewicz, 1990). That of the Upper Disang sandstones range from 1.9 to 6.4 (avg. 3.9) while in shale it varies from 5.4 to 9.3 (avg. 6.7), which is lesser than PAAS values (7.5). This depletion of compatible elements in the Upper Disang sediments

Table 7.1: Elemental ratios of the Upper Disang sediments compared with the ratios in similar fractions derived from felsic rocks, mafic rocks, UCC, PAAS, and their probable source rocks from the adjoining areas. Values in bracket show mean element ratios and standard deviation

Elemental ratio	La/Sc	Th/Sc	Eu/Eu*	$(La/Lu)_N$	$(La/Yb)_N$	Th/Co	Th/Cr
Range of Upper Disang sandstones *(n=15)**	1.15-3.24 (2.18±0.89)	0.42-1.13 (0.71±0.27)	0.56-0.90 (0.71±0.11)	4.61-13.44 (7.76±2.44)	5.07-9.57 (6.6±1.64)	0.38-1.50 (0.83±0.49)	0.16-0.53 (0.30±0.13)
Range of Upper Disang shales *(n=10)**	1.58-2.76 (1.88±0.36)	0.48-0.77 (0.57±0.09)	0.66-0.94 (0.75±0.08)	7.8-19.65 (12.05±4.72)	8.23-15.88 (11.43±3.70)	0.37-0.87 (0.61±0.17)	0.11-0.18 (0.15±0.02)
Range of Basalt from NHO[a] *(n=29)*	0.04-1.14 (0.15±0.16)	0.002-0.01 (0.02±0.02)	0.74-1.09 (0.96±0.07)	0.46-7.09 (1.59±1.63)	0.46-5.54 (1.44±1.25)	0.001-0.03 (0.008±0.007)	0.001-0.02 (0.004±0.007)
Avg. of Granitoids from NHO[b]	1.34	0.20	0.69	1.35	1.24	0.46	0.09
Avg. of Pyroxenite from NHO[c] *(n=18)*	0.007±0.004	0.93±0.58	0.95±0.73	0.54±0.29	0.56±0.57	0.09±0.03	0.007±0.006
Avg. of Gabbro from NHO[c] *(n=11)*	0.001±0.002	0.001±0.0002	9.83±4.1	1.12±0.81	5.04±3.2	0.02±0.04	0.005±0.005
Range of sediments from felsic sources[d]	2.50–16.30	0.84–20.50	0.40–0.94	3.00–27.00	3.0-27.00	0.67-19.40	0.13-2.70
Range of sediments from mafic sources[d]	0.43–0.86	0.05–0.22	0.71–0.95	1.10–7.00	1.1-7.00	0.04-1.40	0.018-0.046
UCC[e]	2.21	0.79	0.63	9.73	9.21	0.63	0.31
PAAS[f]	3.45	1.33	0.65	-	9.17	1.46	0.13

[a] Srikanth *et al.* (2004)
[b] Ghose and Chatterjee (2010)
[c] Chisoi (2011)
[d] Cullers (1994, 2000)
[e,f] Taylor and McLennan (1985)
*Present study
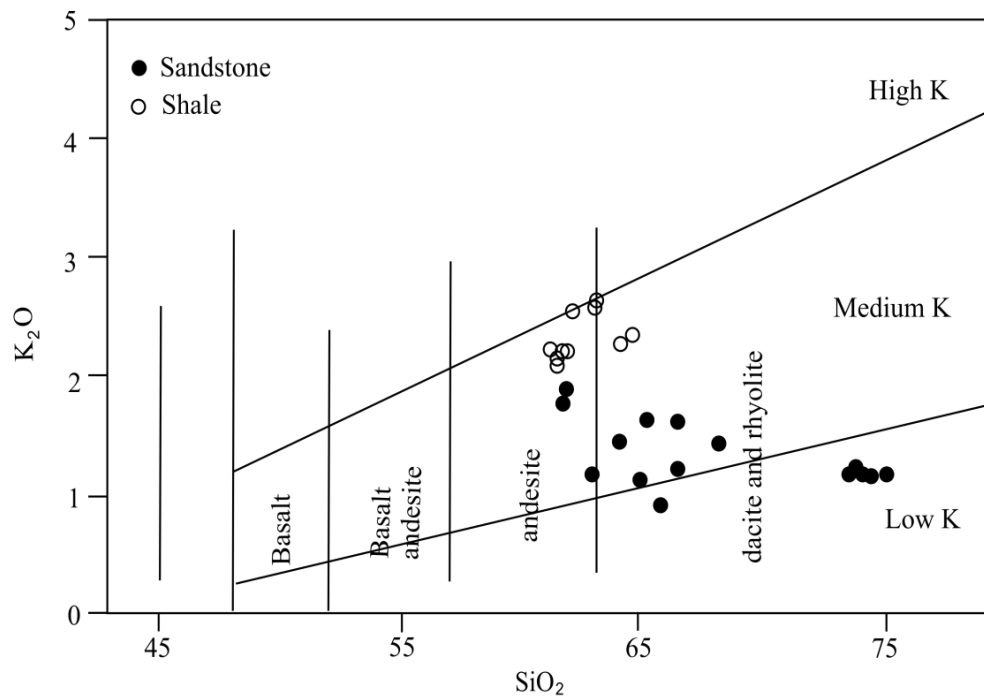
Fig. 7.23: K$_2$O-SiO$_2$ plots showing sub-alkaline composition of Upper Disang sediments (after Le Maitre *et al.*, 1989)
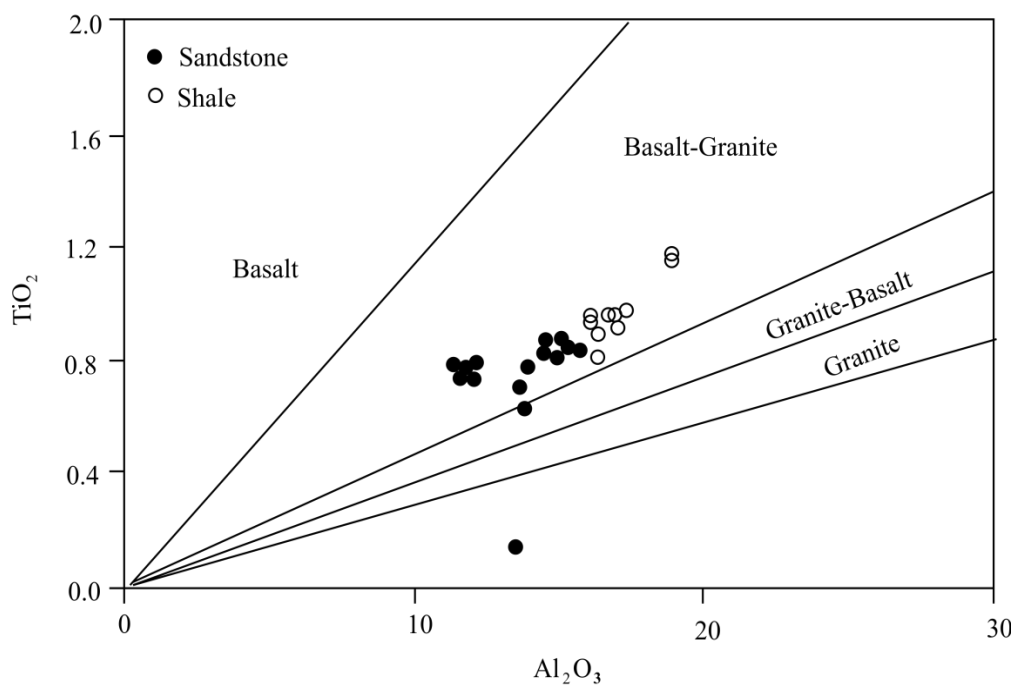
Fig. 7.24: Provenance plots of Upper Disang sediments (after Amajor, 1987)
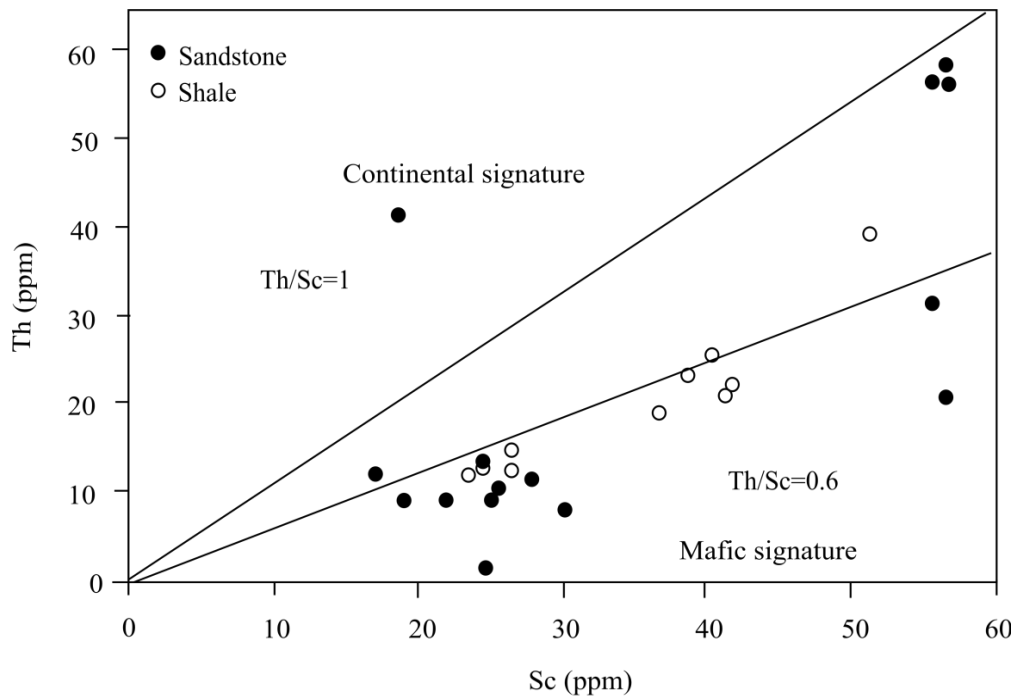
Fig. 7.25: Comparison of Sc and Th concentrations with linear provenance indicators for continental or more mafic influenced materials (after Chakrabarti *et al.*, 2009)

1 = Granite Gneiss sources (Cullers, 1995)

2 = Clay, silt, sand and gravels from mixed sources

3 = Metabasic sources

4 = Clay, silt and sand from amphibolite source

5 = Amphibolite source
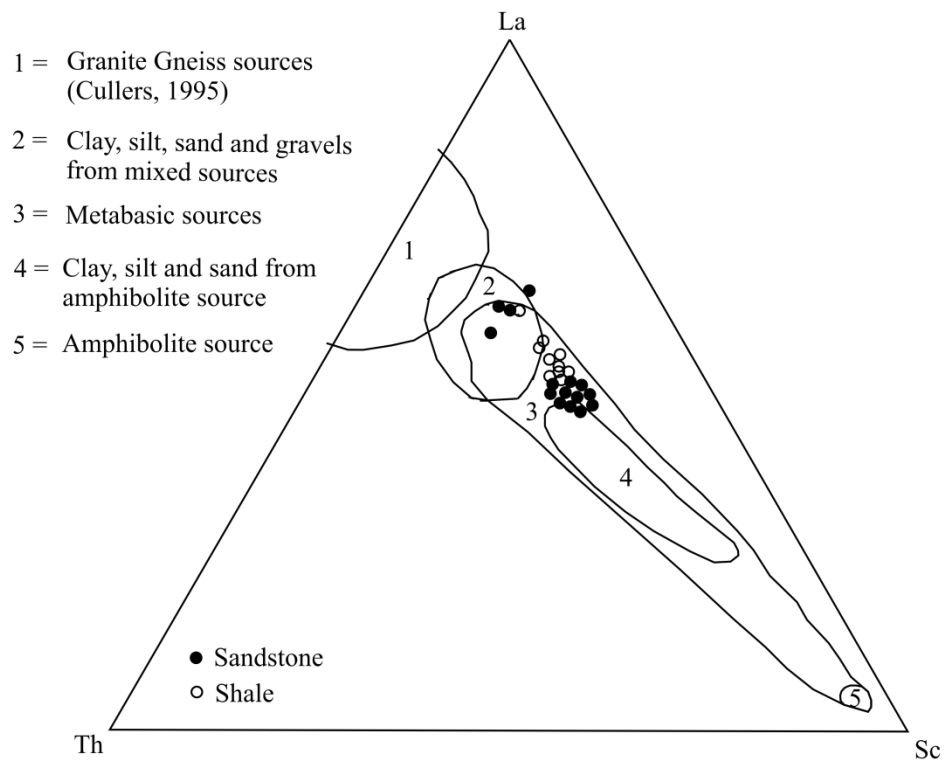
Fig. 7.26: Provenance discrimination plots of La-Th-Sc for Upper Disang sediments (after Bhatia and Crook, 1986 and Cullers, 1994)
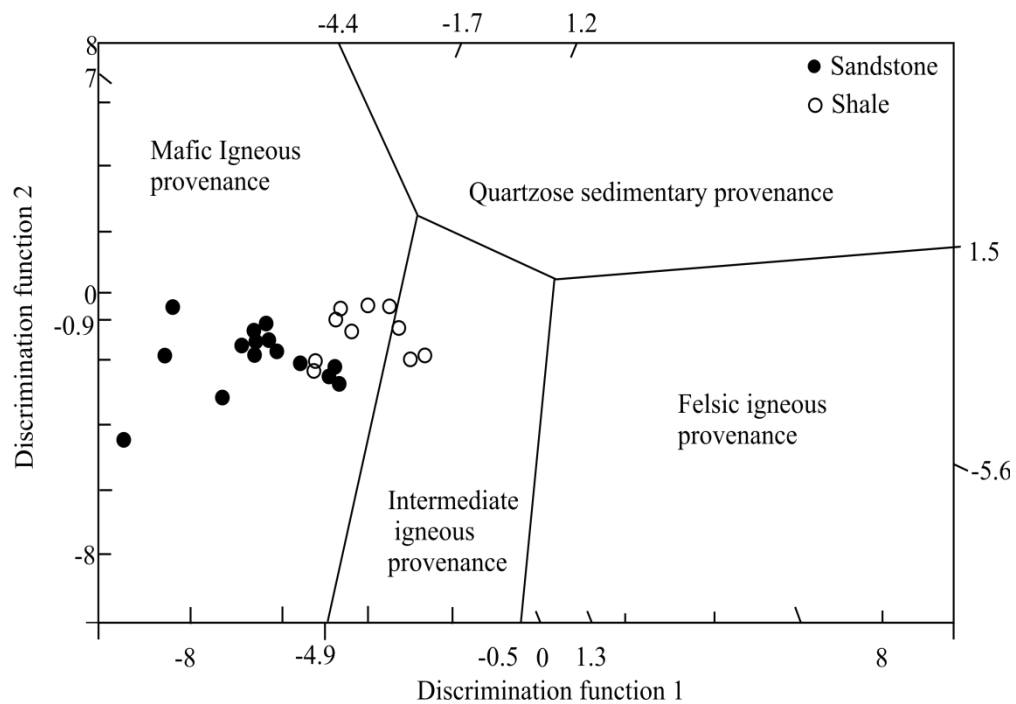
Fig. 7.27: Discrimination function diagram for provenance signatures of sandstone-mudstone suites using major element ratios (after Roser and Korsch, 1988)
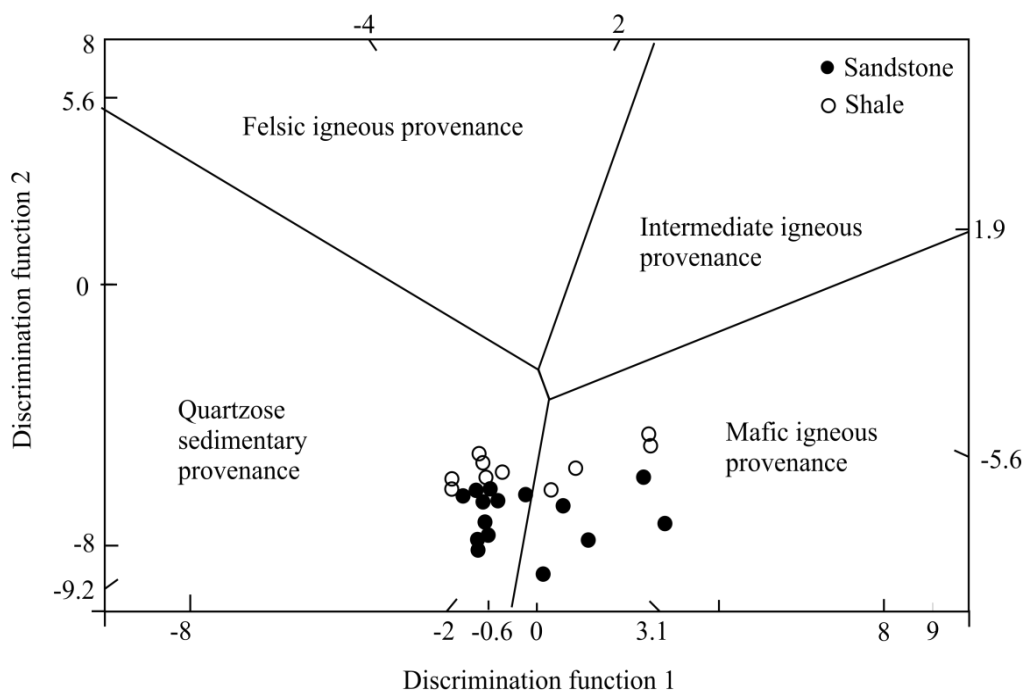
Fig. 7.28: Discrimination function diagram for provenance of sandstone-mudstone suites using major element ratios (after Bhatia, 1983)
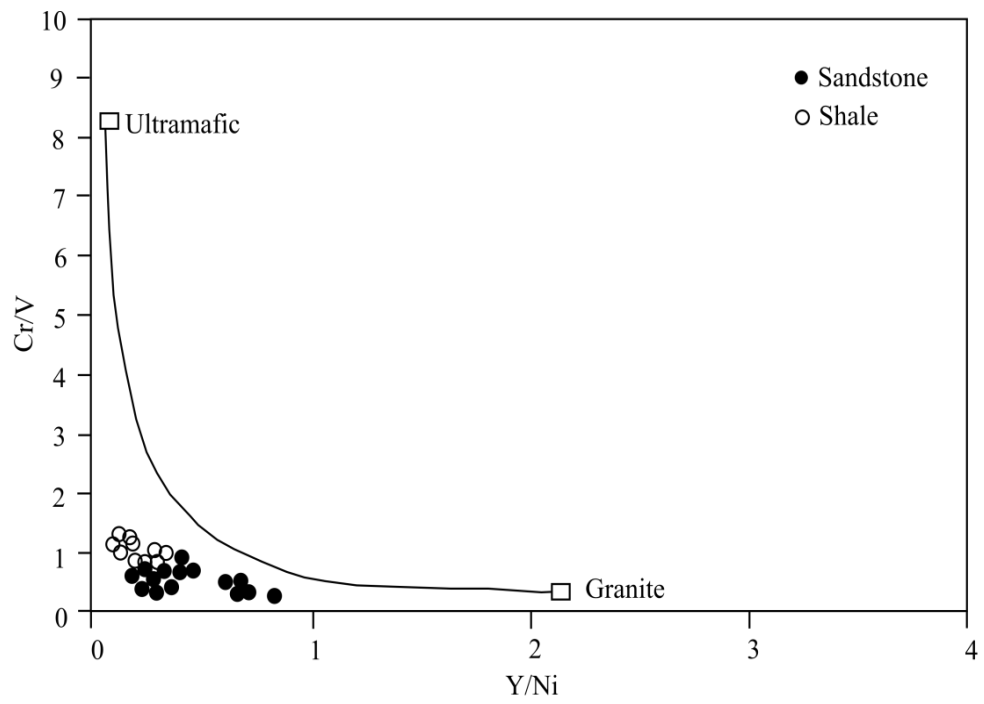
Fig. 7.29: Cr/V vs Y/Ni plots showing mixing between granite and ultramafic end-members (after Mongelli *et al*., 2006)

suggests some contribution of detritus from felsic sources. Garver *et al.* (1996) opine that high values of Cr (>150 ppm) and Ni (>100 ppm) and a range of Cr/Ni ratios from 1.2 to 1.5 may be due to contributions from ultramafic sources. The Cr concentrations of the Upper Disang sandstone and shale range from 42 to 136 (avg. 82 ppm) and 85 to 212 (avg. 132 ppm) respectively, which is comparatively depleted. Roy and Kacker (1980) state that Naga ophiolite ultramafics are depleted in Cr and Ni relative to the average ophiolitic peridotites. Besides source rock composition, post depositional alteration of the sediments may also be responsible for such depletion. The relatively greater depletion in the sandstone may be a reflection of much mixing of sediments from two or more sources. Ni concentrations range from 97 to 342 (avg. 189 ppm) and 22 to 291 (avg. 182 ppm) in the sandstone and shale respectively. Since mafic and ultramafic rocks are repositories of Ni, it is most likely that some sediments were contributed from the NHO that lies in the vicinity of the study area. Cr/Ni ratios of the sandstone and shale range from 0.39 to 0.68 and 0.5 to 0.6 respectively. Cr depletion and/or mixing of acid and mafic sources may be the cause of such lowered values. A high correlation coefficient exists between Cr and Ni ($r= 0.94$ sandstone; 0.59 shale) and corresponding high correlation of Cr and Ni with Co ($r= 0.8$ and 0.9 for sandstone and 0.7 and 0.8 for shale respectively). In such cases Asiedu *et al.* (2000) suggest significant contribution from ultramafic rocks.

Heavy mineral association is indispensable for provenance studies (Mange and Maurer, 1992; Morton and Hurst, 1995). Heavy minerals can be effectively used for tracing sediment transport path. Vital *et al.* (1999) used clay and heavy minerals to deduce provenance. Heavy minerals identified in the Upper Disang sandstone are euhedral, rounded and zoned zircon, rutile, tourmaline, garnet, corundum, wollastonite and scapolite. Euhedral zircon is a derivative of acid rocks. Zircon is among the most stable minerals commonly found in rocks. Zircon survives erosion during transportation and is much less altered than most other accessory minerals. Consequently, detrital zircon may be recycled many times, and multicycle sands may contain zircon from a variety of original source rocks. Zircon has therefore, been commonly used in provenance studies (Poldervaart, 1955; Larsen and Poldervaart, 1957; El-Hinnawi, 1973; El-Shazly, 1981). Some well preserved euhedral crystals of zircon in the sandstone point to possible granite or granite gneiss terrain in the vicinity. The angular and sub-rounded nature of the detritals indicates considerable textural immaturity. Such grains are products of rapid erosion of crystalline rocks and

short transportation of the debris over low relief areas. Granite gneiss is noted in the Naga Metamorphics in the vicinity of the study area. Zircon is also reported in eclogite (Ghose *et al*., 2010) that occurs as isolated, narrow lenses, bands and tectonic slices associated with lava flows and ultramafic cumulates in the NHO (Agrawal and Ghose, 1986). Such rocks that may have been exposed in the vicinity of the depositional site during the Middle Eocene (Fig. 7.30a) may well be the source for the euhedral zircon crystals. Most Upper Disang zircon however evolved in the Karbi Anglong crystalline complex which is the eastern extension of the Meghalaya massif. These two bodies are separated by the Kopili Graben of probable Paleocene-Eocene age; hence contribution from the latter may be ruled out. The granite gneiss of the Shillong Plateau has been dated at 1720 Ma, indicating a Paleoproterozoic age (Ghosh *et al*., 1994). Bidyananda and Deomurari (2007) estimated the age of zircon of the basement gneissic rocks at 1.9 Ga. Another episode of felsic magma activity gave rise to the Neoproterozoic porphyritic granite, which intruded the Shillong basin as plutons; these have been dated at 500 Ma (Chatterjee *et al*., 2007). The provenance of the well rounded and zoned zircon may be this multiple episodic terrain of Karbi Anglong that lies in the western proximity of the study area. The high degree of rounding of much zircon points to intense reworking of former sediments, probably in a foreland basin and their further prolonged transport to the depositional site by turbidity currents. Flow of turbidity currents and consequent transport of sediments through relatively long distances would require gravitational aid. This would be possible only if the seafloor was appreciably tilted towards the east. Such a condition would have existed due to the enormous compression that caused the buckling and tilting of the seafloor eastward. The presence of garnet suggests low to medium grade metamorphic sources. Detrital rutile inclusions suggest medium grade metamorphic parent rocks.

Rutile occurs in recrystallized basalt and oceanic sediments of the NHO, particularly in eclogite, garnet-glaucophane schist, greenschist and metachert (Ghose *et al*., 2010). Tourmaline is found in metamorphic rocks with a wide range of bulk compositions, developing under most grades of metamorphism (Henry and Guidotti, 1985) including ophiolite belts. Corundum in the Upper Disang sandstones may have been contributed from portions of the ultramafic suite. Normative values indicate that the ophiolite basalt (Ezung, 2007) and gabbro (Chisoi, 2011) are devoid of corundum. This may be due to the exhaustion of Al_2O_3 during the formation of the potash and

sodic feldspars. However, normative values indicate small amounts of corundum in pyroxenite (Chisoi, 2011) and serpentinite (Merangsoba, 2012). Petrographic studies show corundum as an accessory mineral in the ultramafics of Phek district (Chisoi, 2011). The angularity of the corundum grains suggests nominal transportation. Wollastonite is characteristic of contact metamorphic zones and is found as inclusions in volcanic rocks. Scapolite is a product of metamorphic rocks such as marble and schist. It is relatively common but confined to the upper horizons of the Upper Disang. Much evidence points to the presence of the Naga Metamorphics during Mid-Eocene but the schist of this formation has apparently not yielded any scapolite. Hence, it may be reasonably assumed that the probable source is the low grade metamorphosed limestone and/or quartz-sericite schist of the Nimi Formation. These exotic limestones defining the paleoplate boundary were emplaced on the Upper Disang due to gravity gliding (Robertson, 1977). However, this was most probably during the Oligocene with the dispersal of the Tethyan Sea in this region. But their unroofing from deeper levels definitely began earlier. It is assumed that these metamorphics were thrust over the obducted ophiolite during Late Eocene (Fig. 7.30b). The angularity of the scapolite grains points to a near source supply of sediments such as the Nimi formation in the vicinity. The presence of chert and abundance of basaltic opaques in the Disang sandstone are strong indications of contribution from the NHO. These are products of ocean floor material that were probably scraped and thrust above sea level during Middle and Late Eocene. It is known that Qmt and Qpt are contributed from igneous and metamorphic sources respectively. Qmt dominates over Qpt in these rocks indicating mainly plutonic sources. These plutonic sources would have been from both east and west of the basin as noted from other evidences. The small amounts of Qpt have most likely been contributed from metamorphic terrains in the east.

Plagioclase dominates over K-feldspar in sediments contributed from basic sources. Hence it may be assumed that the part of the Disang sediments was contributed from basic sources. Positive correlation coefficients of Al_2O_3 with Fe_2O_3 and MgO of the Upper Disang sandstone ($r= 0.72$ and 0.82 respectively) and Al_2O_3 with Fe_2O_3 in shale ($r= 0.69$) indicate an inclination towards basic sources. However, negative correlation of Al_2O_3 with MgO in shale ($r= -0.83$) suggest probable acidic sources. Hence, in the overall analyses it can be confidently assumed that both acid and basic rocks contributed to the formation of the Upper Disang.
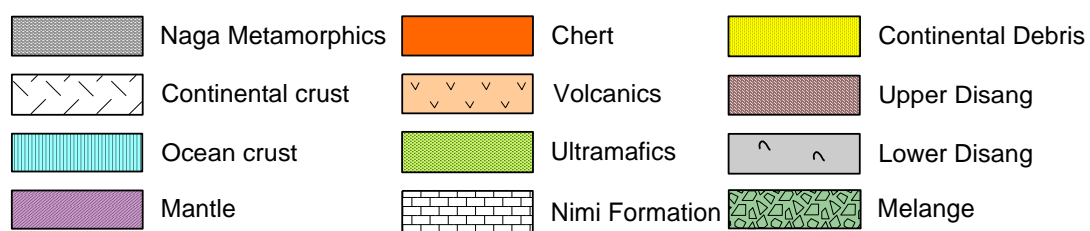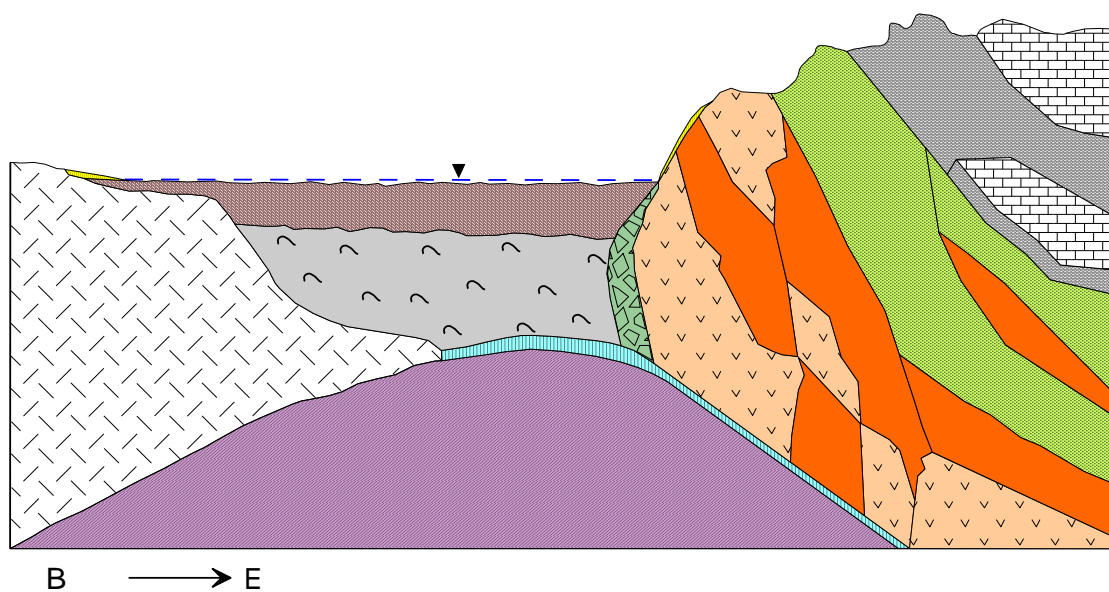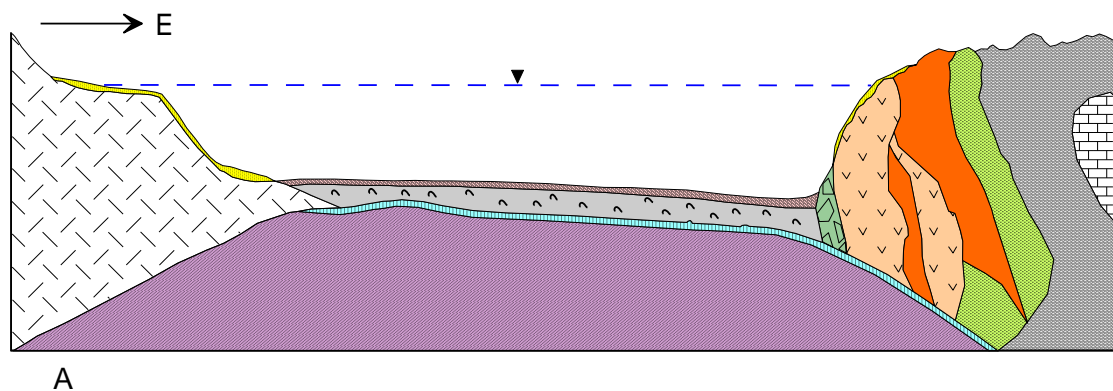
Fig. 7.30: Conceptual basin models of Upper Disang sediments (a) Middle Eocene, (b) Late Eocene

Hot and wet climates would have caused intense chemical weathering and erosion of the rapidly rising ophiolite. The resulting debris would have been rapidly transported and dumped into the basin formed due to subduction of the Indian plate. Similarly, the Karbi Anglong crystallines would have been rapidly weathered and eroded and the resulting debris brought down by fast flowing rivers into the shallowing sea. These sediments were transported further offshore into the slanting, quick shallowing deep sea floor by turbidity currents to their burial sites. Hence, detritus was supplied both from the east and west simultaneously to this turbidite basin. The detritus from the Karbi Anglong source was transported through long distances, possibly through a series of canyons as proposed by Allen *et al*. (2008) and got thoroughly mixed with detritus derived from the ophiolite and metamorphic terrains.

7.3   Age of NHO Basalt

In the NHO, basic to intermediate volcanic rocks are intercalated with variegated chert and occasionally with limestone. Previous workers have assigned the NHO rocks an Upper Jurassic to Upper Cretaceous age (Chattopadhyay *et al*., 1983; Acharyya *et al*., 1986; Sarkar *et al*., 1996; Baxter *et al*., 2011). Data scatter in most of the bivariate plots. LILE enrichment and unusually high Na_2O contents suggest hydrothermal alteration of most samples. Plots after Hughes (1972) suggest alkali metasomatism of most basalt into spilite. Calc-alkaline affinity of some samples may be ascribed to probable alkali enrichment due to seawater alteration. Undulose extinction and dissolution of plagioclase indicate effects of metamorphism. Very poor paleomagnetic results of most basalt samples may be attributed to the same.

The paleomagnetic pole position for the ChRM lies at 42.27°N and 315.5°E. Paleopole of basalt plotted in the APWP (Fig. 7.31) following Vandamme *et al*. (1991) indicates a Maestrichtian age of 70±5 Ma.
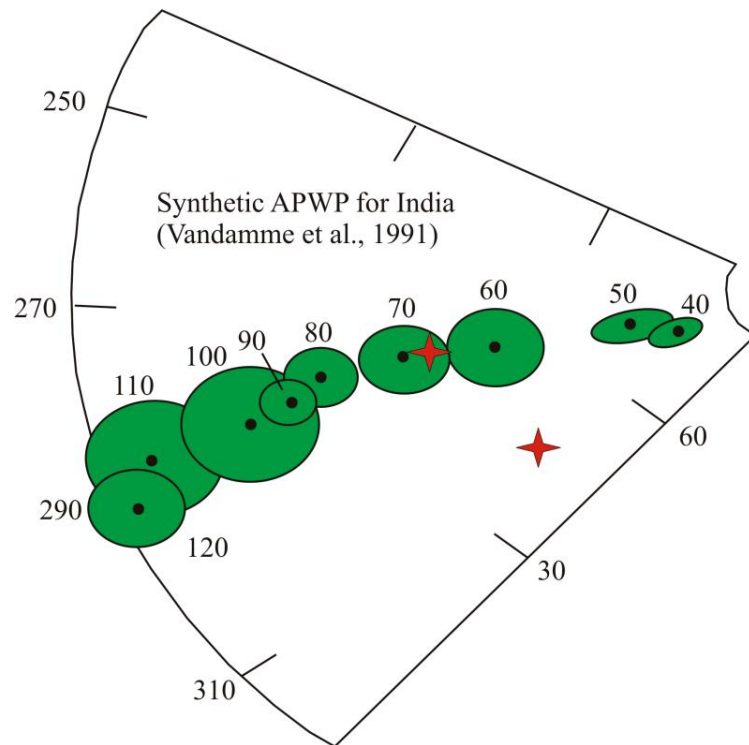
Fig. 7.31: Paleo pole of basalt plotted in synthetic apparent polar wandering path of India (after Vandamme *et al.*, 1991)

7.4. Magnetostratigraphic Correlation and Age of Paleogene Sediments

Magnetostratigraphy has been effectively used throughout the world in varied depositional environments for stratigraphic correlation (Harsland *et al.*, 1990; Opdyke and Channel, 1996). Magnetic polarity reversal is a global event that provides a robust tool for correlation. Magnetic polarity is independent of lithogenic constraints such as lateral litho-facies variations, permitting good correlation amongst Cenozoic successions (Tauxe and Opdyke, 1982; Sangode and Bloemendal, 2004).

From a 234 m thick composite sequence of the upper horizon of the Upper Disang at Leshimi, the age is constrained between 36.6 to 34.9 Ma (Fig. 7.32). The base of this section corresponds to chron C16r (36.618 - 36.341 Ma) and top to chron C15r (35.343 - 34.940 Ma).The correlation of this section is based on the presence of index planktic foraminifers such as *Globogerinatheka semiinvoluta, Cribrohantkenina inflate* and *Turborotalia cerroazulensis* indicating Bartonian to Priabonian age (Lokho and Kumar (2008). This horizon coincides at 175 m stratigraphic level corresponding to chron C15r of Cande and Kent (1995) at 35.940 Ma. After correlating C15r the rest of the section matches well with the GPTS which is justified by sediment accumulation rates. Mention may be made here that the base of the

Fig. 7.32: Correlation of Leshimi section MPTS with Cande and Kent (1995) GPTS (Black and white intervals of polarity column indicate normal and reverse polarity respectively)

Upper Disang is not exposed in this section but for correlation MPTS is extrapolated to the base of C16r and top of C15r. This work is corroborated by Basu and Raju (1964) favouring an Upper Eocene age for the Upper Disang based on foraminiferal assemblages including *Discocyclina dispensa, Numulites margoclaria and Discocyclina amphohus*. The base of this section corresponds to the upper part of E14 foram zone and nano zone NP18 within Chron C16r. Lithounits show rythmites of sandstone, siltstone and shale with an overall fining upward cycle of a transgressive phase. The upper part of this section is relatively more arenaceous and coarser than the underlying units, indicating shallowing of the basin. This corresponds to E15 foram zone and nanno zone NP19 within Chron 15r. Samples from the uppermost horizon of the Upper Disang near the contact with the overlying Laisong Formation could not be collected for this study. Thus, the upper age limit of the Leshimi section may be 34.9±0.01 Ma. However, this section is but a portion of a much thicker Upper Disang sequence. It may thus be reasonably assumed that the Upper Disang rocks range in age from Middle to Late Eocene. Leshimi composite section covers a time interval of 1.678 Ma.

Viswema section shows an overall coarsening upwards regressive sequence. Though no fossils are recorded from this section for magnetostratigraphic age calibration, numerous fossils have been reported in the adjoining areas. The presence of *Nummulites chavanensis*, *Dictyoconoides sp.*, *Operculina sp.*, *Reticulate Nummulites* and *Biplanispira sp.* from Laisong Formation suggest Upper Eocene age (Acharyya, 1982; Rao, 1983). *Assilina sp.* of Eocene affinity has also been documented from the same (Mishra, 1984). This section can therefore be matched with the GPTS pattern of Late Eocene. Based on this paleontological data and a distinct reverse polarity at C13r, a tie point with GPTS for this section is considered. Iterative matching of the present MPTS with the GPTS of Cande and Kent (1995) constrained the age of this sediments between 34.940 and 33.058 Ma (Fig. 7.33). The basal part of this section exposes thin interbeds of shale, sandstone and siltstone, which corresponds to the upper part of foram zone E15 and nanno zone NP19 within Chron C15n. This composite section covers a time interval of 1.882 Ma. The base of the section corresponds to chron C15n (34.940 - 34.655 Ma) and top to chron C13n (33.545 - 33.058 Ma). It is estimated that the 483 m thick sedimentary pile was deposited over 1.882 million years at an average rate of 25.
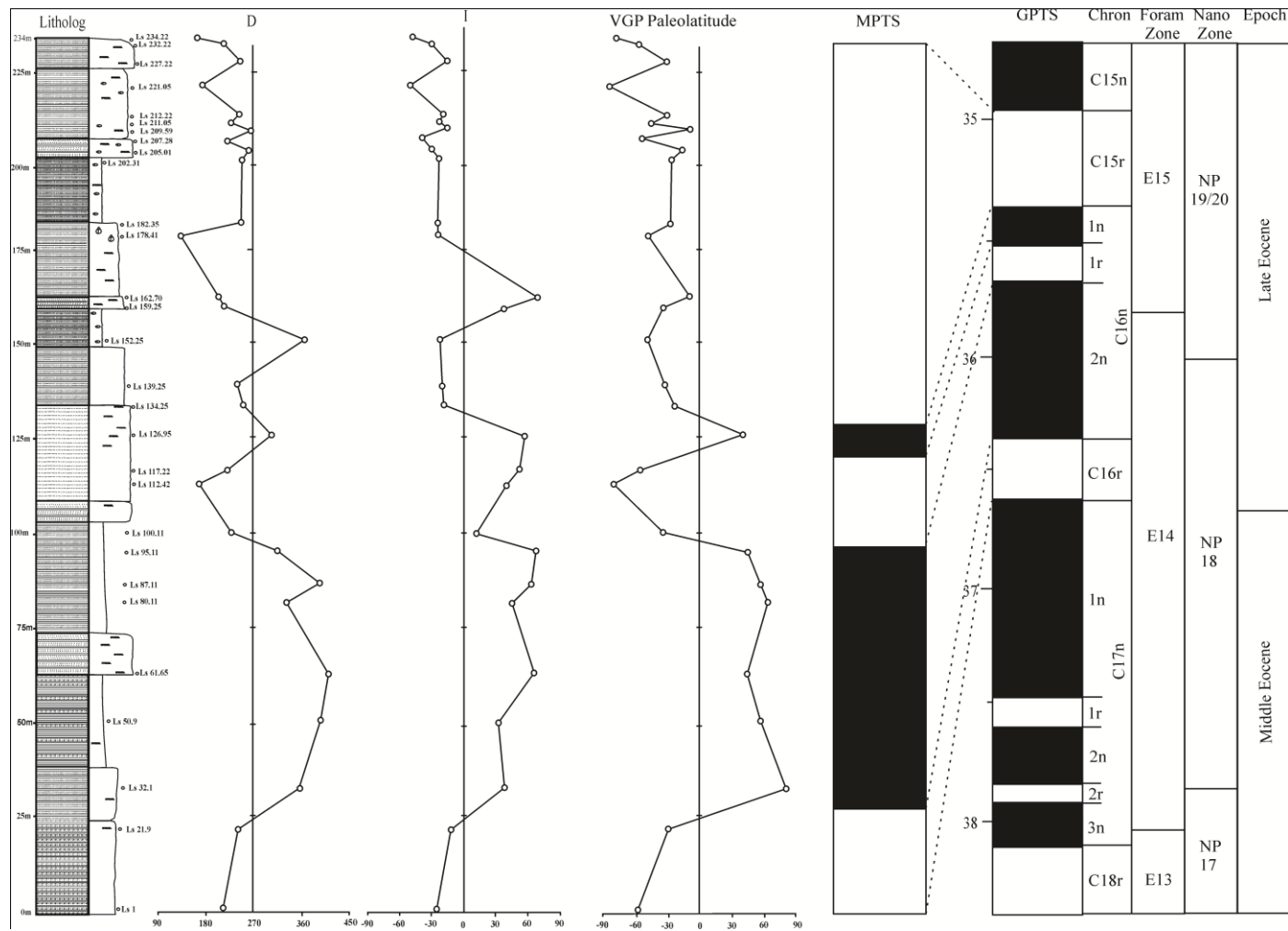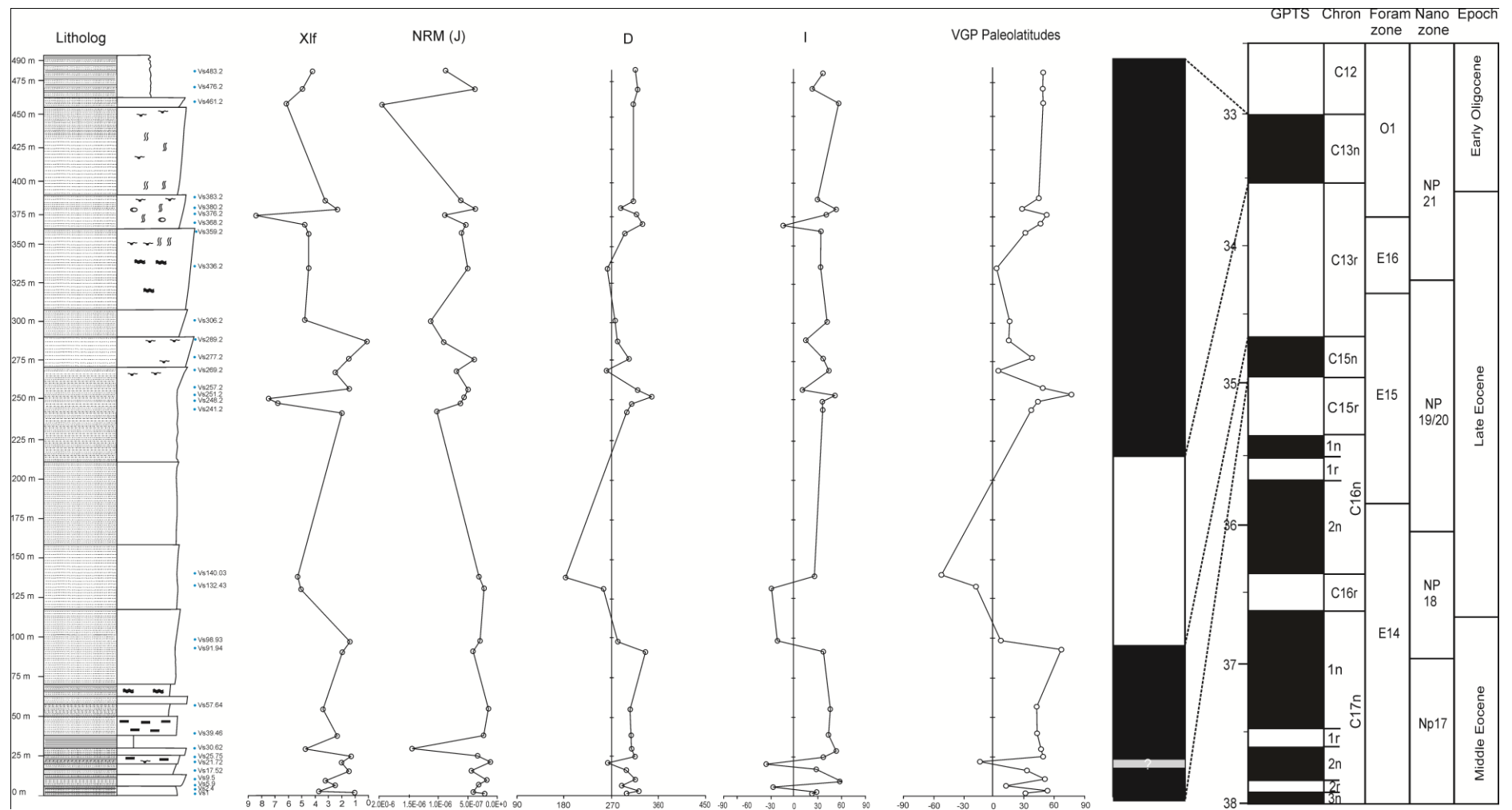
Fig. 7.33: Correlation of Viswema section MPTS with Cande and Kent (1995) GPTS (Black and white intervals of polarity column indicate normal and reverse polarity respectively)

The orientation of K_{max} trending NE-SW and NW-SE from AMS studies may be related to F_2 and F_3 regional folds. Jelinek plots indicate progressive increase in the intensity of deformation of the sediments. Since these magnetic lineations are sub-parallel to the regional fold axes / bedding strikes / thrusts it may be inferred that they are a consequence of an initial sedimentary compactional fabric and a later secondary tectonic fabric.

7.5   Sediment Accumulation Rate

Determination of SAR is one of the most powerful applications of magnetostratigraphy. SAR curves provide validity and check for successful correlation to GPTS by displaying justifiable rates for the given sequence (Malsawma, 2011). If the correlation is inaccurate, it produces anomalous and unexpected rates of sedimentation thus defying age correlation. However, its correlation needs careful examination since SAR varies with location (distal-proximal) and a tectonic setting of the given sedimentary section within the basin (Sangode and Kumar, 2003). SAR has not been corrected for post-depositional compaction because of unknown compaction history.

7.5.1   Implications of SAR Variations

Change in SAR is one of the most important proxies in basin tectonics inferred from magnetostratigraphy (Sangode and Kumar, 2003). Abrupt changes in the slope of a sediment accumulation curve commonly indicate timing of major thrusting events, basin subsidence or uplift (Burbank *et al*., 1996). The rate of sediment accumulation has been successfully used in the Himalayan foreland basin as an important proxy to discriminate thrust activity and reactivations, events of rapid or slow subsidence and several changes related to depocentre migrations (Burbank *et al*., 1996; Sangode *et al*., 1999). Sediment supply is a function of climate which enhances the runoff and thus available stream power for fluvial erosion (Molnar, 2004), source-rock lithology that is easily denuded, re-deposited or resistant and thus not readily available for re-deposition (Carroll *et al*., 2006) and the proximity of the sediment source (Burbank and Beck, 1991). Variations in SAR in the present study exhibits upward concavity (Fig. 7.34). Manifold increase in sedimentation rates observed at 35.343 Ma in the Leshimi section (25.81 cm/ka) may be attributed to gradual facies change from argillaceous dominant units of shale, siltstone and fine grained sandstone
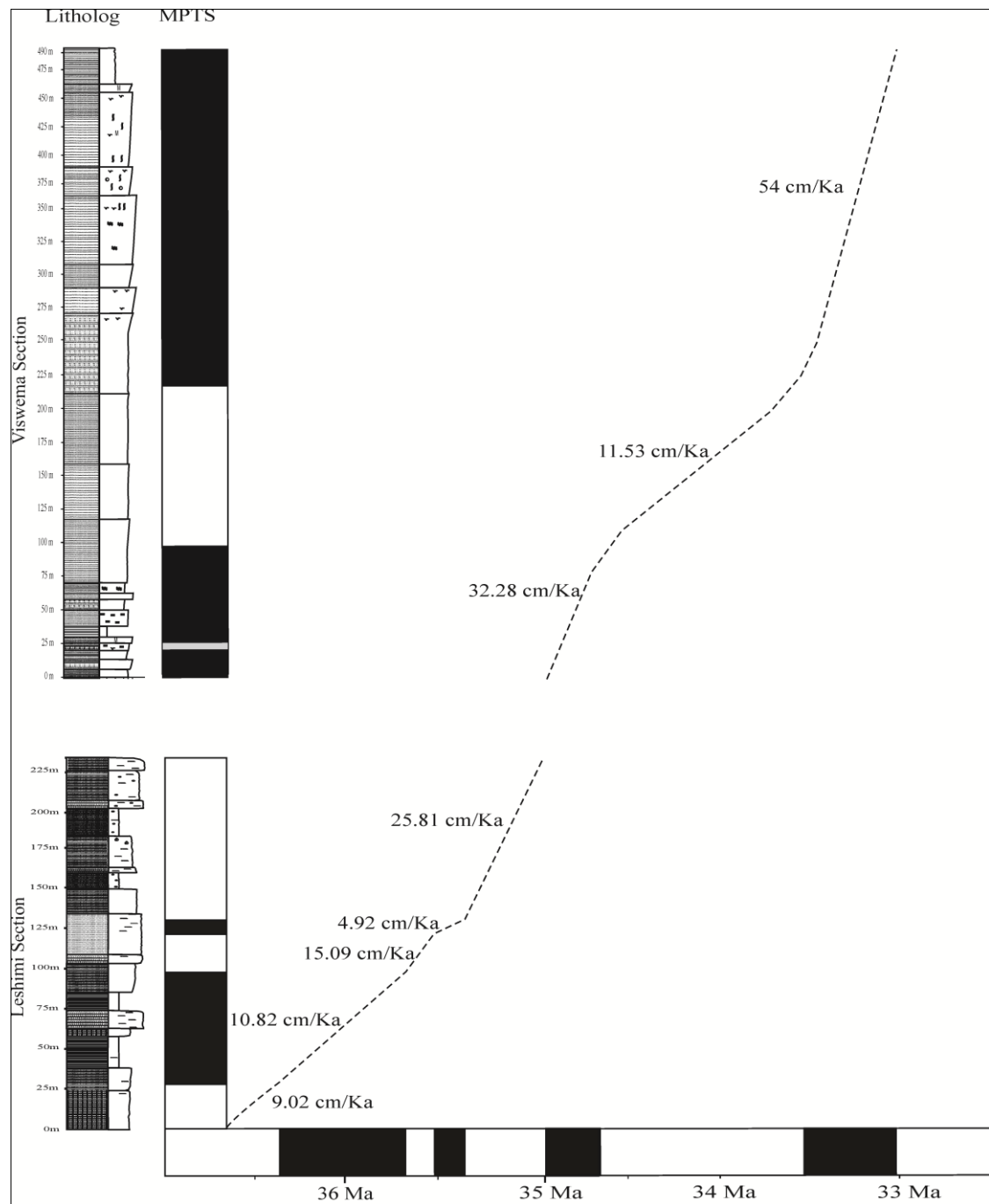
Fig. 7.34: Sediment accumulation rate of study area (after Cande and Kent, 1995)

to more arenaceous units. Abrupt drop in SAR in both sections suggest sluggishness in sedimentation rate due to basin subsidence and/or decrease in sediment influx. Enhanced SAR (54 cm/ka) is conspicuous at 33.545 Ma in the Viswema section which may be ascribed to gradual shallowing of the depositional basin. This is corroborated by the prevalence of Ophiomorpha ichnofossils characteristic of shallow marine environments (Pemberton and Jones 1988; Uchman and Gazdzicki, 2006). It may also be attributed to major tectonic reactivation of the positive areas during this period, which enhanced denudation and caused greater influx into the basin.

Conclusions

The NHO tholeiitic basalts have an E-MORB affinity. Poor fractionation of the parent magma is due to a slightly evolved magmatic source from shallower depths. The probable age of the NHO basalt is 70±5 Ma. These basalts underwent variable degrees of alteration and metamorphism. The enrichment of the MORB is due to aqueous fluid addition from a dehydrating subducting oceanic crust in a supra-subduction zone during collision of the Indian and Burmese plates.

Titano-magnetite is the main remanence carrier in the Upper Disang sediments. Magnetostratigraphic correlation of an Upper Disang section at Leshimi indicates ages between 36.6 to 34.9±0.01 Ma. These sediments were deposited at an average rate of 13.94 cm/ka. Laisong sediments of the Barail Group are conformably deposited over the Upper Disang sediments. Magnetite is the dominant magnetic mineral in the Laisong sediments with minor goethite and hematite. The age of the Laisong sediments from the Viswema section is constrained between 34.94 and 33.058 Ma. These sediments were deposited at an average rate of 25.66 cm/ka.

The Upper Disang turbidites are derivatives of felsic and mafic sources with minor contribution from low to medium rank metamorphic horizons. Much of the felsic components have been transported from distal sources. The most likely source rocks are the granite/granite gneiss of the Karbi Anglong crystalline complex on the west of the study area. However, the bulk of the sediments have been contributed from nearby basic and ultrabasic sources. This corresponds to the fast rising Naga Ophiolite which probably emerged above sea level during Mid-Eocene. Prevailing high temperatures and humid climate caused intense chemical weathering of the source rocks. The sediments from the west were transported great distances by

turbidity currents along an eastward slanting seafloor. Sediments from the nearby east were rapidly dumped onto the seafloor causing rapid mixing resulting in textural and chemical immaturity. Paleomagnetic studies endorse various paleontological evidences to indicate that the Upper Disang sediments were deposited from Middle to Late Eocene. Deposition took place in a subduction zone, most likely a closed wedge of an accretionary complex. This was a rapidly-closing turbidite basin where anoxic conditions prevailed. Towards the end of the Eocene this basin almost completely closed with the dispersal of the Tethyan Sea.

BIBLIOGRAPHY

Acharyya, S.K., 1982. Structural framework and tectonic evolution of the Eastern Himalaya. Him. Geol., v. 10, pp. 412-429.

Acharyya, S.K., 2007. Collisional emplacement history of the Naga-Andaman ophiolites and the position of the eastern Indian suture. Jour. Asian Earth Sci., v. 29, pp. 229-242.

Acharyya, S.K. Roy, D.K. and Mitra, N.D., 1986. Stratigraphy and palaeontology of the Naga Hills Ophiolite belt. Mem. Geol. Surv. India., v. 119, pp. 64-74.

Agarwal, R.K. and Madhav, C., 1988. Systematic geological mapping in parts of Phek district, Nagaland. Unpubl. Prog. Rep., FS 1987-88.

Agrawal, O.P., 1977. Prospects of refractory mineral in the ophiolite belt of Nagaland. Proc. Sem. Raw mat. Glass, Cer., Ref. Ind., Shillong, pp. 51-56.

Agrawal, O.P., 1985. Geology and geochemistry of the mafic-ultra mafic complex of Indo-Burman ranges between Meluri and Awankhoo, Phek district, Nagaland, India, Ph.D. thesis (Unpubl.), Patna University, Patna.

Agrawal, O.P. and Ghose, N.C., 1986. Geology and stratigraphy of the Naga Hills Ophiolite between Meluri and Awangkho, Phek district, Nagaland, India. In: N.C. Ghose and S. Varadaranjan (Eds.), Ophiolite and Indian plate margin. Sumna Publ., Patna, pp. 163-195.

Agrawal, O.P. and Ghose, N.C., 1989. Mineral resources in the ophiolite belt of Nagaland, NE India. In: N.C. Ghose (Ed.), Phanerozoic Ophiolites of India, Sumna Publ., Patna, pp. 245-280.

Agrawal, O.P. and Kacker, R.N., 1980. Nagaland ophiolites, India: A subduction zone ophiolite complex in a Tethyan orogenic belt. Intl. Ophiolite Sym., Cyprus, 1979. pp. 454-461.

Aier, I., Luirei, K., Bhakuni, S.S., Thong, G.T. and Kothyari, G.C., 2011. Geomorphic evolution of Medziphema intermontane basin and Quaternary deformation in the schuppen belt, Nagaland, NE India. Z. Geomorph., v. 55, pp. 247-265.

Aissaoui, D.M., McNeill, D.F. and Kirshvink, J.L., 1990. Magnetostratigraphic dating of shallow-water carbonates from Mururoa Atoll, French Polynesia: Implications for global eustasy. Earth Planet Sci. Lett., v.97, pp. 102-112.

Allen, R., Najman, Y., Carter, A., Barfod, D., Bickle, M.J., Chapman, H.J., Garzanti, E., Vezzoli, G., Ando, S. and Parrish, R.R., 2008. Provenance of the Tertiary sedimentary rocks of the Indo-Burman Ranges, Burma (Myanmar): Burman arc or Himalayan-derived? Jour. Geol. Soc. Lond., v. 165, pp. 1045-1057.

Alva-Valdivia L.M., Goguitchaichvii, A., Grajales, M., de Dios, A.F., Urrutia-Fucugaughi, J. and Roseles, C., 2002. Further constraints for Permo-Carboniferous magnetostratigraphy: Case study of the sedimentary sequence from San Salvador-Patlanoaya (Mexico). Comptes Rend Geosci., v. 334, pp. 811- 817.

Alva-Valdivia, L.M., Goguitchaichvili, A., Urrutia-Fucugauchia, J., Riisager, J., Riisager, P. and Lopesc, O.F., 2003. Paleomagnetic poles and paleosecular

variation of basalts from Parana Magmatic Province, Brazil: Geomagnetic and geodynamic implications. Phy. Earth Planet. Inter., v. 138, pp. 183-196.

Amajor, L.C., 1987. Major and trace element geochemistry of Albin and Touronian shales from the Southern Benue trough, Nigeria. Jour. Afr. Earth Sci., v. 6, pp. 633-641.

Appel, E., Rostler, W. and Corvinus, G., 1991. Magnetostratigraphy of the Miocene-Pleistocene Surai Khola Siwaliks in West Nepal. Intl. Jour. Geophy., v. 105. pp. 191-198.

Argast, S. and Donnelly, T.W., 1987. The chemical discrimination of clastic sedimentary components. Jour. Sed. Pet., v. 57, pp. 813-823.

Armstrong-Altrin, J.S., Verma, S.P., Madhavaraju, J. and Ramaswami, S., 2004. Geochemistry of sandstones from the Upper Miocene Kudankulam Formation, Southern India: Implications for provenance, weathering and tectonic setting. Jour. Sed. Res., v. 74, pp. 285-297.

Arndt, N.T., Czamanske, G.K., Wooden, J.L. and Fedorenko, V.A., 1993. Mantle and crustal contributions to continental flood volcanism. Tectonophysics, v. 223, pp. 39-52.

Asiedu, D.K., Dampare, S.B., Sakyi, P.A., Banoeng-Yakubo, B., Osae, S., Nyarko, B.J.B. and Manu, J., 2004. Geochemistry of Paleoproterozoic metasedimentary rocks from the Birim diamondiferous field, southern Ghana: Implications for provenance and crustal evolution at the Archaean-Proterozoic boundary. Geochem. Jour. v. 38, pp. 215-228.

Asiedu, D.K., Suzuki, S., Nogami, K. and Shibata, T., 2000. Geochemistry of Lower Cretaceous sediments, inner zone of SW Japan: Constraints on provenance and tectonic environment. Jour. Geochem., v. 14, pp. 155-173.

Athavale, R.N., Radhakrishnamurthy, C. and Sahasrabudhe, P.W., 1963. Paleomagnetism of some Indian rocks. Jour. Geophys., v. 7, pp. 304-313.

Bagci, U., 2013. The geochemistry and petrology of the ophiolitic rocks from the Kahramanmaras region, Southern Turkey. Turk. Jour. Earth Sci., doi:10.3906/yer-1203-1.

Balsley, J.R. and Buddington, A.F., 1960. Magnetic susceptibility anisotropy and fabric of some Adirondack granites and orthogneisses. Am. Jour. Sci., v. 2, pp. 6-20.

Banerjee, D.M. and Bhattacharya, P., 1994. Petrology and geochemistry of greywackes from the Aravalli Supergroup, Rajasthan, India and the tectonic evolution of a Proterozoic sedimentary basin. Precamb. Res., v. 67, pp. 11-35.

Banerjee, R.K., 1979. Disang shales: It's stratigraphy, sedimentary history and basin configuration in northeast India and Burma. Qtly. Jour. Geol. Min. Metal. Soc. Ind., v. 5, pp. 113-142.

Bareille, G., Grousset, F.E., Labracherie, M., Labeyrie, L.D. and Petit, J.R., 1994. Origin of detrital fluxes in the southeast Indian Ocean during the last climatic cycles. Paleoceanography, v. 9, pp. 799-819.

Baruah, R., 2003. Sedimentology and diagenetic environment of Paleogene Disang sediments in parts of Kohima and Phek districts, Nagaland. Ph.D. thesis (Unpubl.), Nagaland University, Kohima.

Basu, A., 1976. Petrology of Holocene fluvial sand derived from plutonic source rocks: Implications of paleoclimate interpretation. Jour. Sed. Pet., v. 46, pp. 694-709.

Basu, A., Young, S.S., Suttner, L.G., James, W.C. and Mack, G.W., 1975. Re-evaluation of the use of undulatory extinction and polycrystalline detrital quartz in provenance interpretation. Jour. Sed. Pet., v. 45, pp. 873-882.

Basu, D.N. and Ranga Raju, K.M., 1964. Geology of the Manipur valley and adjacent Hills. Unpubl. Rep. ONGC.

Baxter, A.T., Aitchison, J.C., Zyabrev, S.V. and Ali, J.R., 2011. Upper Jurassic radiolarians from the Naga ophiolite, Nagaland, northeast India. Gond. Res., doi:10.1016/j.gr.2011.02.001.

Bellanca, A., Claps, M., Erba, E., Masetti, D., Neri, R., Premoli-Silva, I. and Venezia, F., 1996. Orbitally induced limestone / marlstone rhythms in the Albian-Cenomanian Cismon section (Venetian región, northern Italy): Sedimentology, calcareous and siliceous plankton distribution, elemental and isotope geochemistry. Palaeogeog., Palaeoclim., Palaeoeco., v. 126, pp. 227-260.

Best, R.C. and Bothner, W.A., 1971. Petrographic observations on the cooling history of some oceanic basalts (abst.) Eos. Trans., AGU, v. 52, p. 375.

Bezos, A., Escrig, S., Langmuir, C.H., Micheal, P.J. and Asimow, P.D., 2009. Origin of chemical diversity of back arc basin basalt: A segment scale study of the eastern Lau spreading centre. Jour. Geophy. Res., v. 114, p. B06212.

Bhandari, L.L., Fuloria, R.C. and Sastry, V.V., 1973. Stratigraphy of Assam Valley, India. Bull. AAPG, v. 57, pp. 642-650.

Bhatia, M.R., 1983. Plate tectonics and geochemical composition of sandstones. Jour. Geol., v. 91, pp. 611-627.

Bhatia, M.R., 1985a. Rare earth element geochemistry of Australian Paleozoic graywackes and mudrocks: Provenance and tectonic control. Sed. Geol., v. 45, pp. 97-113.

Bhatia, M.R., 1985b. Composition and classification of Paleozoic flysch mudrocks of eastern Australia: Implications in provenance and tectonic setting interpretation. Sed. Geol., v. 41, pp. 249-268.

Bhatia, M.R. and Crook, K.A.W., 1986. Trace element characteristics of greywackes and tectonic setting discrimination of sedimentary basins. Contri. Min. Pet., v. 92, pp. 181-193.

Bhatia, M.R. and Taylor, S.R., 1981. Trace element geochemistry and sedimentary provinces: A study from the Tasman Geosyncline, Australia. Chem. Geol., v. 33, pp. 115-125.

Bhatt, M.I., Ghosh, S.K., 2001. Geochemistry of 2.51 Ga old Rampur Group pelites, western Himalayas: Implications from their provenance and weathering. Precamb. Res., v. 108, pp. 1-16.

Bhattacharjee, C.C., 1991. The Ophiolites of northeast India: A subduction zone Ophiolite Complex of Indo-Burman Orogenic Belt. Tectonophysics, v. 191, pp. 213-222.

Bhattacharjee, C.C., 1997. Tectonism and sedimentation in the Indo-Burman Sedimentary basin. Jour. Geosci., v. 2, pp. 1-8.

Bidyananda, M. and Deomurari, M.P., 2007. Geochronological constraints on the evolution of Meghalaya massif, Northeastern India: An ion microprobe study. Curr. Sci., v. 93, pp. 1620-1623.

Bjorlykke, K., 1974. Geochemical and mineralogical influence of Ordovician island arcs on epicontinental clastic sedimentation: A study of Lower Paleozoic sedimentation in the Oslo region, Norway. Sedimentology, v. 2, pp. 251-272.

Blatt, H., 1967. Provenance determination and recycling of sediments. Jour. Sed. Pet., v. 37, pp. 1031-1044.

Blatt, H. and Christie, J.M., 1963. Undulatory extinction in quartz of igneous and metamorphic rocks and its significance in provenance study of sedimentary rocks. Jour. Sed. Pet., v. 33, pp. 559-579.

Blatt, H., Middleton, G.V. and Murray, R.C., 1980. Origin of sedimentary rocks. Prentice-Hall, New Jersey, 634p.

Bloemendal, J., Barton, C.E. and Radhakrishnamurthy, C., 1985. Correlation between Rayleigh loops and frequency dependent and quadrature susceptibility: Applications to magnetic granulometry of rocks; Jour. Geophy. Res., v. 90, pp. 8789-8792.

Bloemendal, J., King, J.W., Hall, F.R. and Doh, S.J., 1992. Rock magnetism of late Neogene and Pleistocene deep sea sediments: Relationship of sediment source, diagenetic processes and sediment lithology. Jour. Geophy. Res., v. 97, pp. 4361-4375.

Borradaile, G.J. and Henry, B., 1997. Tectonic applications of the magnetic susceptibility and its anisotropy. Earth Sci. Rev., v. 42, pp. 49-93.

Boynton, W.V., 1983. Geochemistry of the rare earth elements: meteorite studies. In: P. Henderson (Ed.), Rare Earth Element Geochemistry. Elsevier, Amsterdam, pp. 63-114.

Breit, G.N. and Wanty, R.B., 1991, Vanadium accumulation in carbonaceous rocks: A review of geochemical controls during deposition and diagenesis: Chem. Geol., v. 91, pp. 83-97.

Brooks, C.K., 1973. Rifting and doming in Southern East Greenland. Nature, v. 244, pp. 23-24.

Brozovik, N. and Burbank, D.W., 2000. Dynamic fluvial systems and gravel progradation in the Himalayan foreland. Geol. Soc. Am. Bull., v. 112, pp. 394-412.

Brunnschweiler, R.O., 1966. On the geology of Indo-Burman Ranges. Jour. Geol. Soc., Aust., v. 13. pp. 137-195.

Brunnschweiler, R.O., 1974. Indo-Burman Ranges. In: A.M. Spencer (Ed.), Mesozoic-Cenozoic Orogenic belts. Data Orogenic Stud. Edinburgh, pp. 279-299.

Burbank, D.W. and Beck, R.A., 1991. Rapid, long-term rates of denudation. Geology, v. 19, pp.1169-1172.

Burbank, D.W., Beck, R. and Mulder, T., 1996. The Himalayan foreland basin. In: M. Harrison (Ed.), Tectonic evolution of Asia. Cambridge University Press, pp. 149-188.

Butler, R.F., 1992. Paleomagnetism. Blackwell Scientific Publ., Oxford.

Butler, R.F., 1998. Paleomagnetism: Magnetic domains to geologic terranes. Blackwell Science Inc.

Butler, R.F. and Opdyke, N.D., 1979. Magnetic polarity stratigraphy. Rev. Geophy. Space Phy., v. 17. pp. 235-244.

Cande, S.C. and Kent, D.V., 1992. A new geomagnetic polarity timescale for the Late Cretaceous and Cenozoic. Jour. Geophy. Res., v. 97, pp. 13917-13951.

Cande, S.C. and Kent, D.V., 1995. Revised calibration of the geomagnetic polarity timescale for the Late Cretaceous and Cenozoic. Jour. Geophy. Res., v. 100, pp. 6093-6095.

Cann, J.R., 1970. Rb, Sr, Y, Zn, Nb in some ocean floor basaltic rocks. Earth Planet. Sci. Lett., v. 10, pp. 7-11.

Carroll, A.R., Chetel, L.M. and Smith, M.E., 2006. Feast to famine: Sediment supply control on Laramide basin. Geology, v. 34, pp. 197-200.

Chadima, M. and Hrouda, F., 2006. Remasoft 3.0 - A user friendly paleomagnetic data browser and analyzer. Travaux G´eophysiques, v. 27, pp. 20-21.

Chakrabarti, G., Shome, D., Bauluz, B. and Sinha, S., 2009. Provenance and weathering history of Mesoproterozoic clastic sedimentary rocks from the basal Gulcheru Formation, Cuddapah basin, India. Jour. Geol. Soc. Ind., v. 74. pp. 119-130.

Channell, J.E.T., Lowrie, W., Pailli, P. and Venturi, E., 1984. Jurassic magnetic stratigraphy from Umbrian (Italian) land section. Earth Planet. Sci. Lett., v. 68. pp. 309-325.

Chatterjee, N., Mazumdar, A.C., Bhattacharya, A. and Saikia, R.R., 2007. Mesoproterozoic granulites of the Shillong-Meghalaya Plateau: Evidence of westward continuation of the Prydz Bay Pan-African suture into Northeastern India. Precamb. Res., v. 152, pp. 1-26.

Chattopadhyay, B. and Roy R.K., 1975. Systematic geological mapping and mineral investigation in Manipur east district, Manipur. Unpubl. Prog. Rep., Geol. Surv. Ind.

Chattopadhyay, B. and Roy, R.K., 1977. Systematic geological mapping in Phek district, Nagaland. Unpubl. Prog. Rep., Geol. Surv. Ind., FS 1975-1979.

Chattopadhyay, B., Venkataramana, P., Roy, D.K., Bhattacharya, S. and Ghosh, S., 1983. Geology of Naga Hills Ophiolite. Geol. Surv. Ind. Rec. 112, v. 2. pp. 59-115.

Chaudhuri, S. and Cullers, R.L., 1979. The distribution of REE in deeply buried Gulf Coast sediments. Chem. Geol., v. 24, pp. 327-338.

Chirouze, F., Dopont-Nivet, G., Huyghe, P., Van der Beek, P., Chakraborti, T., Bernet, M. and Erens, V., 2012. Magnetostratigraphy of the Neogene Siwalik

Group in the far eastern Himalaya: Kameng section, Arunachal Pradesh, India. Jour. Asian Earth Sci., v. 44, pp. 117-135.

Chisoi, 2011. Petrography and geochemistry of mafic and ultramafic cumulates from parts of Phek district, Nagaland with special reference to platinum group mineralization. Ph.D. thesis (Unpubl.), Nagaland University, Kohima.

Coish, R.A., 1977. Ocean floor metamorphism in the Belts Cove Ophiolite, Newfoundland. Contrib. Min. Pet., v. 60, pp. 255-270.

Coleman, D. and Walker, J.D., 1990. Geochemistry of Mio-Pliocene volcanic rocks from around Panamint Valley, Death Valley area, California. In: B.P. Wernicke, (Ed.), Basin and Range extensional tectonics near the latitude of Las Vegas, Nevada: Boulder Colorado. Geol. Soc. Am. Mem., pp. 391-411.

Collinson, D.W., 1983. Methods in rock magnetism and paleomagnetism: Techniques and instrumentation. Chapman and Hall, London, 503p.

Condie, K.C., 1991. Another look at rare earth elements in shales. Geochim. Cosmochim. Acta, v. 55, pp. 2527-2531.

Condie, K.C., 1993. Chemical composition and evolution of the upper continental crust: Contrasting results from surface samples and shales. Chem. Geol. v. 104, pp. 1-37.

Condie, K.C. and Allen, P., 1984. Origin of Archaean charnockites from southern India. In: A. Kroner, G.N. Hanson and A.M. Goodwin (Eds.), Archaean Geochemistry. Springer-Verlag, Berlin, pp. 182-203.

Condie, K.C., Boryta, M.D., Liu, J. and Quian, X., 1992. The origin of Khondalites: Geochemical evidence from the Archaean to Early Proterozoic granulitic belt in the north China Craton. Precamb. Res., v. 59, pp. 207-223.

Condie, K.C. and Wronkiewicz, D.J., 1990. The Cr/Th ratio in Precambrian pelites from the Kaapvaal Craton as an index of craton evolution. Earth Planet. Sci. Lett., v. 97, pp. 256-267.

Conolly, J.R., 1965. The occurrence of polycrystallinity and undulatory extinction in quartz in sandstone. Jour. Sed. Pet. v. 35, pp. 116-135.

Cox, K.G., Bell, J.D. and Parkhurst, R.J., 1979. The interpretation of igneous rock. George Allen and Unwin, London, pp. 1-450.

Cox, K.G. and Hawkesworth, C.J., 1984. Relative contributions of crust and mantle to flood basalt magmatism, Mahabaleshwar area, Deccan Traps. Phil. Trans. Roy. Soc. Lond., Series A, v. 310, pp. 627-641.

Cox, R., Lowe, D.R. and Cullers, R.L., 1995. The influence of sediment recycling and basement composition on evolution of mudrock chemistry in the southwestern United States. Geochim. Cosmochim. Acta, v. 59, pp. 2919-2940.

Creaser, R.A., Erdmer, P., Stevens, R.A. and Grant, S.L., 1997. Tectonic affinity of Nisutlin and Avil assemblages strata from the Teslin tectonic zone, northern Canadian Cordillera: Constraints from neodymium isotope and geochemical evidence. Tectonics, v. 16, pp. 107-121.

Crook, K.A.W., 1974. Lithogenesis and geotectonics: The significance of compositional variation in flysch arenites (greywackes). In: R.H. Dott and R.H.

Shavar (Eds.), Modern and ancient geosynclinal sedimentation. Soc. Econ. Paleont. Min. Spl. Publ., v. 19, pp. 304-310.

Cullers, R.L., 1988. Mineralogical and chemical changes of soil and stream sediment formed by intense weathering of the Danburg granite, Georgia. Lithos, v. 21, pp. 301-314.

Cullers, R.L., 1994. The controls on the major and trace element variation of shales, siltstones, and sandstones of Pennsylvanian-Permian age from uplifted continental blocks in Colorado to platform sediment in Kansas, USA. Geochim. Cosmochim. Acta, v. 58, pp. 4955-4972.

Cullers, R.L., 2000. The geochemistry of shales, siltstones and sandstones of Pennsylvanian-Permian age, Colorado, USA: Implications for provenance and metamorphic studies. Lithos, v. 51, pp. 181-203.

Cullers, R.L., Barrett, T., Carlson, R. and Robinson, B., 1987. REE and mineralogic changes in Holocene soil and stream sediment. Chem. Geol., v. 63, pp. 275-297.

Cullers, R.L., Basu, A. and Suttner, L.J., 1988. Geochemical signature of provenance in sand-size material in soils and stream sediments near the Tobacco Root batholith Mt, USA. Chem. Geol., v. 70, pp. 335-348.

Cullers, R.L. and Berendsen, P., 1998. The provenance and chemical variation of sandstones associated with the Midcontinent rift system, USA. Euro. Jour. Min., v. 10, pp. 987-1002.

Cullers, R.L., Chaudhuri, C., Kilbane, N. and Koch, R., 1979. REE in size fractions and sedimentary rocks of Pennsylvanian-Permian age from the mid-continent of the USA. Geochim. Cosmochim. Acta, v. 43, pp. 1285-1301.

Cullers, R.L. and Podkovyrov, V.N., 2000. Geochemistry of the Mesoproterozoic Lakhanda shales in southeastern Yakutia, Russia: Implications for mineralogical and provenance control and recycling. Precamb. Res. v. 104, pp. 77-93.

Cummins, W.A., 1962. The greywacke problem. Geology, v. 13, pp. 51-72.

Currie, R.G. and Bornhold, B.D., 1983. The magnetic susceptibility of continental-shelf sediments, West coast Vancouver Island, Canada. Mar. Geol. v. 51, pp. 115-127.

Dampare, S.B., Asiedu, D.K., Osae, S., Manu, J. and Banaoeng-Yakuba, B., 2004. Geochemistry of the Lower Proterozoic greywackes from the Birm diamondiferous field, Ghana. Afri. Jour. Sci. Tech., v. 5, pp. 9-18.

Dasgupta, A., 1977. Geology of Assam-Arakan Region. Quart. Jour. Geol. Mini. Min. Soc. Ind., v. 49, pp. 20-36.

Dearing, J.A., Dann, R.J.L., Hay, K., Lees, J.A., Loveland, P.J., Maher, B.A. and O'Grady, K., 1996. Frequency dependent susceptibility measurements of environmental materials. Geophy. Jour. Intl, v. 124, pp. 228-240.

Dekkers, M.J., 1997. Environmental magnetism: An introduction. Geologie Mijnbouw., v. 76, pp. 163-182.

Desikachar, S.V., 1974. A review of tectonic and geological history of Eastern India in terms of plate tectonics theory. Jour. Geol. Soc. Ind., v. 15, pp. 137-149.

Dickinson, W.R., 1970. Interpreting detrital modes of graywacke and arkose. Jour. Sed. Pet., v. 40, pp. 695-707.

Dickinson, W.R., 1985. Interpreting provenance relations from detrital modes of sandstones. In: G.G. Zuffa (Ed.), Provenance of arenite. In: Nato ASI series C, Reidel Dordrecht, v. 148, pp. 333-361.

Dickinson, W.R., Beard, L.S., Brokenridge, G.R., Erjavec, J.L., Ferguson, R.C., Inman, K.F., Knopp, R.A., Lindberg, F.A. and Ryberg, P.T., 1983. Provenance of North America Phanerozoic sandstone in relation to tectonic setting. Bull. Am. Geol. Soc., v. 94, pp. 222-235.

Dickinson, W.R. and Suczek, C.A., 1979. Plate tectonics and sandstone composition. Bull. AAPG, v. 63, pp. 2165-2182.

Dill, H., 1986. Metallogenesis of early Paleozoic graptolite shales from the Graefenthal Horst (northern Bavaria-Federal Republic of Germany). Econ. Geol., v. 81, pp. 889-903.

Dill, H., Teschner, M. and Wehner, H., 1988. Petrography, inorganic and organic geochemistry of Lower Permian Carbonaceous fan sequences ("Brandschiefer Series"), Fedral Republic of Germany: Constraints to their paleogeography and assessment of their source rock potential. Chem. Geol., v. 67, pp. 307-325.

Directorate of Geology and Mining, Nagaland, 1978. Misc. Publ., No. 1.

Dokuz, A. and Tanyolu, E., 2006. Geochemical constraints on the provenance, mineral sorting and sub-areal weathering of Lower Jurassic and Upper Cretaceous clastic rocks of the eastern Pontides, Yusufeli (Artvin), NE Turkey. Turk. Jour. Earth Sci., v. 15, pp. 181-209.

Donnelly, K. E., Goldstein, S. L. and Langmuir, C. H., 2004. Origin of enriched ocean ridge basalts and implications for mantle dynamics. Earth Planet. Sci. Lett., v. 226, pp. 347-366.

Drever, J.I., 1977. Seawater: Cycles of the major elements. Dowden, Hutchinson and Ross, Stroudsburg, 344p.

Dunlop, D.J. and Ozdemir, O., 1997. Rock magnetism: Fundamentals and frontiers. Cambridge Univ. Press, Cambridge, UK, 573p.

Dypvik, H., 1979. Mineralogy and geochemistry of the Mezozoic sediments of Andoya, Northern Norway. Sed. Geol., v. 24, pp. 45-67.

Dypvik, H., 1984. Geochemical compositions and depositional conditions of Upper Jurassic and Lower Cretaceous Yorkshire clays, England. Geol. Mag., v. 121, pp. 489-504.

Elderfield, H. and Sholkovitz, E.R., 1987. REE in the pore waters of reducing marine sediments. Earth Planet. Sci. Lett., v. 82, pp. 280-288.

El-Hinnawi, E., 1973. Mineralogy and Chemistry of Nubian sandstones from the central Eastern Desert of Egypt. N. Jb Miner. Abh., v. 118, p. 211.

El-Shazly, E.M., 1981: Distribution of beach zircon along the Mediterranean Coast, Egypt. Egypt. Jour. Geol, v. 25, p. 113.

Ernst, W., 1970. Geochemical facies analysis, methods in geochemistry and geophysics. Elsevier, Amsterdam, 152p.

Evans, M.E. and Heller, F., 2001. Magnetism of loess/paleosol sequences: Recent developments. Earth Sci. Rev., v. 54, pp. 129-144.

Evans, P., 1932. Tertiary succession in Assam. Trans. Min. Geol. Inst. Ind., v. 27, pp. 155-260.

Evans, P., 1964. The tectonic framework of Assam. Jour. Geol. Soc. Ind., v. 5, pp. 80-96.

Evensen, N.M., Hamilton, P.J. and O'nions, R.K., 1978. Rare earth abundances in chondritic meteorites. Geochim. Cosmochim. Acta, v. 42, pp. 1199-1212.

Ezung, O.C., 2007. Petrography and geochemistry of volcanic rocks of the ophiolite suite in and around Zipu, Phek district, Nagaland. Ph.D. thesis (Unpubl.), Nagaland University, Kohima.

Fairbridge, R.W., 1972. The encyclopaedia of geochemistry and environmental sciences. Encyclopaedia of Earth Science Series No. 4. Van Nostrand Reinhold Co., New York.

Fedo, C.M., Eriksson, K.A. and Krogstad, E.J., 1996. Geochemistry of shales from the Archean ($\sim$3.0 Ga) Buhwa Greenstone belt, Zimbabwe: Implication for provenance and source area weathering. Geochim. Cosmochim. Acta, v. 60, pp. 1751-1763.

Fedo, C.M., Nesbitt, H.W. and Young, G.M., 1995. Unraveling the effect of potassium metasomatism in sedimentary rocks and paleosols, with implications for paleoweathering conditions and provenance. Geology, v. 23, pp. 921-924.

Feng, R. and Kerrich, R., 1990. Geochemistry of fine-grained clastic sediments in the Archaean Abitibi greenstone belt, Canada: Implications for provenance and tectonic setting. Geochim. Cosmochim. Acta, v. 54, pp. 1061-1081.

Floyd, P.A. and Leveridge, B.E., 1987. Tectonic environment of the Devonian Gramscatho basin, Cornwall: Framework mode and geochemical evidence from turbiditic sandstones. Jour. Geol. Soc. Lond., v. 144, pp. 531-542.

Folk, R.L., 1960. Petrography and origin of the Tuscarora Rose Hill and Keefer Formations, Lower and Middle Silurian of eastern West Virginia. Jour. Sed. Pet., v. 30, pp. 1-58.

Folk, R.L., 1968. Bimodal supermature sandstones: Product of the desert floor. Intl. Geol. Cong., 23rd Session, v. 8, pp. 9-32.

Folk, R.L., 1980. Petrology of sedimentary rocks. Hemphill, Austin, Texas 183p.

Freyer, B.J., 1977. Rare earth evidence in iron formations for changing Precambrian oxidation states. Geochim. Cosmochim. Acta, v. 41, pp. 361-367.

Ganguly, S., 1993. Stratigraphy, sedimentation and hydrocarbon prospects of the Tertiary succession of Tripura and Cachar (Assam). Ind. Jour. Geol., v. 65. pp. 145-180.

Ganju, J.L., Khar, B.M. and Chaturvedi, J.G., 1986. Geology and hydrocarbon prospects of Naga Hills, south of 27° latitude. Bull. ONGC, v. 23, pp. 129-145.

Garcia, O.M., 1978. Criteria for the identification of ancient volcanic arcs. Earth Sci. Rev., v. 14, pp. 147-165.

Garrels, R.M. and Christ, C.L., 1965. Solution, minerals and equilibria. Harper and Row Publishers, New York, 450p.

Garver, J.I., Royce, P.R. and Smick, T.A., 1996. Chromium and nickel in shale of the Taconic foreland: A case study for the provenance of fine-grained sediments with an ultramafic source. Jour. Sed. Res., v. 66, pp. 100-106.

Garver, J.I. and Scott, T.J., 1995. Trace elements in shale as indicators of crustal provenance and terrain accretion in south Canadian Cordillera. Geol. Soc. Am. Bull., v. 107, pp. 440-453.

Gazzi, P., 1966. Le Arenarie del Flysch Sopracretaceo dell'Appennino Modenese: Correlazioni con il Flysch di Monghidoro. Mineralogica e Petrografica Acta, v. 12, pp. 69-97.

Geological Survey of India, 1986. Geology of Nagaland ophiolite. In: D.B. Ghosh commemorative volume. Mem. Geol. Surv. Ind., v. 119, pp. 1-113.

Ghose, N.C., 1979. Composition and origin of serpentinite in the ophiolite belt of Naga Hills, NE India. 26th Intl. Geol. Cong., Paris (Abs.).

Ghose, N.C., Agrawal, O.P. and Chatterjee, N., 2010. Geological and mineralogical study of eclogite and glaucophane schists in the Naga Hills Ophiolite, Northeast India. Island Arc, v. 19, pp. 336-356.

Ghose, N.C., Agrawal, O.P. and Srivastava, S.C., 1987. Metamorphism of the ophiolite belt of Nagaland, NE India. Proc. Natl. Sem. Tert. Orog., pp. 189-213.

Ghosh, S., Chakraborthy, S., Paul, D.K., Bhalla, J.K., Bishui, P.K., Gupta, S.N., 1994. New Rb-Sr ages and geochemistry of granitoids from Meghalaya and their significance in middle-late Proterozoic crustal evolution. Ind. Min., v. 48, pp. 33-44.

Ghose, N.C. and Singh, R.N., 1980. Occurrence of blue schist facies in the ophiolite belt of Naga Hills, east of Kiphire, NE India. Geol. Surv. Ind. Rec., v. 68, pp. 41-43.

Ghose, N.C. and Singh, R.N., 1981. Structure of the Naga Hills Ophiolite and associated sedimentary rocks in the Tuensang district of Nagaland, NE India. Ofioliti, v. 6. pp. 237-254.

Gilkson, M., Chappell, B.W., Freeman, R.S., Webber, E., 1985, Trace elements in oil shales, their source and organic association with particular reference to Australian deposits: Chem. Geol., v. 53, pp. 155-174.

Goswami, D.N.D., 1960. Geology of Assam. Dept. Publ., University of Guwahati.

Gradstein, F.M., Ogg, J.G. and Smith, A.G., 2004. A geologic time scale 2004. In: F.M. Gradstein, J.G. Ogg and A.G. Smith (Eds.). Cambridge University Press, Cambridge, UK, 610p.

Gromet, L.P., Dymek, R.F., Haskin, L.A. and Korotev, R.L., 1984. The North American shale composite: Its composition, major and trace element characteristics. Geochim. Cosmochim. Acta, v. 48, pp. 2469-2482.

Hallberg, R.O., 1976. A geochemical method for investigation of paleoredox conditions in sediments. Ambio. Spl. Rep., v. 4, pp. 139-147.

Halliday, A.N., Lee, D.C., Tommasini, S., Davies, G.R., Paslick, C.R., Fitton, J.G. and James, D.E., 1995. Incompatible trace elements in OIB and MORB and source enrichments in the sub-oceanic mantle, Earth Planet. Sci. Lett., v. 133, pp. 379-395.

Han, J. and Jiang, W., 1999. Particle size contributions to bulk magnetic susceptibility in Chinese loess and paleosol. Quat. Intl., v. 62, pp. 103-110.

Hariharan, G.N. and Nambiar, C.G., 1998. Rare earth element geochemistry of modern detrital sediments from Chaliyar River, northern Kerala. Jour. Geol. Soc. Ind., v. 52, pp. 213-217.

Harnois, L., 1988. The CIW index: A new chemical index of weathering. Sed. Geol., v. 55, pp. 319-322.

Harsland, W.B., Armstrong, R.L., Cox, A.V. Craig, L.E., Smith, A.G. and Smith, D. G., 1990. A geologic time scale 1989. Cambridge Univ. Press, Cambridge.

Hart, S.R., Erlank, A.J. and Kable, E.J.D., 1974. Seafloor basalt alteration: Some chemical and Sr isotope effects. Contrib. Min. Pet., v. 44, pp. 219-240.

Hassan, S., Ishiga, H., Roser, B.P., Dozen, K. and Naka, T., 1999. Geochemistry of Permian-Triassic shales in the Salt Range, Pakistan: Implications for provenance and tectonism at the Gondwana margin. Chem. Geol., v. 168, pp. 293-314.

Hatch, J.R. and Leventhal, J.S., 1992, Relationship between inferred redox potential of the depositional environment and geochemistry of the Upper Pennsylvanian (Missourian) Stark shale member of the Dennis Limestone, Wabaunsee County, Kansas, USA. Chem. Geol., v. 99, pp. 65-82.

Hawkesworth, C.J., O'Nions, R.K., Pankhurst, R.J., Hamilton, P.J. and Evensen, N.M., 1977. A geochemical study of island arc and back arc tholeiites from the Scotia Sea. Earth Planet. Sci. Lett. v. 36, pp. 253-62.

Hawkins, J.W. (Jr) and Whetten, J.T., 1969. Greywacke matrix minerals: Hydrothermal reactions with Columbia river sediments. Science, v. 66, pp. 868-870.

Hayden, H.H., 1910. Some coalfields in Northeastern Assam. Rec. Geol. Surv. Ind., v. 12.

Heald, M.T. and Laresse, R.E., 1974. The significance of the solution of feldspar in porosity development. Jour. Sed. Pet., v. 43, pp. 457-460.

Heller, F.W., Lowrie, H., Li and Wang, J., 1988. Magnetostratigraphy of the Permo-Triassic boundary section at Shangai. Earth Planet. Sci. Lett., v. 88, pp. 348-356.

Henry, D.J. and Guidotti, C.V., 1985. Tourmaline as a petrogenetic indicator mineral: An example from the staurolite grade metapelites of NW Maine. Am. Min., v. 70, pp. 1-15.

Herron, M.M., 1988. Geochemical classification of terrigenous sands and shales from core or log data. Jour. Sed. Pet., v. 58, pp. 820-829.

Holland, H.D., 1978. The chemistry of the atmosphere and the oceans. John Wiley, New York, 351p.

Hrouda, F., 1982. Magnetic anisotropy of rocks and its application in geology and geophysics, Geophy. Surv., v. 5, pp. 37-82.

Huerta-Diaz, M.A. and Morse, J.W., 1992, Pyritization of trace metals in anoxic marine sediments: Geochim. Cosmochim. Acta, v. 56, pp. 2681-2702.

Hughes, J.C., 1972. Spilites, kerotophyres and the igneous spectrum. Geol. Mag. v. 109, pp. 513-527.

Ingersoll, R.V., Bullard, T.F., Ford, R.L., Grimm, J.P., Pickle, J.D. and Sares, S.W.,

1984. The effect of grain size on detrital modes: A test of the Gazzi-Dickinson point counting method. Jour. Sed. Pet., v. 54, pp. 103-16.

Irvine, T.N. and Baragar, W.R.A., 1971. A guide to the chemical classification of the common volcanic rocks. Can. Jour. Earth Sci., v. 8, pp. 523-548.

Ising, G., 1942. On the magnetic properties of varved clay, Arkiu Mat. Astro. Phy., v. 29, pp. 1-37.

Jacobson, A.D., Blum, J.D., Chamberlian, C.P., Craw, D. and Koons, P.O., 2003. Climate and tectonic controls on chemical weathering in the New Zealand Southern Alps. Geochim. Cosmochim. Acta, v. 37, pp. 29-46.

Jakes, P. and Gill, J., 1970. Rare earth elements and the island arc tholeiitic series. Earth Planet. Sci. Lett., v. 9, pp. 17-28.

Jakes, P. and White, A.J.R., 1972. Major and trace element abundances in volcanic rocks of orogenic areas. Geol. Soc. Am. Bull., v. 83, pp. 29-40.

Jayaram, V., Chakradhar, N., Srivastava, M.P., Gandhi, P., Naik, K.K. and Roy, B., 1987. Systematic geological mapping of Kohima and Phek districts, Nagaland. Unpubl. Prog. Rep., FS 1986-87.

Jelinek, V., 1981. Characterization of the magnetic fabric of rocks. Tectonophysics, v. 79, pp. 63-67.

Johnson, N.M., Stix, J., Tauxe, L., Cerveny, P.F. and Taherkhelli, R.A.K., 1985. Paleomagnetic chronology, fluvial processes and tectonic implications of the Siwalik deposits near Chinji village, Pakistan. Jour. Geol., v. 93, pp. 27-40.

Johnsson, M.J., Stallard, R.F. and Meade, R.H., 1988. First cycle quartz arenites in the Orinoco River basin, Venezuela and Colombia. Jour. Geol., v. 96, pp. 263-277.

Jones, B. and Manning, D.C., 1994. Comparison of geochemical indices used for the interpretation of paleo-redox conditions in ancient mudstones: Chem. Geol., v. 111, pp. 111-129.

Kacker, R.N., Roy, R.K. and Agrawal, O.P., 1984. Exploration of ophiolite related mineral resources in Naga Hills. Sem. Rec. Adv. Cainozoic Geol., NER, Dibrugarh University.

Kent, D.V., Olsen, P.E. and Witte, W.K., 1995. Late Triassic-earliest Jurassic geomagnetic polarity sequence and paleolatitudes from drill cores in the Newark rift basin, NE America. Jour. Geophy. Res., v. 100, pp. 14965-14998.

King, J.W. and Channell, J.E.T., 1991. Sedimentary magnetism, environmental magnetism and magnetostratigraphy. In: US National Report to International Union of Geodesy and Geophysics. Rev. Geophy. Supp., pp. 358-370.

Kirschvink, J.L., 1980. The least-square line and plane and the analysis of paleomagnetic data. Geophy. Jour. Res. Astr. Soc., v. 62, pp. 699-718.

Kloowijk, C.T., 1976. The drift of the Indian sub-continent: An interpretation of recent paleomagnetic data. Geol. Rundschau, v. 65, pp. 885-909.

Kloowijk, C.T., 1979. A review of paleomagnetic data from the Indian fragment of the Gondwanaland. In: A. Farah and K.A. De Jong (Eds.), Geodynamics of Pakistan. Geol. Surv. Pak., Quetta. pp. 41-80.

Knight, C.A., 1971. Breeding of crystal nuclei by classical nucleation: Theory and some observations and experiments, Jour. Cryst. Grow., v. 11, pp. 201-217.

Kotlia, B.S., Nakayama, K., Bhalla, M.S., Phatiyal, B., Kosaka, T., Joshi, M., Sanwal, J. and Pande, R.N. 2002. Lithologic and magnetic polarity stratitgraphy of the Lower-Middle Siwalik succession between Kathgodam and Ranibagh, Kumaun Himalaya. Jour. Geol. Soc. Ind., v. 58, pp. 411-423.

Krishnan, M.S., 1968. Geology of India and Burma. Higginbothams (P) Ltd., Madras.

Kruiver P.P., Dekkers M.J. and Heslop D., 2001. Quantification of magnetic coercivity components by the analysis of acquisition curves of isothermal remanent magnetisation. Earth Planet. Sci. Lett., v. 189, pp. 269-276.

Kukal, Z., 1968. Origin, development and chemical classification of Early Paleozoic sandstones of central Bohemia. Intl. Geol. Cong., 23rd Session, Prague, Section 8, pp. 61-72.

Larsen, L.H. and Poldervaart, A., 1957. Measurement and distribution of zircon in some granitic rocks of magmatic origin. Miner. Mag., v. 31, p. 544.

Le Bas, M.J., Le Maitre, R.W., Streckeisen, A. and Zanettin, B., 1986. A chemical classification of volcanic rocks based on the total alkali-silica diagram. Jour. Pet., v. 27, pp. 745-750.

Le Maitre, R.W., 1989. A classification of igneous rocks and glossary of terms, recommendations of the International Union of Geological Sciences Sub commission on the Systematics of Igneous Rocks. Blackwell Scientific Publications, Oxford.

Levanthal, J.S. and Hosterman, J.W., 1982. Chemical and mineralogical analysis of Devonian black-shale samples from Martin County, Kentucky; Carroll and Washington counties, Ohio; Wise County, Virginia; and Overton County, Tennessee, USA. Chem. Geol., v. 37, pp. 239-264.

Lewan, M.D., 1984. Factors controlling the proportionality of vanadium to nickel in crude oils. Geochim. Cosmochim. Acta, v. 48, pp. 2231-2238.

Lewan, M.D. and Maynard, J.B., 1982. Factors controlling enrichment of vanadium and nickel in the bitumen of organic sedimentary rocks. Geochim. Cosmochim. Acta, v. 46, pp. 2547- 2560.

Liu, S., Lin, G., Liu, Y., Zhou, Y., Gong, F. and Yan, Y., 2007. Geochemistry of Middle Oligocene-Pliocene sandstones from the Nangpu Sag, Bohia Bay basin (Eastern China): Implications for provenance, weathering and tectonic setting. Geochem. Jour., v. 41, pp. 359-378.

Lokho, K. and Kumar, K., 2008. Fossil pteropods (Thecosomata, holoplanktonic Mollusca) from the Eocene of Assam-Arakan Basin, northeastern India. Curr. Sci. v. 94, pp. 647-652.

Lowrie, W. and Alvarez, W., 1977. Upper Cretaceous-Paleocene magnetic stratigraphy at Gubbio, Italy. III. Upper Cretaceous magnetic stratigraphy. Geol. Soc. Am. Bull., v. 88, pp. 374-377.

Mack, G.H., 1984. Exception to the relationship between plate tectonics and sandstones composition. Jour. Sed. Pet., v. 54, pp. 121-220.

Madhavaraju, J. and Ramasamy, S., 2002. Petrography and geochemistry of Late Maastrichtian-Early Paleocene sediments of Tiruchirapalli Cretaceous, Tamil Nadu: Paleoweathering and provenance implications. Jour. Geol. Soc. Ind., v. 59, pp. 133-142.

Maher B.A., 1986. Characterization of soils by mineral magnetic measurements. Phy. Earth Planet. Intl., v. 42, pp. 76-91.

Maher, B.A., 1988. Magnetic properties of some magnetites. Geophy. Jour., v. 94, pp. 83-96.

Maher, B.A. and Taylor, R.M., 1988. Formation of ultrafine-grained magnetite in soils. Nature, v. 366, pp. 368-370.

Majumdar, T., Pal, J.C. and Das, S.B., 1980. Trace element study of Banded Iron Formation and associated rocks of Orissa. Geol. Surv. Ind. Spl. Publ., No. 1, pp. 587-597.

Mallet, F.R., 1876. On the coalfields of Naga Hills bordering Lakhimpur and Sibsagar districts, Assam. Geol. Surv. Ind., Mem., v. 12.

Malsawma, J., 2011. Magnetostratigraphic study of the Bhuban Formation (Surma Group) around Aizawl, Mizoram. Ph.D. thesis (Unpubl.), Mizoram University, Aizawl.

Mange, M.A. and Maurer, H.F.W., 1992. Heavy minerals in colour. Chapman and Hall, London.

Mason, B. and Moore, C., 1982. Principles of geochemistry (4th Ed). John Willey and Sons. 350p.

Mathur, L.P. and Evans, P., 1964. Oil in India. Intl. Geol. Cong. (22nd Session), New Delhi.

Maynard, J.B., Valloni, R. and Yu, H.S., 1982. Composition of modern deep sea sands from arc related basins. In: J.K. Legget (Ed.), Trench-fore arc geology: Sedimentation and tectonics on modern and ancient active plate margins. Geol. Soc. Lond. Spl. Publ., v. 10, pp. 551-561.

McElhinny, M.W., 1973. Paleomagnetism and plate tectonics. Cambridge University Press, 230p.

McElhinny, M.W. and McFadden, P.L., 2000. Paleomagnetism: Continents and Oceans. Academic Press, San Diego, 386p.

McKenzie, D.P. and O'Nions, R.K., 1995. The source regions of ocean island basalts, Jour. Pet., v. 36, pp. 133-159.

McKenzie, D.P. and Sclater, J.G., 1971. The evolution of the Indian ocean since the Late Cretaceous. Roy. Astr. Soc. Geophy. Jour., v. 25, pp. 437-528.

McLennan, S.M., 1989. Rare earth elements in sedimentary rocks: Influences of provenance and sedimentary processes. Rev. Min., v. 21, pp. 169-200.

McLennan, S.M., 1993. Weathering and global denudation. Jour. Geol., v. 101, pp. 295-303.

McLennan, S.M., Hemming, S., McDaniel, D.K. and Hanson, G.N., 1993. Geochemical approaches to sedimentation, provenance and tectonics. Geol. Soc. Am. Spl. Paper, v. 285, pp. 21-40.

McLennan, S.M. and Taylor, S.R., 1980. Th and U in sedimentary rocks: Crustal evolution and sedimentary recycling. Nature, v. 285, pp. 621-624.

McLennan, S.M. and Taylor, S.R., 1991. Sedimentary rocks and crustal evolution: Tectonic setting and secular trends. Jour. Geol. v. 99, pp. 1-21.

McLennan, S.M., Taylor, S.R., McCulloch, M.T. and Maynard, J.B., 1990. Geochemical and Nd-Sr isotopic composition of deep-sea turbidites: Crustal evolution and plate tectonic associations. Geochim. Cosmochim. Acta, v. 54, pp. 2015-2050.

McNeill, D.F., Ginsburg, R.N., Chang, S.B.R. and Kirsvink, J.R., 1988. Magnetostratigraphic dating of shallow water carbonates from San Salvador, the Bahamas. Geology, v. 16. pp. 18-12.

Merangsoba, 2012. Petrology and geochemistry of serpentinites in the ophiolite suite from parts of Phek district, Nagaland with emphasis on their genesis. Ph.D. thesis (Unpubl.), Nagaland University, Kohima.

Meschede, M., 1986. A method of discriminating between different types of mid-ocean ridge basalts and continental tholeiites with the Nb-Zr-Y diagram. Chem. Geol., v. 56, pp. 207-218.

Middlemost, E.A.K., 1994. Naming materials in the magma/igneous rock system. Earth Sci. Rev., v. 37, pp. 215-224.

Migdisov, A.A., 1960. On the titanium/aluminum ratios in sedimentary rocks. Geochemistry (USSR), English Transl., v. 2, pp. 178-194.

Mishra, U.K., 1984. Paleontological studies of Disang and Barail sedimentaries in a part of Manipur East district. Unpubl. Geol. Surv. Ind., Prog. Rep.

Mitchell, A.H.G., 1981. Phanerozoic plate boundaries in mainland SE Asia, the Himalayas and Tibet. Jour. Geol. Soc. Ind., v. 138, pp. 109-122.

Mitchell, A.H.G. and McKerrow, W.S., 1975. Analogous evolution of the Burma Orogen and the Scottish Caledonides. Geol. Soc. Am. Bull., v. 86, pp. 305-315.

Miyashiro, A., 1974. Volcanic rock series in island arcs and active continental margins. Am. Jour. Sci., v. 274, pp. 321-355.

Miyashiro, A. and Shido, F., 1975. Tholeiitic and calc-alkalic series in relation to the behaviors of titanium, vanadium, chromium and nickel. Am. Jour. Sci., v. 275, pp. 265-277.

Molnar, P., 2004. Late Cenozoic increase in accumulation rates of terrestrial sediment: How might climate change have affected erosion rates? An. Rev. Earth Planet. Sci., v. 32, pp. 67-89.

Molnar, P. and Tapponnier, P., 1975. Cenozoic tectonics of Asia: Effects of a continental collision. Science, v. 189, pp. 419-425.

Mongelli, G., Critelli, S., Perri, F., Sonnino, M. and Perrone V., 2006. Sedimentary recycling, provenance and paleoweathering from chemistry and mineralogy of Mesozoic continental red bed mudrocks, Peloritani mountains, southern Italy. Jour. Geochem., v. 40, pp. 197-209.

Mooney, S.D., Geiss, C. and Smith, M.A., 2002. The use of mineral magnetic parameters to characterize archaeological ochres. Jour. Arch. Sci., v. 29, doi10.1006/jasc.2002.0856.

Morton, A.C. and Hurst, A., 1995. Correlation of sandstones using heavy minerals: An example from the Statfjord Formation of the Snorre field, northern North Sea. In: R.E. Dunay and E.A. Hailwood (Eds.), Non-biostratigraphical methods of dating and correlation. Geol. Soc. Spl. Publ., v. 89, pp. 3-12.

Mullins, C.E., 1977. Magnetic susceptibility of soil and its significance in soil science: A review. Jour. Soil Sci., v. 28, pp. 223-246.

Mullins, C.E. and Tite, M.S., 1973. Magnetic viscosity, quadrature susceptibility and frequency dependence of susceptibility in single-domain assemblages of magnetite and maghaemite. Jour. Geophy. Res., v. 78, pp. 804-809.

Murphy, J.B., 2000. Tectonic influence on sedimentation along the southern flank of the late Paleozoic Magdalen basin in the Canadian Appalachians: Geochemical and isotopic constrains on the Horton Group in the St. Mary's basin, Nova Scotia. Geol. Soc. Am. Bull., v. 112, pp. 997-1011.

Nagata, T., 1961. Rock magnetism (2nd Ed). Maruzan, Tokyo, 350p.

Naik, G.C., 1994. Subsurface geology and tectono-sedimentary evolution pre-Miocene sediments of Upper Assam, India. Ph.D. thesis (Unpubl.), ISM, Dhanbad.

Nandy, D.R., 1976. The Assam syntaxis of the Himalaya: A re-evaluation. Sem. Rec. Geol. Study. Him. Misc. Pub., Geol. Surv. Ind., v. 24, pp. 363-368.

Nandy, D.R., 1980. Tectonic pattern in India. Ind. Jour. Earth Sci., v. 7, pp. 103-107.

Nandy, D.R., 1982. Geological setup of the eastern Himalaya, the Patkai-Naga-Arakan-Yoma (Indo-Burman) hill ranges in relation to the Indian plate movement. Geol. Surv. Ind., Misc. Publ., v. 41, pp. 305214.

Naqvi, S.M., Sawkar, R.H., Subba Rao, D.V., Govil, P.K. and Rao, T.G., 1988. Geology, geochemistry and tectonic setting of Archaean greywacke from Karnataka nucleus, India. Precamb. Res., v. 39, pp. 193-126.

Nesbitt, H.W., 1979. Mobility and fractionation of rare earth elements during weathering of a granodiorite. Nature, v. 299, pp. 715-717.

Nesbitt, H.W., Fedo, C.M. and Young, G.M., 1997. Quartz and feldspar stability, steady and non-steady-state weathering and petrogenesis of siliciclastic sands and muds. Jour. Geol., v. 105, pp. 173-191.

Nesbitt, H.W., Markovics, G. and Price, R.C., 1980. Chemical processes affecting alkalies and alkaline earths during continental weathering. Geochim. Cosmochim. Acta, v. 44, pp. 1659-1666.

Nesbitt, H.W. and Young, G.M., 1982. Early Proterozoic climates and plate motions inferred from major element chemistry of lutites. Nature, v. 299, pp. 715-717.

Nesbitt, H.W. and Young, G.M., 1984. Prediction of some weathering trends of plutonic and volcanic rocks based on thermodynamic and kinetic considerations. Geochim. Cosmochim. Acta, v. 48, pp. 1523-1534.

Nesbitt, H.W. and Young, G.M., 1989. Formation and diagenesis of weathering profiles. Jour. Geol., v. 97, pp. 129-147.

Nesbitt, H.W., Young, G.M., McLennan, S.M. and Keays, R.R., 1996. Effects of chemical weathering and sorting on the petrogenesis of siliclastic sediments with implications for provenance studies. Jour. Geol., v. 104, pp. 525-542.

Odermatt, J.R. and Curiale, J.A., 1991. Organically bound metals and biomarkers in the Monterey Formation of the Santa Maria Basin, California. Chem. Geol., v. 91, pp. 99-113.

Ogg, J.G. and Lowrie, W., 1986. Magnetostratigraphy of the Jurassic-Cretaceous boundary. Geology, v. 4, pp. 547-550.

Ohara, Y., Stern, S., Ishii, T., Yurimoto, H. and Yamazaki, T., 2002. Peridotites from the Mariana Trough: First look at the mantle beneath an active back-arc basin. Contrib. Min. Pet., v. 143, pp. 1-18.

Okada, H., 1971. Classification of sandstone: Analysis and proposal. Jour. Geol., v. 79, pp. 509-525.

Oldham, R.D., 1883. Report on the geology of parts of Manipur and Naga Hills. Geol. Surv. Ind., Mem., v. 14.

Omar, A.A. and Khan, M.M., 2005. Mineralogy and geochemistry of Unayzah Formation, Central Saudi Arabia: Implications for provenance interpretation. Jour. King Saudi University, v. 18, Sci., pp. 35-49.

Opdyke, N.D. and Channel, J.E.T., 1996. Magnetic stratigraphy. Academic Press, pp. 20-25.

O'reilly, W., 1984. Rock and mineral magnetism. Blackie, Chapman and Hall, New York, 220p.

Pascoe, E.H., 1912. A traverse across the Naga Hills of Assam from Dimapur to the neighbourhood of Saramati peak. Rec. Geol. Surv. Ind., v. 42, pp. 254-264.

Pearce, J.A., 1983. Role of sub-continental lithosphere in magma genesis in active continental margins. In: C.J. Hawkesworth and M.J. Norry (Eds.), Continental basalts and mantle xenoliths. Shiva Cheshire UK, pp. 230-249.

Pearce, J.A. and Cann, J.R., 1971. Ophiolite origin investigated by discriminant analysis using Ti, Zr and Y. Earth Planet. Sci. Lett., v. 12, pp. 339-349.

Pearce, J.A. and Cann, J.R., 1973. Tectonic setting of basic volcanic rocks determined by using trace element analysis. Earth Planet Sci. Lett., v. 19, pp. 290-300.

Pearce, J.A., Lippard, S.J. and Robert, S., 1984. Characteristics and tectonic significance of supra-subduction zone ophiolite. In: B.P. Kokellar, and M.F. Howells (Eds.), Marginal Basin Geology. Jour. Geol. Soc. Lond. Spl. Publ., v. 16, pp. 77-94.

Pearce, J.A., Lippard, S.J. and Robert, S.S., 1985. Characteristic tectonic significance of supra-subduction zone ophiolite, reproduced from marginal basin. Geol. Publ. Geol. Soc., Blackwell Scientific Publication, pp. 77-94.

Pearce J.A. and Norry M.J., 1979. Petrogenetic implications of Ti, Zr, Y, and Nb variations in volcanic rocks. Contrib. Min. Pet., v. 69, pp. 33-47.

Pearce, J.A. and Peate, D.W., 1995. Tectonic implications of the composition of volcanic arc lavas. An. Rev. Earth Planet. Sci., v. 23, pp. 251-285.

Pemberton, S.G. and Jones, B., 1988. Ichnology of the Pleistocene Iron Shore Formation, Grand Cayman Island, British West Indies. Jour. Paleon., v. 62, pp. 495-505.

Peng, Z.X., Mahoney, J.J., Hooper, P.R., Harris, C. and Beane, J.E., 1994. A role for lower continental crust in flood basalt genesis: Isotopic and incompatible element

study of the lower six formations of the western Deccan Traps, India. Geochim. Cosmochim. Acta, v. 58, pp. 267-288.

Pettijohn, F.J., 1984. Sedimentary rocks (3rd Ed.), CBS Publishers and Distributor, Ind. Ed., 628p.

Pettijohn, F.J., Potter, P.E. and Seiver, R., 1987. Sand and sandstone (2nd Ed.). Springer-Verlag, New York, 553p.

Pineau, F., Javoy, M. Hawkins, J.W. and Craig, H., 1976. Oxygen isotope variations in marginal basin and ocean ridge basalts. Earth Planet. Sci. Lett., v. 28, pp. 229-307.

Poldervaart, A., 1955. Zircon in rocks 1: Sedimentary rocks. Am. Jour. Sci., v. 86, pp. 433-461.

Potter, P.E., 1978. Petrology and chemistry of modern big river sands. Jour. Geol., v. 86, pp. 423-449.

Prange, A. and Kremling, K., 1985. Distribution of dissolved molybdenum, uranium and vanadium in Baltic Sea waters. Mar. Geol., v. 16, pp. 259-274.

Prothero, D.R. and Schwab, F.L, 2003. Sedimentary geology. W.H. Freeman and Co. pp. 99-126.

Raju, A.T.R., 1968. Geological evolution of the Assam and Cambay Tertiary basins in India. Bull. AAPG, v. 52, pp. 2422-2437.

Ranjan, N. and Banerjee, D.M., 2009. Central Himalayan crystallines as the primary source for the sandstone-mudstone suites of the Siwalik Group: New geochemical evidence. Gond. Res., v. 16, pp. 687-696.

Rao, B.V., Subba Rao, M.V., Charan, S.N., Srikanth, B., Balaram, V. and Ezung, O.C., 2003. Major, trace and platinum group element geochemistry of ultramafic rock assemblages of the Nagaland ophiolite belt: Implications for petrogenesis and PGE occurrence. Nat. Sym., Hyderabad.

Rao, R.A., 1983. Geology and hydrocarbon potential of a part of Assam Arakan basin and its adjacent regions. In: L.L. Bhandari (Ed.), Petroleum. Asia Jour., pp. 127-158.

Rao, R.A., 1993. Magnetic polarity stratigraphy of Upper Siwalik of north western Himalayan foothills. Curr. Sci., v. 64, pp. 863-873.

Rao, R.A. and Samanta, M.K., 1987. Structural style of the Naga overthrust belt and its implications on exploration. Bull. ONGC, v. 24.

Ray, D., Rajan, S. and Ravindra, R., 2012. Role of subducting component and sub-arc mantle in arc petrogenesis: Andaman volcanic arc. Curr. Sci., v. 102, pp. 605-609.

Raynolds, R.G.S. and Johnson, G.D., 1985. Rates of Neogene depositional and deformational processes, northwest Himalayan foredeep margin, Pakistan. In: N.J. Snelling, (Ed.), The chronology of geological records. Mem. 10th Geol. Soc. Ind., pp. 307-311.

Reichow, M.K., Saunders, A.D. and White, R.V., 2005. Geochemistry and petrogenesis of basalts from the west Siberian basin: An extension of the Permo-Triassic Siberian Traps, Russia. Lithos, v. 79, pp. 435-452.

Renne, P.R., Scott, G.R. and Bazard, D.R., 1988. Multi-component paleomagnetic data from the Nosoni Formation, eastern Klamath Mountains, California: Cratonic

Permian directions with Jurassic overprints. Jour. Geophy. Res., v. 93, pp. 3387-3400.

Resimic-Saric, K., Koroneos, A., Cvetkovic, V. and Balogh, K., 2004. Origin and evolution of the ophiolitic complex of Zdraljica (Central Serbia). Jour. Geol. Soc. Greece, v. 36, pp. 597-606.

Ringwood, A.E., 1976, Composition and petrology of the Earth's mantle. McGraw Hill Book Company, New York, 618 p.

Roaldest, E., 1978. Mineralogical and chemical changes during weathering, transportation and sedimentation in different environments with particular references to the distribution of yttrium and lanthanide elements. Ph.D. thesis (Unpubl.), Geol. Inst., University of Oslo, Norway.

Robertson, A.H.F., 1977. The Moni Melange, Cyprus: An olistrome formed at a destructive plate margin. Jour. Geol. Soc. Lond., v. 133, pp. 447-466.

Robertson, D.J. and France, D.E., 1994. Discrimination of remanence-carrying minerals in mixtures, using isothermal remanent magnetization acquisition curves. Phy. Earth Planet. Inter., v. 82, pp. 223-234.

Robinson, S.G., 1986. The late Pleistocene palaeoclimatic record of North Atlantic deep sea sediments revealed by mineral magnetic measurements. Phy. Earth Planet. Inter., v. 42, pp. 22-47.

Rochette, P., Lorand, J.P., Fillion, G. and Sautter, V., 2001. Pyrrhotite and the remanent magnetization of SNC meteorites: A changing perspective on Martian magnetism. Earth Planet. Sci. Lett., v. 190, pp. 1-12.

Rollinson, H.R., 1993. Using geochemical data: Evaluation, presentation, interpretation. John Wiley and Sons, New York.

Roser, B.P., Cooper, R.A., Nathan, S. and Tulloch, A.J., 1996. Reconnaissance sandstone geochemistry, provenance and tectonic setting of the Lower Palaeozoic terranes of the West Coast and Nelson, New Zealand. New Zeal. Jour. Geol. Geophy., v. 39, pp. 1-16.

Roser, B.P. and Korsch, R.J., 1985. Plate tectonics and geochemical composition of sandstones: A discussion. Jour. Geol., v. 93, pp. 81-84.

Roser, B.P. and Korsch, R.J., 1986. Determination of tectonic setting of sandstone-mudstone suites using SiO_2 content and K_2O/Na_2O ratio. Jour. Geol. v. 94, pp. 635-650.

Roser, B.P. and Korsch, R.J., 1988. Provenance signatures of sandstone-mudstone suites determined using discriminant function analysis of major-element data. Chem. Geol., v. 67, pp. 119-139.

Roy, A., Bandyopadhyay, B.K. and Huin, A.K., 1997. Geology and geochemistry of basic volcanics from the Sakoli schist belt of Central India. Jour. Geol. Soc. Ind., v. 50, pp. 209-221.

Roy, R.K., 1989. Meso-Cenozoic accretionary prism on the margin of Indo-Burman range ophiolite and its implications. Suran Publication, Patna.

Roy, R.K. and Kacker, R.N., 1980. Tectonic analysis of Naga Hills orogenic belt along eastern Peri-Indian suture. Him. Geol. v. 10, pp. 374-402.

Roy, R.K. and Kacker, R.N., 1986. Cenozoic deformation pattern and mechanism in the belt of schuppen and their role in hydrocarbon accumulation: Further exploratory concepts for Assam-Arakan basin. In: N.C. Ghose and S. Varadarajan (Eds.), Ophiolites and Indian plate margin. Sumna Publishers, Patna, pp. 197-221.

Roy, R.K., Kacker, R.N. and Chattopadhyay, B., 1982. Geochemical characteristic and tectonic setting of the Naga Hills ophiolite volcanics, India. Ofioliti, v. 2, pp. 479-498.

Sadler, P.M., 1981. Sediment accumulation rates and the completeness of stratigraphic sections, Jour. Geol., v. 89, pp. 569-584.

Sangode, S.J. and Bloemendal, J., 2004. Pedogenic transformation of magnetic minerals in Pliocene-Pliestocene palaeosols of the Siwalik Group, NW Himalaya, India. Palaeogeog. Palaeoclim. Palaeoeco., v. 212, pp. 95-118.

Sangode, S.J. and Kumar, R., 2003. Magnetostratigraphic correlation of the Late Cenozoic fluvial sequence from NW Himalaya, India. Curr. Sci., v. 84, pp. 1014-1024.

Sangode, S.J., Kumar, R. and Ghosh, S.K., 1996. Magnetic polarity stratigraphy of the Siwalik sequence of Haripur area (HP), NW Himalaya. Jour. Geol. Soc. Ind., v. 47, pp. 683-704.

Sangode, S.J., Kumar, R. and Ghosh, S.K., 1999. Paleomagnetic and rock magnetic perspectives on the post collision continental sediments of the Himalaya. In: T. Radhakrisna and J.D.A. Piper (Eds.), The Indian sub-continents and the Gondwana: A paleomagnetic and rock magnetic perspective. Mem. Geol. Soc. Ind., v. 44, pp. 221-248.

Sarkar, A., Datta, A.K., Poddar, B.C., Bhattacharyya, B.K., Kollapuri, V.K. and Sanwal, R., 1996. Geochronological studies of Mesozoic igneous rocks from eastern India. Jour. SE Asian Earth Sci., v. 13, pp. 77-81.

Sarmah, R.N., 1983. Sedimentology and geochemistry of the sandstones of the Disang and Barail groups, Kohima, Nagaland. Ph.D. thesis (Unpubl.), Gauhati University, Guwahati.

Saunder, A.D. and Tarney, J., 1979. The geochemistry of basalts from a back arc spreading centre in the East Scotia Sea. Geochim. Cosmochim. Acta, v. 43, pp. 555-72.

Saxena, A. and Pandit, M.K., 2012. Geochemistry of Hindoli Group metasediments, SE Aravalli Craton, NW India: Implications for weathering and provenance. Jour. Geol. Soc. Ind., v. 79, pp. 267-278.

Schilling, J.G., 1973. Iceland mantle plume: Geochemical study of the Reykjanes Ridge. Nature, v. 242, pp. 565-571.

Schwab, F.L., 1975. Framework mineralogy and chemical composition of continental margin type sandstones. Geology, v. 3, pp. 487-490.

Seifert, K. and Brunotte, D., 1996. Geochemistry of weathered mid oceanic ridge basalt and diabase clasts from hole 899B in the Iberia abyssal plain. In: R.B. Whitemarsh, D.S. Sawyer, A. Klaus and D.G. Masson, (Eds.), Proceedings of the ocean drilling program. Scientific Results, v. 149, pp. 497-515.

Seiver, R., 1979, Plate tectonic controls on diagenesis. Jour. Geol., v. 87, pp. 127-155.

Selvaraj, K. and Chen, C.A., 2006. Moderate chemical weathering of subtropical Taiwan: Constraints from solid-phase geochemistry of sediments and sedimentary rocks. Chic. Jour. Geol., v. 114, pp. 101-116.

Sen, S. and Chattopadhyay, B., 1978. The ophiolite belt north-eastern India and associated mineralization. Proc. 3rd Reg. Conf. Geol. Miner. Res. SE Asia. Asian Inst. Tech., Bangkok, pp. 281-284.

Shaw, T.J., Geiskes, J.M. and Jahnke, R.A., 1990. Early diagenesis in differing depositional environments: The response of transition metals in pore water. Geochim. Cosmochim. Acta, v. 54, pp. 1233-1246.

Shervais, J.W., 1982. Ti-V plots and petrogenesis of modern ophiolitic lavas. Earth Planet. Sci. Lett., v. 59, pp. 101-118.

Shervais, J.W., 2001. Birth, death and resurrection: The life cycle of supra-subduction zone ophiolites. Geochem. Geophys. Geosyst., v. 2.

Sholkovitz, E.R., 1978. The flocculation of dissolved Fe, Mn, Al, Cu, Ni, Co and Cd during estuarine mixing. Earth Planet. Sci. Lett., v. 41. pp. 77-86.

Singer, M.J. and Fine, P., 1989. Pedogenic factors affecting magnetic susceptibility of northern California soils. Soil Sci. Soc. Am. Jour., v. 53, pp. 1119-1127.

Singh, R.N., 1979. Geochemistry of the ophiolite suite, east of Kiphire, Tuensang district, Nagaland. Ph.D. thesis (Unpubl.), Patna University, Patna.

Singh, R.N. and Adiga, K.S., 1976. Systematic mapping in parts of ultramafic belt, Tuensang district, Nagaland. Unpubl. Prog. Rep. Geol. Surv. Ind., FS 1975-76.

Singh, S.K., Vidhyadharan, K.T. and Ray, S.B., 1983. Systematic geological mapping of Naga Hill ophiolites in the Phek district, Nagaland. Unpubl. Prog. Rep. Geol. Surv. Ind., FS 1981-1982.

Smewing, J.D. and Potts, P.J., 1976. Rare-earth abundances in basalts and metabasalts from the Troodos massif, Cyprus. Contrib. Min. Pet., v. 57, pp. 245-257.

Sofy, M.M., 2003. Petrochemistry and petrogenesis of Bulfat mafic layered igneous intrusion around Herro (Qaladizeh)-Iraq Kurdistan. M.Sc thesis, Salahaddin University, Erbil, 123p.

Spears, D.A. and Sotiriou, R.K., 1976. Titanium in some carboniferous sediment from Great Britain. Geochim. Cosmochim. Acta, v. 40, pp. 345-351.

Spooner, E.T. and Fyfe, W.S., 1973. Sub-seafloor metamorphism, heat and mass transfer. Contrib. Min. Pet., v. 42, pp. 287-304.

Srikanth, B., Rao, M.V.S., Rao, B.V., Charan, S.N., Balaram, V. and Ezung, O.C., 2004. Geochemical signatures in the basaltic rocks of Naga Hills Ophiolite (NHO) belt: Implication for petrogenesis and tectonic environment of emplacement. Jour. App. Geochem., v. 6, pp. 177-189.

Srinivasan, V., 2007. Regional structural configuration and seismic pattern of "Belt of Schuppen" in northeast India. Jour. Geol. Soc. Ind., v. 70. pp. 801-814.

Srivastava S.K. and Pandey., N. 2011. Search for provenance of Oligocene Barail Sandstones in and around Jotsoma, Kohima, Nagaland. Jour. Geol. Soc. Ind., v. 77, pp. 433-442.

Srivastava, S.N.P., Roy, R.K., Singh, R.N. and Adiga, K.S., 1978. Tectono-stratigraphy of the ophiolite belt of the Naga Hills, NE India. Him. Geol., v. 8, pp. 531-559.

Stacey, F.D. and Banerjee, S.K., 1974. The physical principles of rock magnetism. Der. Solid Earth Geophy., v. 5, 195p.

Stacey, F.D., Joplin, G. and Lindsay, J., 1960. Magnetic anisotropy and fabric of some foliated rocks from SE Australia. Geofis. Pura Appl., v. 47, pp. 30-40.

Stoneley, R., 1974. Evolution of the continental margins bounding a former southern Tethys. In: C.A. Burk and C.L. Drake (Eds.), The Geology of Continental Margins. Springer-Verlag, New York, 1009p

Subba Rao, M.V., Balaram, V., Rao, B.V., Charan S.N. and Ezung O.C., 2005. Prospects of Platinum Group Element (PGE) occurrence in the mafic and ultramafic cumulate rocks of the Naga Ophiolite (NHO) belt, Northeast India. Proc. Sem. Sci. Tech. Reg. Dev. - Case for Northeast India. In: S.K. Dolui and Mahanta (Eds.), pp. 84-88.

Subba Rao, M.V., Srikanth, B., Balaram, V., Charan, S.N., Rao, B.V., Ezung, O.C. and Chisoi, 2004. Estimation of platinum group elements by ICP-MS in the ultramafic and mafic cumulates of the Naga Hills Ophiolite Belt, Nagaland: Implications for petrogenesis and potential of PGE occurrence in the belt. 11th ISMAS Workshop on Mass Spectrometry, Shilon Bagh, Shimla, pp. 210-214.

Suess, E., 1904. The face of the earth. Oxford University Press.

Sun, S.S. and McDonough, W.F., 1989. Chemical and isotopic systematics of oceanic basalts: Implications for mantle composition and processes. In: S.D. Saunders and M.J. Norry (Eds.), Magmatism in Ocean Basins. Geol. Soc. Lond. Spl. Publ., v. 42, pp. 313-345.

Suttner, L.J., 1974. Sedimentary petrographic provinces: An evaluation. In: C.A. Ross (Ed.), Paleogeographic provinces and provincialibility. Soc. Eco. Pal. Min. Spl. Publ., v. 21, pp. 25-84.

Suttner, L.J., Basu, A. and Mack, G.H., 1981. Climate and the origin of quartz arenites. Jour. Sed. Pet., v. 51, pp. 1235-1246.

Suttner, L.J. and Dutta, P.K., 1986. Alluvial sandstone composition and paleoclimate: Framework and mineralogy. Jour. Sed. Pet., v. 56, pp. 329-345.

Tandon, S.K., 1991. The Himalayan foreland: Focus on Siwalik Basin. In: S.K. Tandon, C.C. Pant and S.M. Casshyap (Eds.), Sedimentary Basins of India: Tectonic context, Nainital, pp. 177-201.

Tandon, S.K., Kumar, R., Koyama, M. and Niitsuma, N. 1984. Magnetic polarity stratigraphy of the Upper Siwalik Subgroup, east of Chandigarh, Punjab Sub-Himalaya, India. Jour. Geol. Soc. Ind., v. 25, pp. 45-55.

Tarling, D.H., 1971. Principles and applications of paleomagnetism. Chapman and Hall, London.

Tarling, D.H. and Hrouda, F., 1993. The magnetic anisotropy of rocks, Chapman and Hall, London, 217p.

Tatsumi, Y., Hamilton, D.L. and Nesbitt, R.W., 1986. Chemical characteristics of fluid phase released from a subducted lithosphere and origin of arc magmas:

Evidence from high-pressure experiments and natural rocks. Jour. Volcan. Geotherm. Res., v. 29, pp. 293-309.

Tauxe, L. and Opdyke, N.D., 1982. A time framework based on magnetostratigraphy for the Siwalik sediments of the Kaur area, Northern Pakistan. Palaeogeo. Palaeoclim. Palaeoeco., v. 37. pp. 43-61.

Taylor, S.R. and McLennan, S.M., 1985. The continental crust: Its composition and evolution. Blackwell Scientific Publ., 312p.

Thompson, G., 1973. A geochemical study of the low-temperature interaction of sea water and oceanic igneous rocks. EOS Trans., v. 54, pp. 1015-1019.

Thompson, R. and Oldfield, F., 1986. Environmental magnetism. Allen and Unwin, London.

Thong, G.T., 1993. Sedimentological studies of the Palaeogene sandstones around Botsa, Kohima district, Nagaland. Ph.D. thesis (Unpubl.), North Eastern Hill University, Shillong.

Thong, G.T. and Rao, B.V., 2006. Geochemical investigations of the Disang sandstones of Botsa, Nagaland, NE India. Jour. Geol. Soc. Ind., v. 68, pp. 715-722.

Tian, L.L., Zhu, R.X., Pan, Y.X., 2002. Rock magnetic properties of Hannuoba basalts, Zhangbei, China. Chin. Jour. Geophy., v. 45, pp. 872-878.

Tiwari, R.P., Malsawma, J., Sangode, S.J. and Arora, B.R., 2007. Magnetostratigraphy of a part of Middle Bhuban sequence (Surma Group), Aizawl, Mizoram. Jour. Geol. Soc. Ind., v. 70, pp. 667-674.

Tiwari, R.P., Sangode, S.J., Patil, S.K., Sivaji, C. and Arora, B.R., 2006. Status of paleomagnetic and magnetostratigraphic studies in the northeast India and the new initiatives. DCS-DST News, pp. 16-20.

Tribovillard, N.P., Desprairies, A., Lallier-Verges, E., Bertrand, P., Moureau, N., Ramdani, A. and Ramanampisoa, L., 1994. Geochemical study of organic-matter rich cycles from the Kimmeridge Clay Formation of Yorkshire (UK): Productivity versus anoxia: Palaeogeo. Palaeoclim. Palaeoeco., v. 108, pp. 165-181.

Tripathi, C., 1989. Tectonic implications of Greater Himalayan ophiolites: Strategy for mineral exploration in the India-Asia collision zone. In: N.C. Ghose, (Ed.), Phanerozoic Ophiolites of India. Sumna Publishers, Patna, pp. 17-38.

Uchman, A. and Gazdzicki, A., 2006. New trace fossils from the La Meseta Formation (Eocene) of Seymour Island, Antarctica. Polish Pol. Res., v. 27, pp.153-170.

Vance, R.K. and Condie, K.C., 1987. Geochemistry of footwall alteration associated with the Early Proterozoic United Verde massive sulfide deposit, Jerome, Arizona. Econ. Geol., v. 82, pp. 571-586.

Vandamme, D., Courtillot, V., Besse, J. and Montigny, R., 1991. Paleomagnetism and age determination of the Deccan Traps (India): Results of a Nagpu-Bombay traverse and review of earlier work. Rev. Geophy., v. 29, pp. 159-190.

Velbal, M.A., 1985. Mineralogically mature sandstones in accretionary prisms. Jour. Sed. Pet., v. 55, pp. 685-690.

Verma, R.K., 1985. Gravity field, seismicity and tectonics of the Indian Peninsula and the Himalaya. Allied Publ., New Delhi, pp. 155-189.

Verma, R.K., Mukhopadhyay, M. and Ahluwalia, M.S., 1976. Earthquake mechanism and tectonic features of the northern Burma. Tectonophysics, v. 32, pp. 387-399.

Verma, S.P., 1992. Seawater alteration effects on REE, K, Rb, Cs, Sr, U, Th, Pb and Sr-Nd-Pb isotope systematics of mid-ocean ridge basalt. Geochem. Jour., v. 26, pp. 159-177.

Verosub, K.L. and Roberts, A.P., 1995. Environmental magnetism: Past, present, and future. Jour. Geophy. Res., v. 100, pp. 2175-2192.

Vidyatharan, K.T., Srivastava, R.K., Bhattacharyya, S., Joshi, A. and Jena, S.K., 1986. Distribution and description of major rock types. Geol. Surv. Ind., Mem., v. 119, pp. 18-27.

Vigliotti, L., 1997. Magnetic properties of light and dark sediment layers from the Japan Sea: Diagenetic and paleoclimatic implications. Quat. Sci. Rev., v. 16, pp. 1093-1114.

Vineetha, K. 2004. Chemical and geochemical aspects of the shales in and around Kohima, Nagaland. Ph.D. thesis (Unpubl.), Nagaland University, Kohima.

Vital, H. and Stattegger, K., 2000. Major and trace elements of stream sediments from the Amazon River. Chem. Geol., v. 168, pp. 151-168.

Vital, H., Stattegger, K. and Garge-Schonberg, C.D., 1999. Composition and trace element geochemistry of detrital and clay and heavy mineral suites of the lowermost Amazon river: A provenance study. Jour. Sed. Res., v. 69, pp. 563-565.

Wager, L.R. and Mitchell, R.L., 1951. The distribution of trace elements during strong fractionation of basic magma: A further study of the Skeergaard intrusion East Greenland. Geochim. Cosmochim. Acta, v. 1, pp. 129-208.

Wang, K., Plank, T., Walker, J.D. and Smith, E.I., 2002. A mantle melting profile across the Basin and Range, SW USA, pp. ECV 5-1-19.

Waugh, B., 1970. Petrology, provenence and silica diagenesis of the Penrith Sandstone (Lower Permian) of northwest England. Jour. Sed. Pet., v. 40, pp. 1226-1240.

Weiguo, Z. and Lizhong, Y., 2003. Magnetic properties of tidal flat sediments of the Yangtze estuary and its relationship with particle size. Sci. China (Series D), v. 46.

Wildeman, T.R. and Haskin, L.A., 1973. Rare earths in Precambrian sediments. Geochim. Cosmochim. Acta, v. 37, pp. 419-438.

Willis, K.M., Stern, R.J. and Claur, N., 1988. Age and geochemistry of Late Precambrian sediments of the Hammamat Series from the northeastern desert of Egypt. Precamb. Res., v. 42, pp. 173-187.

Wilson, M., 1989. Igneous petrogenesis: A global tectonic approach. Harper Collins Academic Publisher, London, 240p.

Winchester, J.A. and Floyd, P.A., 1976. Geochemical magma type discrimination: Application to altered and metamorphosed basic igneous rocks. Earth Planet. Sci. Lett., v. 28, pp. 459-469.

Winchester, J.A. and Floyd, P.A., 1977. Geochemical discrimination of different magma series and their differentiation products using immobile elements. Chem. Geol., v. 20, pp. 325-343.

Wood, D.A., Gibson, I.L. and Thompson, R.N., 1976. Elemental mobility during zeolite facies metamorphism of the Tertiary basalts of eastern Iceland. Contrib. Min. Pet., v. 55, pp. 224-254.

Wood, D.A., Joron, J.L. and Treuil, M., 1979. A re-appraisal of the use of trace elements to classify and discriminate between magma series erupted in different tectonic settings. Earth Planet. Sci. Lett., v. 45, pp. 326-336.

Wooden, J.L., Czamanske, G.K., Fedorenko, V.A., Arndt, N.T., Chauvel, C., Bouse, R.M., King, B.S.W., Knight, R.J. and Siems, D.F., 1993. Isotopic and trace element constraints on mantle and crustal contributions to Siberian continental flood basalts. Noril'sk area, Siberia. Geochim. Cosmochim. Acta, v. 57, pp. 3766-3704.

Wronkiewicz, D.J. and Condie, K.C., 1987. Geochemistry of Archaean shales from the Witwatershrand Supergroup, South Africa: Source area weathering and provenance. Geochim. Cosmochim. Acta, v. 51, pp. 2401-2416.

Zachos, J.C., Dickens, G.R. and Zeebe, R.E., 2008. An early Cenozoic perspective on greenhouse warming and carbon cycle dynamics. Nature, v. 451, pp. 279-283.

Zhou, L.P., Oldfield, F., Wintle, A.G., Robinson, S.G. and Wang, J.T., 1990. Partly pedogenic origin of magnetic variations in Chinese loess. Nature, v. 246, pp. 737-739.

Zhu, R.X., Guo, B. and Zong, L., 2000. Gauss-Matuyama polarity transition obtained from a loess section at Weiman, North-Central China. Chin. Jour. Geophy., v. 43, pp. 621-634.

(Appendix I)

Paleomagnetic basalt samples from Zipu and adjoining area (in degree decimals)

Sl. No.	Sample	Latitude (N)	Longitude (E)
1	Bs 1	25.68430	94.75908
2	Bs 2	25.68453	94.75919
3	Bs 4	25.68584	94.75721
4	Bs 5	25.68764	94.75701
5	Spl 1	25.65501	94.73769
6	Spl 2	25.65506	94.73769
7	Spl 3	25.66176	94.74413
8	Spl 4	25.66230	94.74471
9	Spl 5	25.65950	94.75217
10	Spl 6	25.66856	94.76081
11	Spl 7	25.67168	94.76278
12	Spl 8	25.68249	94.76020
13	Spl 9	25.69146	94.75817
14	Spl 10	25.60889	94.75590
15	Spl 11	25.60498	94.76736
16	Spl 12	25.59800	94.76801
17	Spl 13	25.59102	94.76603
18	Spl 14	25.55895	94.77506
19	Spl 18	25.59231	94.76700

I. Journals (Papers communicated)

1. **Watitemsu Imchen**, Glenn T. Thong, and Temjenrenla Pongen. Provenance, tectonic setting, and age of the Upper Disang sediments of Phek District, Nagaland.

2. S.K. Patil, **Watitemsu Imchen**, V. Rino, Temjenrenla, Glenn T. Thong, and B.V. Rao. Geochemistry and paleomagnetism of the basalt of the ophiolite suite in parts of Phek District, Nagaland.

II. Abstracts

1. S.K. Patil and **Watitemsu Imchen**. Geochemistry and paleomagnetism of the basalt of the ophiolite suite in parts of Phek District, Nagaland. National Symposium on Recent Advances in Applied Geochemistry: Current Status and Future Trends. Atomic Minerals Division, Hyderabad, 19-21 December, 2011. Organised by Indian Society of applied Geochemists (ISAG).

III. Workshop / Training Attended

1. Workshop on Paleomagnetism and Magnetostratigraphy. Department of Geology, Mizoram University & Department of Science & Technology, New Delhi (Aizawl), 17-19 March 2008.

2. Brainstorming Session on Landslides of NE India. Department of Geology, Nagaland University & Department of Science & Technology, New Delhi (Kohima), 5-6 May 2009.

IV. Junior Research Fellow

1. Shillong Basin and the Thrust and Ophiolite Belts of Indo-Myanmar Mobile Belt, North Eastern India: An Integrated Approach from Magnetostratigraphy and Paleomagnetism. Department of Science & Technology, Govt. of India, New Delhi.